Fluorescent Molecular Crystals and Nanocrystals: Templated Assembly, Amorphous-to-Crystalline Transformation and Hierarchical Growth

A Thesis Submitted for the Degree of

DOCTOR OF PHILOSOPHY

by

Ch. Gupta Chandaluri

School of Chemistry

University of Hyderabad

Hyderabad 500 046

INDIA

April 2013

DECLARATION

I hereby declare that the matter embodied in this thesis is the result of investigations carried out by me in the School of Chemistry, University of Hyderabad, Hyderabad under the supervision of Prof. T. P. Radhakrishnan.

In keeping with the general practice of reporting scientific observations, due acknowledgements have been made wherever the work described is based on the findings of other investigators.

Ch. Gupta Chandaluri

CERTIFICATE

This is to certify that the work described in this thesis entitled "**Fluorescent Molecular Crystals and Nanocrystals: Templated Assembly, Amorphous-to-Crystalline Transformation and Hierarchical Growth**" has been carried out by Ch. Gupta Chandaluri, under my supervision and the same has not been submitted elsewhere for any degree.

Prof. T. P. Radhakrishnan
(Thesis Supervisor)

DEAN
School of Chemistry
University of Hyderabad
Hyderabad 500 046

CONTENTS

LIST OF ACRONYMS

ACT	amorphous-to-crystalline transformation
AFM	atomic force microscope
AIE	aggregation induced emission
AM1	austin model 1
br	broad
CI	configuration interactions
COSMO	conductor-like screening model
d	doublet
DADQ	diaminodicyanoquinodimethane
dec.	decomposition
DMSO	dimethylsulfoxide
FESEM	field emission scanning electron microscope
IC	internal conversion
ISC	intersystem crossing
kDa	kilo Dalton
LED	light emitting diode
m	multiplet
μm	micrometer
μl	microliter
M_w	weight average molecular weight
nm	nanometer
ns	nanosecond
PS	polystyrene
quin	quintet
SEM	scanning electron microscope
TEM	transmission electron microscope

Synopsis

This thesis addresses several issues related to the assembly of molecular materials which exhibit enhanced fluorescence in the assembled state. Therefore this chapter provides an introduction to fluorescence and fluorescent materials followed by an overview of some basic aspects of molecular assembly that leads to nucleation and crystal growth. Different fluorescent materials are introduced, highlighting their emergence and relevance (Sec. 1.1). The uniqueness and significance of molecular materials and the influence of molecular packing on their optical responses are discussed, followed by a brief look at the important phenomenon of aggregation-induced fluorescence enhancement (Sec. 1.2). Special attention is paid to molecular nanomaterials based on small organic molecules; factors such as size and shape that impact upon their optical properties are described along with the significance of controlling their self assembly (Sec. 1.3). Turning to the fundamental aspects of nucleation and crystal growth involved in materials assembly, significance of the amorphous phase in materials in general and molecular materials in particular is highlighted, along with the approaches to realize amorphous-to-crystalline transformation (Sec. 1.4), of specific interest to some of the work presented in this thesis. Finally, the salient features of the subsequent chapters in the thesis are outlined (Sec. 1.5).

1.1. Fluorescent Materials

1.1.1 *Fluorescence phenomenon*

The phenomena of fluorescence was first reported in 1845 by Herschel who observed a quinine solution in sunlight.[1] Fluorescence is one of the phenomena of photoluminescence, in which a substance absorbs radiations or light followed by emission of light. The absorption of radiation by a molecule causes electronic excitation from its ground state to any of the higher excited states. The excited molecule returns to the ground state by releasing the energy as radiation. Fluorescence process is explained using the well-known Jablonski diagram (Fig. 1.1).

Jablonski diagram is named after Prof. Alexander Jablonski, who is generally considered to be the father of fluorescence spectroscopy. This diagram is used to explain the processes that occur between the absorption and emission of light that is transitions between electronic states of a molecule. Fluorescence phenomenon is explained as follows; molecule absorbs UV-Vis radiation by which it gets excited from the ground state S_0 (which has several vibrational states) to the excited state S_1 or higher electronic energy states. This process is very fast, occurring in the order of 10^{-15} s. Now the molecule has some additional energy that can be dissipated through non-radiative or radiative paths. Non-radiative paths include vibrational relaxation and internal conversion; these processes are very fast, occurring in the order of 10^{-14} to 10^{-11} s. Radiative pathways like fluorescence, are slow processes compared to vibrational relaxation, occurring in the order of 10^{-9} to 10^{-7} s. Other processes like phosphorescence may also occur.

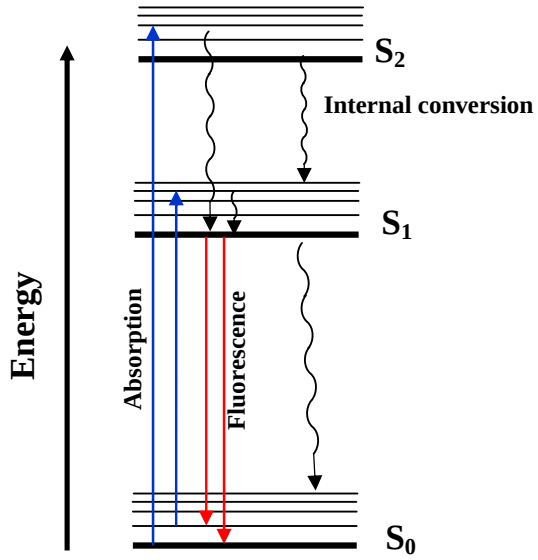

Figure 1.1. *Jablonski diagram*

The intensities of the vibronic transitions between states can be determined using the Franck Condon (FC) selection rules for UV-Vis spectroscopy. According to the FC principle electronic motion is much faster than the nuclear motion, so the molecule retains the same geometry in the excited state as the ground state. This excited state is called the FC excited state. After absorption, molecules reorganize to a different geometry to reach the lowest vibrational state of the lowest excited state. Due to the energy loss during these non-radiative pathways, the emission energy is lower, red-shifted, compared to the absorption energy. This phenomenon is known as Stokes shift. In this process, the molecule is stabilized through changes in the molecular geometry and rearrangement of the solvent environment, in accordance with the electron density distribution. Molecule retains its equilibrium excited state and emission of a photon from this state produces the FC ground state. Molecule reaches the equilibrium ground state by releasing energy through vibrational relaxation again.

These processes influence the way in which the molecular geometry and the environment affect the fluorescence emission energy.

Quantum yield and excited state lifetime measurements are also important to understand the fluorophore properties. These quantities are generally independent of the concentration of fluorophore and intrinsic properties of the system in a given environment. Quantum yield is defined as the ratio between the number of emitted photons to the number of absorbed photons. It provides the efficiency of conversion of the absorbed light to emitted light by the fluorophore. Lifetime measurements provide a fundamental characterization of the excited state of the fluorophore. Time-resolved measurements provide information on the decay of the excited state and can be used to distinguish dynamic and static quenching processes, nature and number of the emitting states etc. Resonance energy transfer between molecules can be explored through the lifetime measurements. Measurement of the excited state lifetime of a sample with high spatial resolution allows an advanced fluorescence based imaging, known as the fluorescence lifetime imaging microscopy (FLIM).

Fluorescence quenching

Fluorescence quenching is a process in which the fluorescence intensity decreases due to non-radiative energy loss pathways. In solution state different types of quenching processes are known. These include molecular rearrangements, energy transfer, collisional or dynamic quenching and static quenching. Consider the dynamic and static quenching processes (Fig. 1.2); in these two processes fluorophore and quencher should be in contact.[2] In dynamic quenching, the quencher diffuses to the excited fluorophore and the energy is transferred to it causing the fluorophore to come to the ground state without emission of a photon. In the case of static quenching, the

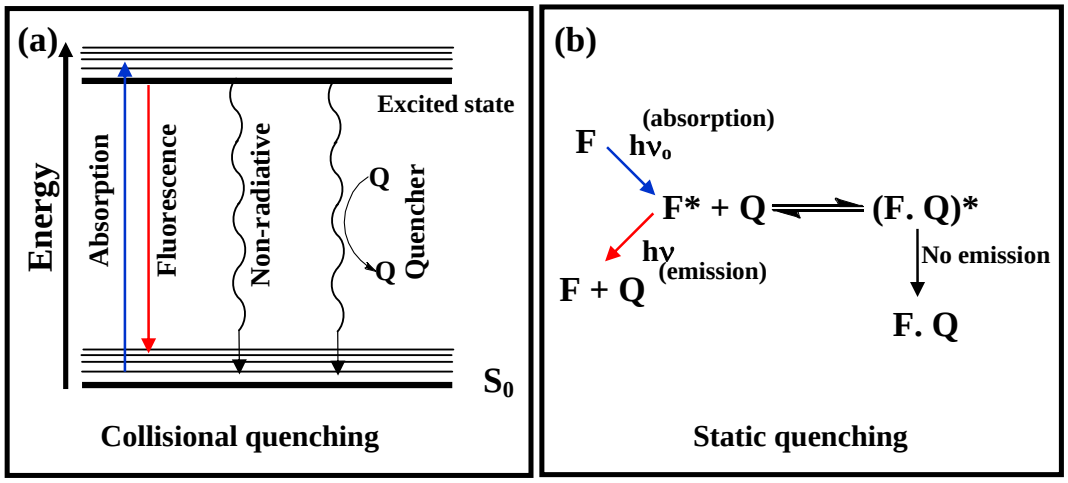

Figure 1.2. ***(a)*** *Jablonski diagram for collisional quenching and* ***(b)*** *schematic representation of static quenching; Q represents the quencher.*

fluorophore and the quencher form a nonfluorescent complex. Many quenchers are known in the literature; a commonly used quencher is molecular oxygen.[3] Aromatic and aliphatic amines also act as quenchers to most of the unsubstituted aromatic hydrocarbons. Halogenated compounds can also behave as quenchers.[2] Uridine acts as a quencher to coumarin derivative due to static interactions. Stern-Volmer equation is used to understand the quenching (Eq. 1.1) phenomenon. F_o and F are fluorescence

$$\frac{F_0}{F} = 1 + K_D[Q] \qquad \text{----- (1.1)}$$

intensities of the fluorophore in the absence and presence of the quencher. [Q] is the concentration of the quencher, K_D is the Stern-Volmer quenching constant. In the case of static quenching the association constant, K_S replaces K_D.

Resonance energy transfer is a quenching process in which spatial interactions matter. This process occurs between energy donor (D) and acceptor (A) systems. Initially D accepts photons and gets excited; while returning to the ground state, it

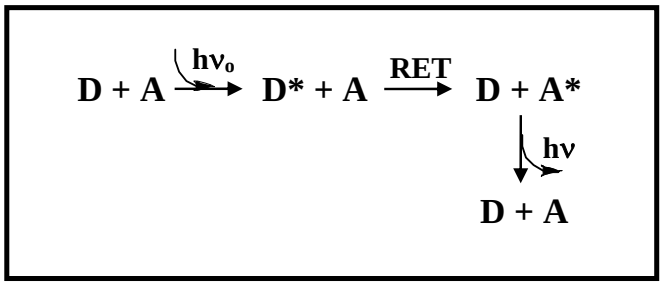

Figure 1.3. *Schematic representation of resonance energy transfer (RET).*

transfers the energy to A. It is not necessary that D and A should be in contact; however the distance between the two is important and are typically ~10 to 100 Å. A schematic representation of the process is shown in Fig. 1.3. Equation for the rate of energy transfer is given by Förster (Eq. 1.2). τ_D is the life time of D in the absence of A, r is the distance between the centers of D and A and R_0 is known as the Förster distance.

$$k_T(r) = \frac{1}{\tau_D}\left(\frac{R_0}{r}\right)^6 \qquad \text{----- (1.2)}$$

In the solid state, aggregation of molecules generally leads to fluorescence quenching through intermolecular energy transfer pathways. In selected classes of molecules, however, aggregation can lead to fluorescence enhancement. We discuss the latter case in Sec.1.2.3.

1.1.2 *Classes of fluorophores*

In the past few decades, there has been tremendous interest in the development of fluorescent materials, for a wide range of applications especially related to biology and device technologies. Some of the important applications are chemical sensors, biological labeling, medical diagnostics, DNA sequencing, forensics, genetic analysis, cellular and molecular imaging, fluorescent lamps, lasers, light emitting diodes and displays.[2,4] Many of the biochemical measurements which depended on radioactive

tracers now exploit fluorescence based probes. Different types of fluorophores that have been developed and their areas of application are discussed briefly below.

Organic molecules

Organic luminescent materials have been widely studied and surveyed in several books.[2,5] Condensed aromatic hydrocarbons such as pyrene are well-known fluorophores.[6] Some of the well known dye molecules that show efficient fluorescence are shown in Fig. 1.4. Fluoresceine, rhodamine, 4,4-difluoro-4-bora-3a,4a-diaza*s*-indacene, squaraine and cyanine derivatives show fluorescence emission in the 500–900 nm range. Fluorophores based on oxygen, sulfur, nitrogen heterocycles and naphthalene derivatives show fluorescence emission between near ultraviolet to 500 nm; these are used for fluorescent labeling of peptides and other biomolecules.[7]

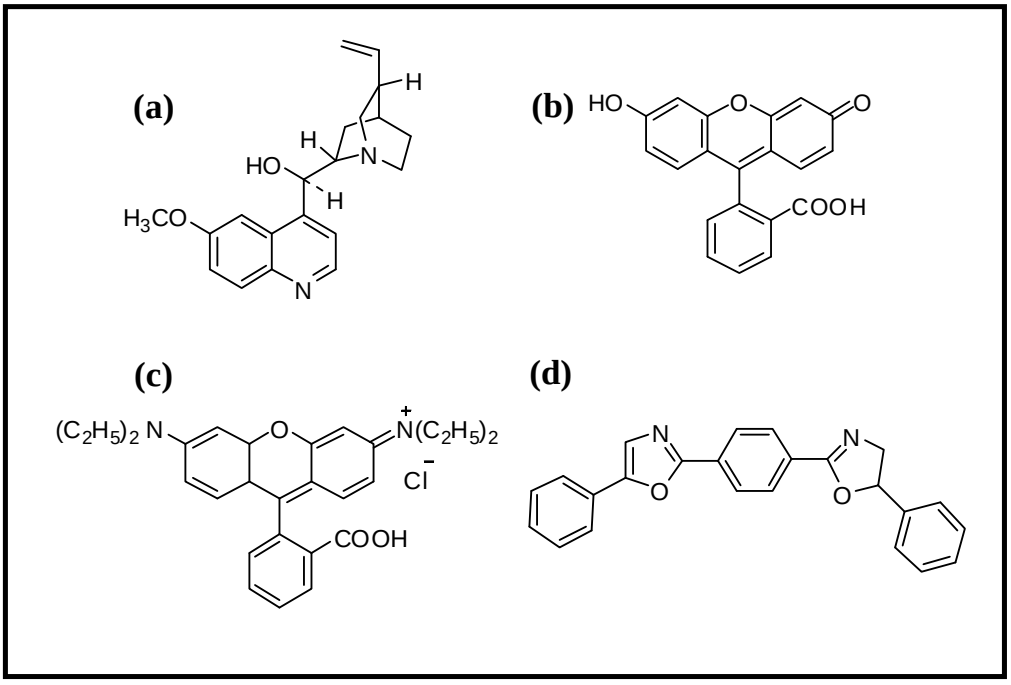

Figure 1.4. *Molecular structure of some well-known organic fluorophores:* ***(a)*** *quinine,* ***(b)*** *fluorescein,* ***(c)*** *rhodamine B and* ***(d)*** *1,4-bis(5-phenyloxazol-2-yl)benzene.*

Fluorescence intensity changes that accompany the spiro ring opening of xanthene derivatives is used for the detection of different metal ions.[8] Fluorescent organic molecules are used in the fabrication of LEDs and lasers.[9] They are of particular interest in reducing cost as well as environmental hazard effects. Relatively lower weights and the possibility of developing large area devices make them attractive choices for display systems in mobile phones, cameras and flat panel televisions. Organic transistors and LED's have become viable alternatives to their inorganic counterparts. Broad emission spectral feature of organic molecules is useful to produce tunable lasers.[10] Dye doped polymer lasers were developed in 1967;[11] dopedcrystals[12] and anthracene crystals[13] were developed in 1972 and 1974 respectively.

Light emission in conjugated polymers was discovered in 1990.[14] Semiconducting laser using conjugated polymer[15] solution was reported in 1992, followed by solid state conjugated polymers in 1996. Molecular structures of small

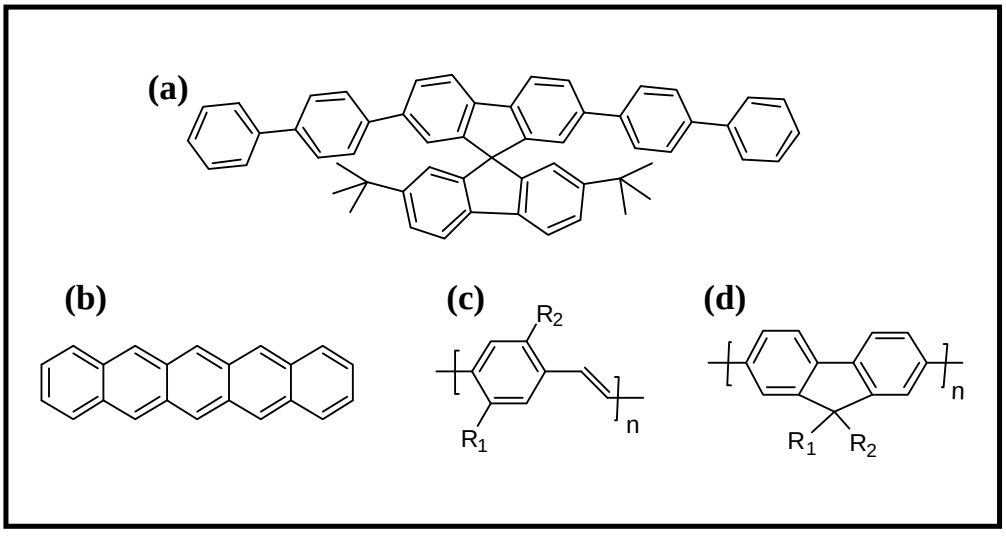

Figure 1.5. *Molecular structure of typical fluorophores based on monomer, oligomer and polymer:* ***(a)*** *spiro-linked oligomer,* ***(b)*** *pentacene,* ***(c)*** *generic poly (p-phenylene vinylene) derivative and* ***(d)*** *generic polyfluorene derivative.*

molecules and polymers which act as organic semiconductors for lasers and electroluminescent devices are shown in Fig. 1.5. Highly fluorescent semiconducting polymer dots are fabricated and used in biology and medicine applications.[16] Fluorescent polymer films also find application as highly sensitive sensors.[17]

Lanthanides and transition metal-ligand complexes

Lanthanide materials have generally sharper emission than organic luminescent materials. They cover the entire UV-Vis and near IR range; some are fluorescent, and several are phosphorescent and some show both phenomena. Lanthanides have low extinction coefficient, so these are not excited directly. Therefore complexes of these ions with chelators containing fluorophores are used often. The fluorophore is excited which then transfers the energy to the metal ion.[18] Chelators are chosen based on their ability to excite the metal ion. Some of typical chelators are shown in Fig. 1.6. Some of the most popular luminescent lanthanide coordination complexes are based on

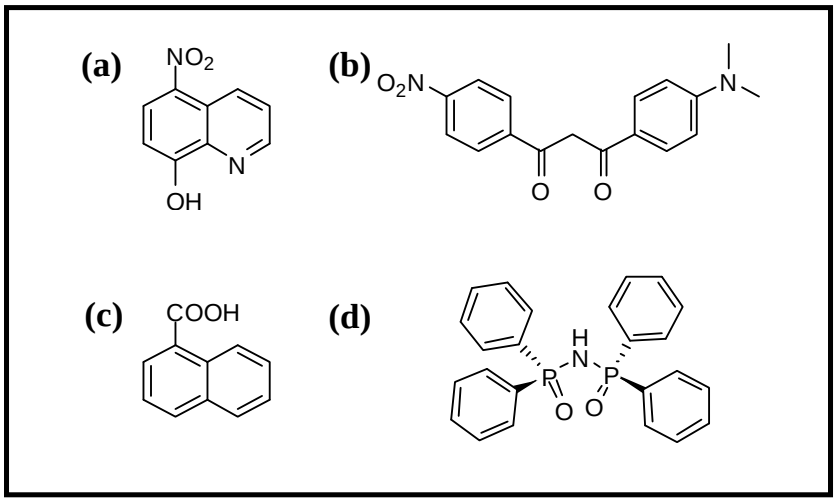

Figure 1.6. *Molecular structure of typical ligands for luminescent metal ions:* ***(a)*** *8-hydroxyquinoline derivative,* ***(b)*** *β-diketone derivative,* ***(c)*** *carboxylic acid derivative and* ***(d)*** *phosphinic acid derivative.*

β-diketone ligands. Chelators are used to increase the quantum yield and thus, the application potential. Lanthanide luminescent materials are interesting due to their application in many optoelectronic devices, bio-imaging and sensing.[19] Y_2O_3:Eu^{III} material is used extensively in fluorescent lamps. Nd-YAG[20] is one of the most popular lasing materials and Er-doped[21] optical fibers are used in telecommunications. Usage of lanthanides in biology is limited by the commercial availability of chelators.

Several transition metal complexes are well-known fluorescent systems, and act as fluorescent probes. A typical example is the $[Ru(bpy)_3]^{+2}$ ion (Fig. 1.7).[2,22] Many organometallic and coordination complexes which show strong fluorescence find application as chemical sensors.[18] Several Pt(II) and Au(I) compounds are strong fluorophores; some examples are shown in Fig. 1.7.[23]

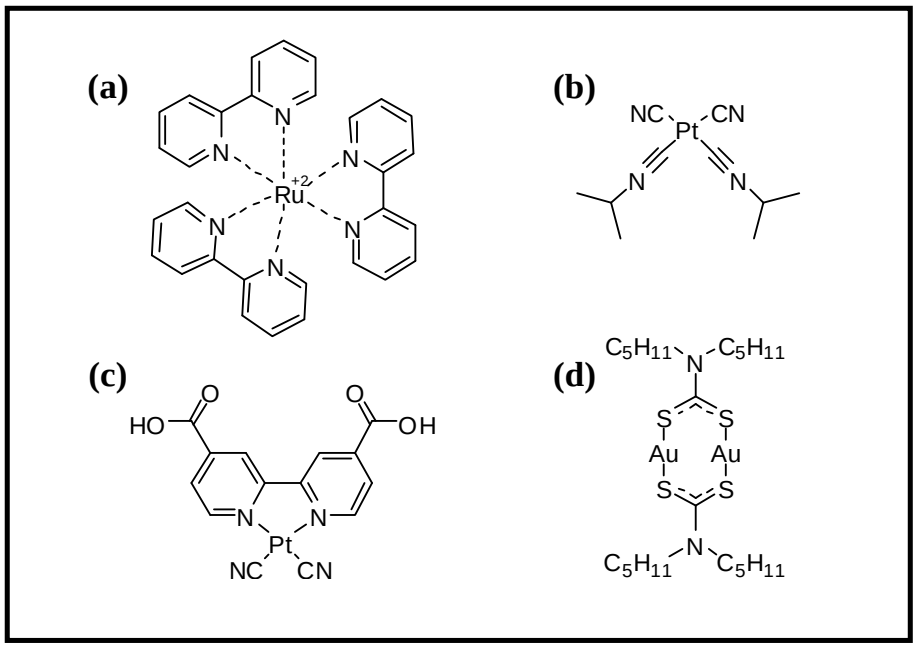

Figure 1.7. *Molecular structure of some fluorescent transition metal compounds:* ***(a)*** *$[Ru(bpy)_3]^{2+}$,* ***(b)*** $[Pt(CN^iC_3H_7)_2(CN)_2]$ ***(c)*** *$[Pt(4,4'\text{-}H_2dcbpy)(CN)_2]$ and* ***(d)*** $[Au(S_2CN)(C_5H_{11})_2]_2$.

bpy = 4,4'-bipyridine, 4,4′-H_2dcbpy = 4,4′-dicarboxyl-2,2′-bipyridine.

Metal organic frameworks

Metal-organic frameworks (MOF's) are hybrid materials contain inorganic and organic moieties. Luminescence of these materials can arise from the organic ligand, the metal center or the charge transfer (metal to ligand or ligand to metal) transition. Examples of fluorescent MOF's are listed in the Table 1.1. MOF's find use in sensing, gas storage, catalysis, magnetism and biomedical applications.[24] They are promising candidates for multifunctional luminescent materials. One of the first lanthanide MOF's used for sensing of cations is $Na[EuL(H_2O)_4]2H_2O$ (L = 1,4,8,11-tetraazacyclotetradecane-1,4,8,11-tetrapropionic acid).[25] Cu_6L_6 (H_2O) (DMSO) (HL = 5,6-diphenyl-1,2,4-triazine-3-thiol) MOF exhibits luminescence that is sensitive to the

Table 1.1. *Examples of fluorescent MOF's.*

Name	Formula	Ref.
Lanthanide-Based MOFs	$[La(pmtz)(TzC)(H_2O)_3](H_2O)$, $Eu(1,4\text{-}BDC)_3(H_2O)_4$	28, 29
Transition-Metal-Based MOFs	$Zn_4O(1,4\text{-}BDC)_3$, $Cd_4(BTC)_3(DMF)_2(H_2O)_2$ $6H_2O$	30, 31
Heterometal-Organic Frameworks	$Pr(pydc)_3Cu_3(bipy)_3$ $m(H_2O)$, $[Eu(PDA)_3Mn_{1.5}(H_2O)_3]$ $3.25H_2O$	32, 33
Main Group Metal-Organic Frameworks	$In_2(OH)_2(TBAPy)$, $Mg(DHT)(DMF)_2$	34, 35

Abbreviations used in the table are BDC= benzenedicarboxylate, bipy = 4,4'-bipyridine, BTC = 1,3,5-benzenetricarboxylate, DHT = 2,5-dihydroxyterephthalate, DMF= dimethylformamide, PDA= pyridine-2,6-dicarboxylic acid, pmtz = 5-(pyrimidyl)-tetrazolato, pydc = pyridine-dicarboxylate, TBAPy = 1,3,6,8-tetrakis(p-benzoic acid)pyrene and TzC = 5-carboxylato-tetrazolato.

presence of small aromatic organic molecules.[26] Doping of Eu^{+3} in Tb(1,3,5-BTC)(H_2O) $3H_2O$ (BTC = benzenetricarboxylate) MOF's produce LED materials with emission colors ranging from green to red.[27]

Semiconductor nanoparticles

Semiconductor nanoparticles or quantum dots form an important class of strongly luminescent materials. These nanoparticles are typical model systems for quantum mechanical particle in a 3-D box, and the optical properties follow this model. Due to the confinement effects, optical properties of quantum dots can be tuned based on size and shape.[36] The nearly discrete energy levels lead to narrow emission features, and the quantum yields are generally very high. Examples of fluorescent semiconductor nanoparticles are PbSe, CdSe, CdS, InP and InAs. Stability of these particles can be improved by different capping agents. Photochemical stability of CdSe particles has been improved by coating with high band gap material like ZnS. These particles are coated with polymer or silica to make them soluble in water for use in biological systems (Fig. 1.8).[2] These materials are useful in many applications due to their high photo stability, high extinction coefficient, broad absorption and long life time. Quantum dots are relatively large in size compared to organic molecules for labeling

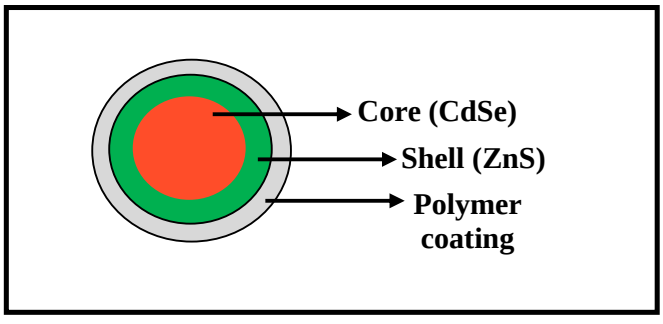

Figure 1.8. *Schematic representation of core-shell quantum dot nanoparticle.*

bio-systems. Cd used in many quantum dots is toxic; there has been attempts to develop non toxic quantum dots.[2,37] Quantum dots find extensive applications in areas such as solar cells, optoelectronic devices and cell imaging.[38]

Metal nanoclusters

Metal nanoclusters are emerging as an important class of fluorescent materials.[39] Metal nanoclusters can be considered to be a state between atoms and their nanoparticles. Size of the noble metal nanoclusters is typically less than 2 nm and contains several to ~100 atoms.[40] They usually have an arrangement of atoms reminiscent of a molecule, rather than a translationally periodic lattice. They show molecule like behavior in terms of discrete electronic states and size dependent fluorescence emission. Metal nanoclusters can show properties like chirality,[41] ferromagnetism[42] and photoluminescence[43] and find applications in sensing[44] and bio-imaging.[45] Fluorescence emission of these nanoclusters can be tuned by varying the size and the capping molecules. Fluorescent emission wavelength increases with increasing number of atoms in the cluster. Fluorescent nanoclusters of Au and Ag using poly(amidoamine) dendrimers have been reported.[46] The metal nanoclusters are synthesised using templates like polymer microgel,[47] copolymers,[48] polyelectrolytes[49] and organic-inorganic hybrids.[50] Another approach is to prepare them as monolayer-protected nanoclusters. In this method, they are protected by using different molecules such as glutathione, tiopronin, phenylethylthiolate, dodecanethiol and mercaptoundecanol. Highly fluorescent nanoclusters of Ag, Au, Pt and Cu have been prepared using electrostatically induced reversible phase transfer method.[51]

1.2. Fluorescent Molecular Materials

1.2.1 *Molecular materials*

Molecular materials built up of molecules and molecular ions exploiting a wide range of weak non-covalent interactions, form an important class of soft materials. Typical weak interactions present between molecules in molecular materials include H-bonds, π-stacking and dispersion forces. The hallmark of molecular materials is the tailorability of their assembly, structure and function, realized through the fine-tuning of the relatively weak intermolecular interactions. This flexibility is generally unavailable in the case of solids like sodium chloride, metals and metal oxides in which the constituent atoms/ions are assembled through strong ionic and covalent bonding interactions. The range of weak non-covalent interactions allows the assembly of molecules to yield desired molecular materials. A schematic diagram representing the formation of molecular materials in different forms is shown in Fig. 1.9. Some of the common methods used to fabricate molecular materials include crystallization, self-

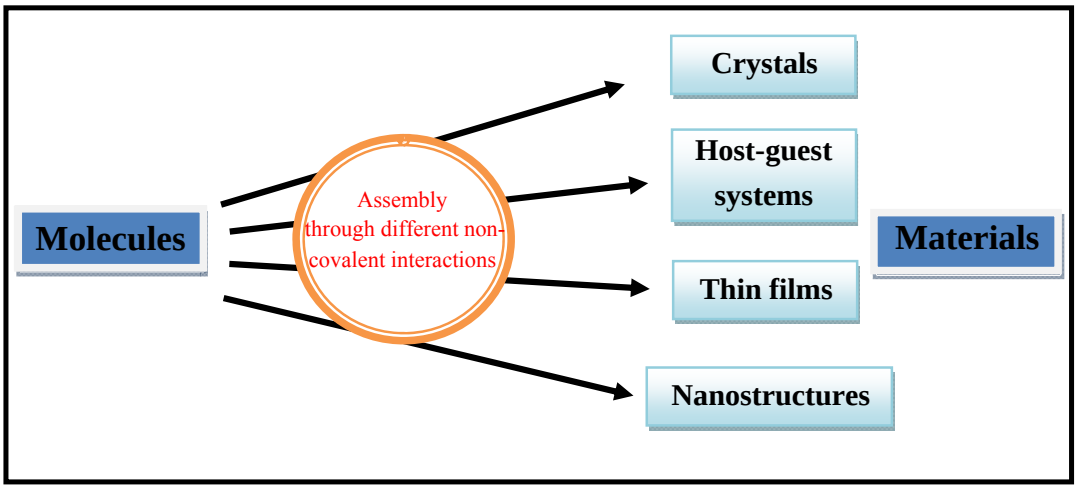

Figure 1.9. *Schematic representation of the fabrication of molecular materials.*

assembly, host-guest complexation, and Langmuir-Blodgett deposition.[52] Different classes of molecular materials exhibiting electrical, magnetic, superconducting, optical and ferroelectric properties have been developed. These can be used in a wide range of areas such as electronics,[53] energy storage,[54] memory devices,[55] sensors[56] and photonics.[57]

A major area of research in the field of molecular materials relates to the development of optical materials exhibiting strong linear and nonlinear responses. In the former case, materials capable of efficient light emission are of great interest from both fundamental materials chemistry and application perspectives. We have listed in Sec. 1.1.2, a wide range of molecules capable of strong light emission. However, in order to develop a strongly fluorescent material, it is essential that the specific molecular assembly and interactions involved are able to circumvent the problem of aggregation-induced fluorescence quenching commonly observed in dyes. The critical factors involved in the fabrication of such materials are the design of the molecular building blocks and the control of their assembly patterns.

1.2.2 *Impact of molecular aggregation*

Properties of organic dye molecular aggregates are strongly influenced by their assembly patterns which in turn are governed by the intermolecular interactions from weak van der Waals forces to strong electrostatic interactions. Two types of molecular aggregates are generally important – H-type (H stands for Hypsochromic) and the J-type (J stands for Jelly).[58] H-aggregates are formed by parallel or plane-to-plane stacking of molecules. Due to H-aggregation, the electronic absorption shifts to a higher energy level compared to the isolated dye molecule (hypsochromic shift). J-aggregates formed

by head-to-tail or tail-to-tail intermolecular interactions show electronic absorption at a lower energy compared to the isolated dye molecule (bathochromic shift).

The exciton coupling theory is used to understand these interactions between dye molecules.[59] The relation between the molecular arrangements and spectral shifts based on molecular exciton theory are schematically represented in Fig. 1.10. S_0 and S_1 are the energy levels of the isolated molecule, typically in a dilute solution state. When the concentration increases, molecules come close together, the transition dipoles interact and monomer excitation energy level splits into multiple levels. The extent of splitting mainly depends on factors like the distance and angle between the interacting transition dipole moments of the molecules and the number of molecules involved in the

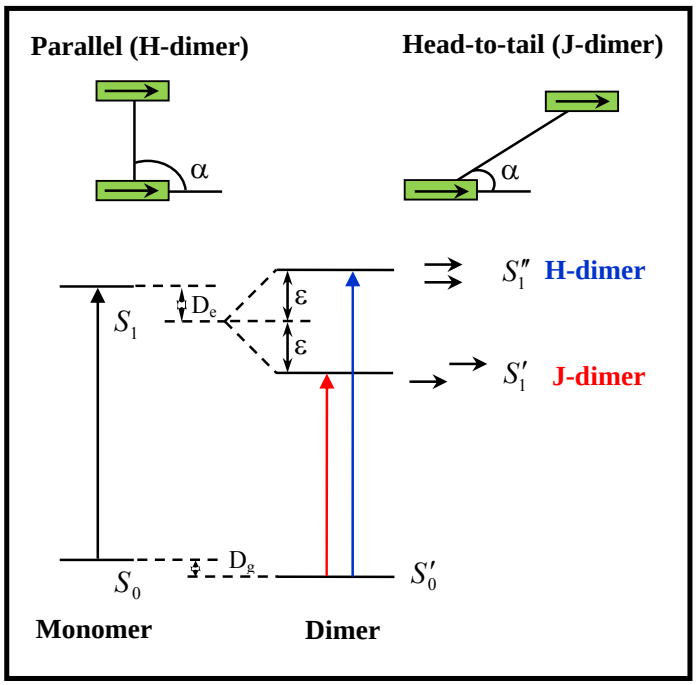

Figure 1.10. *Schematic representation of the relationship between molecular arrangement in a dimer and spectral shift based on the molecular exciton theory (see text for details).*

interaction. The transition energies for a simple dimer are given by equation 1.3.

$$\Delta E_{dimer} = \Delta E_{monomer} + \Delta D \pm \varepsilon \qquad \text{----- (1.3)}$$

where ΔE is the transition energy from the ground to the excited state of the monomer or dimer, ΔD is the van der Waal dispersion energy given by $D_g - D_e$ (Fig. 1.8) and ε is the interaction energy. α is the angle between the vector connecting the centers of the two interacting molecules and the dipole vector of one of the molecules. In the case of H-dimer α is ~ 90°. In many J-dimers α < 32°;[58] α = 0° represents the extreme case of perfect head-to-tail organization. J-aggregates generally show smaller Stokes shift and strong emission compared to H-aggregates.

Fluorescence of dyes in the solid state is often quenched partially or fully due to aggregation induced effects. Radiative decay is reduced due to energy transfer from the

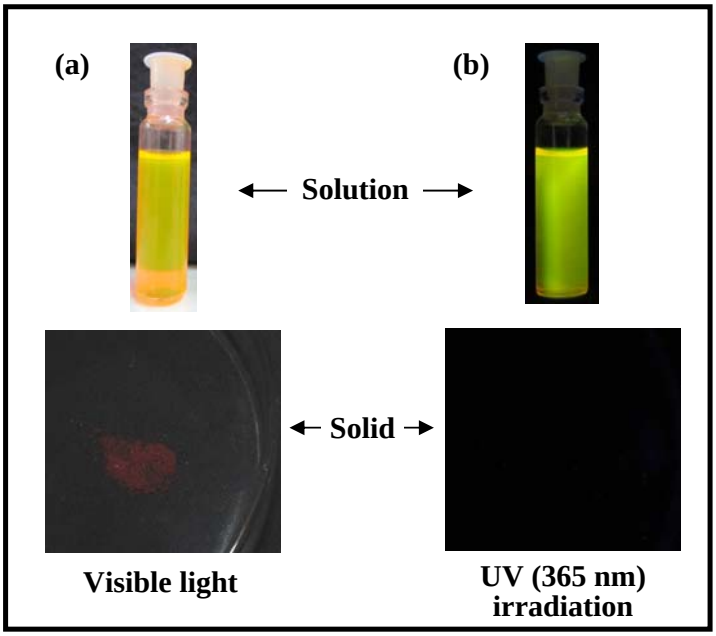

Figure 1.11. *Photographs of rhodamine solution and solid under* ***(a)*** *visible light and* ***(b)*** *UV-365 nm irradiation.*

excited molecule to its neighbors and further cascades. The situation is clearly demonstrated for the case of rhodamine which shows strong fluorescence in solution state but none in the solid state (Fig. 1.11). Fluorescence quenching can also happen due to various intramolecular relaxation pathways. Strong light emitting property in the solid state is important for potential applications like light-emitting diodes[6] and sensors.[8] A detailed discussion on materials exhibiting strong fluorescence in the solid state is presented in the following section.

1.2.3 *Fluorescent organic materials*

Solutions of organic dyes are not quite suitable for many applications.[60] Dye molecules in dilute solution can be quickly photobleached under intense laser beams. High concentration of dyes is not useful due to aggregation-induced quenching effects. For example pyrene shows strong emission in solution state but quenches in aggregated and crytstalline states.[61] This is due to the presence of π-π interactions in the solid state which causes the excited states of the aggregate to decay via non-radiative pathways. Even though fluorophores are commonly characterized in the solution state, the practical applications often require them in the solid state, such as thin films for organic light emitting diodes.[62] Therefore extensive research has addressed the issue of synthesizing new molecules that show strong or even enhanced fluorescence in the solid material state.

Some of the systems that have been developed, showing strong fluorescence in the solid state are shown in Fig. 1.12. Different mechanistic pathways have been used to explain aggregation-induced emission (AIE); they include J-aggregate formation, conformational planarization and restricted intramolecular rotation (RIR). A typical example of an AIE system is hexaphenylsilole,[63] synthesized by the research group of

B. Z. Tang; RIR was shown to be the basis for the fluorescence enhancement in the aggregated state. Increasing water content in an acetonitrile-water mixture of the silole solution produces enhanced fluorescence intensity due to the formation of aggregate structures. Solution state fluorescence of the siloles is weak due to the loss of the

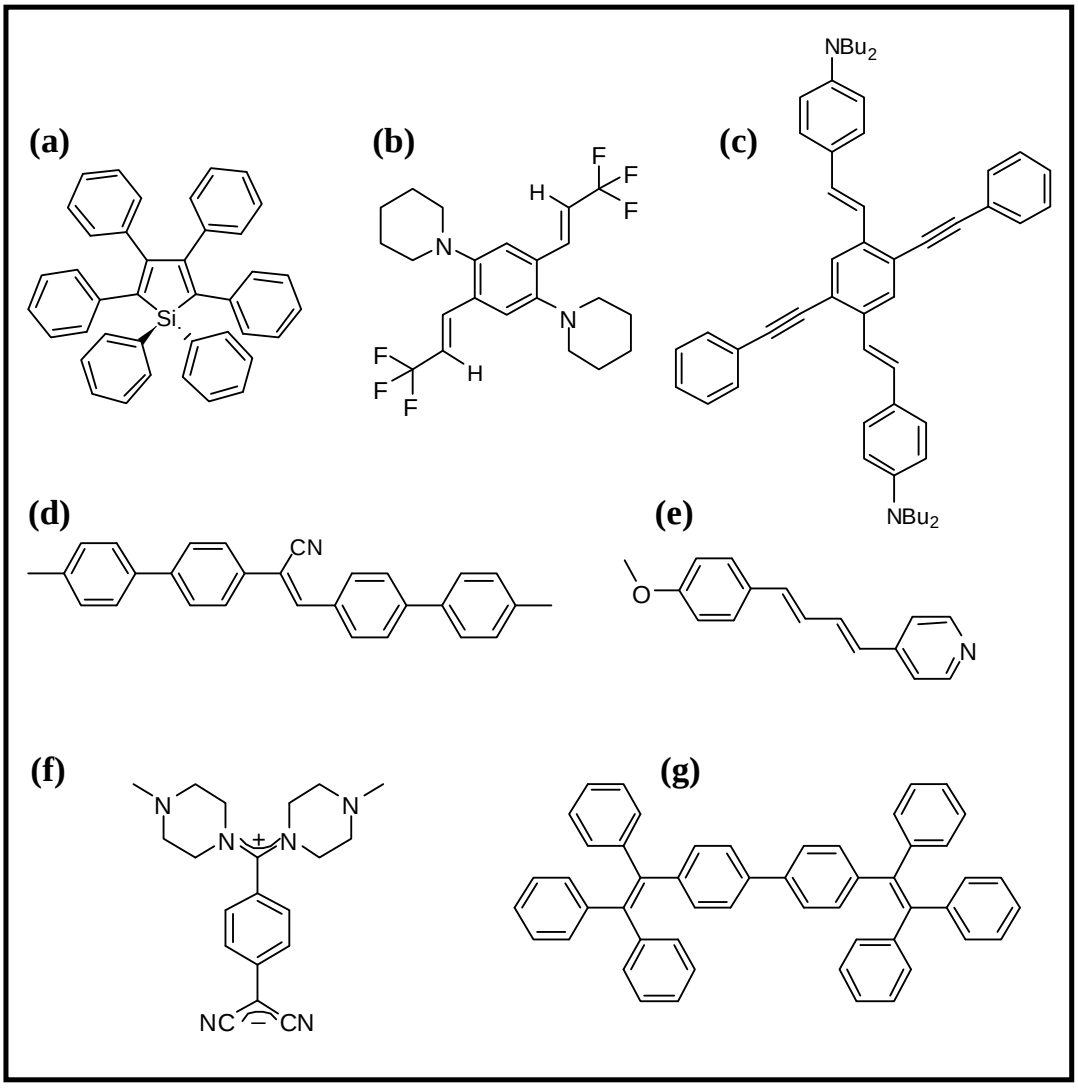

Figure 1.12. *Examples of molecules showing strong fluorescence in the solid state are* ***(a)*** *hexaphenylsilole,* ***(b)*** *1,4-bis(alkenyl)-2,5-dipiperidinobenzenes,* ***(c)*** *cruciforms,* ***(d)*** *1-cyano-trans-1,2-bis-(4'-methylbiphenyl)ethylene,* ***(e)*** *4-alkoxy-pyridine butadiene,* ***(f)*** *7,7-bis(N-methylpiperazino)-8,8-dicyanoquinodimethane and* ***(g)*** *4,4'-bis(1,2,2-triphenylvinyl)biphenyl.*

excited state energy as heat through intramolecular rotations. Structural tuning of silole molecule by introducing bulky isopropyl groups produces strong fluorescence emission in both the solution and solid state. 1,4-bis(alkenyl)-2,5-dipiperidinobenzenes show strong emission in crystals and polymer films.[64] The emission color can be tuned from blue to red by modifying the alkenyl group. Cruciforms[65] show different fluorescence emission in the crystalline phase, thin films and nanoparticles indicating the influence of intermolecular interactions. The enhanced emission of 1-cyano-trans-1,2-bis-(4'-methylbiphenyl)ethylene[66] (CN-MBE) in the solid state and aggregated nanoparticles is due to both planarization and J-aggregate formation. 4-alkoxy-pyridine butadiene[67] derivatives are nonfluorescent in solution but show strong fluorescence in thin films and the solid state. One of the 4-alkoxy-pyridine butadiene derivatives forms polymorphs showing different fluorescence emissions. It shows clearly that molecular packing influences the fluorescence emission. Organic salts of anthracene-2,6-disulfonic acids[68] (ADS) with different primary amines have been reported. ADS salts exhibit different fluorescence properties based on their molecular arrangement in the crystal lattice. This system also proves that prevention of π-π interaction of the anthracene moity and rigidification of the molecules due to packing produces strong emission in the solid state. Several diaminodicyanoquinodimethane derivatives which shows strong fluorescence in the solid state have been developed in our laboratory. 7,7-bis(N-methylpiperazino)-8,8-dicyanoquinodimethane[69] is a typical example that shows fluorescence enhancement of ~170 in the solid state compared to its solution state. Enhancement of fluorescence in the aggregated state of these systems has been attributed to the inhibition of the relaxation of the vertical excited state to a non-emitting state through an intramolecular twist. 4,4'-bis(1,2,2-triphenylvinyl)biphenyl shows high quantum yield in the solid state due to the suppression of intramolecular rotation.[70]

In the case of some organic molecules, it has been shown that simple aggregation is not sufficient to enhance the fluorescence. The amorphous packing does not suppress the RIR process and collective hydrogen bonds are required to rigidify the molecules and enhance the emission intensity. This has been termed as crystallization induced emission.

1.3. Fluorescent Molecular Nanomaterials

A major part of contemporary nanomaterials research is focused on metal and semiconductor nanoparticles, constituted of extended lattices of atoms or ions. Molecular nanoparticles assembled from small molecules through non-covalent interactions are relatively less explored but equally fascinating materials. The richness and versatility of molecular materials in general, has been unraveled by the research over the last several decades. Electrical, superconducting, magnetic, optical and ferroelectric properties have been realized in this class of materials.[71-75] Effective utilization of the special attributes of molecular materials discussed in Sec. 1.2.1, is found to be reflected in the emerging field of molecular nanomaterials. The unique and versatile characteristics of molecular nanomaterials have attracted considerable attention in recent years, establishing their identity and status as a novel class of nanomaterials. Optical characteristics of molecular nanoparticles capture the essence of their nanoscale features and form the basis of a variety of applications.

1.3.1 *Fabrication*

The fundamental events in the fabrication of nanocrystals are the nucleation and growth processes (discussed further in Sec. 1.4.). A number of parameters involved in the fabrication protocol can influence these events, often in complex ways. Some

studies have demonstrated that these stages can be steered through logical design. Nanocrystals of zinc tetraphenylporphyrin were fabricated by colloid chemical reduction of the cation leading to controlled release of the neutral molecule; the high and tunable supersaturation thus obtained cannot be realized in conventional crystallization.[76] Morphology of the nanocrystals could be smoothly varied through polyhedral shapes such as cubes, cubooctahedron and octahedron by manipulating the growth kinetics, effectively separated from the nucleation stage. Efficient size-tuning was realized in a similar synthesis of perylene nanocrystals by adjusting the monomer concentration and injection method; once again a facile separation of the nucleation and growth stages was realized.[77] Nucleation and growth processes have been explored in detail with rubrene,[78] magnesium phthalocyanine[79] and 2,5,8,11-tetra-*tert*-butylperylene[80] nanocrystals as well.

Design of the molecular building blocks and the supramolecular entities with specific structure, shape and interactions that will lead to the desired aggregate ensembles is the key step in the fabrication of molecular nanostructures. Several nanostructures have been fabricated through the self-assembly of molecules in solution. Various amphiphilic molecules with tailored structure have been self-assembled into organic nanotubes, nanofibers and nanoplates.[81]

Reprecipitation

The reprecipitation method developed primarily by Nakanishi and coworkers[82] and applied extensively over the past decade, offers a simple and convenient route for the fabrication of molecular nanoparticles. It is essentially a process based on quick exchange of the solvent environment that leads to limited crystal growth. Microliter quantities of a solution of the compound of interest in a good solvent are injected

rapidly into excess of a second liquid which while being miscible with the first liquid, acts as a nonsolvent or poor solvent for the compound of interest. This addition is commonly carried out under vigorous stirring or ultrasonication. Replacement of the good solvent environment of the molecules by that of the poor solvent causes prompt aggregation and formation of nano/microparticles dispersed homogeneously in the bulk medium.

Drop-cast

Drop-casting is another method that is commonly employed technique for the fabrication of molecular nanostructures. The control of solvent evaporation provides one of the simplest and most efficient approaches to tune molecular nanostructure fabrication by self-assembly from solution.[52] The critical factors involved in the formation of nanostructures through the drop casting technique are the polarity and volatility of the solvent, concentration of the solution, chain-length of any amphiphilic molecules present and nature of the surface on to which solutions are cast.[83] The interplay of interactions between the molecule, solvent and substrate determine the dewetting and evolution of the self-assembled structures.[84]

Crystallization in confined environment

Crystallization in the spatially restricted environments of microemulsions,[85,86] sol-gel matrices,[87] nanoporous glasses,[88] and porous alumina templates[89-91] provides direct control on the growth of crystals and access to tailored nanostructures. Crystallization in porous alumina template wherein the desired material is grown within the nanopores of an alumina membrane is perhaps one of the most popular techniques in this area.[90] The first step involves the infiltration of a solution of the molecule of

interest into commercially available or custom made alumina membranes with uniform pore distribution by direct capillary forces or by pressure filtration. After the membrane is air dried, excess organic materials may be removed by grinding and polishing the membrane and the process repeated till the pores are fully packed with the solution. Finally the polished membrane is heated under optimal conditions of temperature and time, either in an inert atmosphere or in the environment of the solvent vapor. Dissolution of the alumina template in concentrated alkali solution frees the organic nanorods or nanotubes formed within the pores.[89,90] Monodispersed perylene nanotubes have been fabricated by a simple dip-and-dry procedure, in which the porous alumina membrane is repeatedly immersed into a saturated solution of perylene and the solvent evaporated during the intervals between dipping.[91] The diameter, length, and wall thickness of the nanotubes can be controlled by the choice of the template and the solution concentration. Chiral quinidine nanotubes[92] and dibenzoylmethane nanotubes of various diameters[93] are other examples of molecular nanostructures that have been fabricated using porous alumina templating.

Porous glasses, gels and polymers offer a convenient form of confined space for growing molecular nanoparticles of varying shapes. The latter can be obtained by preferential etching of shear aligned diblock copolymers. Crystals of 2,2,3,3,4,4-hexafluoro-1,5-pentanediol and (*R*)-(+)-3-methyladipic acid grown in such matrices showed size and environment dependent melting temperatures.[88] Microemulsions allow restricted growth of molecular crystals, which in some cases follow a miniature version of the reprecipitation protocol. Cholesterol and retinol nanoparticles have been fabricated in various heptane-water microemulsions by precipitation of the organic material in the aqueous cores.[85] In a stabilizer-free approach, nanocrystals of polycyclic aromatic hydrocarbons and fullerene were fabricated in an oil-in-water emulsion made

from low-molecular-weight hydrocarbons.[86] Dispersion of a hot solution of the target molecule in an organic solvent, into aqueous medium at the same temperature produced the emulsion, which on cooling led to the confined crystal growth of the target molecule.

Organized structures through template control

A general mechanical approach to the formation of molecular nanostructures involves the use of functional molecules as 'ink' on a rubber stamp which can be deposited on appropriate surfaces. Such an approach forms the basis of various techniques such as soft lithography and microcontact printing, with special relevance to the formation of large area structures and automation. Nanofabrication can be achieved through a variety of processes including molding, embossing, printing and template-controlled molecular assembly.[94] Particle replication in non-wetting templates (PRINT) is an efficient 'top-down' protocol for the fabrication of organic nanoparticles.[95] It follows the general principle of soft imprint lithography, but the deployment of nonwetting molds and substrate surfaces enables the fabrication of isolated particles with superior size, shape and composition control. Photocurable perfluoropolyether molds and highly fluorinated surfaces provide the nonwetting environment for the nanofabrication. The technique is compatible with a wide range of polymeric materials and sophisticated biomaterials enabling encapsulation of bioactive agents for delivery applications.[96] Another important approach to molecular printing involves dip pen nanolithography.[97]

1.3.2 *Size and Shape Dependent Optical Properties*

Like other classes of nanomaterials, molecular nanoparticles and nanostructures also exhibit optical properties that can be tuned by their size and shape. However, a systematic and general understanding of these effects is only emerging and potential applications are beginning to be explored.

Size dependent optical responses

A unique feature that makes nanomaterials interesting from fundamental as well as application perspectives is their size-dependent photophysical properties. While confinement effects make the optical responses of metal and semiconductor nanoparticles especially sensitive to size variation, factors that lead to size-dependent optical responses in molecular nanoparticles are likely to be complex. It has been suggested that the so-called "quantum size effect" may not dominate in small molecule crystals, with their relatively more localized excitons normally spanning just a few molecules.[98] The increasing proportion of surface molecules to bulk ones in the nano regime makes the lattice of nanoparticles relatively softer. As the particle size increases this ratio decreases resulting in an increase in the average crystal cohesive energy, concomitantly strengthening the intermolecular interactions.[99] These effects could have an impact on the optical responses of molecular nanoparticles.

Size-dependent optical properties were first observed in perylene nanocrystals.[100] Another early investigation relates to the effect of supramolecular structure and particle size on the absorption spectra of β-carotene nanoparticles.[101] A large number of studies demonstrating size-dependent optical absorption and emission in a wide variety of molecular nanostructures including spherical particles,[99,102]

wires,[103,104] tubes[105,93] and plates[106] have appeared over the last decade. A series of substituted pyrazoline compounds have been investigated for the size-tunable optical properties of their nanoparticles. With increasing size, nanoparticles of 1,3-diphenyl-5-(2-anthryl)-2-pyrazoline show a red shift in the absorption band in the 330 – 410 nm range and splitting of a higher energy band.[107] In the emission spectrum however, the main peak shifts to the blue and a lower energy band emerges and grows in intensity. These size-dependent changes are attributed to the increase in intermolecular interactions with increasing particle size and the consequent inhibition of vibronic relaxation and configurational reorganization. Increase in the size of nanoparticles of (*R*)-(+)-1,1′-bi-2-naphthol dimethyl ether is accompanied by reduction in the emission intensity as well as red shift in the circular dichroism spectrum.[108] The size-dependence of exciton chirality has also been attributed to the emergence and growth of intermolecular interactions. Nanowires of 2,4,5-triphenylimidazole fabricated by the adsorbent assisted physical vapor deposition method show not only a blue shift of the absorption, but also a gradual emergence of vibrational fine structure in the emission spectrum with decrease in the wire diameter from 500 nm to 40 nm.[102] The fine structure appears to be a consequence of the increase in the long range and configurational order, and enhancement in the degree of orientation of the nanowires with decreasing diameter. Nanotubes of dibenzoylmethane display increase in fluorescence intensity with decrease in diameter.[93] Raman spectroscopic investigations revealed increasing fraction of the enol isomer as the nanotubes became thinner. The improved π-stacking of the enol structures leads to aggregation induced emission enhancement. Size tunable nano/microcrystals of a zwitterionic diaminodicyanoquino-dimethane molecule with a plate-like morphology, fabricated in our laboratory through a reprecipitation-digestion protocol, showed optical responses dependent on the particle

size.[106] Absorption is gradually red shifted with sequential emergence of additional peaks in the longer wavelength region and fluorescence intensity is enhanced with increase of particle size (Fig. 1.13). A model that explains these observations has been developed based on quantum chemical computations.

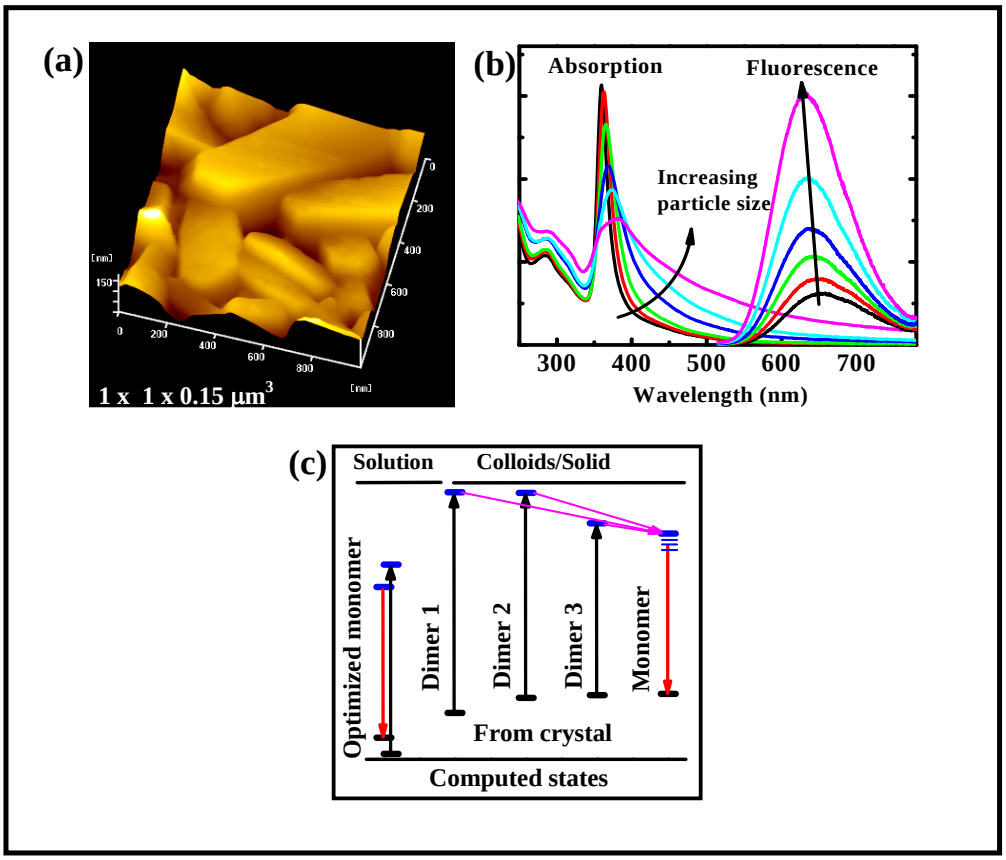

Figure 1.13. ***a)*** *AFM image of BCADQ nanocrystals fabricated by reprecipitation and digestion at 30°C.* ***(b)*** *Absorption and emission (λ_{exc} = 365 nm) spectra of BCADQ colloids digested at 0, 30, 45, 60, 75 and 90°C resulting in increasing size of nanoparticles.* ***(c)*** *Schematic drawing of the computed ground and excited electronic states of BCADQ monomer and dimers (1: H-bonded, 2: antiparallel, 3: parallel) used to model the absorption (black arrow) and emission (red arrow) of solution, colloids and solid (adapted from Ref. 106)*

Far-field microspectroscopy combined with atomic force microscopy has been developed as a powerful tool to examine the optical properties of single nanoparticles. Such an approach allows the evaluation of the precise relationship between optical response and particle size, as individual particles are examined rather than ensembles.[109] A typical example is the critical analysis of the size dependent excimer emission of perylene nanocrystals which led to the development of a model based on the inhibition of lattice vibration and consequent raising of the excimer energy level, with decrease in the crystal size. Single particle spectroscopy combined with microscopy has also been used to investigate the sensitive dependence of emission color on the morphology of organic nanoparticles discussed below.[110]

Shape dependent optical responses

The shape of molecular nanocrystals and their surface structure can be modified by a number of factors including the method of fabrication, solvent composition, presence of stabilizers and annealing or aging. The shape is influenced by the extent of crystallinity, molecular packing and growth kinetics. Several reports exist on the impact of the shape and surface features of molecular nanoparticles on their optical responses. The surface structure of 9,10-bis(4-(N-carbazolyl)phenyl)anthracene nanocrystals was shown to depend on whether they were formed through an emulsion or reprecipitation route.[111] While the photoluminescence spectrum of the former with a rough surface morphology showed clear fine structure, the spectrum of the latter with a smooth surface was very different with no fine structure; interestingly, the absorption spectra were insensitive to the surface morphology. Single molecule spectroscopy of nanoparticles of the bis(2,5-di-*tert*-butylphenyl) showed that small amorphous particles produced blue emission characteristic of the monomer and larger crystalline particles

produced red emission reminiscent of excimers.[110] Nanotubes and nanorods of 2,4,5-triphenylimidazole fabricated by varying the type of solvent (ethanol and acetone) and solution concentrations, were found to show different extents of J-aggregation leading to shift of absorption peak and change in emission intensity.[112] The size and shape of perylene nanoparticles fabricated through a hydrothermal process were shown to be controlled by the temperature of the process; the optical absorption and photoluminescence could be tuned through the control of size and shape.[113]

As in the case of metal and semiconductor nanoparticles, surfactants can be used to conveniently control the shape of molecular nanoparticles as well.[114,115] Self-assembly of a simple molecule like pyrene could be tuned to generate nanoparticles, short nanorods and nanowires by optimizing the relative amount of sodium dodecyl sulfate template molecules.[114] Increase in the aspect ratio led to the gradual transition of emission characteristics such as peak position, life time and anisotropy, from those of isolated molecules to those of aggregates. Cubic to rhombic dodecahedral nano/microcrystals and nanowires of 2,5,8,11-tetra-*tert*-butylperylene fabricated by tuning the solvent composition in the reprecipitation process showed different photoluminescence spectra.[115] 1-D ribbons and 2-D plates of rubrene microcrystals fabricated by tuning the nucleation and growth processes show distinct optical responses owing to the polymorphic structures formed.[78] Annealing of rubrene nanocrystals produced by the reprecipitation process in a solvent vapor environment led to significant changes in the morphology; the changes are sensitive to the nature of the substrate on which the nanocrystals are deposited.[116] Rectangular and hexagonal nanocrystals formed by the annealing process were shown to produce considerably enhanced photoluminescence over the pristine ones. Simple aging process can also induce morphological changes in molecular nanocrystals. An interesting case is that of

N,*N*'-bis(salicylidene)-*p*-phenylenediamine which changes from spherical particles to rods and belt-like aggregates with aging; the fluorescence emission of the nanoparticles enhanced in intensity over that in solution, however diminishes with the aging time, possibly due to increasing intermolecular interactions.[117] Reversible photoinduced shape changes have been observed in organic nanorods of 9-anthracene carboxylic acid which undergo dimerization on irradiation with 365 nm light with concomitant switching off of the fluorescence emission.[118] The study showed that strain-induced mechanical damage familiar in macroscopic crystals does not occur in the nanoscopic crystals; this would of considerable interest in photomechanically driven actuators.

1.3.3 *Applications*

Last several years have witnessed an exponential growth of nanotechnology, and device applications of nanomaterials based primarily on metals, semiconductors and solids like carbon and silicon with extended covalent bonding. Compared to these, the direct application of molecular nanoparticles and optical materials based on them is still in its infancy. However a range of potential areas of application have emerged in recent years throwing up unique challenges and opportunities to unveil a new vista of nanotechnology. Some representative examples are considered below.

Sensors

A traditional technique like fluorescence based sensing can achieve higher levels of sensitivity and sophistication by making use of the versatility and efficient response of molecular nanoparticles. The photostability of these nanosensors are generally found to be superior to that of fluorophore molecules dispersed in solvent media. Highly fluorescent perylene nanoparticles synthesized through the reprecipitation route and

stabilized with CTAB have been shown to readily interact with DNA leading to fluorescence based detection of the latter down to 10^{-2} μg ml^{-1}.[119] The fluorescence responses including excited state decay kinetics, of rubrene nanocrystals grown in silicate thin films have been shown to be very sensitive to the presence of analytes like methylene blue.[120] Molecular nanoparticles based on pyrene and its derivatives serve as efficient sensors for a variety of analytes like chromium (VI) ions,[121] nucleic acids[122] and proteins such as γ-globulin.[123] Nanofiber based sensors for vapors of explosives (eg. TNT) and organic amines have been developed using an alkoxycarbonyl-functionalized carbazole-cornered, ethynylene-bridged tetracycle,[124] and the n-type organic semiconductor molecule, *N*-(1-hexylheptyl)perylene-3,4,9,10-tetracarboxyl-3,4-anhydride-9,10-imide[125] respectively. Selective and sensitive detection of Hg^{2+} down to a few tens of ppb has been demonstrated using a ratiometric fluorescence sensor based on thiourea-thiadiazole-pyridine linked organic nanoparticles.[126]

Photonics and optoelectronics

Organic nanophotonics is emerging as a field of exciting research, holding considerable promise for a variety of applications in areas such as photoswitching,[127] waveguiding,[128-130] ultraviolet lasers,[130] and optical memory.[131] Single crystalline nanowires of 2,4,5-triphenylimidazole have been demonstrated to serve as nanoscale active waveguides and optically pumped UV lasers.[130] Nanodot arrays of photochromic fulgide molecules fabricated on patterned substrates covering millimeter-squared areas have been shown to function as optical memory devices with remarkable storage capacity;[131] a storage density of 74 $Tbit/in^2$ has been achieved. Based on their efficient electroluminescence (EL) responses, molecular nanoparticles can form the active elements in light emitting diodes.[132] Nanoparticles of 4,4'-bis(1,2,2-

triphenylvinyl)biphenyl formed by reprecipitation from THF-water show aggregation induced emission with 100% quantum efficiency and efficient EL response at low bias voltages in multi-layer devices.[70] Single layer EL devices with visible emission have been fabricated using nanocrystalline J-aggregated phase of a cyanine dye in an electron-hole transporting aromatic polyimide film.[133] Similar polymer composites based on organic nanocrystals have been used to fabricate devices showing efficient EL in the near infra red as well.[134] Enclosing luminescent small molecules inside an active polymer shell that controls electron/hole migration, has been shown to be an effective route to fabricate EL nanocapsules.[135]

Molecular nanocrystals also find application in improving the photovoltaic performance of organic solar cells. An illustrative case is that of hydrothermally treated perylene nanoparticles with tunable emission which was used to enhance the power conversion efficiency of bulk heterojunction devices based on poly(3-hexylthiophene) and [6,6]-phenyl-C_{61}-butyric acid methyl ester.[113] Organized assemblies of fullerene-encapsulated zinc *meso*-tetra(4-pyridyl)porphyrin nanorods display controlled photoinduced electron transfer and efficient solar energy conversion.[136] Single crystalline organic semiconducting nanowires fabricated from small molecules have been investigated extensively in field-effect transistor devices as well.[137-141]

Medicine

Small molecule based nanoparticles have been used for probing biological systems such as cells and their constituent organelles. Coating or functionalization on the surface of the nanoparticles and their successful integration with a host of biomolecular moieties open up a range of applications in molecular biology and biomedicine. Low inflammatory activation of the human Calu-3 epithelial cell by water

soluble, self-assembling lysine functionalized organic nanotubes has been demonstrated.[142] Prolyl functionalized amphiphilic resorcinarenes form stable nanoparticles which could further be functionalized at the surface with proteins such as bovine serum albumin (BSA).[143] Demonstration of its interaction with surface bound anti-BSA antibodies suggests the potential application of these nanoparticles in drug targeting. Organic nanoparticle based agents developed for biosensing and bioanalytical applications include antibody conjugated fluorescein diacetate nanocrystals with releasable fluorophores for immunoassays,[144] hexabenzocoronene functionalized with fluorescein labeled peptides for developing novel bioprobes[145] and rhodamine based nanocrystals anchored in a sol-gel film and grafted with hairpin shaped DNA for detection of the complementary DNA.[146] Aggregation induced enhancement of fluorescence has been exploited in the development of organic nanoparticles useful in bioimaging applications. 10H-phenothiazine based donor-acceptor molecules upon protonation and aggregation form fluorescent nanoparticles in the lysosomes of cancer cells but not in normal cells, facilitating selective imaging.[147] Similar applications have been investigated using nanoparticles of novel naphthalimide derivatives as well.[148]

1.4. Molecular Assembly–Nucleation and Crystal Growth

1.4.1 *Basic concepts*

Crystallization is a fundamental process occurring in nature; and is of great interest in the laboratory and industry as well. The lattice structure plays a critical role in the properties of crystals, and the quality of crystal is of great interest in various applications. The lattice structure, morphology and quality of crystals are controlled by the basic processes of nucleation and growth. The classical nucleation theory was

developed by Gibbs, Volmer, Weber, Becker, Döring, Turnbull and Fisher. The first stage in the crystallization from solution is the formation of a supersaturated solution. The molecules then begin to aggregate and form nuclei (process of nucleation) that can act as the center for crystallization. Nuclei are essentially metastable, dissolving and reforming until they reach a critical size, which then is followed by the growth stage and formation of the stable crystal. Size of the critical nuclei ranges from 100 – 1000 atoms/molecules.

There are two types of nucleation; homogeneous and heterogeneous. The parent phase starts the nucleation without the help of other substances in the homogeneous nucleation process. If nucleation starts on another substance or a substrate like impurity or glass, it is called heterogeneous nucleation. The total free energy of a cluster (assumed to be spherical, with radius, r) can be expressed by Eq. 1.4, where γ is the

$$\Delta G\,(r) = -\,g_v \,.\frac{4}{3}\pi r^3 + \gamma.4\pi r^2 \qquad \text{----- (1.4)}$$

surface tension and g_v is the free energy gain per unit volume. It may be noted that the surface contribution is positive (destabilizing) and the bulk one is negative (stabilizing).

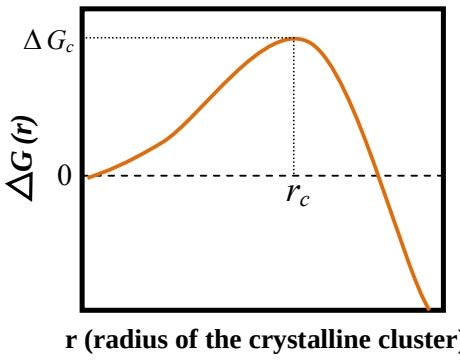

Figure 1.14. *Schematic representation of the free energy change in the nucleation process.*

ΔG (r) is positive at small values of r, increases with r and reaches a maximum at a critical value of r (r_c) and then decreases and reaches negative value (Fig.1.14). r_c is called the critical radius; when $r < r_c$, the nucleus dissolves back and when $r > r_c$ it grows into a crystal.[149]

Classical nucleation theory does not explain many of the experimental observations related to nucleation and crystal growth, for example the rates involved.[150] This suggests that the nucleation is a more complex process than that is suggested by the simple classical model. It has been suggested that the crystallization process involves a two-step process. The two-step model was first proposed for protein crystallization, and then applied to macromolecules and small organic molecules. In this model, a liquid-like cluster of solute molecules forms which then reorganizes to forms the ordered structure (Fig. 1.15). Essentially, the classical nucleation theory suggests that the two order parameters, density and structure, are realized concomitantly in a single step, but the two-step model suggests that these occur in a serial fashion, the density first, followed by the structure.

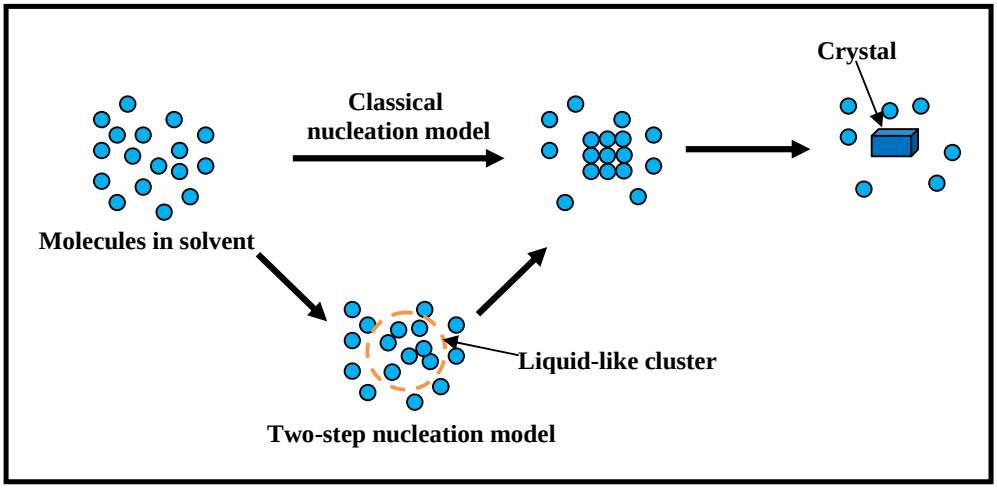

Figure 1.15. *Schematic representation for classical nucleation model and two-step nucleation model.*

1.4.2 *Amorphous and Crystalline Materials*

Understanding of crystallization process, amorphous and crystalline phases and the transformation between the two phases are important from both fundamental and application perspectives. The liquid-like clusters involved in the two-step nucleation theory are essentially amorphous aggregates and their visualization is important to understand the crystallization process. A case of great practical interest involves the so called phase change materials (PCM) that are capable of reversible amorphous-to-crystalline transformation (ACT). A major application of PCM is in memory storage devices such as compact discs.

The most promising and successful material for the reversible ACT is $Ge_2Sb_2Te_5$ (GST).[151] The phase transition happens on time scales that are useful for applications such as memory storage. Amorphous GST deposited as a layer, when exposed to a laser beam that produces sufficient heat, melts; controlled cooling results in the crystalline form. A short laser pulse can melt the crystalline material which if followed by fast quenching, produces the amorphous phase again. Phase change properties of GST nanowires have been studied under high resolution transmission electron microscopy.[152] AgInSbTe[153] and GeTe[154] are also good PCM's. Magnetic properties of amorphous and crystalline materials of doped GST are also known.[155] The different optical characteristics of the amorphous and crystalline phases, and the fast switching between the two can be exploited in several applications including data storage and retrieved.

In the case of molecular materials, the amorphous phase is important in terms of several applications. Solubility of materials is a critical issue in pharmaceutical applications.[156] Amorphous materials often have higher rate of dissolution compared to

their crystalline counterparts. Different methods are adopted to realize amorphous pharmaceutical ingredients. Melt quenching, ball milling and cryogrinding are used to make small quantities of amorphous materials. Lyophilization, spray drying and precipitation are used for large scale preparations. Amorphous molecular materials are of great interest in the area of organic light emitting diode owing to their isotropic structure and efficient contact with metal electrodes and the other active organic layers. Amorphous nature of molecular materials can be designed through the control of molecular structure; nonplanar structure, existence of different conformers and large size and complex shapes often tend to produce amorphous particles. Examples of molecules that form amorphous materials include 4,4',4"-tris(diphenylamino)-triphenylamine, 1,3,5-tris(diphenylamino)benzene, 4-diphenylaminobenzaldehyde diphenylhydrazone, oligothiophenes with triaryl amine group, oligo(diphenylsilane)s and spiro compounds.[157] Several photochromic compounds in the amorphous are also known. Photochromic compounds have applications in near-field optical recording, holographic memory and surface relief grating. Examples of photochromic compounds are stilbene, spirooxazines, diarylethenes and furylfulgides. Amorphous materials offer advantages such as high optical anisotropy, high concentrations of dyes and ease of film fabrication.

Crystallization of macromolecules has been investigated carefully to explore the relevance of the two-step nucleation theory. A typical example is the crystallization of sickle cell hemoglobin upon crossing that supersaturation and ACT of the liquid-like cluster.[158] The process of ACT has been observed in small molecule based materials through techniques such as heating or fuming with solvent vapors. In some of the cases, the fluorescence response is sensitive to the transition, and has been attributed to the change in the structural arrangement. Heating-cooling cycles on solid thin films of (4-

biphenylyl)phenyldibenzofulvene[159] produces phase transition and fluorescence switching. Phenomena such as mechanochromism have been attributed to the transition between the amorphous and crystalline forms. However, a detailed examination of the ACT and visualization of the amorphous state especially at the nanoscale of small molecule based materials, has not been reported prior to the work presented in this thesis.

1.5. Layout of the Thesis

The main focus of the investigations presented in this thesis is the fabrication of novel, strongly fluorescent molecular crystals and nanostructures of diaminodicyanoquinodimethane (DADQ) based molecules. The new concepts developed include a polyelectrolyte-assisted reprecipitation strategy to produce colloids, a simple approach to generate amorphous nanoparticles and carry out their transformation to crystalline structures and a new dimension involving the amorphous phase in the hierarchical assembly of molecular materials. All these molecular assembly processes are accompanied by significant changes and evolution in the fluorescence emission characteristics.

The specific achievements reported in the thesis are the: (i) synthesis and detailed characterization of several molecular crystals based on DADQ derivatives exhibiting significant fluorescence enhancement in the solid state and tuning of the emission from green to blue, (ii) optimization of a strategy for fabrication of molecular nano/microcrystals of highly soluble DADQ derivative using a polyelectrolyte as a template, (iii) fabrication of amorphous nanoparticles of specially designed DADQ derivatives and development of a simple protocol to transform them into crystalline nanoparticles and (iv) hierarchical assembly of molecules to nano/microcrystals with

increasing extent of crystallinity. The detailed spectroscopy and microscopy investigations are supported by quantum chemical modeling studies aimed at developing an understanding of the observed optical responses.

Chapter 2

The facile tailorability of molecular materials coupled with the wide spectrum of physical attributes and functions that can be realized in them have led to their emergence as promising candidates for various applications. One of the critical problems in the area of optical applications such as displays and sensors is the fabrication of molecular assemblies capable of strong light emission, circumventing the inherent self-quenching effects. Some selected classes of molecules have been shown to produce strongly enhanced emission in aggregates and the crystalline solid state. Even though it is possible to achieve wide structural variations in molecular materials and thus tune the electronic energy levels, a combination of high fluorescence quantum yield in the solid state and efficient tuning of the emission color through simple and systematic structural variations have been demonstrated only in a few cases.

Earlier work in our laboratory has established that DADQ's is one of the families of small molecule based materials that exhibit enhanced fluorescence in the solid state. Based on computational studies, it was proposed that the weak fluorescence of the DADQ fluorophore in solution can be attributed to the relaxation of the excited state geometry through an intramolecular twisting, and the associated non-radiative decay channel. This excited state geometry relaxation is prevented in the rigid solid state, leading to strong fluorescence. DADQ's having amino groups based on saturated heterocycles with remote functional groups exhibit strong green fluorescence and aromatic amine based derivatives show red emission.

In this chapter we present novel DADQ derivatives mainly based on primary amine substituents, along with their crystallographic and spectroscopic characterization. Detailed studies on two of the systems that show strong solid state emission in the blue-green region are reportd. The emission in the solid state is found to be ~ 400 times stronger than that in solution in these systems. Semiempirical computational studies provide useful insight into the various structural and spectroscopic features. Exploration of several more primary amine derivatives of DADQ provided molecular crystals showing emission color spanning the entire blue-green region; culminating in nearly pure blue-emitting ones.

Chapter 3

Several of the molecules exhibiting enhanced fluorescence in the bulk solid state are also capable of strong light emission when formed as nanoparticles in the colloidal state. Such luminescent nanomaterials are useful in applications like organic LED's, biological probes and sensors. The most general and widely used route to the formation of molecular nanocrystals is the reprecipitation technique, wherein the solution of the compound in a suitable solvent is rapidly injected into a nonsolvent, under vigorous stirring or ultrasonication. The simple reprecipitaion technique is unviable in the case of molecules such as the remote functionalized DADQ's that show appreciable solubility in aqueous and the common organic solvents.

We present a solution to the above mentioned problem taking a DADQ derivative as an example; the approach is likely to have broad applicability in similar situations with other molecules. The protocol involves the introduction of a polyelectrolyte template that can bind the DADQ derivative bearing ionic groups and impart the required level of insolubility in an appropriate medium. We have chosen 7,7-

bis(piperazinium)-8,8-dicyanoquinodimethane bis(*p*-toluenesulfonate) (BT_2) and sodium poly(styrenesulfonate) (NaPSS) to demonstrate the idea described above. Complexation of BT_2 with NaPSS (essentially the dication B and the polyanion PSS) in aqueous solution produces appreciable fluorescence enhancement. Nanoparticles are prepared by injecting the aqueous solutions containing an optimum ratio of NaPSS to BT_2 into methanol. The nanoparticles formed in the colloidal state exhibit an overall fluorescence enhancement of ~ 90 times over the aqueous solutions of the pure compound. A model for the molecular level interactions and aggregation effects is developed through detailed spectroscopy, microscopy and calorimetry investigations and control experiments.

Chapter 4

The classical model for crystallization visualizes the formation of a metastable crystalline nucleus that through density fluctuations reaches a critical size and grows into a stable crystal. The two-step nucleation theory invoking a liquid-like cluster intermediate developed to explain protein crystallization, has been shown to be of more general validity, and applicable to macromolecule as well as small molecule based crystals. Amorphous-to-crystalline transformation (ACT) in small molecule based nanoparticles accompanied by substantial changes in some physical responses is of fundamental interest in the growth of molecular nanocrystals and crystals and their materials applications.

In this chapter we present some novel DADQ derivatives solutions of which upon simple drop-casting on substrates like glass or quartz produce nanoparticles of varying size and morphology. Presence of specific structural motifs such as aromatic groups connected through conformationally labile bonds in the DADQ is shown to

promote the formation of amorphous particles, when solutions are drop-cast on suitable substrates. The detailed investigations are focused on one of the DADQ derivatives, 7,7-bis(2-(4-bromophenyl)ethylamino)-8,8-dicyanoquinodimethane (BBPEDQ). Solution of BBPEDQ shows nearly green emission while microcrystals show blue emission. Electronic structure calculations show that the blue shift of the absorption and fluorescence emission of BBPEDQ, from the solution to the crystalline state is a consequence of the molecular assembly in the crystal lattice. The drop-cast films of BBPEDQ contain spherical nanoparticles and produce green emission on illumination by UV light. The emission color suggests that these particles, even though solid, are far from crystalline. We have developed a simple protocol to transform the amorphous particles to crystalline ones. A free standing polystyrene film with the amorphous particles fixed in it, when exposed to solvent vapors produces crystalline particles with concomitant enhancement and switching of fluorescence emission. The transformation is established using a range of microscopy and diffraction techniques. The amorphous nanostructures provide a model for the liquid-like cluster proposed in the two-step nucleation theory.

Chapter 5

Earlier investigations in our laboratory and in other research groups as well as the various studies presented in the previous chapters in this thesis show that the fluorescence emission wavelength and efficiency of DADQ's is strongly sensitive to the molecular environment as well as rigidification of their structures. Therefore, it would be interesting to explore the hierarchical assembly of these molecules from the amorphous to the crystalline state and observe the consequence to their fluorescence characteristics. Exploration with a variety of derivatives indicated that this was indeed

possible, through fine-tuning the conditions of fabrication of the molecular nanoparticles.

We describe the synthesis and structural characterization of the DADQ derivative, 7-pyrrolidino-7-benzylamino-8,8-dicyanoquinodimethane (PBEDQ). Drop-cast thin films obtained from solutions of PBEDQ with varying compositions of a good solvent and a nonsolvent revealed nanostructures ranging from amorphous spherical particles to fibrous crystals to faceted crystals, including intermediate composite structures. While the solution and the crystalline solid state represent the two extremes of molecular materials commonly studied, the nanostructures of PBEDQ including the amorphous phase represent logical intermediates, in terms of their fluorescence characteristics, both energies and efficiencies. The spherical particles obtained from the acetonitrile solution shows nearly green emission reminiscent of the solution whereas the emission of the nanofibres and nano/microcrystals resemble the blue emission from microcrystalline solid. Spectroscopy and microscopy including fluorescence lifetime imaging shows that the quantum efficiency increases with the crystallinity of the particles. These observations with PBEDQ unravel a new dimension in the hierarchical assembly of molecular materials, with the inclusion of amorphous and related phases.

Chapter 6

This chapter presents a brief overview of the various investigations presented in the thesis on the development of highly fluorescent molecular crystals and nano/microcrystals. The salient aspects of controlling the molecular assembly through extrinsic factors such as template and substrate effects and aggregation conditions are highlighted. The notable consequence to the fluorescence emission characteristics demonstrates the significance of these studies to materials applications. A major

advancement realized through the studies presented in this thesis is the critical importance of the amorphous phase in small molecules based materials.

The chapter also outlines the directions for further investigations in this area. The growth and morphology evolution of the nanoparticles in colloidal medium and its relevance to the optical properties needs careful examination. The correlation between the molecular and crystal structure on the one hand and the fluorescence characteristics including quantum yields on the other, appears to be rather complex. Some of the preliminary attempts in this direction suggest that in addition to the electronic structure of the molecules-in-crystals, the mechanical attributes of the crystals could play a critical role. Fabrication of polymer thin films with embedded molecular nanostructures and exploration of the utility of the novel DADQ derivatives as probes in biological imaging are important applications that are currently being actively pursued in our laboratory.

References

1. J. F. W. Herschel, *Phil. Trans. R. Soc. Lond*. **1845**, *135*, 143.
2. J. R. Lackowicz, *Principles of fluorescence spectroscopy*, Springer, New York, 3rd Edn. **2006**.
3. D. R. Kearns, *Chem. Rev.* **1971**, *71*, 395.
4. E. L. Wehry, *Modern Fluorescence Spectroscopy*, Plenum press, New York, **1976**, Vol. *1 & 2*.
5. a) S. Miyata, H.S. Nalwa, *Organic Electroluminescent Materials and Devices*, Gordon and Breach, Amsterdam, **1997**. b) B. M. Krasovitskii, B. M. Bolotin, *Organic Luminescent Materials*, VCH: Weiheim, **1988**.
6. T. M. Figueira-Duarte, K. M€ullen, *Chem. Rev*. **2011**, *111*, 7260.
7. M. S. T. Gonçalves, *Chem. Rev*. **2009**, *109*, 190.
8. X. Chen, T. Pradhan, F. Wang, J. S. Kim, J. Yoon, *Chem. Rev*. **2012**, *112*, 1910.
9. I. D. W. Samuel, G. A. Turnbull, *Chem. Rev*. **2007**, *107*, 1272.
10. J. P. Webb, *Anal. Chem.* **1972**, *44*, 30.
11. B. H. Soffer, B. B. McFarland, *Appl. Phys. Lett*. **1967**, *10*, 266.
12. N. Karl, *Phys. Stat. Sol. A* **1972**, *13*, 651.
13. O. S. Avanesjan, V. A. Benderskii, V. KH. Brikenstein, V. L. Broudet, L. I. Korshunov, A. G. Lavrushko, I. I. Tartakovskii, *Mol. Cryst. Liq. Cryst*. **1974**, *29*, 165.
14. J. H. Burroughes, D. D. C. Bradley, A. R. Brown, R. N. Marks, K. Mackay, R. H. Friend, P. L. Burns, A. B. Holmes, *Nature* **1990**, *347*, 539.
15. D. Mosses, *Appl. Phys. Lett*. **1992**, *60*, 3215.
16. a) C. Wu, D. T. Chiu, *Angew. Chem. Int. Ed*. **2013**, *52*, 3086. b) A. Vollrath, S. schubert, U. S. Schubert, *J. Mater. Chem. B*, **2013**, *1*, 1994.
17. a) J. S. Yang, T. M. Swager, *J. Am. Chem. Soc*. **1998**, *120*, 5321. b) S. W. Thomas III, G. D. Joly, T. M. Swager, *Chem. Rev*. **2007**, *107*, 1339.
18. K. Binnemans, *Chem. Rev*. **2009**, *109*, 4283.

19. S. V. Eliseeva, J-C. G. Bünzli, *Chem. Soc. Rev*. **2010**, *39*, 189.

20. J. E. Geusic, H. M. Marcos, L. G. Van Uitert, *Appl. Phys. Lett*. **1964**, *4*, 182.

21. R. J. Mears, L. Reekie, I. M. Jauncey, D. N. Payne, *Electron. Lett.* **1987**, *23*, 1026.

22. A. C. Bhasikuttan, M. Suzuki, S. Nakashima, T. Okada, *J. Am. Chem. Soc*. **2002**, *124*, 8398.

23. O. S. Wenger, *Chem. Rev.* dx.doi.org/10.1021/cr300396p.

24. a) J. O. rocha, L. D. Carlos, F. A. A. Paz, D. Ananias, *Chem. Soc. Rev*. **2011**, *40*, 926. b) M. D. Allendorf, C. A. Bauer, R. K. Bhakta, R. J. T. Houk, *Chem. Soc. Rev*. **2009**, *38*, 1330. c) O. Shekhah, J. Liu, R. A. Fischer, Ch. Wo¨ ll, *Chem. Soc. Rev*. **2011**, *40*, 1081. d) Y. Cui, Y. Yue, G. Qian, B. Chen, *Chem. Rev*. **2012**, *112*, 1126.

25. W. Liu, T. Jiao, Y. Li, Q. Liu, M. Tan, H. Wang, L. Wang, *J. Am. Chem. Soc*. **2004**, *126*, 2280.

26. Y. Bai, G. He, Y. Zhao, C. Duan, D. Dang, Q. Meng, *Chem. Commun*. **2006**, 1530.

27. K. Liu, H. You, Y. Zheng, G. Jia, Y. Song, Y. Huang, M. Yang, J. Jia, N. Guo, H. Zhang, *J. Mater. Chem*. **2010**, *20*, 3272.

28. A. Rodriguez-Dieguez, A. Salinas-Castillo, A. Sironi, J. M. Seco, E. Colacio, *CrystEngComm* **2010**, *12*, 1876.

29. C. Daiguebonne, N. Kerbellec, O. Guillou, J.-C. Bünzli, F. Gumy, L. Catala, T. Mallah, N. Audebrand, Y. Gérault, K. Bernot, G. Calvez, *Inorg. Chem.* **2008**, *47*, 3700.

30. P. L. Feng, J. J. Perry Iv, S. Nikodemski, B. W. Jacobs, S. T. Meek, M. D. Allendorf, *J. Am. Chem. Soc.* **2010**, *132*, 15487.

31. Q. Fang, G. Zhu, M. Xue, J. Sun, F. Sun, S. Qiu, *Inorg. Chem.* **2006**, *45*, 3582.

32. Q.-B. Bo, G.-X. Sun, D.-L. Geng, *Inorg. Chem.* **2010**, *49*, 561.

33. B. Zhao, X.-Y. Chen, P. Cheng, D.-Z. Liao, S.-P. Yan, Z.-H. Jiang, *J. Am. Chem. Soc.* **2004**, *126*, 15394.

34. K. C. Stylianou, R. Heck, S. Y. Chong, J. Bacsa, J. T. A. Jones, Y. Z. Khimyak, D. Bradshaw, M. J. Rosseinsky, *J. Am. Chem. Soc.* **2010**, *132*, 4119.

35. K. Jayaramulu, P. Kanoo, S. J. George, T. K. Maji, *Chem. Commun.* **2010**, *46*, 7906.

36. A. M. Smith, S. Nie, *Acc. Chem. Res*. **2010**, *43*, 190.

37. Y. Li, Z. He, P. Zhanq, J. Gao, C. Chenq, H. Zhanq, *J. Nanosci. Nanotechnol.* **2010**, *10*, 520.

38. a) R. Bakalova, Z. Zhelev, H. Ohba, Y. Baba, *J. Am. Chem. Soc.* **2005**, *127*, 11328. b) K. Hoshino, A. Gopal, M. S. Glaz, D. A. V. Bout, X. Zhang, *Appl. Phys. Lett.* **2012**, *101*, 043118. c) J. Vaillancourt, P. Vasinajindakaw, X. Lu, *Optics and Photonics Lett.* **2011**, *4*, 57.

39. a) J. P. Wilcoxon, B. L. Abrams, *Chem. Soc. Rev*. **2006**, *35*, 1162. b) R. C. Jin, *Nanoscale* **2010**, *2*, 343.

40. a) I. Diez, R. H. A. Ras, *Nanoscale* **2011**, *3*, 1963–1970. b) Q. B. Zhang, J. P. Xie, Y. Yu, J. Y. Lee, *Nanoscale* **2010**, *2*, 1962.

41. a) C. Gautier, T. Burgi, *J. Am. Chem. Soc.* **2008**, *130*, 7077. b) C. E. Roman-Velazquez, C. Noguez, I. L. Garzon, *J. Phys. Chem. B* **2003**, *107*, 12035.

42. P. Crespo, R. Litran, T. C. Rojas, M. Multigner, J. M. de la Fuente, J. C. Sanchez-Lopez, M. A. Garcia, A. Hernando, S. Penades, A. Fernandez, *Phys. Rev. Lett.* **2004**, *93*, 087204.

43. a) T. P. Bigioni, R. L. Whetten, O. Dag, *J. Phys. Chem. B* **2000**, *104*, 6983. b) L. A. Peyser, A. E. Vinson, A. P. Bartko, R. M. Dickson, *Science* **2001**, *291*, 103.

44. C. C. Huang, Z. Yang, K. H. Lee, H. T. Chang, *Angew. Chem. Int. Ed.* **2007**, *46*, 6824.

45. N. Makarava, A. Parfenov, I. V. Baskakov, *Biophys. J.* **2005**, *89*, 572.

46. a) J. Zheng, C. W. Zhang, R. M. Dickson, *Phys. Rev. Lett.* **2004**, *93*, 077402. b) J. Zheng, J. T. Petty, R. M. Dickson, *J. Am. Chem. Soc.* **2003**, *125*, 7780.

47. J. G. Zhang, S. Q. Xu, E. Kumacheva, *Adv.Mater.* **2005**, *17*, 2336.

48. Z. Shen, H. W. Duan, H. Frey, *Adv. Mater.* **2007**, *19*, 349.

49. a) H. W. Duan, S. M. Nie, *J. Am. Chem. Soc.* **2007**, *129*, 2412. b) L. Shang, S. J. Dong, *Chem. Commun.* **2008**, *9*, 1088.

50. S. Y. Lin, N. T. Chen, S. P. Sum, L. W. Lo, C. S. Yang, *Chem. Commun.* **2008**, 39, 4762.

51. X. Yuan, Z. Luo, Q. Zhang, X. Zhang, Y. Zheng, J. Y. Lee, J. Xie, *ACS Nano* **2011**, *5*, 8800.

52. E. Gomar-Nadal, J. Puigmartí-Luis, D. B. Amabilino, *Chem. Soc. Rev.* **2008**, *37*, 490.

53. a) C. Joachim, J. K. Gimzewski, A. Aviram, *Nature* **2000**, *408*, 541. b) A. Nitzan, M. A. Ratner, *Science* **2003**, *300*, 1384.

54. C. Julien, J. P. Pereira-Ramos, A. Momchilov, *New Trends in Intercalation Compounds for Energy Storage*, Springer, Berlin, **2002**.

55. H. Dong, H. Zhu, Q. Meng, X. Gong, W. Hu, *Chem. Soc. Rev.* **2012**, *41*, 1754.

56. a) T. M. Swager, *Acc. Chem. Res.* **1998**, *31*, 201. b) L. Basabe-Desmonts, D. N. Reinhoudt, M. Crego-Calama, *Chem. Soc. Rev.* **2007**, *36*, 993.

57. a) D. Holten, D. F. Bocian, J. S. Lindsey, *Acc. Chem. Res.* **2002**, *35*, 57. b) V. A. Mallia, N. Tamaoki, *Chem. Soc. Rev.* **2004**, *33*, 76.

58. a) A. Mishra, R. K. Behera, P. K. Behera, B. K. Mishra, G. B. Behera, *Chem. Rev.* **2000**, *100*, 1973. b) J. Bujdák, N. Iyi, R. Sasai, *J. Phys. Chem. B* **2004**, *108*, 4470. c) H. Yao, K. Domoto, T. Isohashi, K. Kimura, *Langmuir* **2005**, *21*, 1067.

59. M. Kasha, *Rev. Mod. Phys.* **1959**, *31*, 162.

60. a) J. Slavı´k, *Fluorescence Microscopy and Fluorescent Probes*, Plenum, New York, **1996**. b) R. B. Thompson, *FluorescenceSensors and Biosensors*, CRC, Boca Raton, **2006**. c) S. M. Borisov, O. S. Wolfbeis, *Chem. Rev*. **2008**, *108*, 423.

61. J. Duhamel, *Langmuir* **2012**, *28*, 6527.

62. a) J. H. Burroughes, D. D. C. Bradley, A. R. Brown, R. N. Marks, K. Mackay, R. H. Friend, P. L. Burns, A. B. Holmes, *Nature* **1990**, *347*, 539. b) C. W. Tang, S. A. Vanslyke, *Appl. Phys. Lett.* **1987**, *51*, 913.

63. Y. Hong, J. W. Y. Lam, B. Z. Tang, *Chem. Commun.* **2009**, 4332.

64. M. Shimizu, Y. Takeda, M. Higashi, T. Hiyama, *Angew. Chem. Int. Ed.* **2009**, *48*, 3653.

65. J. N. Wilson, M. D. Smith, V. Enkelmann, H. F. Bunz, *Chem. Commun.* **2004**, 1700.

66. B. An, S. Kwon, S. Jung, S. Y. Park, *J. Am. Chem. Soc.* **2002**, *124,* 14410.

67. N. S. S. Kumar, S. Varghese, N. P. Rath, S. Das, *J. Phys. Chem. C* **2008,** *112,* 8429.

68. a) Y. Mizobe, N. Tohnai, M. Miyata, Y. Hasegawa, *Chem. Commun*. **2005**, 1839.

b) Y. Mizobe, T. Hinoue, A. Yamamoto, I. Hisaki, M. Miyata, Y. Hasegawa, N. Tohnai, *Chem. Eur., J.* **2009**, *15*, 8175.

69. S. Jayanty, T. P. Radhakrishnan, *Chem. Eur. J.* **2004**, *10*, 791.

70. Z. Zhao, S. Chen, X. Shen, F. Mahtab, Y. Yu, P. Lu, J. W. Y. Lam, H. S. Kwok, B. Z. Tang, *Chem. Commun.* **2010**, *46*, 686.

71. S. R. Marder, J. W. Perry, *Adv. Mater.* **1993**, *5*, 804.

72. D. Gatteschi, *Curr. Opin. Solid State Mater. Sci.* **1996**, *1*, 192.

73. S. Roth, D. Carroll, *One Dimensional Metals* Wiley-VCH, Weinheim, 2006.

74. A. Lebed, ed. *The Physics of Organic Superconductors and Conductors*, Springer Series in Materials Science, **2008**, *110*.

75. S. Horiuchi, Y. Tokura, *Nature Mater.* **2008**, *7*, 357.

76. L. Kang, H. Fu, X. Cao, Q. Shi, J. Yao, *J. Am. Chem. Soc.* **2011**, *133*, 1895.

77. L. Kang, Z. Wang, Z. Cao, Y. Ma, H. Fu, J. Yao, *J. Am. Chem. Soc.* **2007**, *129*, 7305.

78. L. Huang, Q. Liao, Q. Shi, H. Fu, J. Mab, J. Yao, *J. Mater. Chem.* **2010**, *20*, 159.

79. E. V. Keuren, A. Bone, C. Ma, *Langmuir* **2008**, *24*, 6079.

80. X. Zhang, C. Zhao, J. Lv, C. Dong, X. Ou, X. Zhang, S. Lee, *Cryst. Growth Des.* **2011**, *11*, 3677.

81. a) T. Shimizu, M. Masuda, H. Minamikawa, *Chem. Rev.* **2005**, *105*, 1401. b) P.

K. Vemula, G. John, *Acc. Chem. Res.* **2008**, *41*, 769. c) X. Zhu, Y. Li, P. Duan, M. Liu, *Chem. Eur. J.* **2010**, *16*, 8034. d) D. Wu, R. Liu, W. Pisula, X. Feng, K. Müllen, *Angew. Chem. Int. Ed.* **2011**, *50*, 2791.

82. a) H. Kasai, H. S. Nalwa, H. Oikawa, S. Okada, H. Matsuda, N. Minami, A. Kakuta, K. Ono, A. Mukoh, H. Nakanishi, *Jpn. J. Appl. Phys.* **1992**, *31*, L1132. b) H. Nakanishi, H. Oikawa, in *Single Organic Nanoparticles*, ed. H. Masuhara, H. Nakanishi, K. Sasaki, Springer, Berlin, **2003**, pp. 17–31.

83. L. Jiang, Y. Fu, H. Li, W. Hu, *J. Am. Chem. Soc.* **2008**, *130*, 3937.

84. T. Nguyen, R. Martel, P. Avouris, M. Bushey, L. Brus, C. Nuckolls, *J. Am. Chem. Soc.* **2004**, *126*, 5234.

85. C. Destrée, J. Ghijsen, J. B. Nagy, *Langmuir* **2007**, *23*, 1965.

86. E. Kwon, H. Oikawa, H. Kasai, H. Nakanishi, *Cryst. Growth Des.* **2007**, *7*, 600.

87. V. Monnier, N. Sanz, E. Botzung-Appert, M. Bacia, A. Ibanez, *J. Mater. Chem.* **2006**, *16*, 1401.

88. J. Ha, M. A. Hillmyer, M. D. Ward, *J. Phys. Chem. B* **2005**, *109*, 1392.

89. R. O. Al-Kaysi, C. J. Bardeen, *Chem. Commun.* **2006**, 1224.

90. S. Cui, H. Liu, L. Gan, Y. Li, D. Zhu, *Adv. Mater.* **2008**, *20*, 2918.

91. L. Zhao, W. Yang, Y. Ma, J. Yao, Y. Li, H. Liu, *Chem. Commun.* **2003**, 2442.

92. H. Gan, H. Liu, Y. Li, Y. Liu, F. Lu, T. Jiu, D. Zhu, *Chem. Phys. Lett.* **2004**, *399*, 130.

93. L. Zhao, W. Yang, Y. Luo, T. Zhai, G. Zhang, J. Yao, *Chem. Eur. J.* **2005**, *11*, 3773.

94. B. D. Gates, Q. Xu, M. Stewart, D. Ryan, C. G. Willson, G. M. Whitesides, *Chem. Rev.* **2005**, *105*, 1171.

95. J. P. Rolland, B. W. Maynor, L. E. Euliss, A. E. Exner, G. M. Denison, J. M. DeSimone, *J. Am. Chem. Soc.* **2005**, *127*, 10096.

96. W. Jeong, M. E. Napier, J. M. DeSimone, *Nanomedicine* **2010**,*5*, 633.

97. A. B. Braunschweig, F. Huo, C. A. Mirkin, *Nature Chem.* **2009**, *1*, 353.

98. a) M. Pope, C. E. Swenberg, *Electronic Processes in Organic Crystals and Polymers*, Oxford University Press, Oxford, 2nd edn.,**1999**. b) S. R. Forrest, *Chem. Rev.* **1997**, *97*, 1793. c) M. A. El-Sayed, *Acc. Chem. Res.* **2001**, *34*, 257. d) X. -Y. Zhu, Q. Yang, M. Muntwiler, *Acc. Chem. Res.* **2009**, *42*, 1779.

99. a) H. Kasai, H. Kamatani, Y. Yoshikawa, S. Okada, H. Oikawa, A. Watanabe, O. Itoh, H. Nakanishi, *Chem. Lett.* **1997**, 1181. b) H. Oikawa, T. Mitsui, T. Onodera, H. Kasai, H. Nakanishi, T. Sekiguchi, *Jpn. J. Appl. Phys.* **2003**, *42*, L111.

100. H. Kasai, H. Kamatani, S. Okada, H. Oikawa, H. Matsuda, H. Nakanishi, *Jpn. J. Appl. Phys.*, **1996**, *35*, L221.

101. H. Auweter, H. Haberkorn, W. Heckmann, D. Horn, E. Lüddecke, J. Rieger, H. Weiss, *Angew. Chem. Int. Ed.* **1999**, *38*, 2188.

102. C. J. Bhongale, C. Chang, C. Lee, E. W. Diau, C. Hsu, *J. Phys. Chem. B* **2005**, *109,* 13472.

103. Y. S. Zhao, D. Xiao, W. Yang, A. Peng, J. Yao, *Chem. Mater.* **2006**, *18*, 2302.

104. J. Wang, Y. Zhao, J. Zhang, J. Zhang, B. Yang, Y. Wang, D. Zhang, H. You, D. Ma, *J. Phys. Chem. C* **2007**, *111*, 9177.

105. X. Zhang, X. Zhang, W. Shi, X. Meng, C. Lee, S. Lee, *Angew. Chem. Int. Ed.* **2007**, *46,* 1525.

106. a) A. Patra, N. Hebalkar, B. Sreedhar, M. Sarkar, A. Samanta, T. P. Radhakrishnan, *Small* **2006**, *2*, 650. b) A. Patra, N. Hebalkar, B. Sreedhar, T. P. Radhakrishnan, *J. Phys. Chem. C* **2007**, *111*, 16184.

107. D. Xiao, L. Xi, W. Yang, H. Fu, Z. Shuai, Y. Fang, J. Yao, *J. Am. Chem. Soc.* **2003**, *125,* 6740.

108. D. Xiao, W. Yang, J. Yao, L. Xi, X. Yang, Z. Shuai, *J. Am. Chem. Soc.* **2004**, *126,* 15439.

109. T. Asahi, H. Matsune, K. Yamashita, H. Masuhara, H. Kasai, H. Nakanishi, *Polish J. Chem.* **2008**, *82*, 687.

110. A. J. Gesquiere, T. Uwada, T. Asahi, H. Masuhara, P. F. Barbara, *Nano Lett.* **2005**, *5*, 1321.

111. E. Kwon, H. -R. Chung, Y. Araki, H. Kasai, H. Oikawa, O. Ito, H. Nakanishi, *Chem. Phys. Lett.* **2007**, *441*, 106.

112. Y. S. Zhao, W. Yang, J. Yao, *Phys. Chem. Chem. Phys.* **2006**, *8*, 3300.

113. E. H. Cho, M. S. Kim, D. H. Park, H. Jung, J. Bang, J. Kim, J. Joo, *Adv. Funct. Mater.* **2011**, *21*, 3056.

114. X. Zhang, X. Zhang, W. Shi, X. Meng, C. Lee, S. Lee, *J. Phys. Chem. B* **2005**, *109,* 18777.

115. X. Zhang, C. Dong, J. A. Zapien, S. Ismathullakhan, Z. Kang, J. Jie, X. Zhang, J. C. Chang, C. Lee, S. Lee, *Angew. Chem. Int. Ed.* **2009**, *48*, 9121.

116. D. H. Park, S. G. Jo, Y. K. Hong, C. Cui, H. Lee, D. J. Ahn, J. Kim, J. Joo, *J. Mater. Chem.* **2011**, *21*, 8002.

117. S. Li, L. He, F. Xiong, Y. Li, G. Yang, *J. Phys. Chem. B* **2004**, *108,* 10887.

118. R. O. Al-Kaysi, C. J. Bardeen, *Adv. Mater.* **2007**, *19*, 1276.

119. L. Jinshui, W. Lun, G. Feng, L. Yongxing, W. Yun, *Anal. Bioanal. Chem.* **2003**, *377*, 346.

120. E. Botzung-Appert, V. Monnier, T. Ha Duong, R. Pansu, A. Ibanez, *Chem. Mater.* **2004**, *16*, 1609.

121. L. Wang, L. Wang, T. Xia, L. Dong, G. Bian, H. Chen, *Anal. Sci.* **2004**, *20*, 1013.

122. L. Wang, T. Xia, L. Wang, H. Chen, L. Dong, G. Bian, *Microchim. Acta* **2005**, *149*, 267.

123. L. Wang, L. Wang, L. Dong, G. Bian, T. Xia, H. Chen, *Spectrochim. Acta, part A* **2005**, *61*, 129.

124. T. Naddo, Y. Che, W. Zhang, K. Balakrishnan, X. Yang, M. Yen, J. Zhao, J. S. Moore, L. Zang, *J. Am. Chem. Soc.* **2007**, *129*, 6978.

125. Y. Che, X. Yang, S. Loser, L. Zang, *Nano Lett.* **2008**, *8*, 2219.

126. H. Li, H. Yan, *J. Phys. Chem. C* **2009**, *113*, 7526.

127. Q. Tang, L. Li, Y. Song, Y. Liu, H. Li, W. Xu, Y. Liu, W. Hu, D. Zhu, *Adv.*

Mater. **2007**, *19*, 2624.

128. K. Takazawa, *Chem. Mater.* **2007**, *19*, 5293.

129. M. Schiek, F. Balzer, K. Al-Shamery, J. R. Brewer, A. Lützen, H. Rubahn, *Small* **2008**, *4*, 176.

130. Y. S. Zhao, A. Peng, H. Fu, Y. Ma, J. Yao, *Adv. Mater.* **2008**, *20*, 1661.

131. S. Rath, M. Heilig, H. Port, J. Wrachtrup, *Nano. Lett.* **2007**, *7*, 3845.

132. R. Jagannathan, G. Irvin, T. Blanton, S. Jagannathan, *Adv. Funct. Mater.* **2006**, *16*, 747.

133. E. I. Maltsev, D. A. Lypenko, B. I. Shapiro, M. A. Brusentseva, V. I. Berendyaev, B. V. Kotov, A. V. Vannikov, *Appl. Phys. Lett.* **1998**, *73*, 3641.

134. E. I. Maltsev, D. A. Lypenko, V. V. Bobinkin, A. R. Tameev, S. V. Kirillov, B. I. Shapiro, H. F. M. Schoo, A. V. Vannikov, *Appl. Phys. Lett.* **2002**, *81*, 3088.

135. J. Heo, N. Park, J. Ryu, K. Suh, *Adv. Mater.* **2005**, *17*, 822.

136. T. Hasobe, A. S. D. Sandanayaka, T. Wada, Y. Araki, *Chem. Commun.* **2008**, 3372.

137. A. L. Briseno, S. C. B. Mannsfeld, X. Lu, Y. Xiong, S. A. Jenekhe, Z. Bao, Y. Xia, *Nano Lett.* **2007**, *7*, 668.

138. Y. Zhou, T. Lei, L. Wang, J. Pei, Y. Cao, J. Wang, *Adv. Mater.* **2010**, *22*, 1484.

139. X. Mu, W. Song, Y. Zhang, K. Ye, H. Zhang, Y. Wang, *Adv. Mater.* **2010**, *22*, 4905.

140. L. Jiang, J. Gao, E. Wang, H. Li, Z. Wang, W. Hu, L. Jiang, *Adv. Mater.* **2008**, *20*, 2735.

141. Q. Tang, H. Li, M. He, W. Hu, C. Liu, K. Chen, C. Wang, Y. Liu, D. Zhu, *Adv. Mater.* **2006**, *18*, 65.

142. W. S. Journeay, S. S. Suri, J. G. Moralez, H. Fenniri, B. Singh, *Small* **2008**, *4*, 817.

143. S. Ehrler, U. Pieles, A. Wirth-Heller, P. Shahgaldian, *Chem. Commun.* **2007**, 2605.

144. C. P. Chan, Y. Bruemmel, M. Seydack, K. Sin, L. Wong, E. Merisko-Liversidge, D. Trau, R. Renneberg, *Anal. Chem.* **2004**, *76*, 3638.

145. M. Yin, J. Shen, W. Pisula, M. Liang, L. Zhi, K. Müllen, *J. Am. Chem. Soc.* **2009**, *131*, 14618.

146. E. Dubuisson, S. Szunerits, M. Bacia, R. Pansu, A. Ibanez, *New J. Chem.* **2011**, *35*, 2416.

147. H. Lin, S. Su, C. Chang, *Org. Biomol. Chem.* **2009**, *7*, 2036.

148. H. Lin, Y. Chan, J. Chena, C. Chang, *J. Mater. Chem.* **2011**, *21*, 3170.

149. S. Raoux, M. Wuttig, *Phase Change Materials*, Springer, **2009**, pp. 125-145.

150. a) P. G. Vekilov, *J. Cryst. Growth* **2005**, *275*, 65. b) P. G. Vekilov, *Nanoscale* **2010**, *2*, 2346. c) D. Erdemir, A. Y. Lee, A. S. Myerson, *Acc. Chem. Res.* **2009**, *42*, 621.

151. S. Raoux, D. Ielmini, M. Wuttig, I. Karpov, *MRS Bull.* **2012**, *37*, 118.

152. Y. Jung, S. W. Nam, R. Agarwal, *Nano Lett.* **2011**, *11*, 1364.

153. T. Ohta, S. R. Ovshinsky, *Photo-induced Metastability in Amorphous Semiconductors* ed. A. V. Kolobov, Wiley-VCH, Berlin, **2003**, pp. 310–326.

154. A. V. Kolobov, P. Fons, A. I. Frenkel, A. Ankudinov, J. Tominaga, T. Uruga, *Nature Mater*. **2004**, *3*, 703.

155. W. Zhang, I. Ronneberger, Y. Li, R. Mazzarello, *Adv. Mater*. **2012**, *24*, 4387.

156. K. Nagapudi, J. Jona, *Current Bioactive Compounds* **2008,** *4,* 213**.**

157. Y. Shirota, H. Kageyama, *Chem. Rev.* **2007**, *107*, 953.

158. O. Galkin, K. Chen, R. L. Nagel, R. E. Hirsch, G. Vekilov, *Proc. Natl. Acad. Sci.* **2002**, *99*, 8479.

159. Y. Dong, J. W. Y. Lam, A. Qin, Z. Li, J. Sun, H. H.-Y. Sung, I. D. Williams, B. Z. Tang, *Chem. Commun.* **2007**, *40*.

Synopsis

We have developed diaminodicyanoquinodimethane (DADQ) molecules which show strong solid state emission in the blue-green region. The new materials are structurally characterized; extended supramolecular assemblies mediated by H-bond interactions are observed in the crystal lattice. Spectroscopic studies including excited state life-time and fluorescence quantum yield measurements in the solution and solid states are carried out on two systems, 7,7-bis(benzylamino)-8,8-dicyanoquinodimethane (BBEDQ) and 7,7-bis(2-phenylethylamino)-8,8-dicyanoquinodimethane (BPEDQ). The emission in the solid state is found to be ~ 400 times stronger than that in solution; this can be attributed to the inhibition of the excited state geometry relaxation to a non-radiative state, in the solid. Impact of the molecular structure in the crystals on the solid state light emission is discussed. Semiempirical computational studies provide useful insight into the various structural and spectroscopic features of the new materials. Following the detailed investigation on the two DADQ derivatives, we have synthesized and structurally characterized several more derivatives. The fluorescent color is shown to vary across the entire blue-green region, reaching strongly blue emitting materials.

2.1. Introduction

The facile tailorability of molecular materials coupled with the wide spectrum of physical attributes and functions that can be realized in them have led to their emergence as promising candidates for various applications in fields such as electronics, opto-electronics and photonics. One of the critical problems in the area of optical applications is the fabrication of molecular assemblies capable of strong light emission,

circumventing the inherent self-quenching effects.[1] Some of the families of small organic molecules that exhibit enhanced fluorescence in the solid state (Sec. 1.2.3) are siloles,[2] cyanobis(biphenyl)ethenes,[3] cruciform pentamers,[4] diaminodicyanoquinodimethanes,[5,6] diphenylbutadienes,[7] tetraphenylethenes[8,9] and piperidinobenzenes.[10] Intermolecular interactions as well as geometry relaxations that induce non-radiative decay of the excited state are inhibited in these systems through specific molecular structural features and solid state packing effects. Besides strong emission in the solid state, an important consideration for device applications is the feasibility of tuning the color of light emission in a family of materials, maintaining high quantum yields. Efficient blue emitting systems are less common than the green and red emitting ones, and are of special interest because of the potential for down conversion to other colors.[11-16] The possibility of introducing wide structural variations in molecular materials and thus tuning the electronic energy levels holds great promise in this regard. Besides conjugated macromolecules and coordination polymers that may be confronted with solubility issues, several small molecule based materials showing strong blue or bluish-green fluorescence have been developed. These include derivatives of naphthalene,[11] anthracene,[12,17] coumarin,[18] fluorene,[13,14,19] pyrene[15] and other[10,20,21] fluorophores. However, a combination of high fluorescence quantum yield in the solid state and efficient tuning of the emission color through simple and systematic structural variations have been demonstrated only in a few cases. Emission of 9-anthrylpyrazole derivatives[12] and anthracene-2,6-disulfonic acid salts[17] were rationalized in terms of the packing of the anthracene moiety. Other interesting cases are dipiperidinobenzenes[10] and coumarins[18] with a wide range of emission maxima.

We have demonstrated earlier,[5] the strong fluorescence of a family of zwitterionic diaminodicyanoquinodimethane (DADQ) (Fig. 2.1) molecules in the solid

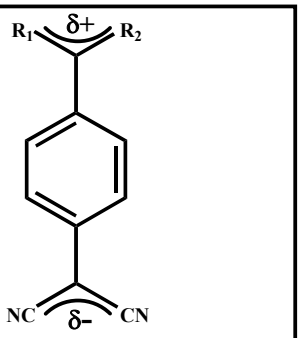

Figure 2.1. *Molecular structure of DADQ. R_1 and R_2 could be same or different amines.*

state and doped polymer films; reversible fluorescence switching induced by solvent vapors was also observed. The molecules reported in earlier work in our laboratory having amino groups based on saturated heterocycles with remote functional groups exhibit green fluorescence; emission maxima typically range from 490 – 550 nm. Computational investigations suggest that the enhanced emission in the solid arises due to the suppression of the excited state geometry relaxation (increased dihedral twist, τ) to a non-radiative state (Fig. 2.2). The matrix dependence of light emission of some DADQ derivatives is consistent with this picture.[6] We have shown also that colloidal aggregates of a DADQ derivative fabricated through a polyelectrolyte-assisted reprecipitation technique produce enhanced green emission[22] (Chapter 3). Aromatic amine based DADQ molecules show red emission[23-25] and the nano/microcrystals of these compounds[24] have enabled systematic investigation of size effects in the optical responses.[23]

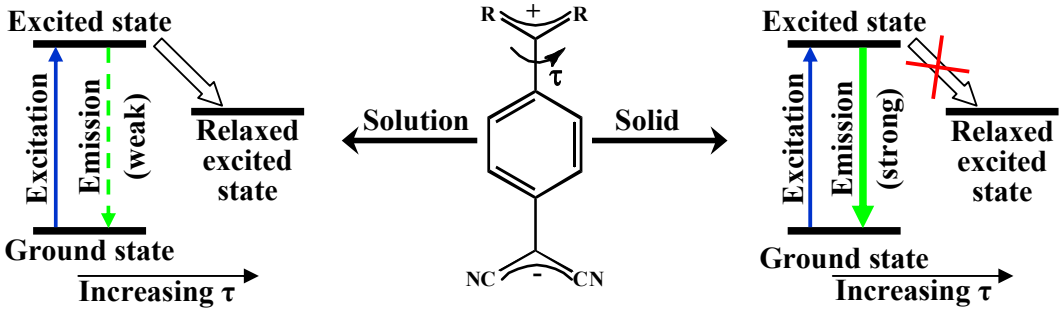

Figure 2.2. *Schematic representation of the mechanism for fluorescence enhancement proposed in Ref. 5.*

Push-pull effect of the amino-cyano groups results in the zwitterionic structure of DADQ's; this feature may induce significant intermolecular phonon contribution to the optical properties of the crystals. The steric interaction between the substituents on the amino group and the *ortho* hydrogen atoms of the benzenoid ring creates a prominent torsion angle between the diaminomethylene and ring planes.[5,26] Computational investigations have shown that the electronic excitation energy of these molecules is sensitive to this torsion angle[27]. Since the synthesis of the DADQ's incorporating a wide range of substitutions on the amino moiety is facile, it should be possible to generate new derivatives using primary amine substitutions that could potentially show higher excitation energies and hence strong light emission towards the blue region. It is notable that a few DADQ derivatives in which the matrix dependence of emission was explored[6] do show blue emission; the emission however was quite weak except in highly viscous solvents.

Some of the significant features of DADQ molecules are the ease of synthesis involving a single step reaction of easily available precursors, amenability to systematic structural variations, appreciable solubility in common organic solvents allowing facile crystallization, and high chemical and thermal stability. They generally possess large ground state dipole moment and hyperpolarizability.[28] The relatively high melting points in the range 200-250^{o}C and thermal stability possibly arise due to the strong electrostatic interactions between the zwitterionic molecules in the solid state. The stability of these compounds would be of special interest from a device application perspective.

2.2. Two new DADQ derivations: BBEDQ and BPEDQ

2.2.1 *Synthesis and characterization*

We have synthesized BBEDQ and BPEDQ by the direct addition of the appropriate amine to 7,7,8,8-tetracyanoquinodimethane (TCNQ).[26,29,30] The general procedure used is as follows. 2 mmol amine was added to a warm solution of 0.5 mmol TCNQ in 10 ml acetonitrile (CAUTION: HCN is a byproduct in this reaction). The solution turned dark green immediately and changed to orange red subsequently. The reaction mixture was stirred at 75^{o}C for 2.5 h and then at -10^{o}C for 4 h or stirring carried out at 30^{o}C for 10 min. The light yellow product which precipitated was filtered out and dried. The compound was recrystallized twice from acetonitrile/methanol. The new compounds were characterized using elemental composition analysis and NMR and IR spectroscopies.

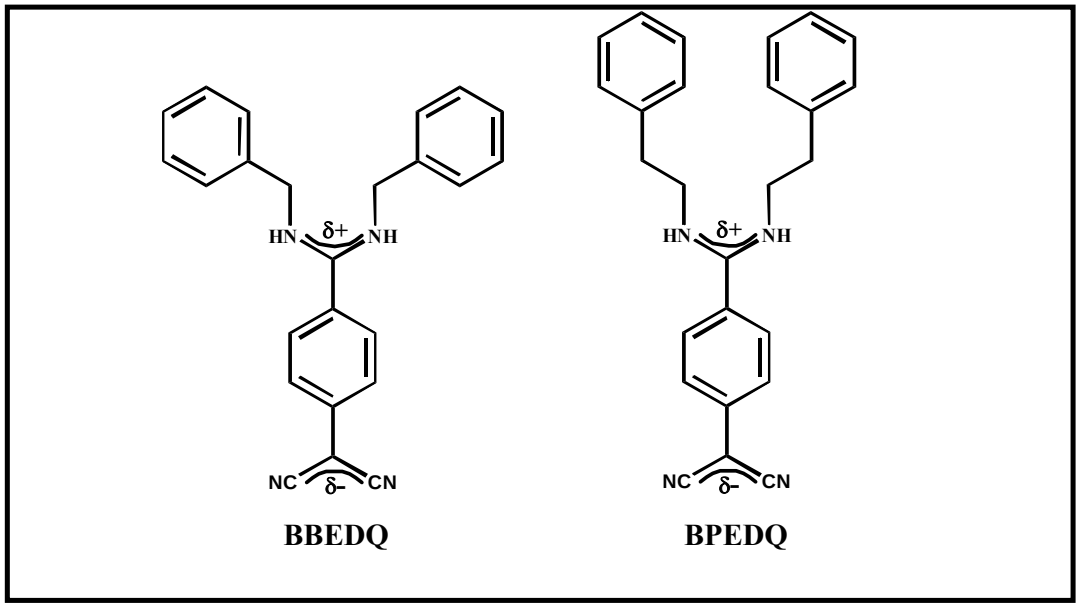

Figure 2.3. *Molecular structure of BBEDQ and BPEDQ.*

BBEDQ: Yield = 60%; M.P. (^oC) = 240 - 242; FTIR (KBr) : $\bar{\upsilon}/cm^{-1}$ = 3026.6, 2181.7, 2129.6; ^{1}H-NMR (d_6-DMSO) : δ/ppm = 9.88 (brs, 1H), 9.28 (brs, 1H), 7.45-7.31 (m, 5H), 7.31-7.21 (m, 5H), 7.03 (brs, 2H), 6.80 (d, 2H), 4.65 (brs, 2H), 4.51 (brs, 2H); elemental analysis (calculated for $C_{24}H_{20}N_4$) : %C = 78.87 (79.10), %H = 5.39 (5.53), %N = 15.05 (15.37).

BPEDQ: Yield = 71%; M.P. (^oC) = 210 - 212; FTIR (KBr) : $\bar{\upsilon}/cm^{-1}$ = 3028.5, 2181.7, 2137.3 ; ^{1}H-NMR (d_6-DMSO) : δ/ppm = 9.21 (brs, 1H), 8.70 (brs, 1H), 7.39-7.31 (m, 2H), 7.31-7.20 (m, 6H), 7.10-7.03 (m, 2H), 6.91 (d, 2H), 6.75 (d, 2H), 3.57-3.46 (m, 4H), 2.85 (t, 2H), 2.79 (t, 2H); elemental analysis (calculated for $C_{26}H_{24}N_4$) : %C = 79.27 (79.56), %H = 5.96 (6.16), %N = 13.73 (14.27).

2.2.2 *Crystal structure information of BBEDQ and BPEDQ*

Crystals of BBEDQ grown from acetonitrile solution belong to the $P2_1/c$ space group with one molecule in the asymmetric unit. The molecular structure and unit cell packing are shown in Fig. 2.4 and the crystallographic data are collected in Table 2.1. The diaminomethylene group is out of plane with respect to the benzenoid ring frame by ~ 46.3^o (dihedral angles: $\tau_{N9\text{-}C7\text{-}C1\text{-}C2}$ = 45.2^o, $\tau_{N10\text{-}C7\text{-}C1\text{-}C6}$ = 47.4^o). This angle is smaller than that observed in the remote functionalized saturated ring derivatives.[5] Both of the amino and cyano groups in BBEDQ are involved in H-bond interactions leading to extended corrugated 2-dimensional supramolecular structures in the crystal lattice. Dimers formed through two identical H-bonds between nearly antiparallel molecules ($r_{N9\ldots N13'}$ = 2.900 Å; $\theta_{N9\text{-}H9\ldots N13'}$ = 155.3^o) are interconnected through further H-bonds ($r_{N10\ldots N14''}$ = 2.856 Å; $\theta_{N10\text{-}H10\ldots N14''}$ = 158.4^o) into extended structures; propagation of the structure along the ***b*** axis is shown in Fig. 2.4c.

Crystals of BPEDQ grown from acetonitrile solution belong to the *C2/c* space group with one molecule in the asymmetric unit. The molecular structure and unit cell packing are shown in Fig. 2.5 and the crystallographic data are collected in Table 2.1.

The twist angle of BPEDQ is ~ 38.0^{o} (dihedral angles: $\tau_{N9\text{-}C7\text{-}C1\text{-}C2}$ = 36.4^{o}, $\tau_{N10\text{-}C7\text{-}C1\text{-}C6}$ = 39.5^{o}), distinctly smaller than that in BBEDQ. The farther placement of the phenyl groups compared to BBEDQ could be an important factor that contributes to the lower twist angle. Once again, both of the amino and cyano groups are involved in H-bond interactions. Each molecule is connected to four different neighbors through two sets of identical interactions ($r_{N9\ldots N14'}$ = 2.893 Å; $\theta_{N9\text{-}H9\ldots N14'}$ = 158.6^{o} and $r_{N10\ldots N13''}$ = 2.942 Å; $\theta_{N10\text{-}H10\ldots N13''}$ = 158.2^{o}). The 2-dimensional structure formed in the ***ab*** plane is shown in Fig. 2.5c; a double helical superstructure extending along the ***b*** direction can be discerned. Powder X-ray diffraction patterns of solid samples from different batches of synthesis were found to be identical and in good agreement with the one simulated using the atom coordinates from single crystal X-ray analysis (Fig. 2.6).[31] These observations confirm the purity of the bulk samples and rule out polymorphic structural variations among the samples.

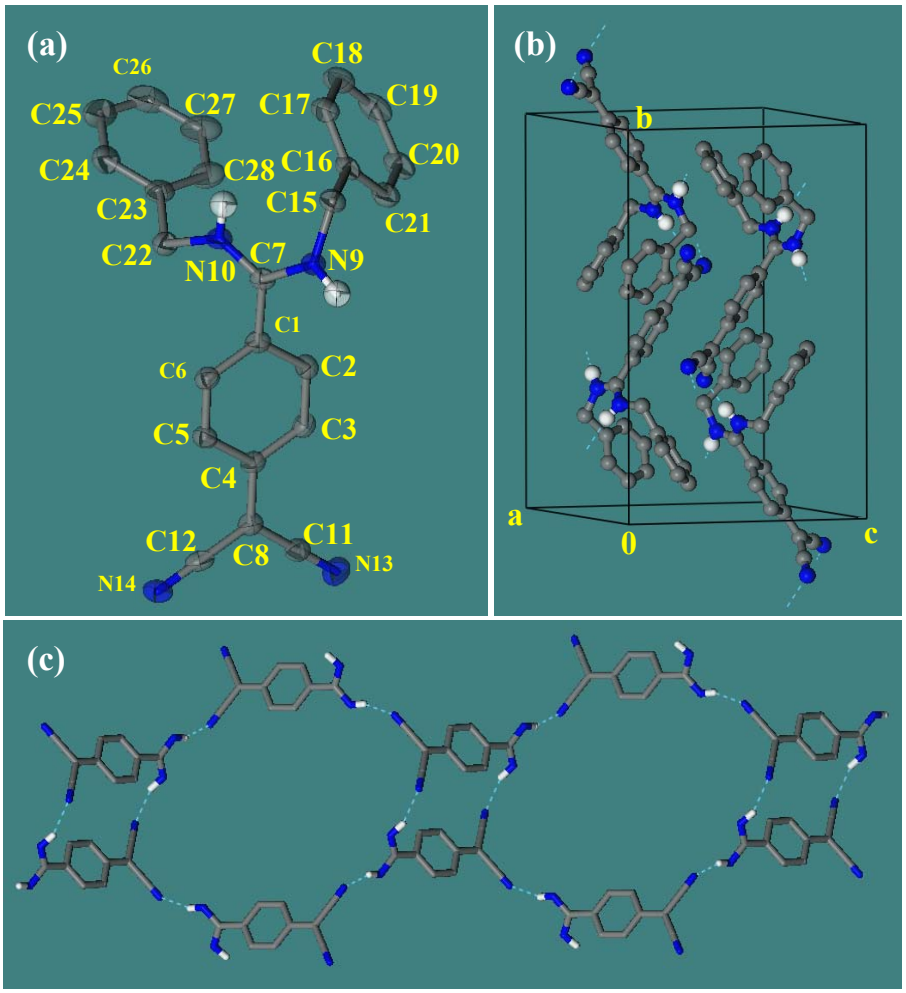

Figure 2.4. *Molecular and crystal structure of BBEDQ from single crystal x-ray analysis:* ***(a)*** *molecular structure indicating 98% probability thermal ellipsoids,* ***(b)*** *unit cell,* ***(c)*** *H-bonded supramolecular assembly along the b-axis. H atoms not involved in H-bonds and the benzyl group [in (c)] are omitted for clarity; C (grey), N (blue), H (white), H-bonds (cyan broken line) are indicated.*

Table 2.1. *Crystallographic data for BBEDQ and BPEDQ.*

	BBEDQ	**BPEDQ**
Empirical formula	$C_{24}H_{20}N_4$	$C_{26}H_{24}N_4$
Crystal system	Monoclinic	Monoclinic
Space group	*$P2_1/c$*	*C2/c*
a / Å	9.4527 (12)	20.3778 (14)
b / Å	18.864 (2)	9.7772 (7)
c / Å	11.6217 (14)	21.7545 (15)
β / deg.	108.287 (2)	92.2280 (10)
V / $Å^3$	1967.7 (4)	4331.0 (5)
Z	4	8
$\rho_{calc.}$ / g cm^{-3}	1.230	1.204
μ / cm^{-1}	0.75	0.72
Temperature / K	100 (2)	293 (2)
λ / Å	0.71073	0.71073
No. of reflections	3498	3804
No. of parameters	253	271
Max., Min. transmission	0.9765, 0.9594	0.9885, 0.9688
GOF	1.057	1.074
R [for $I \geq 2\sigma_I$]	0.0404	0.0497
wR^2	0.0999	0.1188
Largest difference peak and hole / e$Å^{-3}$	0.227 / -0.200	0.217 / -0.269

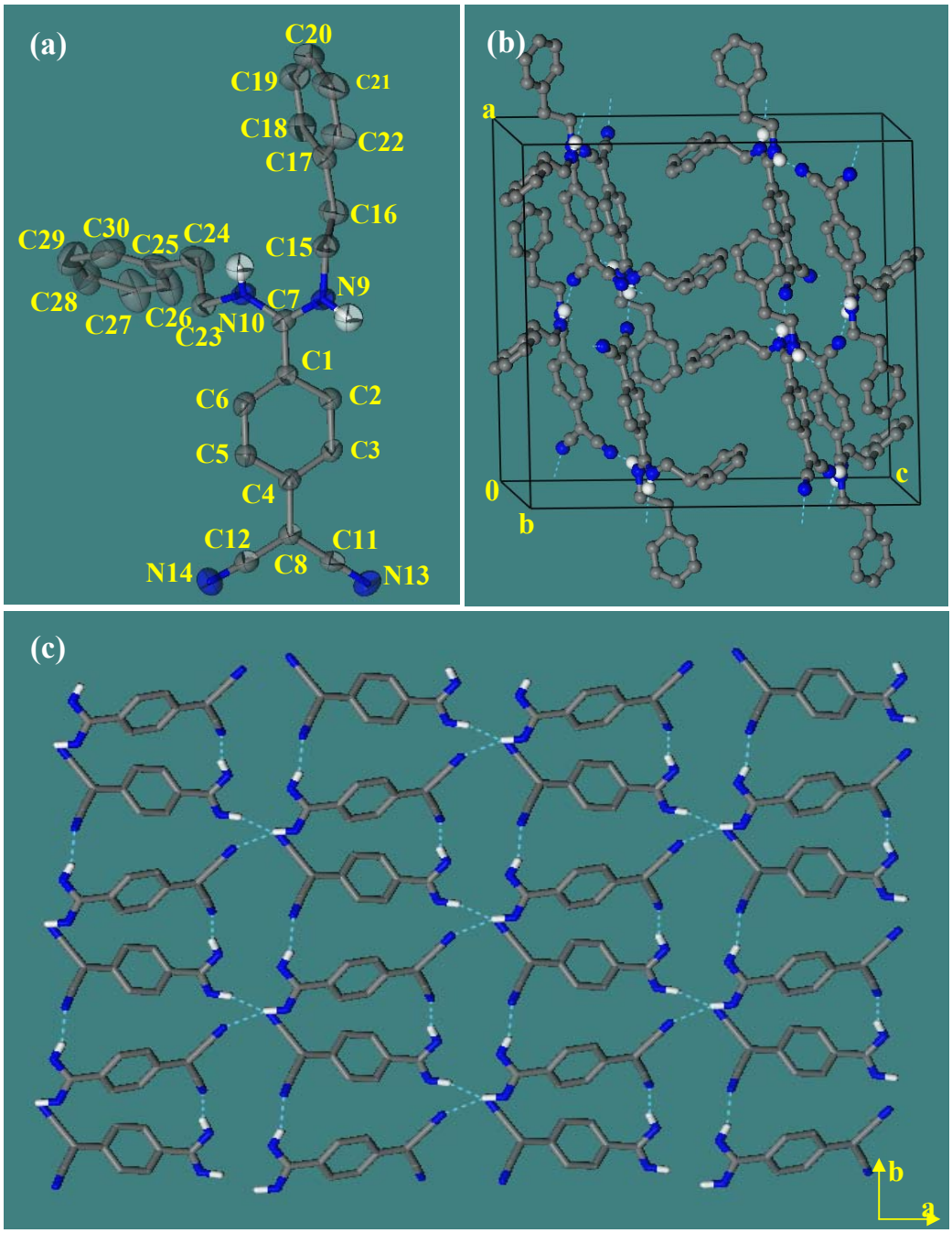

Figure 2.5. *Molecular and crystal structure of BPEDQ from single crystal x-ray analysis:* ***(a)*** *molecular structure indicating 98% probability thermal ellipsoids,* ***(b)*** *unit cell,* ***(c)*** *H-bonded supramolecular assembly in the ab-plane. H atoms not involved in H-bonds and the 2-phenylethyl group [in (c)] are omitted for clarity; C (grey), N (blue), H (white), H-bonds (cyan broken line) are indicated.*

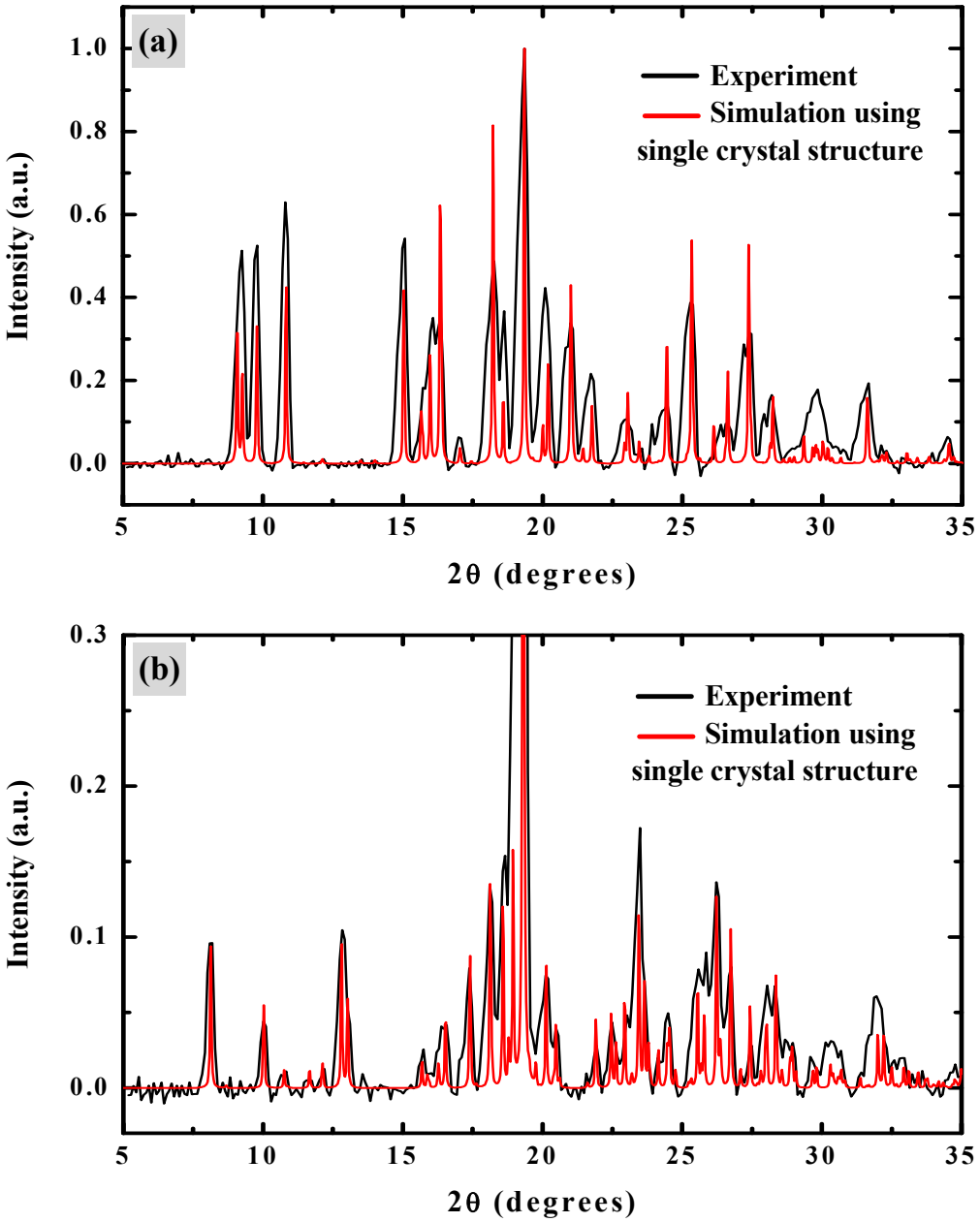

Figure 2.6. *X-ray diffraction pattern of microcrystalline powder samples of* ***(a)*** *BBEDQ and* ***(b)*** *BPEDQ, Compared with the pattern obtained by simulation using the corresponding single crystal structures.*

2.2.3 *Computations*

In order to understand the structural and spectroscopic characteristics of BBEDQ and BPEDQ as isolated molecules and in the crystals, computational studies were carried out using the semiempirical quantum chemical program VAMP in the MS Modeling software.[32] The AM1 method was used for the geometry optimization calculations; effect of the solvent environment was incorporated using the conductor-like screening model (COSMO). Efficacy of these methods in describing the molecular and ground state electronic structure of DADQ molecules has been demonstrated in several earlier studies from our laboratory.[5, 23, 26, 27] Excited state energies and oscillator strengths were computed using the ZINDO method which is specifically parameterized for spectroscopic properties.[33] Configuration interaction (CI) was included using the CI Singles (CIS) option, invoking all single excitations among the 14 MO's bracketing the HOMO/LUMO.

Impact of the molecular and lattice structure on the optical properties of BBEDQ and BPEDQ compounds can be understood in the light of computational studies. Computations were carried out on the molecular structure observed in the crystal lattice as well as the structure obtained by full optimization of this geometry imposing a solvent (acetonitrile) environment. The twist angle in the optimized geometries are compared with those found in the crystal in Table 2.2; even though the angles observed in the two crystals are quite distinct, they both increase to similar values upon geometry optimization. This suggests that the solid state packing effects and non-covalent interactions play a critical role in determining the molecular structure in the BBEDQ and BPEDQ crystals. Both molecules show large ground state dipole moments owing to the zwitterionic nature; the value increases considerably in the more twisted

Table 2.2. *Experimental and computed (AM1/COSMO or ZINDO/CIS) geometric, electronic and spectroscopic parameters of BBEDQ and BPEDQ.*

Parameter	Geometry	BBEDQ	BPEDQ
Twist angle (°)[a]	Crystal[b]	46.3 {45.2, 47.4}	38.0 {36.4, 39.5}
	Optimized[c]	53.9 {52.9, 54.9}	53.5 {52.6, 54.3}
AM1 computed dipole moment (D)	Crystal	20.254	19.589
	Optimized[c]	30.751	30.308
Experimentally observed low energy electronic absorption: λ_{max} (nm)	Crystal	385 [329.0, 393.4, 424.2][d]	376 [315.4, 371.4, 416.7][d]
	Solution	393	386
Computed low energy electronic absorption: λ_{max} (nm) [oscillator strength][e]	Crystal	379.2 [0.55]	371.4 [0.13]
	Optimized[c]	389.6 [0.51]	389.3 [0.12]

[a]The average value and the two dihedral angles involved are indicated.
[b]From X-ray diffraction analysis.
[c]AM1/COSMO (EPS=37.5).
[d]Values from deconvolution of the spectrum.
[e]ZINDO/CIS=14.

optimized geometry as a result of the higher extent of charge localization and the solvent environment imposed.

2.2.4 *Spectroscopic studies*

Electronic absorption and steady state fluorescence emission spectra of BBEDQ and BPEDQ in acetonitrile solution are shown in Fig. 2.7. The lowest energy absorptions due to the characteristic intramolecular charge transfer in the zwitterionic molecules have $\lambda_{max} < 400$ nm. ZINDO/CIS computations carried out on the optimized geometries gave λ_{max} in good agreement with the observed values (Table 2.2); in fact

the computed values are very similar for the two molecules as expected based on the similar twist angles in the optimized geometries. The results suggest that the optimized structures are good models for the molecular geometry in solution. The fluorescence spectra of the solutions show λ_{max} ~ 500 nm indicating nearly green emission from both molecules. The quantum yields[34] for the fluorescence from the solutions are extremely low (Table 2.3). Electronic absorption and fluorescence emission of BBEDQ and BPEDQ in the solid state are shown in Fig. 2.8. The absorption spectra and the λ_{max}

Table 2.3. *Peak maximum (λ_{max}), quantum yield (ϕ) and average lifetime (τ) for fluorescence emission from BBEDQ and BPEDQ in acetonitrile solution and solid states.*

System	Parameter	BBEDQ	BPEDQ
Solution	λ_{max} (nm)	507	503
	ϕ	0.001	0.001
	τ (ns)	< 0.2	< 0.2
Solid	λ_{max} (nm)	474	462
	ϕ	0.40	0.41
	τ (ns)	2.05	1.76

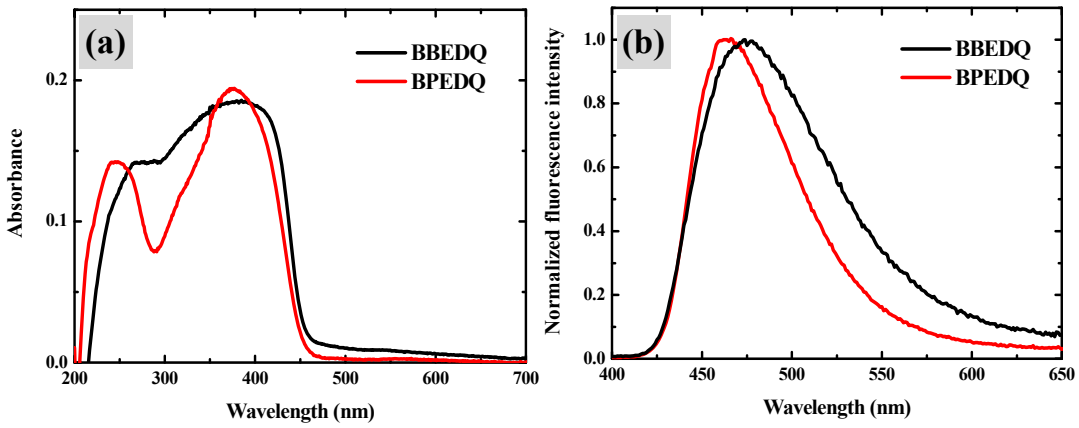

Figure 2.8. ***(a)*** *Electronic absorption and* ***(b)*** *fluorescence emission spectra of BBEDQ and BPEDQ in the solid state (λ_{exc} = 365 nm).*

(Table 2.2) of BPEDQ exhibit a clear blue shift with respect to BBEDQ as expected based on their twist angles.[27] The values computed for the molecular geometry from the respective crystal structures are consistent with the observed peak positions and the relative shift; significantly, they show also the expected blue shift with respect to the values computed for the optimized geometry relevant to the molecular structure in solution. Both absorption spectra show broad peaks possibly due to the intermolecular interactions in the solid state. The multiple excitations likely to be involved are revealed by the deconvolution of the spectra (Fig. 2.9); the positions of the charge transfer peaks obtained from the deconvolution are listed in Table 2.2. The fluorescence spectra of BBEDQ and BPEDQ show λ_{max} at 474 nm and 462 nm respectively, once again consistent with the expected trends in the energy gaps. The solid state absorption as well as emissions spectra of BBEDQ are broader than that of BPEDQ suggesting stronger excitonic interactions in the former. This scenario is supported by the relatively more effective π-π interactions between the chromophores likely to be present in BBEDQ than in BPEDQ (Fig. 2.4b, 2.5b) as indicated by the centroid-centroid distance and interplanar angles between the closest benzenoid rings of the DADQ unit,

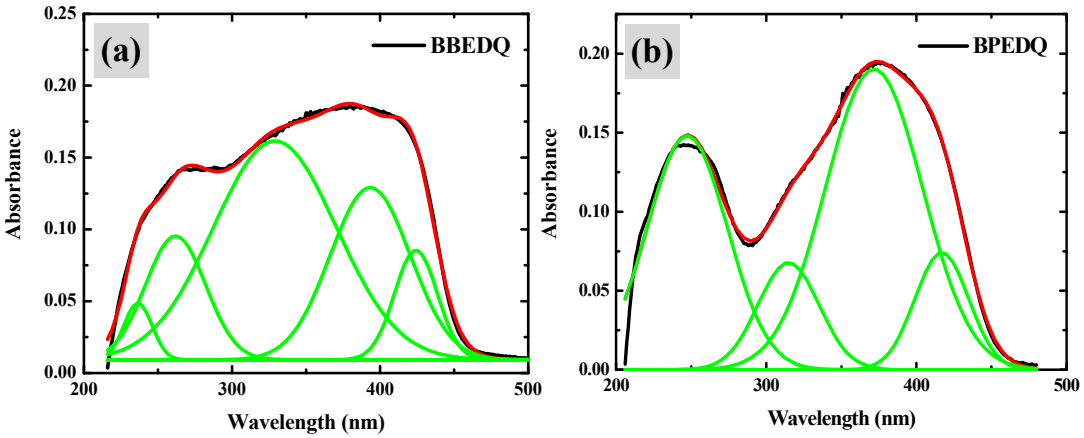

Figure 2.9. *Deconvolution of the solid state absorption spectra of* ***(a)*** *BBEDQ and* ***(b)*** *BPEDQ.*

5.535 Å and 0^o respectively in BBEDQ and 5.691 Å and 52.8^o respectively in BPEDQ. The normalized absorption and fluorescence emission spectra of BBEDQ and BPEDQ solutions show a close to mirror-image relationship; it is not so clear in the case of solids due to the broader absorption peak (Fig. 2.10). The Stokes shift is relatively smaller in the solid than in solution implying less excited state relaxation in the former. There is appreciable similarity between the fluorescence excitation and absorption spectra in the solid and solution states. Based on all these observations it can be inferred that the fluorescence emission occurs primarily from the same state to which absorption occurs in the solid, but there is excited state relaxation in the solution.

The most significant observation in this study is the enhanced intensity of the fluorescence in the solid state compared to the solution (Fig. 2.11); it should be noted that the fluorescence spectra are recorded for samples of same optical density in each case. As waveguide effects in the solid samples are not accounted for in these spectra, the spectra represent an underestimate of the solid state enhancement factor. The enhancement is more accurately reflected in the quantum yield measured for BBEDQ and BPEDQ in the solution and solid states (Table 2.3); the enhancement factor in the solid state is ~ 400 in both compounds. As mentioned earlier, the basis of the enhanced fluorescence is most likely the inhibition of the excited state geometry relaxation to a non-radiative state in the rigid solid structure (Fig. 2.2). The excited state lifetimes in the solids are 2.05 and 1.76 ns for BBEDQ and BPEDQ respectively (Fig. 2.12). These values are considerably higher than that in the respective solutions, consistent with the observed fluorescence enhancement and the proposed mechanism. In the present systems, the solid state emission color is moved well into the blue-green region (Fig. 2.13); the shift from the green emission of the earlier systems is clearly illustrated by the comparison with the case of 7,7-bis(N-methylpiperazino)-8,8-dicyanoquinodimethane

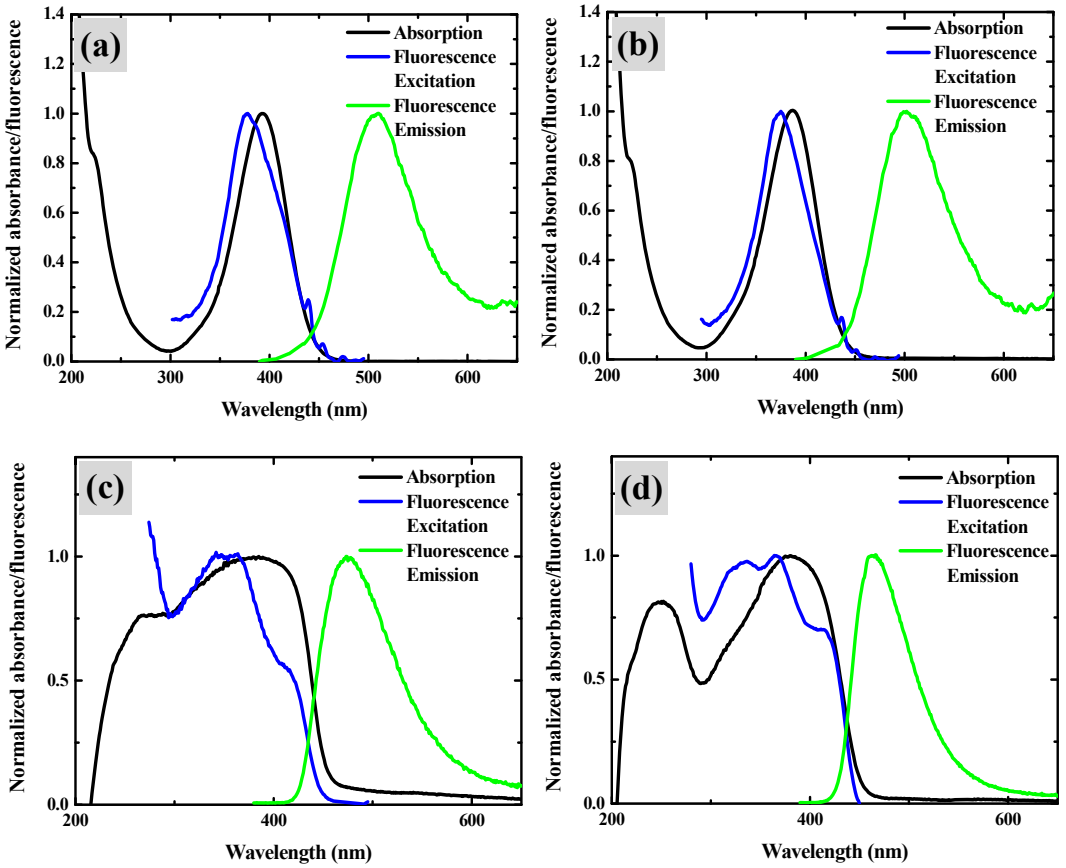

Figure 2.10. *Normalized absorption, fluorescence excitation and fluorescence emission spectra of BBEDQ and BPEDQ:* ***(a)****,* ***(b)*** *in acetonitrile solution, and* ***(c)****,* ***(d)*** *in solid state respectively.*

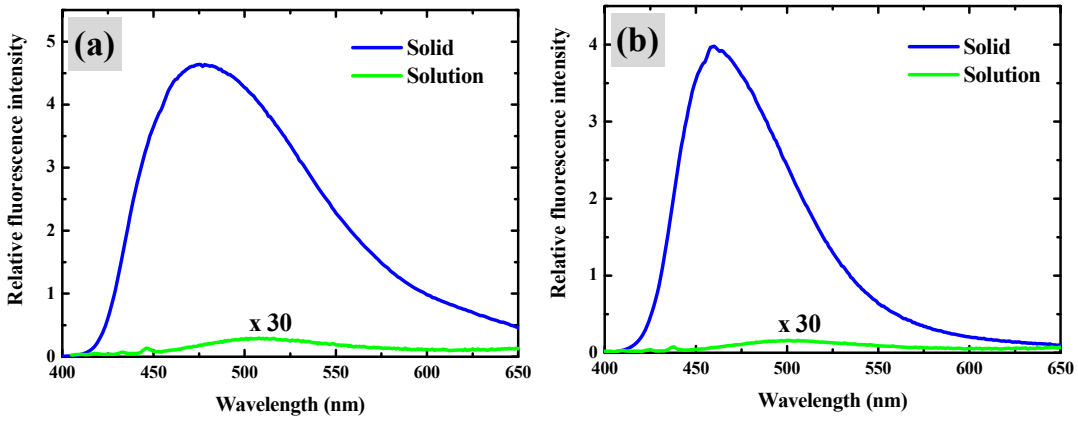

Figure 2.11. *Fluorescence spectra showing the relative intensities of fluorescence emission in acetonitrile solution and solid states of* ***(a)*** *BBEDQ and* ***(b)*** *BPEDQ; note the enlargement of the solution spectra.*

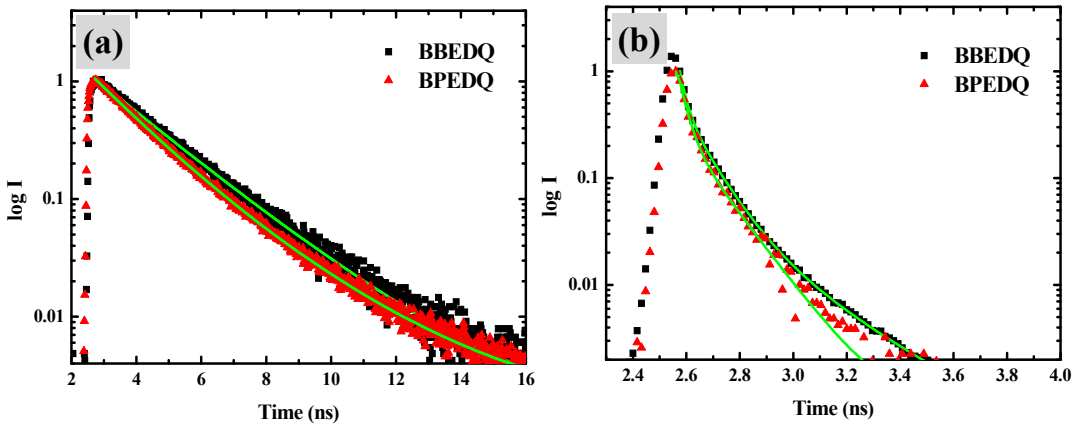

Figure 2.12. *Fluorescence emission decay profiles of BBEDQ and BPEDQ in* ***(a)*** *solid and* ***(b)*** *acetonitrile solution.*

(BMPDQ) reported in Ref. 5. It is also notable that the small blue shift of the fluorescence peak leads to improvement in the CIE coordinates from (0.164, 0.307) in BBEDQ to (0.144, 0.228) in BPEDQ. The study of BBEDQ and BPEDQ unravels an interesting scenario wherein small structural modifications result in subtle changes in the materials responses suggesting possible pathways for further design and optimization.

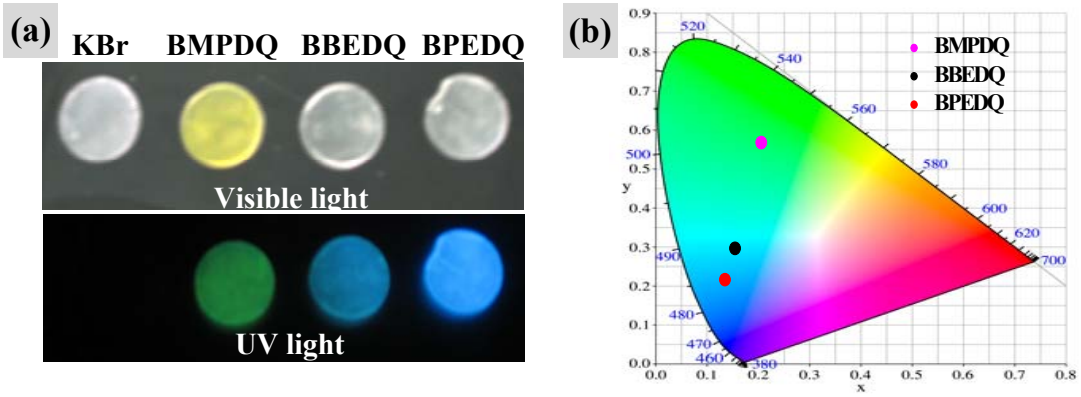

Figure 2.13. ***(a)*** *Photographs of pellets of pure KBr and KBr pellets with BMPDQ, BBEDQ and BPEDQ, under visible and UV (365 nm) light and* ***(b)*** *the CIE chromaticity coordinates of the compounds.*

As noted in the Introduction, there are only limited reports of molecular crystals emitting in the blue and blue-green region with high quantum efficiency. Molecules such as 4,4′-bis(1,2,2-triphenylvinyl)biphenyl,[9] 1,4-bis(alkenyl)-2,5-dipiperidinobenzenes,[10] cis-4,4′-bis(diarylamino)stilbene/fluorene hybrids[13] and tetraphenylmethane derivatives[20] do satisfy these criteria well. However they are relatively complex molecules requiring multi-step synthesis; no crystallographic structural information is available in most cases. Even though 9-anthrylpyrazole derivatives[12] are better in these respects, the thermal stabilities are poor except for one case, possibly due to the solvent molecules in the crystal lattice. The low solubility in the case of molecules like dipyrenylbenzenes[15] is a limiting factor for various applications involving thin film fabrication. DADQ derivatives possess the advantages of simplicity of synthesis with relatively good yields from easily available precursors, amenability to structural variations, easy crystallization, good thermal stability, and high solubility in common organic solvents and in some cases even aqueous medium. Potential requirements for amorphous solids can be met by the incorporation of long alkyl chains on the amino moiety,[35] and as shown in chapters 4 and 5 by other suitable substituents. Therefore the efficient emission of the DADQ systems in the blue-green range is of great interest from the fundamental and application perspectives.

2.3. Exploration of More DADQ Derivatives

The detailed studies on BBEDQ and BPEDQ prompted us to explore more derivatives of DADQ's having primary amine substituents, with a view to developing strongly blue-emitting molecular crystals. The groups of derivatives that we have synthesized and fully characterized are shown in Fig. 2.14. We have investigated their crystal structures and carried out basic spectroscopic measurements to probe the

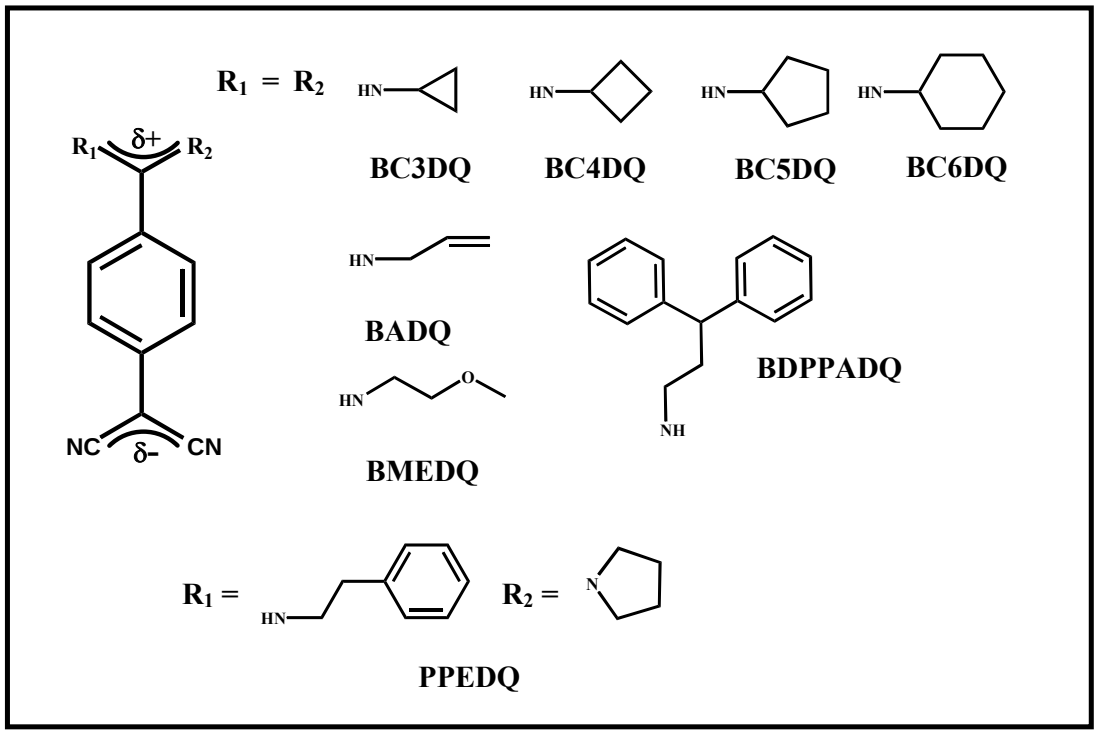

Figure 2.14. *New DADQ derivatives synthesized, and exhibiting strong fluorescence emission in the solid state, in the blue-green region.*

fluorescence emission characterization.

2.3.1 *Synthesis and characterization*

The molecules were synthesized following the same protocol as described in Sec. 2.2.1 for BBEDQ and BPEDQ. In the case of the asymmetrically substituted molecules PBEDQ, the synthesis was carried out in two steps (the detailed protocol is similar to what will be discussed in Sec. 5.2.1). Characterization of each molecule is listed below.

7,7-bis(cyclopropylamino)-8,8-dicyanoquinodimethane (BC3DQ): Yield = 66%; M.P. (^{o}C) = 205 - 210; FTIR (KBr) : $\bar{\upsilon}$/cm^{-1} = 2173.9, 2131.5, 1601.0; ^{1}H-NMR (d_6-DMSO) : δ/ppm = 9.36 (s, 1H), 8.96 (s, 1H), 7.32 (s, 2H), 7.92 (d, 2H), 2.92 (s, 1H), 2.56 (d, 1H), 0.69 (m, 8H).

***7,7-bis(cyclobutylamino)-8,8-dicyanoquinodimethane (BC4DQ)*:** Yield = 84%; M.P. (^{o}C) = 238 - 240; FTIR (KBr) : $\bar{\upsilon}$/cm^{-1} = 2177.8, 2129.6, 1616.5, 1597.2; ^{1}H-NMR (d_6-DMSO) : δ/ppm = 9.44 (s, 1H), 8.54 (s, 1H), 7.13 (d, 2H), 6.83 (d, 2H), 4.20 (s, 1H), 3.90 (s, 1H), 2.00 (m, 12H).

***7,7-bis(cyclopentylamino)-8,8-dicyanoquinodimethane (BC5DQ)*:** Yield = 32%; M.P. (^{o}C) = 240 - 248; FTIR (KBr) : $\bar{\upsilon}$/cm^{-1} = 2185.5, 2133.4, 1626.3, 1604.9 ; ^{1}H-NMR (d_6-DMSO) : δ/ppm = 9.14 (d, 1H), 8.35 (d, 1H), 7.16 (d, 2H), 6.83 (d, 2H), 4.22-4.00 (m, 1H), 3.85-3.70 (m, 1H), 2.05-1.45 (m, 16H)

***7,7-bis(allylamino)-8,8-dicyanoquinodimethane (BADQ)*:** Yield = 70%; M.P. (^{o}C) = 220 - 223; FTIR (KBr) : $\bar{\upsilon}$/cm^{-1} = 2175.90, 2127.68, 1597.20; ^{1}H-NMR (d_6-DMSO) : δ/ppm = 9.505(s, 1H), 8.807(s, 1H), 7.217(d, 2H), 6.821(d, 2H), 5.901 (m, 4H), 4.025 (s, 2H), 3.889 (s, 2H).

***7,7-bis(2-methoxyethylamino)-8,8-dicyanoquinodimethane (BMEDQ)*:** Yield = 65%; M.P. (^{o}C) = 151-154; FTIR (KBr) : $\bar{\upsilon}$/cm^{-1} = 2175.3, 2142.4, 1117.8; ^{1}H-NMR (d_6-DMSO) : δ/ppm = 9.29 (brs, 1H), 8.60 (brs, 1H), 7.22 (d, 2H), 6.82 (d, 2H), 3.61-3.51 (m, 5H), 3.49-3.37 (m, 5H), 3.23-3.15 (m, 4H).

***7,7-bis(3,3-biphenylpropylamino)-8,8-dicyanoquinodimethane (BDPPADQ)*:**
Yield = 90%; M.P. (^{o}C) = 252 - 256; FTIR (KBr) : $\bar{\upsilon}$/cm^{-1} = 3057.45, 2177.83, 2135.39 ; ^{1}H-NMR (d_6-DMSO) : δ/ppm = 9.21 (s, 1H), 8.50 (s, 1H), 7.37-7.7.10 (m, 24H), 6.75 (d, 2H), 4.12 (t, 1H), 3.78 (t, 1H), 3.19-3.11 (m, 4 H), 2.16 (m, 2H).

***7-pyrrolidino-7-(2-phenylethylamino)-8,8-dicyanoquinodimethane (PPEDQ)*:** Yield = 74%; M.P. (^{o}C) = 208 - 212; FTIR (KBr) : $\bar{\upsilon}$/cm^{-1} = 3024.7, 2186.3, 2136.9 ; ^{1}H-NMR (d_6-DMSO) : δ/ppm = 8.64 (brs, 1H), 7.32-7.19 (m, 3H), 7.05 (d, 2H), 6.85 (d, 2H), 6.77 (d, 2H), 3.46 (t, 2H), 3.35-3.30 (m, 2H), 3.23 (t, 2H), 2.75 (t, 2H), 2.00 (quin, 2H), 1.78 (quin, 2H).

2.3.2 *Crystal structure details*

The molecular structure and unit cell packing of the eight DADQ derivatives are presented in Fig 2.15-2.22 and crystallographic information is collected in Table 2.4. It is found that BC3DQ, BC4DQ and PPEDQ centrosymmetric lattice, whereas BC5DQ, BC6DQ, BADQ, BMEDQ and BDPPADQ form noncentrosymmetric ones. The latter are of interest in quadratic nonlinear optical applications. In fact we have found that BC5DQ and BADQ produce appreciable second harmonic generation upon 1064 nm laser irradiation. Since this was not the focus of our work, we have not investigated this area further. The basic DADQ framework is similar in all cases, with significant variation only in the dihedral twist angles τ. These angles are tabulated in Table 2.5. Strong intermolecular H-bonds between the amino and cyano groups, similar to those described in Sec. 2.2.2 are observed in all the crystals.

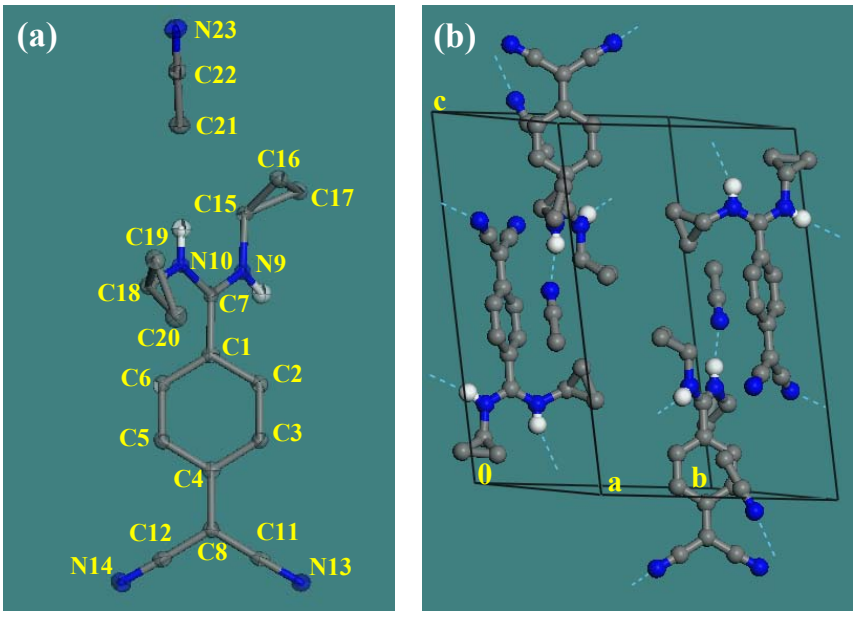

Figure 2.15. *Molecular and crystal structure of BC3DQ from single crystal x-ray analysis:* ***(a)*** *molecular structure and* ***(b)*** *unit cell. H atoms not involved in H-bonds are omitted for clarity; C (grey), N (blue), H (white), H-bonds (cyan broken line) are indicated.*

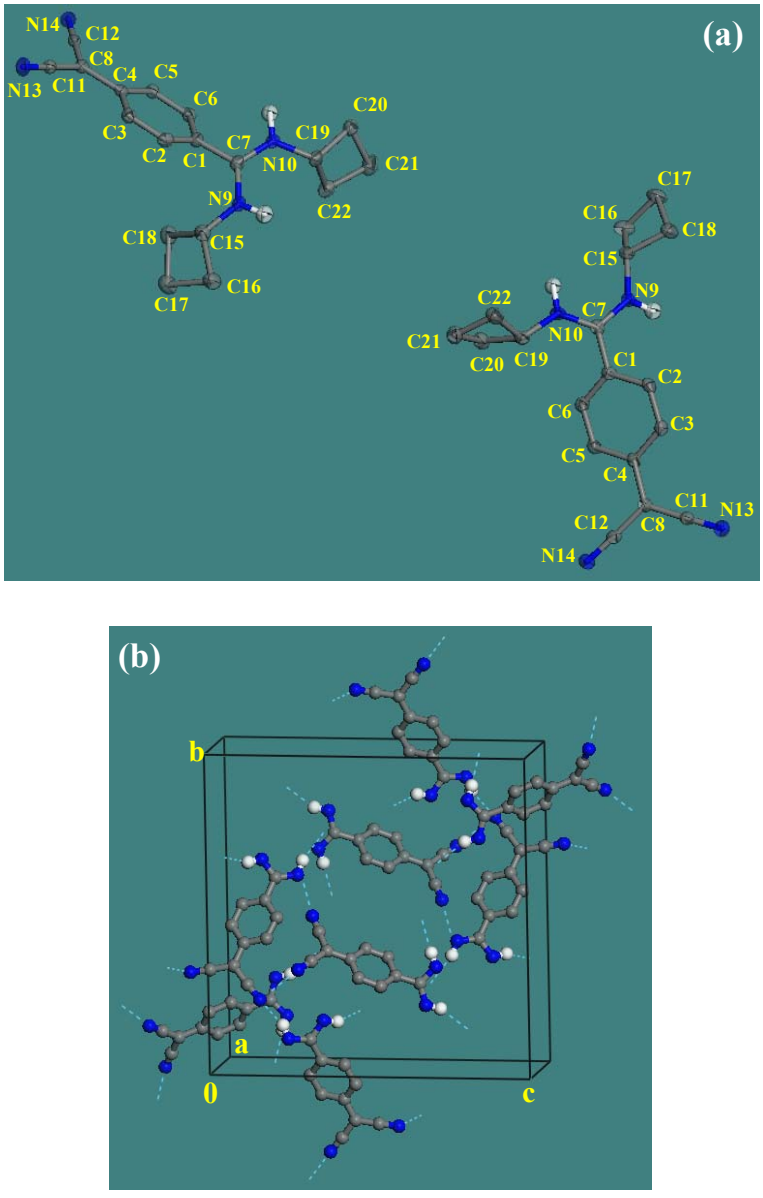

Figure 2.16. *Molecular and crystal structure of BC4DQ from single crystal x-ray analysis:* ***(a)*** *molecular structure and* ***(b)*** *unit cell. H atoms not involved in H-bonds[in (a) and (b)] and the cyclobutyl group [in (b)] are omitted for clarity; C (grey), N (blue), H (white), H-bonds (cyan broken line) are indicated.*

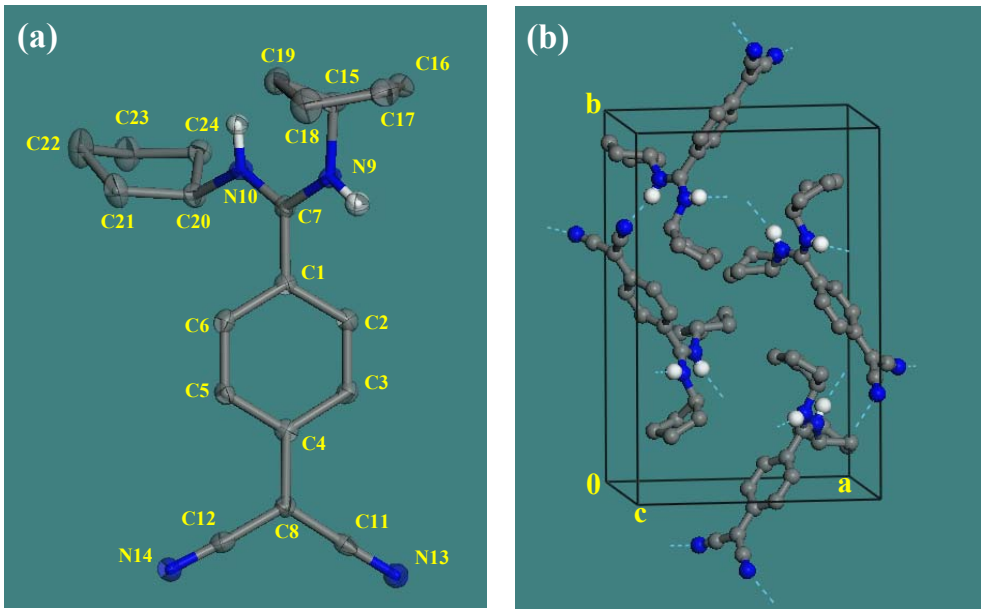

Figure 2.17. *Molecular and crystal structure of BC5DQ from single crystal x-ray analysis:* ***(a)*** *molecular structure and* ***(b)*** *unit cell. H atoms not involved in H-bonds are omitted for clarity; C (grey), N (blue), H (white), H-bonds (cyan broken line) are indicated.*

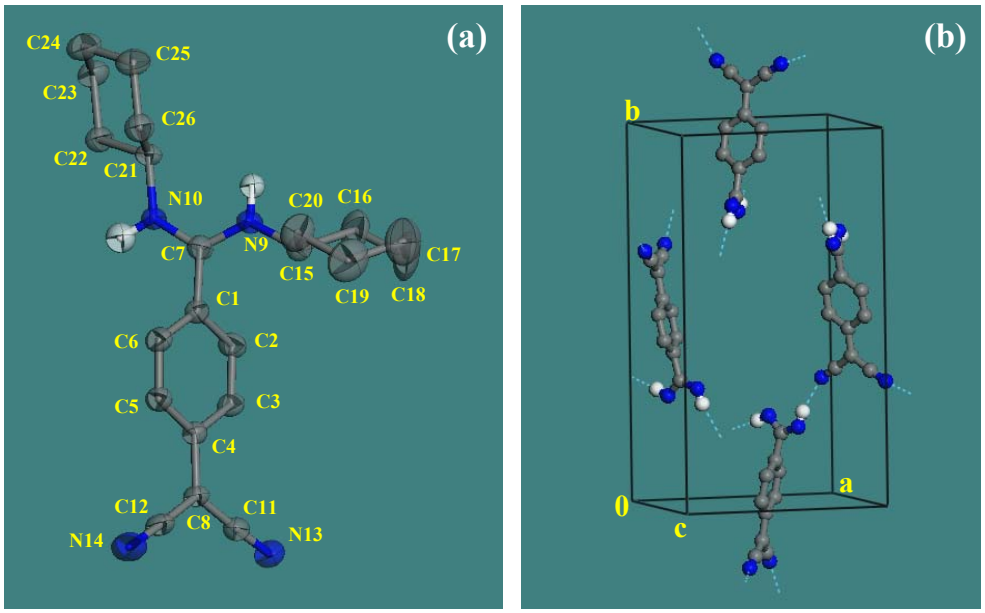

Figure 2.18. *Molecular and crystal structure of BC6DQ from single crystal x-ray analysis:* ***(a)*** *molecular structure and* ***(b)*** *unit cell. H atoms not involved in H-bonds [in (a) and (b)] and the cyclohexyl group [in (b)] are omitted for clarity; C (grey), N (blue), H (white), H-bonds (cyan broken line) are indicated.*

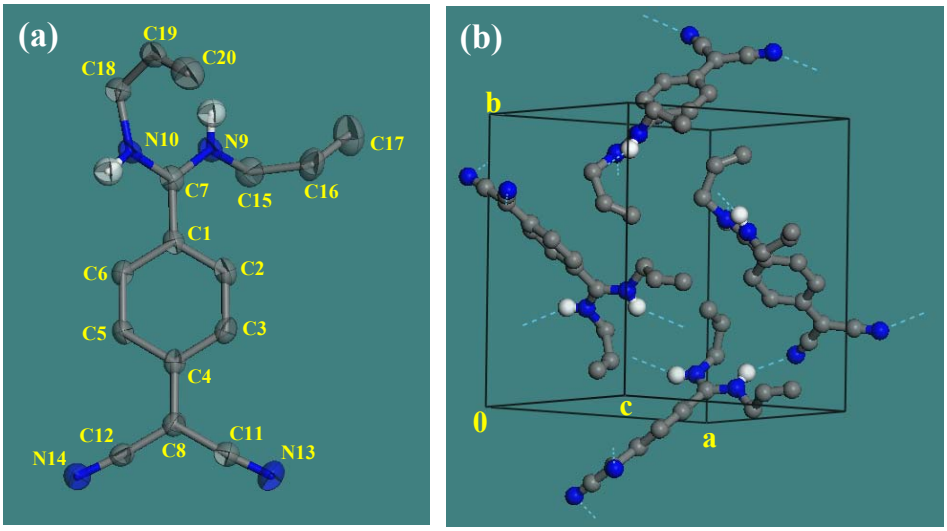

Figure 2.19. *Molecular and crystal structure of BADQ from single crystal x-ray analysis:* ***(a)*** *molecular structure and* ***(b)*** *unit cell. H atoms not involved in H-bonds are omitted for clarity; C (grey), N (blue), H (white), H-bonds (cyan broken line) are indicated.*

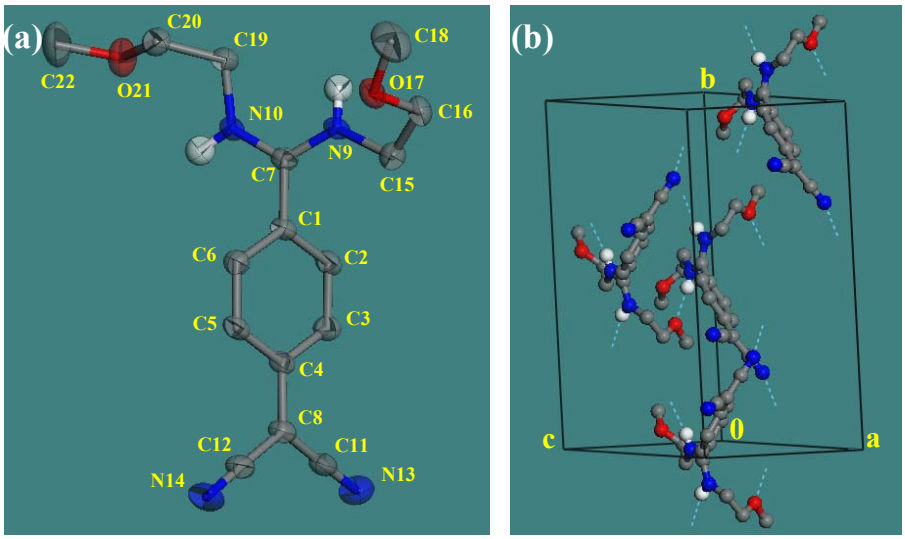

Figure 2.20. *Molecular and crystal structure of BMEDQ from single crystal x-ray analysis:* ***(a)*** *molecular structure and* ***(b)*** *unit cell. H atoms not involved in H-bonds are omitted for clarity; C (grey), O (red), N (blue), H (white), H-bonds (cyan broken line) are indicated.*

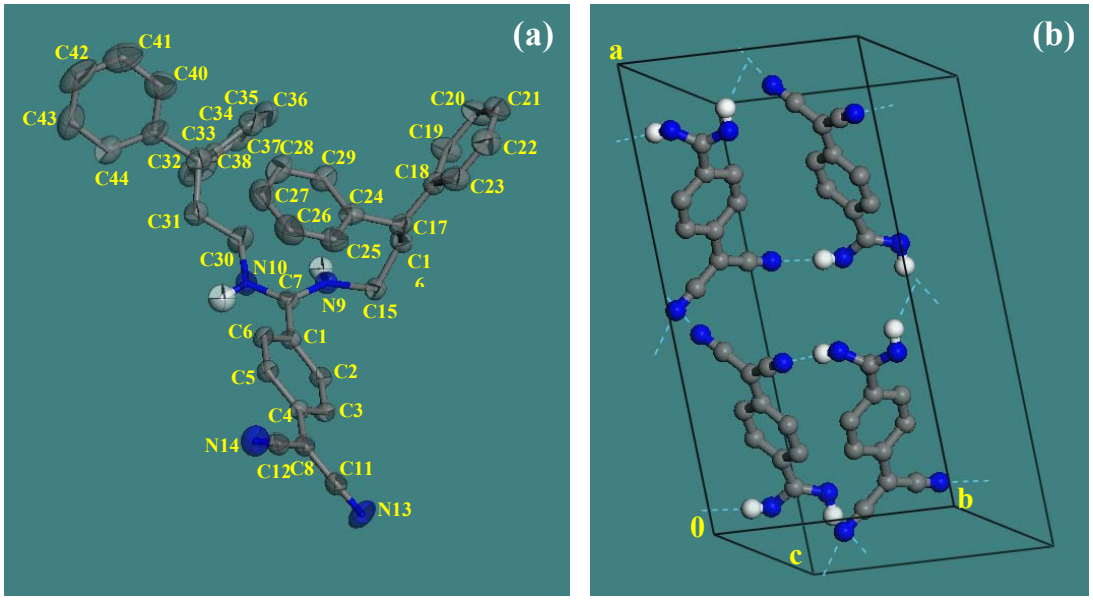

Figure 2.21. *Molecular and crystal structure of BDPPADQ from single crystal x-ray analysis:* ***(a)*** *molecular structure and* ***(b)*** *unit cell. H atoms not involved in H-bonds [in (a) and (b)] and carbon atoms on amine group [in (b)] are omitted for clarity; C (grey), N (blue), H (white), H-bonds (cyan broken line) are indicated.*

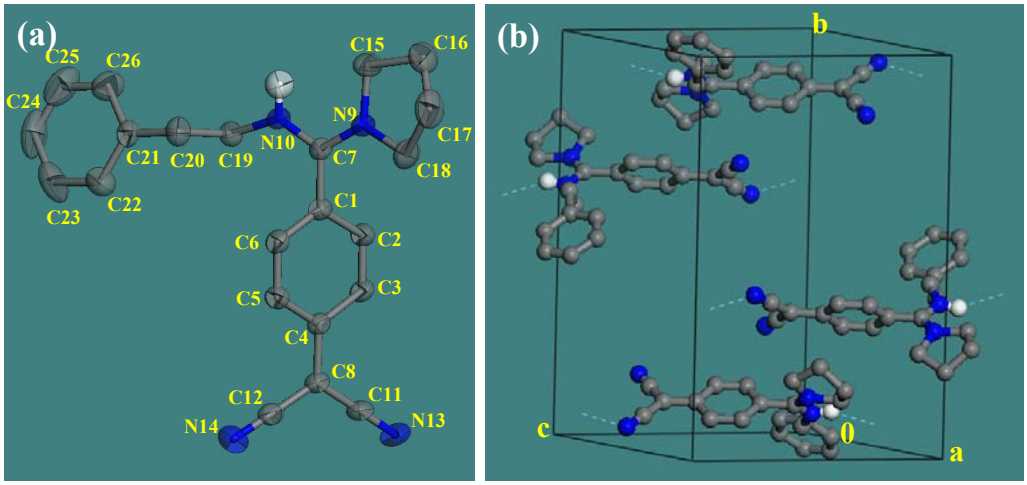

Figure 2.22. *Molecular and crystal structure of PPEDQ from single crystal x-ray analysis:* ***(a)*** *molecular structure and* ***(b)*** *unit cell. H atoms not involved in H-bonds are omitted for clarity; C (grey), N (blue), H (white), H-bonds (cyan broken line) are indicated.*

Table 2.4. *Crystallographic data for DADQ molecules.*

	BC3DQ	**BC4DQ**	**BC5DQ**	**BC6DQ**
Empirical formula	$C_{18}H_{19}N_5$	$(C_{18}H_{20}N_4)_2$	$C_{20}H_{24}N_4$	$C_{22}H_{28}N_4$
Crystal system	Monoclinic	Monoclinic	Orthorhombic	Orthorhombic
Space group	$P2_1/c$	$P2_1/c$	$Pna2_1$	$Pna2_1$
a / Å	8.4964(8)	9.2278(19)	11.4335(14)	10.769(3)
b / Å	13.0741(12)	18.643(4)	17.368(2)	19.652(5)
c / Å	16.0860(14)	19.314(4)	9.2392(11)	9.393(3)
β / deg.	104.178(1)	98.896(3)	90.0	90.0
V / Å^3	1732.4(3)	3282.6(12)	1834.7(4)	1987.8(9)
Z	4	4	4	4
$\rho_{calc.}$ / g cm^{-3}	1.171	1.183	1.160	1.164
μ / cm^{-1}	0.73	0.73	0.71	0.70
Temperature / K	298(2)	100(2)	100(2)	100(2)
λ / Å	0.71073	0.71073	0.71073	0.71073
No. of reflections	3035	5793	3209	3519
No. of parameters	241	413	233	249
Max., Min. transmission	0.9913,0.9713	0.9828,0.9715	0.9805,0.9589	0.992, 0.973
GOF	1.052	1.053	1.062	1.076
R [for $I \geq 2\sigma_I$]	0.0717	0.0477	0.0357	0.0325
wR^2	0.1975	0.1225	0.0895	0.0787
Largest difference peak and hole / eÅ^{-3}	0.267/-0.373	0.296/-0.203	0.280/-0.203	0.162/-0.189

	BADQ	**BMEDQ**	**BDPPADQ**	**PPEDQ**
Empirical formula	$C_{16}H_{16}N_4$	$C_{16}H_{20}N_4O_2$	$C_{40}H_{36}N_4$	$C_{22}H_{22}N_4$
Crystal system	Orthorhombic	Monoclinic	Monoclinic	Monoclinic
Space group	*Pna2₁*	*C_C*	*C2*	*P2₁/c*
a / Å	11.905(7)	12.7001(12)	20.202(10)	10.1985(12)
b / Å	12.592(8)	18.5779(10)	9.455(5)	17.733(2)
c / Å	9.554(6)	8.4195(9)	19.470(9)	11.2140(13)
β / deg.	90.0	125.159(15)	120.456(7)	113.260(2)
V / Å^3	1432.2(15)	1624.1(2)	3206(3)	1863.2(4)
Z	4	4	4	4
$\rho_{calc.}$ / g cm^{-3}	1.226	1.228	1.187	1.221
μ / cm^{-1}	0.76	0.84	0.70	0.74
Temperature / K	298(2)	298(2)	298 (2)	298 (2)
λ / Å	0.71073	0.71073	0.71073	0.71073
No. of reflections	2444	1897	5663	3291
No. of parameters	189	201	411	235
Max., Min. transmission	0.994, 0.979	0.993, 0.972	0.9848, 0.9780	0.991, 0.988
GOF	1.170	1.093	1.035	1.061
R [for $I \geq 2\sigma_I$]	0.0717	0.0310	0.0469	0.0565
wR^2	0.1091	0.0744	0.1231	0.1380
Largest difference peak and hole / eÅ^{-3}	0.134/-0.145	0.132/-0.178	0.414/-0.157	0.163/-0.150

2.3.3 *Tuning of the fluorescence emission color in DADQ derivatives*

The absorption and fluorescence emission peak position of the solid samples of the eight DADQ derivatives are collected in Table 2.5. The absorption appears in the broad range 300 to 440 nm for all the compounds. However, the emission λ_{max} vary from 474 to 440 nm. Combined with the other derivatives reported from our lab earlier, which show emission in the red and green region, the fluorescence of DADQ's can be varied across nearly the full visible range.

The CIE chromaticity coordinates which represents the visible emission colors of the eight DADQ derivatives developed in the present study are shown in Fig. 2.23. The coordinates of BBEDQ, BPEDQ and BMPDQ[5] from Fig. 2.13b are also included to illustrate the broad range and continuous variation achieved using the new DADQ discussed in this chapter. The most significant result is that some of the derivatives show strong solid state emission in a nearly exact blue region (for example, CIE coordinates of BC5DQ are 0.1665, 0.0885). It is also quite remarkable that with the same fluorophore systems, and only peripheral structural changes we are able to tune the emission over a wide range.

We have attempted to explore potential correlations between the observed emission wavelengths and efficiency on the one hand and the molecular structural and assembly patterns on the other. However, the factors that lead to the observed emission characteristics appear to be quite complex and may require several parameters including the mechanical properties of the crystals, their densities etc. to be taken into account. Explorations in such directions are currently under way in our laboratory.

Table 2.5. *Absorption wavelength range, fluorescence emission maximum, quantum yield and average dihedral angles in crystals of the DADQ derivatives.*

Crystal	Absorption wavelength range (nm)	Fluorescence emission maximum λ_{max} (nm)	Quantum yield (%)	Average dihedral angles τ (°)
BBEDQ	300-435	474	40	46.3
BADQ	330-420	473	21	42.3
BC4DQ	300-435	463	33	39.7, 50.2 #
BC6DQ	300-430	463	10	55.9
BPEDQ	315-427	463	41	38.0
PPEDQ	326-423	461	56	54.8
BC3DQ	317-436	459	*	49.7
BMEDQ	320-412	453	17	51.0
BDPPADQ	300-435	450	24	43.1
BC5DQ	300-438	440	25	52.9

* The crystalline powder degrades slowly due to loss of solvent during the sample preparation and measurement.

\# for the two molecules in the asymmetric unit

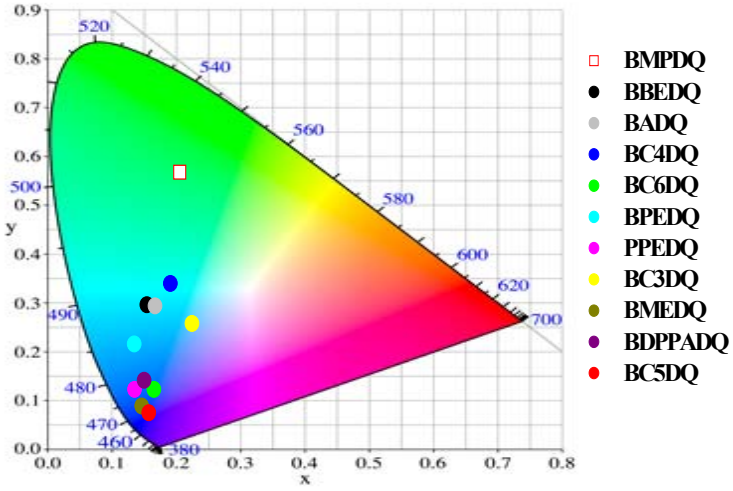

Figure 2.23. *CIE chromaticity coordinates of the various DADQ compounds*

2.4. Conclusions

Zwitterionic diaminodicyanoquinodimethanes are versatile molecules that form crystalline and stable materials exhibiting strong fluorescence in the solid state. In the present study, we have developed new derivatives that exhibit strong light emission, blue shifted with respect to that reported in earlier studies from our laboratory and other research groups; the quantum yields of the solids are high (~ 0.40), strongly enhanced with respect to that of their solution (~ 0.001). Crystallographic investigations reveal the molecular structural features that impact upon the spectroscopic properties. Semiempirical quantum chemical computations provide a platform to understand the observed optical responses of the molecules in solution and in the solid state in the context of the molecular structural features and solid state packing effects. Explorations of a large class of novel derivatives lead to the realization of crystalline solids exhibiting strong emission over a wide blue-green range.

References

1. a) W. E. David, B. S. Solomon, *J. Phys. Chem.* **1967**, *71*, 4467. b) M. V. Auweraer, B. Verschuere, F. C. D Schryver, *Langmuir* **1988**, *4*, 583. c) P. K. Yi, Z. Fang, B. Liu, *Adv. Func. Mater.* **2008**, *18*, 1321.
2. a) J. Luo, Z. Xie, J. W. Y. Lam, L. Cheng, H. Chen, C. Qiu, H. S. Kwok, X. Zhan, Y. Liu, D. Zhu, B. Z. Tang, *Chem. Commun*. **2001**, 1740. b) Y. Hong, J. W. Y. Lam, B. Z. Tang, *Chem. Commun*. **2009**, 4332.
3. a) B. K. An, S. K. Kwon, S. D. Jung, S. Y. Park, *J. Am. Chem. Soc.* **2002**, *124* 14410. b) T. Hirose, K. Matsuda, *Chem. Commun.* **2009**, 5832.
4. J. N. Wilson, M. D. Smith, V. Enkelmann, U. H. F. Bunz, *Chem. Commun.* **2004**, 1700.
5. S. Jayanty, T. P. Radhakrishnan, *Chem. Eur. J.* **2004**, *10*, 791.
6. a) D. Bloor, Y. Kagawa, M. Szablewski, M. Ravi, S. J. Clark, G. H. Cross, L. Pålsson, A. Beeby, C. Parmer, G. Rumbles, *J. Mater. Chem.* **2001**, *11*, 3053. b) M. Szablewski, D. Bloor, Y. Kagawa, R. Mosurkal, J. M. Cole, S. J. Clark, G. H. Cross, L. Pålsson, *J. Phys. Org. Chem.* **2006**, *19*, 206.
7. R. Davis, N. S. S. Kumar, S. Abraham, C. H. Suresh, N. P. Rath, N. Tamaoki, S. Das, *J. Phys. Chem. C.* **2008**, *112*, 2137.
8. Y. Dong, J. W. Y. Lam, A. Qin, J. Liu, Z. Li, B. Z. Tang, J. Sun, H. S. Kwok, *Appl. Phys. Lett.* **2007**, *91*, 011111-1.
9. Z. Zhao, S. Chen, X. Shen, F. Mahtab, Y. Yu, P. Lu, J. W. Y. Lam, H. S. Kwok, B. Z. Tang, *Chem. Commun.* **2010**, *46*, 686.
10. M. Shimizu, Y. Takeda, M. Higashi, T. Hiyama, *Angew. Chem. Int. Ed.* **2009**, *48*, 3653.
11. J. K. Park, K. H. Lee, J. S. Park, J. H. Seo, Y. K. Kim, S. S. Yoon, *Mol. Cryst. Liq. Cryst.* **2010**, *531*, 55.
12. Z. Zhang, Y. Zhang, D. Yao, H. Bi, I. Javed, Y. Fan, H. Zhang, Y. Wang, *Cryst. Growth Des.* **2009**, *9*, 5069.
13. Y. Wei, C. Chen, *J. Am. Chem. Soc.* **2007**, *129*, 7478.

14. S. Jiao, Y. Liao, X. Xu, L. Wang, G. Yu, L. Wang, Z. Su, S. Ye, Y. Liu, *Adv. Funct. Mater.* **2008**, *18*, 2335.
15. K. Wu, P. Ku, C. Lin, H. Shih, F. Wu, M. Huang, J. Lin, I. Chen, C. Cheng, *Adv. Funct. Mater.* **2008**, *18*, 67.
16. K. H. Lee, J. N. You, H. J. Kwon, Y. K. Kim, S. S. Yoon, *Mol. Cryst. Liq. Cryst.* **2010**, *530*, 48.
17. Y. Mizobe, T. Hinoue, A. Yamamoto, I. Hisaki, M.Miyata, Y. Hasegawa, N. Tohnai, *Chem. Eur. J.* **2009**, *15*, 8175.
18. S. Park, M. Ebihara, Y. Kubota, K. Funabiki, M. Matsui, *Dyes Pigments* **2009**, *82*, 258.
19. I. Wang, E. Botzung-Appert, O. Stéphan, A. Ibanez, P. L. Baldeck, *J. Opt. A* **2002**, *4*, S258.
20. H. Yeh, R. Lee, L. Chan, T. J. Lin, C. Chen, E. Balasubramaniam, Y. Tao, *Chem. Mater.* **2001**, *13*, 2788.
21. a) S. Park, O. Kwon, S. Kim, S. Park, M. Choi, M. Cha, S. Y. Park, D. Jang, *J. Am. Chem. Soc.* **2005**, *127*, 10070. b) Z. Li, Y. Dong, B. Mi, Y. Tang, M. Häussler, H. Tong, Y. Dong, J. W. Y. Lam, Y. Ren, H. H. Y. Sung, K. S. Wong, P. Gao, I. D. Williams, H. S. Kwok, B. Z. Tang, *J. Phys. Chem. B* **2005**, *109*, 10061. c) B. J. Liddle, R. M. Silva, T. J. Morin, F. P. Macedo, R. Shukla, S. V. Lindeman, J. R. Gardinier, *J. Org. Chem.* **2007**, *72*, 5637. d) Y. Ooyama, H. Egawa, T. Mamura, K. Yoshida, *Tetrahedron* **2008**, *64*, 7219. e) X. Cai, R. M. Adhikari, K. C. Anyaogu, S. S. Palayangoda, L. A. Estrada, P. K. De, D. C. Neckers, *J. Am. Chem. Soc.* **2009**, *131*, 1648.
22. C. G. Chandaluri, A. Patra, T. P. Radhakrishnan, *Chem. Eur. J.* **2010**, *16*, 8699.
23. A. Patra, N. Hebalkar, B. Sreedhar, M. Sarkar, A. Samanta, T. P. Radhakrishnan, *Small* **2006**, *2*, 650.
24. A. Patra, N. Hebalkar, B. Sreedhar, T. P. Radhakrishnan, *J. Phys. Chem. C* **2007**, *111*, 16184.
25. A. Patra, T. P. Radhakrishnan, *Chem. Eur. J.* **2009**, *15*, 2792.

26. a) M. Ravi, D. N. Rao, S. Cohen, I. Agranat, T. P. Radhakrishnan, *J. Mater. Chem.* **1996**, *6*, 1119. b) M. Ravi, D. N. Rao, S. Cohen, I. Agranat, T. P. Radhakrishnan, *J. Mater. Chem.* **1996**, *6*, 1853. c) M. Ravi, D. N. Rao, S. Cohen, I. Agranat, T. P. Radhakrishnan, *Chem. Mater.* **1997**, *9*, 830. d) M. Ravi, P. Gangopadhyay, D. N. Rao, S. Cohen, I. Agranat, T. P. Radhakrishnan, *Chem. Mater.* **1998**, *10*, 2371. e) S. Jayanty, T. P. Radhakrishnan, *Chem. Mater.* **2001**, *13*, 2460. f) S. Jayanty, P. Gangopadhyay, T. P. Radhakrishnan, *J. Mater. Chem.* **2002**, *12*, 2792. g) S. Jayanty, T. P. Radhakrishnan, *Chem. Eur. J.* **2004**, *10*, 2661.

27. P. Gangopadhyay, M. Ravi, T. P. Radhakrishnan, *Ind. J. Chem.* **2000**, *39A*, 106.

28. a) M. Ravi, T. P. Radhakrishnan, *J. Phys. Chem.* **1995**, *99*, 17624. b) T. P. Radhakrishnan, *Acc. Chem. Res.* **2008**, *41*, 367.

29. Synthesis of BBEDQ is mentioned in US Patent No. 3115506 19631224, **1963**; however, no structural data or optical properties are reported.

30. W. R. Hertler, H. D. Hartzler, D. S. Acker, R. E. Benson, *J. Am. Chem. Soc.* **1962**, *84*, 3387.

31. PowderCell for Windows Version 2.4, W. Kraus and G. Nolze.

32. a) MS Modeling Version 5.5.0.0 (Materials Studio), Accelrys Inc. b) VAMP Version 10.0, T. Clark, A. Alex, B. Beck, F. Burkhardt, J. Chandrasekhar, P. Gedeck, A. Horn, M. Hutter, B. Martin, G. Rauhut, W. Sauer, T. Schindler, T. Steinke; Erlangen, **2003**.

33. a) Y. A. Mantz, R, L. Musselman, *Inorg. Chem.* **2002**, *41*, 5770. b) A. G. Eshimbetov, E. L. Kristallovich, N. D. Abdullaev, T. S. Tulyaganov, Kh. M. Shakhidoyatov, *Spectrochim. Acta A* **2006**, *65*, 299. c) N. A. Murugan, S. Chakrabarti, H. Ågren, *J. Phys. Chem. B* **2011**, *115*, 4025. d) C. Cocchi, D. Prezzi, A. Ruini, M. J. Caldas, E. Molinari, *J. Phys. Chem. Lett.* **2011**, *2*, 1315. e) J. Gao, M. A. Loi, E. J. F. de Carvalho, M. C. dos Santos, *ACS Nano* **2011**, 5, 3993.

34. J. N. Demas, G. A. Crosby, *J. Phys. Chem.* **1971**, *75*, 991.

35. K. Rajesh, T. P. Radhakrishnan, *Chem. Eur. J.* **2009**, *15*, 2801.

Synopsis

A polyelectrolyte-assisted reprecipitation method is developed to fabricate nanoparticles of highly soluble molecules. The approach is demonstrated using a zwitterionic diaminodicyanoquinodimethane molecule bearing remote ammonium functionalities with high solubility in water as well as organic solvents. Nanoparticles are prepared by injecting its aqueous solutions containing an optimum concentration and relative amount of sodium poly(styrenesulfonate), into methanol. The strong fluorescence exhibited by the compound in the aggregated state is reflected in the enhanced fluorescence of the polyelectrolyte complex in water. The nanoparticles formed in the colloidal state manifest even stronger fluorescence leading to an overall enhancement of ~ 90 times over the aqueous solutions of the pure compound. The polyelectrolyte complexation allows tuning of the aggregation of the fluorophore molecules and hence their fluorescence response. The conditions for achieving the emission enhancement are optimized and a model for the molecular level interactions and aggregation effects is developed through a range of spectroscopy, microscopy and calorimetry investigations and control experiments.

3.1. Introduction

The enhanced fluorescence in the solid state exhibited by remote functionalized diaminodicyanoquinodimethanes investigated in our laboratory has been discussed in the previous chapter. The remote functionalities not only facilitate the induction of various intermolecular interactions, but also improve the solubility in aqueous and organic solvents.[1]

Several of the molecules exhibiting enhanced fluorescence in the bulk solid state

are also capable of strong light emission when formed as nanoparticles in the colloidal state.[2-4] Such luminescent nanomaterials are useful in applications like organic LED's, biological probes and sensors.[5] The size dependence of optical[6] and nonlinear optical[7] responses of molecular nano/microcrystals of bis(haloanilino)dicyanoquinodimethanes and the strong blue fluorescence of nanocrystals of tris(cyanophenyl)amine,[8] have been investigated in our laboratory earlier. The most general and widely used route to the formation of molecular nanocrystals is the reprecipitation technique, wherein the solution of the compound in a suitable solvent is rapidly injected into a nonsolvent, under vigorous stirring or ultrasonication.[9] This approach is unviable in the case of molecules such as the remote functionalized diaminodicyanoquinodimethanes that show appreciable solubility in most of the common solvents.[1] We have considered a solution to this problem, that may have broad applicability in similar situations with other molecules; it involves the introduction of a polyelectrolyte that can bind the diaminodicyanoquinodimethanes bearing ionic groups and impart the required level of insolubility in an appropriate medium. Such an approach also raises fundamental questions related to the interaction of dye molecules or their aggregates with polymers including biological macromolecules, and its impact on the optical responses of the resulting nanostructures. Macromolecules present in the nonsolvent during reprecipitation are known to modify the size, shape and agglomeration of microcrystals and affect their optical spectra.[10] Polyelectrolytes have been used to isolate fluorophores, for example in layer-by-layer assemblies, in order to circumvent self-quenching and enhance the fluorescence.[11] However, to the best of our knowledge, utilization of polyelectrolytes to induce the reprecipitation itself and the formation of molecular nanoparticles exhibiting strongly enhanced fluorescence, has not been demonstrated. This templating approach can also provide a route to tune the extent of

molecular aggregation and hence the materials responses.

We have chosen 7,7-bis(piperazinium)-8,8-dicyanoquinodimethane bis(*p*-toluenesulfonate) ($B^{2+}[T^-]_2$ or simply BT_2) and sodium poly(styrenesulfonate), (NaPSS) (Fig. 3.1) to explore the idea described above. Synthesis and crystal structure[12] as well as the enhanced fluorescence in the solid state and doped polymer films[1] of BT_2 have been reported from our laboratory earlier. Due to the solubility of BT_2 in water and common organic solvents, attempts to prepare its nanocrystals by reprecipitation were unsuccessful. We have therefore developed a simple polyelectrolyte-assisted reprecipitation method for the fabrication of its nanoparticles in a colloidal state, and their characterization by microscopy studies. In the aqueous medium, complexation with the polyelectrolyte enhances the fluorescence of BT_2, the effect increasing with the ratio of the polymer to BT_2 and saturating at high values. This demonstrates the feasibility of tuning the aggregation of the molecules and its consequence for the fluorescence response. Significantly, the colloids formed by injecting the aqueous

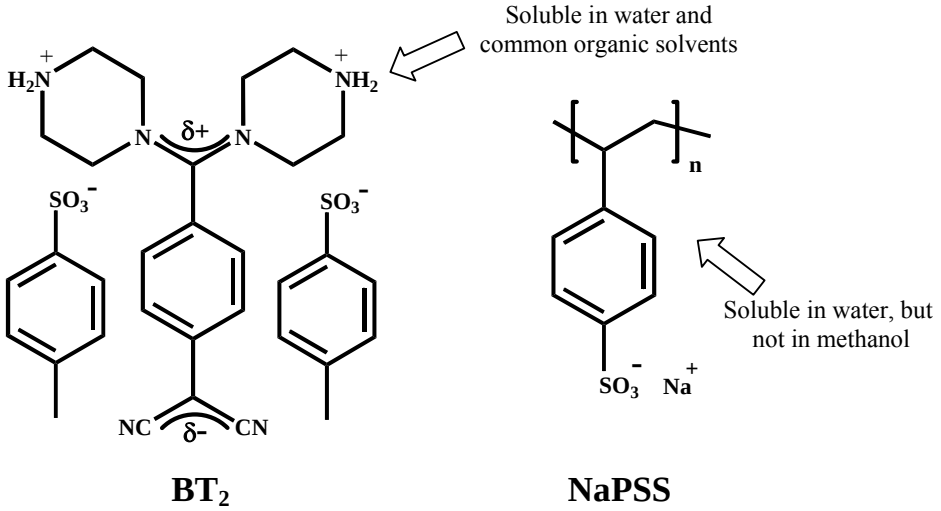

Figure 3.1. *Molecular structure of BT_2 (the water of crystallization observed in the crystal is not shown) and NaPSS. The solubility characteristics are indicated.*

solution into methanol exhibit very high fluorescence enhancement (~ 90 times) over the aqueous solution of BT_2. These observations are in sharp contrast with the report of the suppression or limited increase (in a narrow range of stoichiometries) of the fluorescence response of dyes such as rhodamine and cyanine upon interaction with poly(styrenesulfonate).[13] Several experiments are carried out to assess the conditions required to obtain maximum fluorescence enhancement of BT_2, establish the role of the polyelectrolyte and gain a molecular level understanding of the phenomenon. Potential impact of the medium viscosity and ionic strength are probed. Isothermal titration calorimetry (ITC) provides information on the interactions between BT_2 and NaPSS. The study presented in this chapter thus illustrates a simple methodology to fabricate strongly fluorescent, stable aggregates of highly soluble compounds, using the reprecipitation approach.

3.2. Fabrication of Molecules and Materials

3.2.1 *Synthesis of the molecules and characterization*

BT_2 was prepared in two steps as reported earlier[1] with small modifications in the procedure.

7,7-bis(piperazino)-8,8-dicyanoquinodimethane (DPZDQ): 0.17g (2.07 mmol) of piperazine dissolved in 2.5 ml of acetonitrile was added to a warm solution of 0.1 g (0.49 mmol) of TCNQ in 10ml of acetonitrile. The solution turned dark green immediately and changed to orange yellow subsequently. The reaction mixture was stirred for 2.5 h at 75^{o}C and then for 5 h at 30^{o}C. The yellow product which precipitated was filtered out and dried (0.119 g, yield = 75%).

BT_2: A solution of 0.118 g (0.62 mmol) of *p*-toluenesulfonic acid in 5ml acetonitrile was added to a warm solution of 0.1 g (0.31 mmol) of DPZDQ in 25 ml of acetonitrile:DMSO mixture (7.5 : 1 by volume). The reaction mixture was stirred for 2 h at 75°C and then for 1 h at 30°C. The yellow compound that precipitated was filtered out and dried. The compound was recrystallized thrice from water and dried under vacuum at 70°C for 3 h.

Yield = 74%. FTIR (KBr) : $\bar{\upsilon}$/cm^{-1} = 2177.8, 2139.3, 1153.5 ; ^{1}H-NMR (d_6-DMSO) : δ/ppm = 8.96 (s, 4H), 7.47 (d, 4H), 7.37 (d, 2H), 7.11 (d, 4H), 6.88 (d, 2H), 3.78 (m, 4H), 3.44 (m, 4H), 2.28 (s, 6H); elemental analysis (calculated for $BT_2.H_2O$ *i.e.* $C_{32}H_{40}N_6O_7S_2$) : %C = 55.79 (56.14), %H = 5.71 (5.85), %N = 12.09 (12.28), %S = 9.31 (9.36).

Purification of NaPSS: NaPSS (Aldrich, average molecular weight = 70,000) was purified by dissolving in high purity water followed by precipitation using methanol, centrifugation, filtering and drying under vacuum. The purity and extent of sulfonation (> 95%) was confirmed by NMR.

^{1}H-NMR (D_2O) : δ/ppm = 7.51 (m, 2H), 6.60 (m, 2H), 1.43 (m, 3H).

The sulfonation level f_{NMR} (determined by NMR) is estimated using the ratio (α) of intensities of the peaks due to *meta* and *para* protons on the phenyl rings of polystyrene.[14]

$$\alpha = 1/0.067 = 14.93$$

$$f_{NMR} = 100[3\alpha/(2 + 3\alpha)] = \mathbf{95.74}$$

3.2.2 *Preparation of colloids*

Solutions of BT_2-NaPSS and their nano/microparticles were prepared as follows. 1 mM solution of BT_2 and 1 M solution of NaPSS in high purity water were mixed so as to prepare BT_2–NaPSS mixtures with a wide range of weight ratios (NaPSS : BT_2, x); the pH of all solutions at 25°C was found to be ~ 6.0. Colloids were prepared by injecting 40 µl of the solution (x = 500) rapidly into 3 ml of methanol at 25°C under ultrasonication which was continued for 2 min. Colloid formation was immediately noticeable.

3.3. Spectroscopic Studies

Absorption and emission spectra of BT_2 in water and methanol are presented in Fig. 3.2. The absorption with λ_{max} ~ 410 nm is due to the characteristic intramolecular charge transfer of the zwitterionic diaminodicyanoquinodimethanes, and the small red shift in methanol results from solvatochromic effects.[12,15] Fig. 3.3 shows the

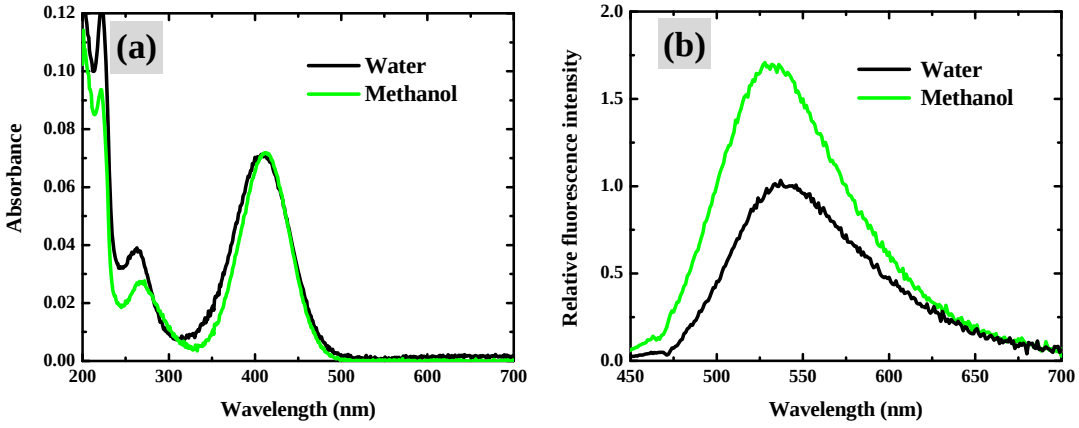

Figure 3.2. ***(a)*** *Electronic absorption and* ***(b)*** *fluorescence emission spectra of BT_2 in water and methanol solutions; λ_{exc} for the fluorescence spectra are 410 and 412 nm in water and methanol respectively.*

absorption and emission spectra of aqueous solutions with a fixed concentration (6.5 μM) of BT_2 and increasing concentrations of NaPSS; x ranges from 20 to 500, the corresponding mol ratios being 66 to 1660 (based on the molecular weight of NaPSS monomer). The increasing optical density in the UV region is due to the polyelectrolyte absorption. There is a red shift of the absorption peak of BT_2 when NaPSS is introduced, from 410 to ~ 426 nm; the gradual increase of the λ_{max} and its saturation beyond a mol ratio of ~ 5.0 are seen in the of Fig. 3.3c. The red shift suggests that the

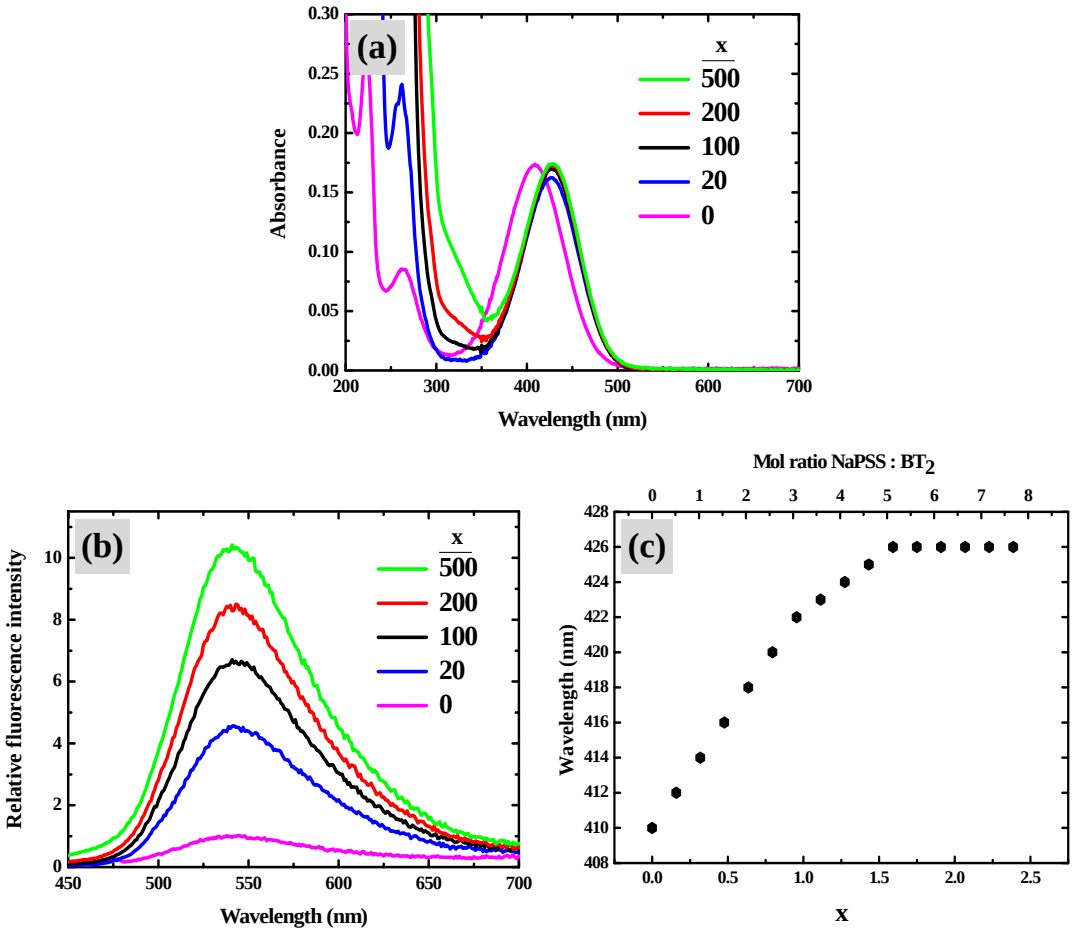

Figure 3.3. ***(a)*** *Electronic absorption and* ***(b)*** *fluorescence emission spectra of BT_2-NaPSS (with different weight ratios NaPSS:BT_2, x) in water; λ_{exc} are 409 nm for pure BT_2 and 428 nm for BT_2-NaPSS.* ***(c)*** *Shift of the λ_{max} of the absorption at low x.*

B^{2+}, initially solvated by pure water, move to a relatively less polarizable local environment upon binding to the polyelectrolyte chain. The mol ratio at which the shift saturates is higher than that expected based on the charge on B^{2+}, possibly due to the influence of neighboring ionic sites. More interestingly, the increasing content of the NaPSS leads to appreciable enhancement of the emission intensity; the optical density is similar in all cases (Fig. 3.3a). The emission spectra recorded on solutions with exactly matched optical density at their absorption (Fig. 3.4) or excitation (Fig. 3.5) λ_{max} appear very similar to those in Fig. 3.3b. When x = 500, the fluorescence intensity is ~ 10 times higher than that of pure BT_2 in water. With further increase of NaPSS, the growth is less pronounced (Fig. 3.6). As the polyelectrolyte absorption dominates in solutions with x > 500, further studies are focused on solutions with x = 500. We consider below, various factors that can possibly give rise to the fluorescence enhancement.

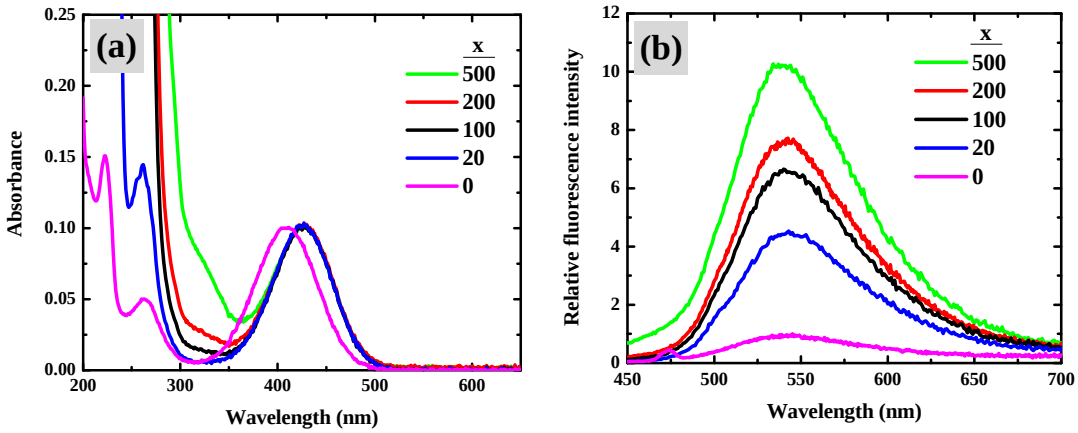

Figure 3.4. ***(a)*** *Electronic absorption and* ***(b)*** *fluorescence emission spectra of BT_2-NaPSS (with different weight ratios, NaPSS:BT_2 (x)) in water with the optical density of the solutions at their respective absorption maxima matched by appropriate dilution. λ_{exc} for the spectra in (b) are 410 nm for pure BT_2 and 428 nm for BT_2-NaPSS.*

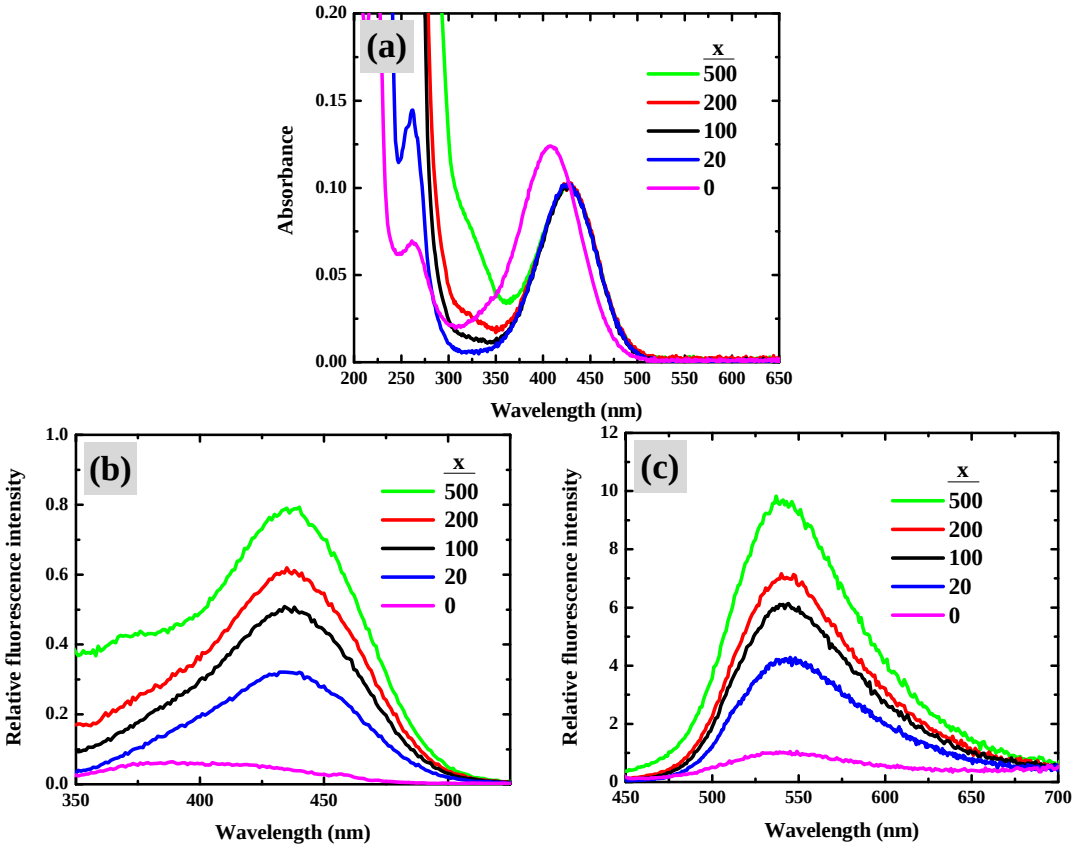

Figure 3.5. ***(a)*** *Electronic absorption and* ***(b)*** *fluorescence excitation and* ***(c)*** *fluorescence emission spectra of BT_2-NaPSS (with different weight ratios, NaPSS:BT_2 (x)) in water, with the optical density of the solutions at their respective excitation maxima matched by appropriate dilution. λ_{em} for the spectra in (b) is 543 nm. λ_{exc} for the spectra in (c) are 385 nm for pure BT_2 and 435 nm for BT_2-NaPSS.*

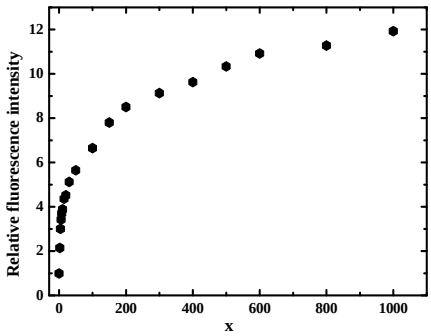

Figure 3.6. *Variation of the intensity of fluorescence emission of BT_2 upon addition of NaPSS in aqueous solution (x = NaPSS:BT_2 weight ratio).*

NaPSS has an absorption peak at 258 nm and when excited close to this wavelength, produces a weak emission at 500 nm. Experiments on solutions of pure NaPSS, with the same molar content as in the measurements with BT_2, showed negligible contribution to fluorescence at 542 nm where the BT_2 emission is observed, ruling out a direct involvement of the polymer in the latter emission. We have considered another scenario wherein the absorption due to the NaPSS units at the

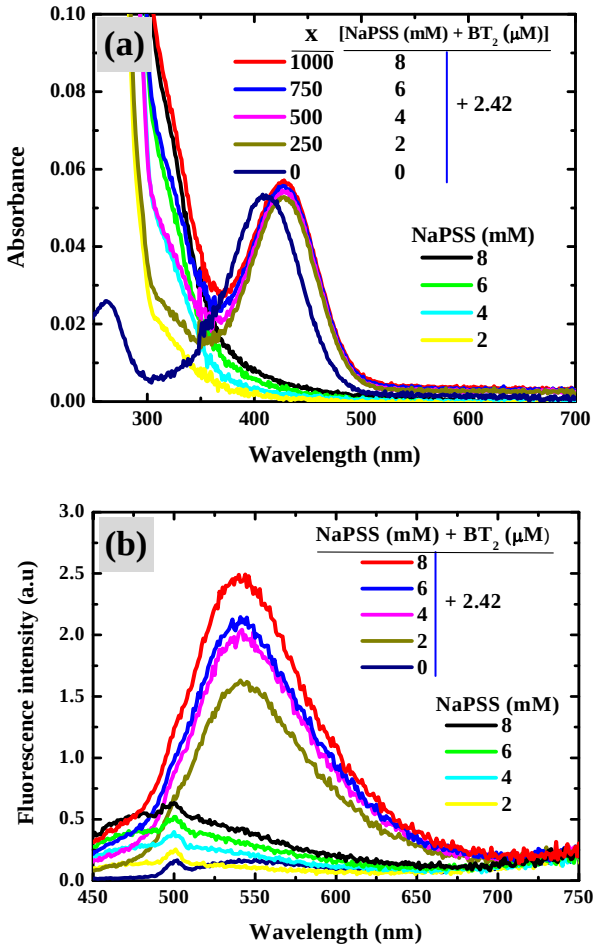

Figure 3.7. ***(a)*** *Electronic absorption and* ***(b)*** *fluorescence emission spectra (λ_{exc} = 428 nm) of BT_2-NaPSS (with different weight ratios, NaPSS:BT_2 (x)) and pure NaPSS with the corresponding concentrations in water illustrating that the growth of the fluorescence below 500 nm, due to NaPSS alone and NaPSS in the BT_2-NaPSS system are very similar.*

exciting wavelength of 428 nm followed by energy transfer to the BT_2 molecules can lead to enhancement of the emission. Observation of similar increase in the emission near 500 nm with increasing concentration of NaPSS both in the presence and absence of BT_2 (Fig. 3.7) rules out this possibility. We have also examined the possibility of increasing ionic strength of the medium affecting the fluorescence emission of BT_2, by carrying out an experiment wherein BT_2 emission in water containing increasing concentration of sodium chloride was monitored (Fig. 3.8). Even at very high levels of salt concentration, the enhancement of the fluorescence was found to be negligible compared to that seen in Fig. 3.6. In view of all these observations, the enhancement of fluorescence with increasing ratio of NaPSS to BT_2 appears to result from the increasing restriction of the geometry relaxation of the excited state of B^{2+}, as proposed earlier for the solid state and doped polymer films.[1]

An important question that arises at this point relates to how the polyelectrolyte restricts the geometry relaxation in B^{2+} – through local viscosity effects or molecular level complexation mediated by ionic interactions. We have carried out the following

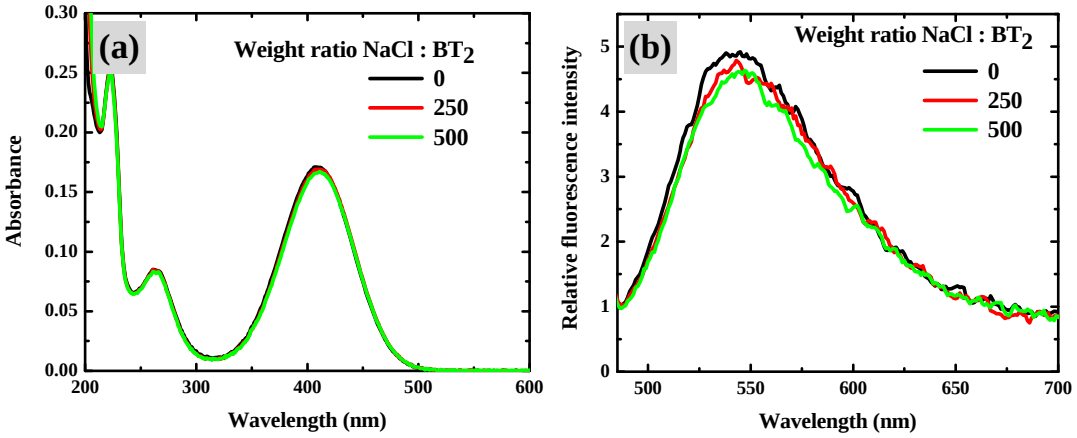

Figure 3.8. ***(a)*** *Electronic absorption and* ***(b)*** *fluorescence emission spectra of BT_2-NaCl (with different weight ratios) in water. λ_{exc} for the spectra in (b) is 410 nm.*

control experiments to explore the potential role of viscosity. Aqueous solutions of BT_2 mixed with each of the following polyelectrolytes, NaPSS (average MW = 70,000), NaPSS1 (average MW = 1,000,000), NaCMC (sodium salt of carboxymethylcellulose, average MW = 90,000) and NaPAA (sodium salt of poly(acrylic acid), average MW = 170,000) were prepared; the concentration of BT_2 was 10 μM and that of the polyelectrolyte 50 mM (based on monomers) in each case. The measured viscosities of the solutions are collected in Table 3.1. The absorption and emission spectra are shown in Fig. 3.9. As the concentration of BT_2 is the same in all, the absorbances at ~ 410 nm are similar. The solutions with NaPSS and NaPSS1 show slightly red shifted peaks compared to the other two; this is reminiscent of the observation in Fig. 3.3a. Absence of such shifts with NaCMC and NaPAA points to the lack of strong interactions with B^{2+}. The relative fluorescence intensities estimated from the spectra are collected in Table 3.1. Even though the viscosity is much higher for the mixture with NaPSS1, a consequence of the higher average molecular weight, the fluorescence is very similar to that of the mixture with NaPSS. Solutions with NaCMC and NaPAA with higher

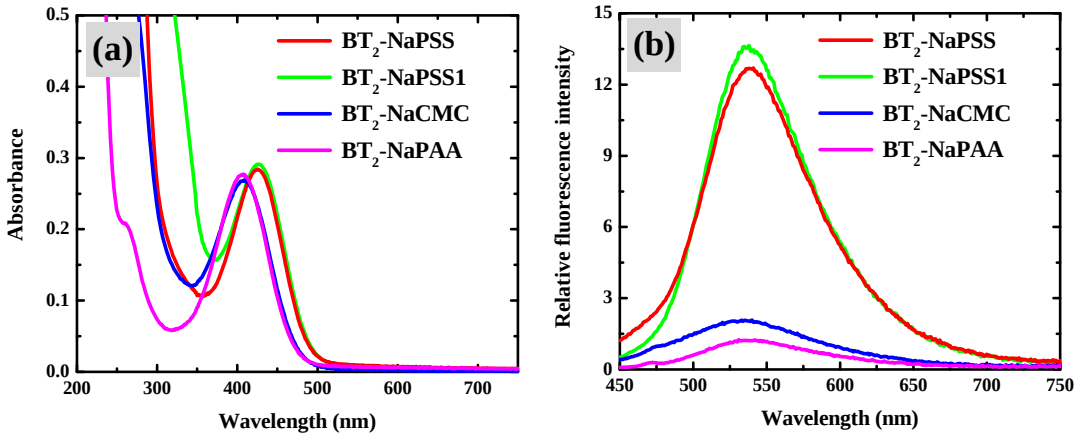

Figure 3.9. ***(a)*** *Electronic absorption and* ***(b)*** *fluorescence emission spectra of aqueous solutions of BT_2 (10 μM) with different polyelectrolytes (50 mM); λ_{exc} for the fluorescence spectra are the λ_{max} from the corresponding absorption spectra.*

Table 3.1. *Viscosity and relative fluorescence intensity of aqueous solutions containing BT_2 (10 μM) and different polyelectrolytes (50 mM).*

Polyelectrolyte	Average Molecular Weight	Viscosity (cP)	Relative fluorescence intensity
NaPSS	70,000	1.34 - 1.50	1.00
NaPSS1	1,000,000	6.90 - 7.20	1.05
NaCMC	90,000	11.90 -12.60	0.16
NaPAA	170,000	2.90 - 3.30	0.10

viscosities exhibit considerably lower fluorescence than that of the solution with NaPSS. These experiments suggest strongly that the bulk viscosity due to the polymer is not the determining factor for the fluorescence enhancement, but some molecular level interactions. The extent of ionization of the carboxylate sites on NaCMC and NaPAA is likely to be relatively less compared to that of the sulfonate sites on NaPSS and NaPSS1 in the neutral aqueous solution. Therefore any ionic complexation with B^{2+} will be more efficient in the latter two compared to the former. It is also possible that the aromatic groups in NaPSS and NaPSS1 facilitate binding with B^{2+} through favorable π-π interactions. We examine later, the molecular level picture of complexation between BT_2 and NaPSS.

In view of the preliminary insight gained from the experiments above regarding the complexation of B^{2+} with PSS^{n-} chains, and the fact that methanol is a solvent for BT_2 but not for NaPSS, we have investigated the solutions/colloids obtained by injecting the aqueous solution containing BT_2 and NaPSS into methanol. Clear

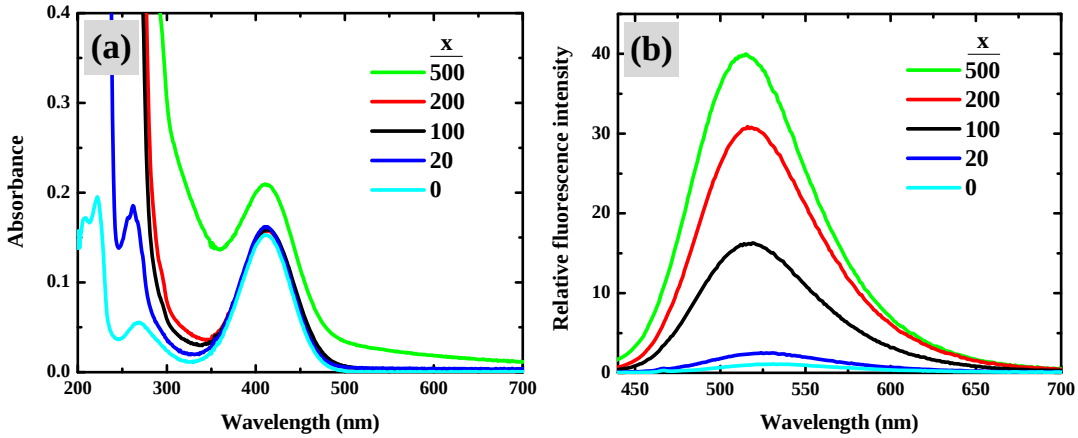

Figure 3.10. ***(a)*** *Electronic absorption and* ***(b)*** *fluorescence emission spectra of BT_2-NaPSS (with different weight ratios NaPSS:BT_2, x) in water (40 µl) injected into 3 ml methanol. λ_{exc} for the spectra in (b) is 412 nm. Concentration of BT_2 is 5 µM in all cases.*

formation of colloids and significant spectral changes are not observed with solutions having x < 500 (Fig. 3.10). In order to assess the relevance of the water-methanol composition, we have injected small aliquots (40 µl) of the aqueous solution with x = 500 into solvent mixtures (3 ml) with increasing methanol fractions. The absorption and emission spectra of the resulting solutions/colloids are collected in Fig. 3. 11. As significant changes in the trends emerge when the fraction of methanol becomes

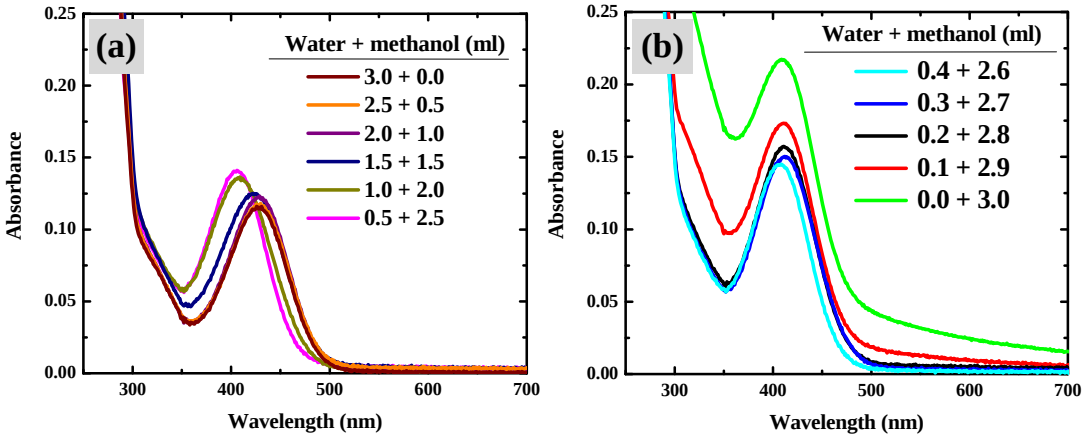

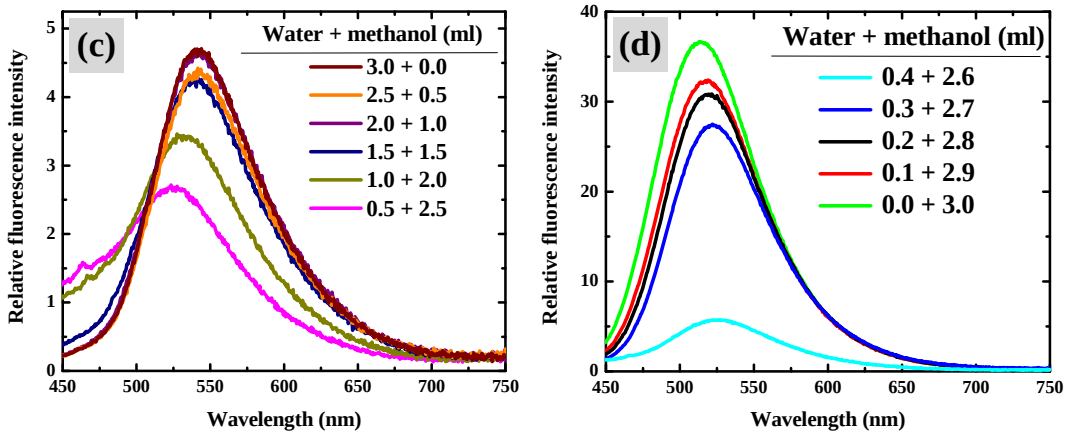

Figure 3.11. ***(a, b)*** *Electronic absorption and* ***(c, d)*** *fluorescence emission spectra of BT_2-NaPSS (x = 500) in water - methanol mixtures having different compositions.*

dominant, solvent mixtures with proportions changing through closer intervals are explored in this regime (Fig. 3.11b, d). Variation of the peak maxima and intensities of the absorption and emission, with the volume fraction of methanol are plotted in Fig. 3.12. The blue shift of the absorption when the methanol fraction increases from ~ 0.3 – 0.8 possibly reflects an increasing aggregation of the ionic sites of the NaPSS chains induced by methanol and partitioning of excess water into this region, effectively increasing the dielectric constant of the local environment around B^{2+} and stabilizing its ground state. The excited state is stabilized less as its dipole moment is lower than that of the ground state, causing the fluorescence peak also to show a blue shift; the intensity remains nearly constant in this range. The abrupt change in the absorption λ_{max} coupled with increased scattering when the fraction of methanol is > 0.8 suggest the formation of colloids. The fluorescence intensity shows dramatic enhancement at this point, indicating that the chromophores enter a rigid phase wherein the geometry relaxations are completely arrested. The most likely scenario is the formation of nano/microparticles of B^{2+} together with the styrenesulfonate units within the NaPSS aggregate structures that emerge due to the dominantly methanolic medium.

Intermolecular interactions contributing to the fluorescence enhancement in these particles cannot be ruled out. Table 3.2 compares the relative fluorescence intensities of

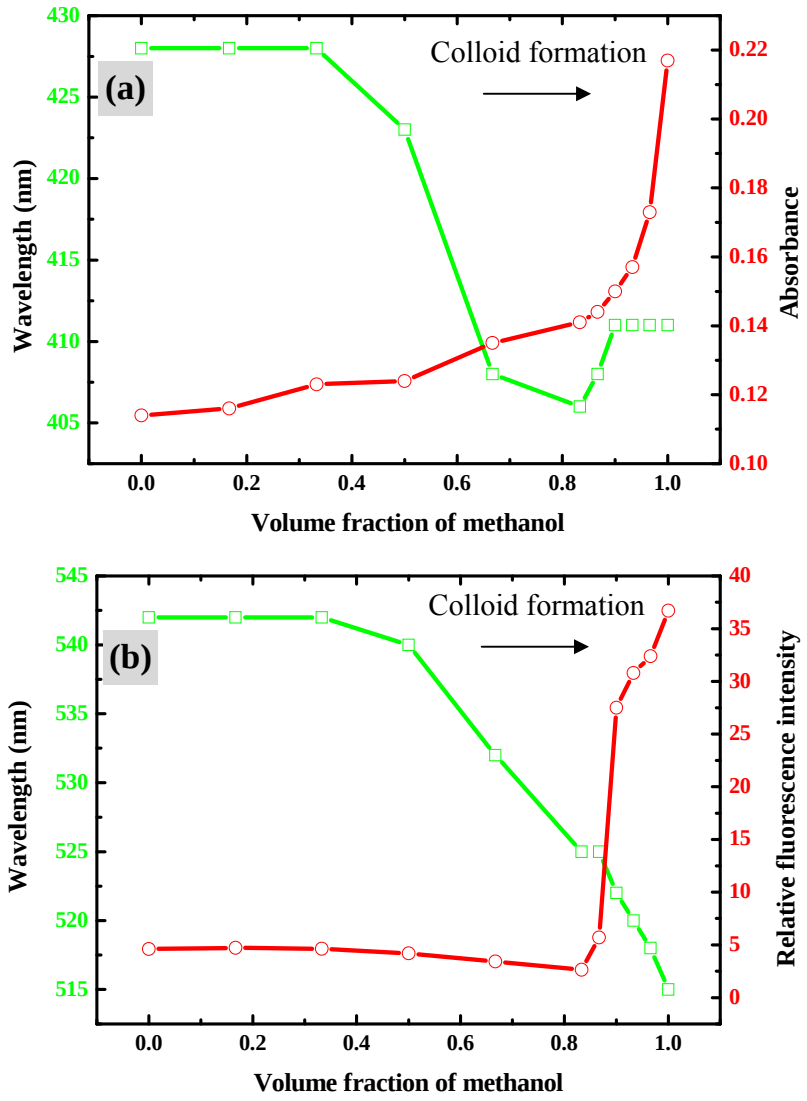

Figure 3.12. *Variation of the λ_{max} and intensity of the **(a)** electronic absorption and **(b)** fluorescence emission of BT_2-NaPSS (x = 500) in water - methanol mixtures with different fractions of methanol. The lines are only guides to the eye.*

Table 3.2. *Relative fluorescence intensities, quantum yields and excited state lifetimes of BT_2 and BT_2-NaPSS solutions and BT_2-NaPSS colloid; the comparisons are based on solutions having the same molar content of BT_2.*

System	Relative fluorescence intensity	Quantum yield	Average lifetime of excited state (ns)
BT_2 (solution in water)	1.0	0.08	< 0.04
BT_2 (solution in methanol)	1.7	0.14	< 0.04
BT_2-NaPSS (x = 500; solution in water)	10.2	1.20	0.08
BT_2-NaPSS (x = 500; colloid in methanol)	81.6	10.40	1.70

BT_2 and BT_2-NaPSS (x = 500) solutions in water and the colloid formed by injecting 40 μl of the BT_2-NaPSS (x = 500) aqueous solution into 3 ml methanol. The table also lists the values of quantum yields measured in each case. The enhancement of fluorescence of the colloids formed in methanol over that of the aqueous solution of pure BT_2 is of the order of 80 - 100 !

We have carried out time-resolved fluorescence measurements (with a time resolution of 40 ps) to probe the excited state dynamics of the various systems (Fig. 3.13). Fluorescence decay of BT_2 solutions in water as well as methanol are found to be too fast to measure with the setup used. BT_2-NaPSS (x = 500) in water decays slower and the corresponding colloid prepared in methanol even more slowly (Table 3.2). These observations are consistent with the relative fluorescence intensities of the various systems and follow the trends expected based on the model invoking suppression of excited state geometry relaxation leading to enhanced fluorescence.

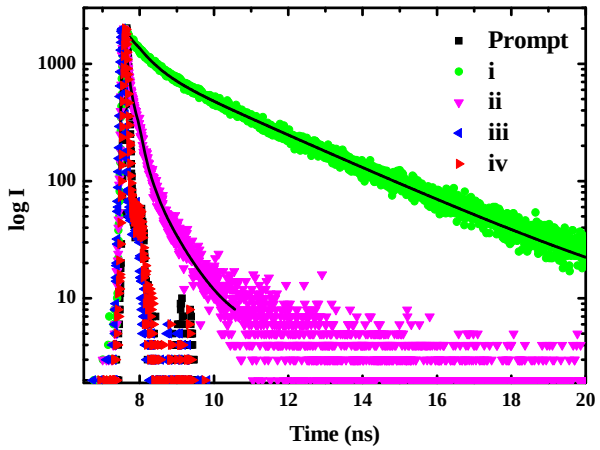

Figure 3.13. *Fluorescence emission decay profiles of (i) BT_2-NaPSS (x = 500) colloid in methanol, (ii) BT_2-NaPSS (x = 500) solution in water, (iii) BT_2 (solution in methanol) and (iv) BT_2 (solution in water). The black lines indicate the fitting of (i) and (ii) to (multi)exponential decays.*

In order to confirm the significance of these observations, we have carried out a control experiment using an analog of BT_2, 7,7-bis(N-methylpiperazino)-8,8-dicyanoquinodimethane (BMPDQ).[1] BMPDQ has exactly the same fluorophore unit as B^{2+}, but has no net charge as N-methyl replaces ammonium as the remote group. Spectroscopic experiments indicate fluorescence enhancement in aqueous solutions of BMPDQ- NaPSS; however, when injected into methanol medium, the enhancement is significantly lower than that observed in BT_2-NaPSS (Fig. 3.14).

Control experiments carried out with a simple sulfonate surfactant, sodium dodecylbenzenesulfonate (SDBS) in place of NaPSS showed that even though complexation occurs in aqueous medium as revealed by absorption spectral shifts, the colloid formed in methanol is not stable and exhibits no fluorescence enhancement (Fig. 3.15). This demonstrates clearly the critical role played by the polyelectrolyte chains in the formation of the colloids and fluorescence enhancement as described above.

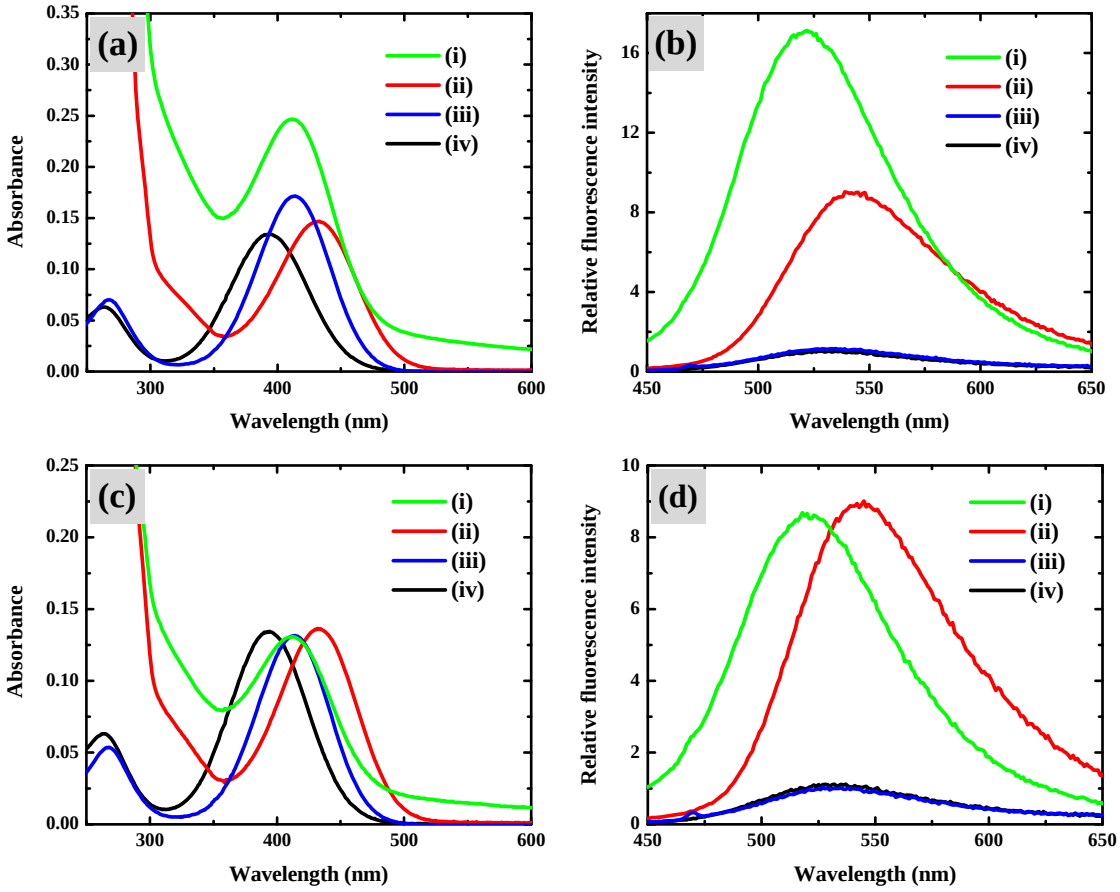

Figure 3.14. ***(a)*** *Electronic absorption and* ***(b)*** *fluorescence emission spectra of (i) BMPDQ-NaPSS (weight ratio, NaPSS:BMPDQ, x = 500) colloid in methanol, (ii) BMPDQ-NaPSS (x = 500) solution in water, (iii) BMPDQ (solution in methanol) (iv) BMPDQ (solution in water).* ***(c)*** *Electronic absorption and* ***(d)*** *fluorescence emission spectra of the solutions in (a) and (b), with the optical density at their respective absorption maxima matched by appropriate dilution.* λ_{exc} *for the fluorescence spectra are the corresponding absorption maxima; concentration of BMPDQ is 5 μM in all cases.*

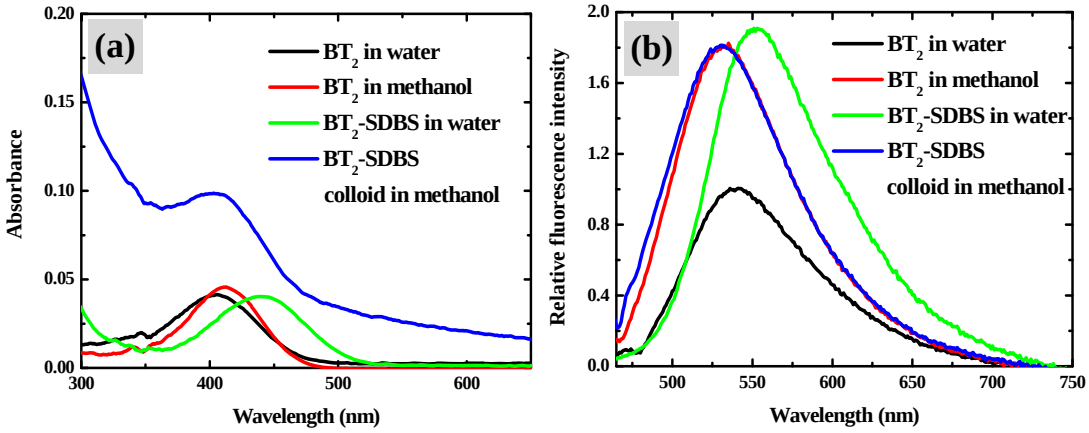

Figure 3.15. ***(a)*** *Electronic absorption and* ***(b)*** *emission spectra of BT2-SDBS. A mol ratio, BT2:SDBS = 1660 is used in the mixtures. It may be noted that this is the mol ratio of BT2-NaPSS having weight ratio, x = 500. The fluorescence spectra were recorded by exciting each of the solutions at their excitation peaks; BT2 (in water) – 408 nm, BT2 (in methanol) – 411 nm, BT2 – SDBS (in water) – 440 nm, BT2 – SDBS (in methanol) – 408 nm.*

3.4. Microscopy

As noted above, BT_2-NaPSS (x = 500) injected into methanol is likely to yield nanoparticles. We have investigated the formation of nano/microparticles in the colloid using different microscopy experiments. The colloids were either drop-cast on suitable substrates and dried or filtered through nanoporous membranes to prepare the samples for imaging. TEM, SEM and AFM images are collected in Fig. 3.16. The grain-like structures observed are ~ 200 - 550 nm long and 100 - 200 nm wide. The AFM images indicate that the structures have a thickness of ~ 15 - 25 nm. As BT_2 is soluble in methanol, the particles observed cannot be due to pure BT_2. In order to verify whether NaPSS forms such nanostructures, aqueous solutions of pure NaPSS were injected into methanol (keeping the concentrations and volumes of solutions the same as in the case of BT_2-NaPSS) and the resulting colloids examined. Only some diffuse aggregates (Fig.

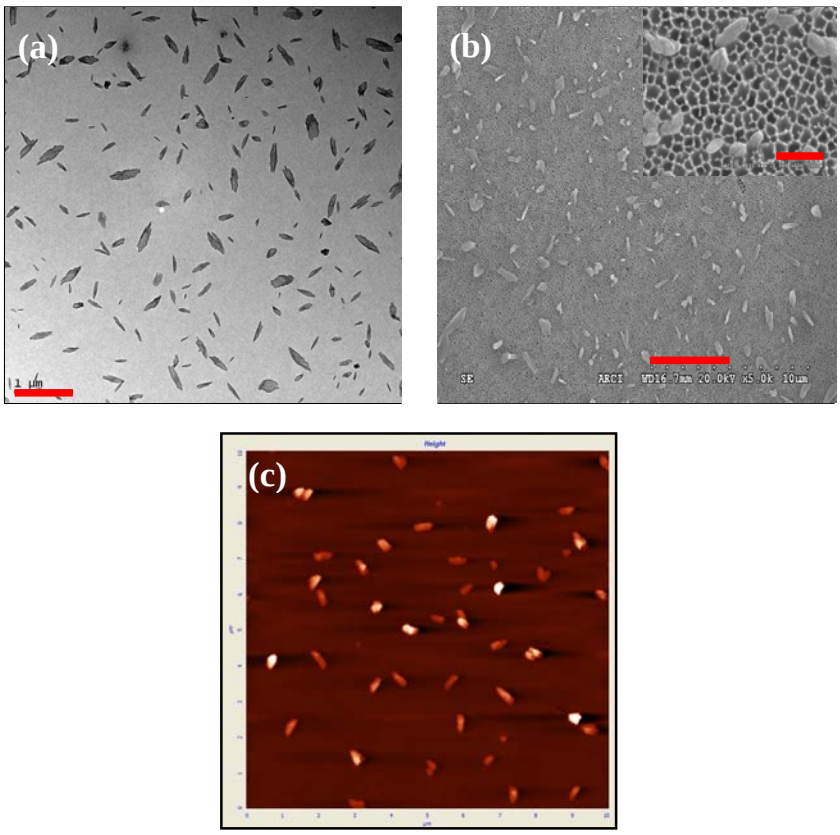

Figure 3.16. ***(a)*** *TEM (scale bar = 1 μm)* ***(b)*** *FESEM (scale bar = 5 μm; inset: scale bar = 500 nm) and* ***(c)*** *AFM topography (10 μm × 10 μm) images of BT_2-NaPSS colloidal particles.*

3.17) were obtained and no structures similar to those in Fig. 3.16 could be found. These experiments prove that the particles are indeed formed by the aggregation of BT_2 together with NaPSS. The finer details of whether the crystals of BT_2 are formed embedded inside the polyelectrolyte chains or the two are enmeshed in an aggregate structure, is not clear at the moment. Laser confocal microscopy images are shown in Fig. 3.18. It shows large features due to clusters of the nanoparticles; excitation of these clusters by 458 nm laser produces emission with a peak maximum at ~ 520 nm consistent with the spectroscopic studies.

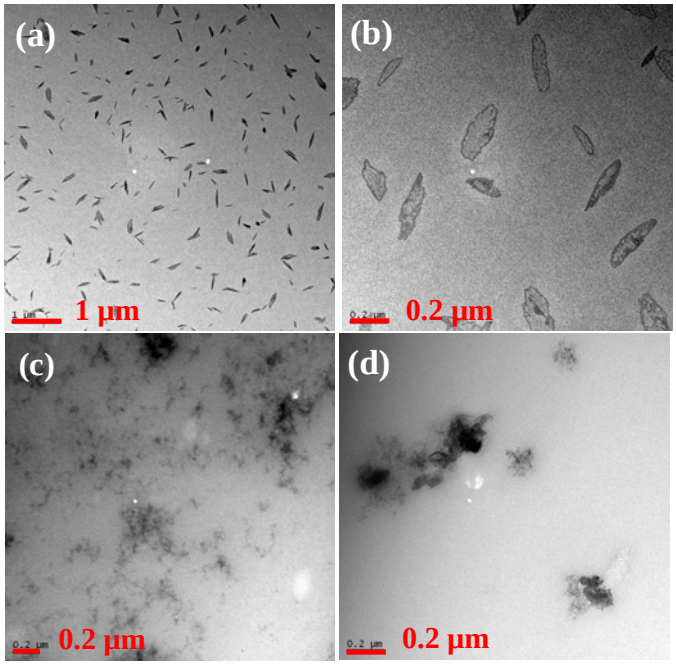

Figure 3.17. *TEM images of* ***(a, b)*** *BT_2-NaPSS colloid formed by injecting 40µl of aqueous solution of BT_2-NaPSS (x = 500) into 3 ml of methanol* ***(c, d)*** *NaPSS colloid formed by injecting aqueous solution of NaPSS into methanol (keeping the concentrations and volumes of solutions the same as in (a and b).*

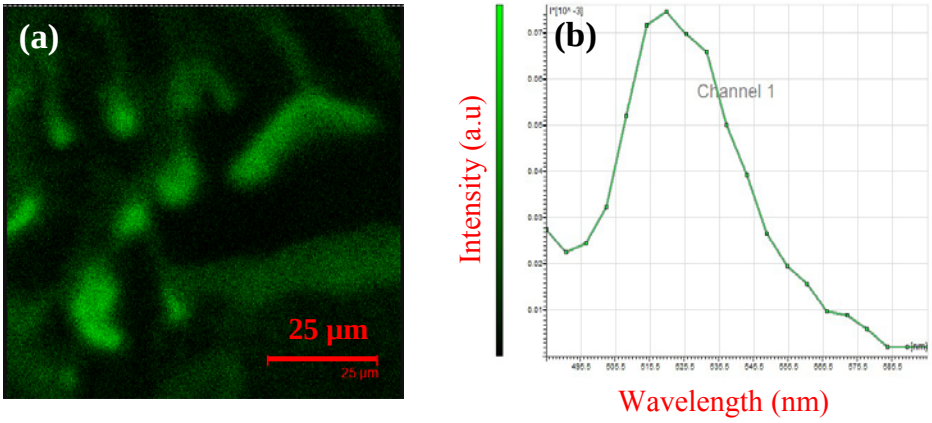

Figure 3.18. ***(a)*** *Laser confocal microscopy image and* ***(b)*** *fluorescence emission spectrum of colloid drop on glass substrate recorded by excitation at 458 nm.*

3.5. Isothermal Titration Calorimetry

In order to gain insight into the nature of the interactions between B^{2+} and PSS^{n-}, we have carried out ITC experiments by titrating aqueous solution of NaPSS into aqueous solution of BT_2. In a typical experiment, 1.44 ml of a 0.05 mM solution of BT_2 was taken in the cell and 7 µl aliquots of 2 mM solution of NaPSS were injected at time

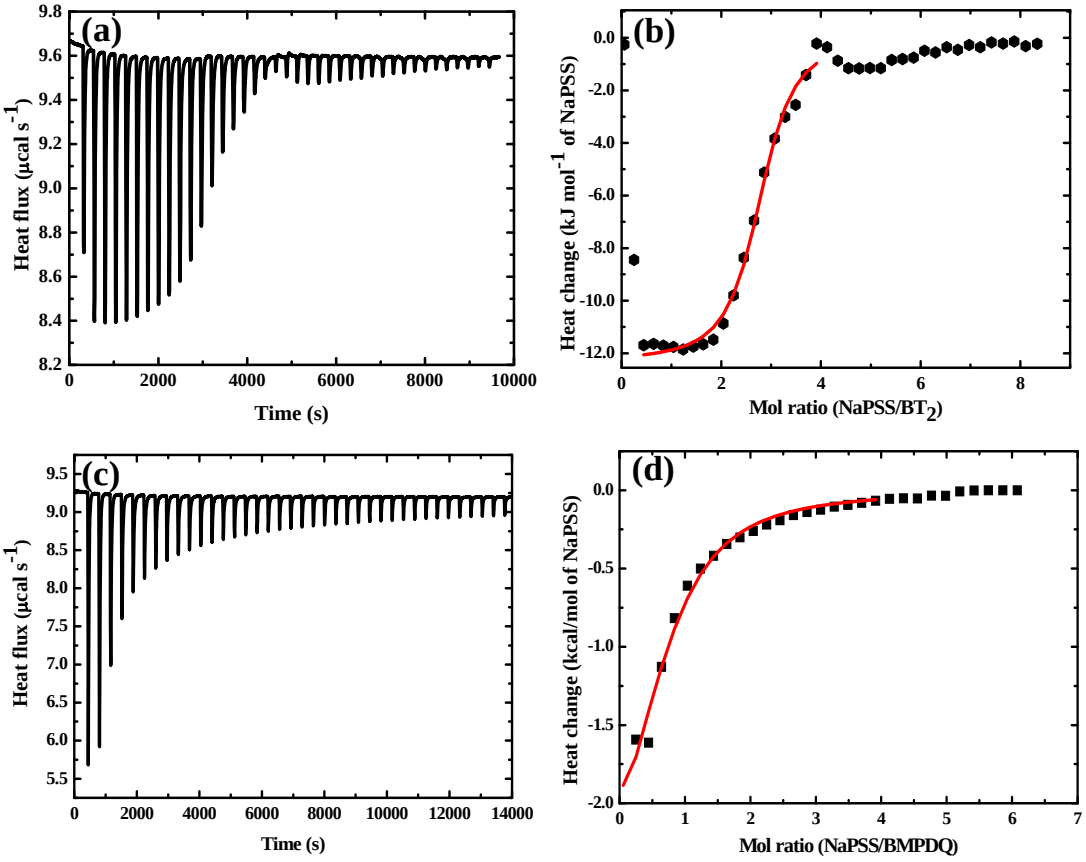

Figure 3.19. ***(a)*** *Raw and* ***(b)*** *integrated thermograms from the isothermal titration of NaPSS into BT_2 in aqueous solution.* ***(c)*** *Raw and* ***(d)*** *integrated thermograms from the isothermal titration of NaPSS into BMPDQ in aqueous solution. Fitting of the data in the low mol ratio region are indicated.*

intervals of 240 s (first injection alone was 2 μl). Thermograms (raw and integrated) obtained are shown in Fig. 3.19a, b. The heat changes follow a complicated pattern and the full thermogram cannot be fitted to standard binding models. However, some salient features of the molecular interaction can be inferred. Appreciable heat changes remaining nearly constant upto a mol ratio of ~ 2.0 are indicative of a strong binding interaction. In the mol ratio range 2.0 – 4.0, the heat changes diminish tending towards zero. This points to a binding stoichiometry in this range, *i.e.* ~ 3 monomer sites per B^{2+}. As PSS^{n-} is almost completely sulfonated (Sec. 3.2.1), this implies that one B^{2+} engages two sulfonate sites, and on an average, an additional one becomes unavailable for binding further B^{2+} possibly due to steric congestion. If the binding events were completed following this, the thermogram would have approached zero heat change smoothly. However, a further small dip appears near the mol ratio of ~ 5.0, indicating possible aggregation of the polyelectrolyte chains. As these special features of the thermogram are quite reproducible, we have attempted a partial fitting of the data in the low mol ratio regime (0.4 – 4.0) to a single site binding model; it may be noted that such partial analysis is common with systems showing complex behavior.[16] The fitting is shown in Fig. 3.19b; the parameters estimated in Table 3.3 are consistent with the general inferences drawn above. In order to confirm the significance of these observations, we have carried out a control experiment using BMPDQ, the analog of BT_2 noted earlier.[1] In this experiment, 1.44 ml of a 0.25 mM solution of BMPDQ was taken in the cell and 7 μl aliquots of 10 mM solution of NaPSS were injected at time intervals of 360 s (first injection alone was 2 μl). The thermogram recorded for the titration against NaPSS is very different (Fig. 3.19c, d); even though some binding interaction is observed (possibly due to the highly dipolar structure of BMPDQ similar to that of B^{2+}), it is considerably weaker (the difference appears to be primarily entropy

Table 3.3. *Binding and thermodynamic parameters from the isothermal titration calorimetry experiments on NaPSS against BT_2 and BMPDQ. Percentage error for the parameters estimated by the nonlinear least square fitting (Fig. 3.19b, d) are indicated in brackets; the fitting was carried out for the mol ratios in the range 0.4 - 4.0 in both*

Parameter	Value [% error]	
	BT_2-NaPSS	**BMPDQ-NaPSS**
N (stoichiometry)	2.73 [1.1]	0.67 [1.2]
K / dm^3 mol^{-1}	4.4×10^5 [15.3]	1.0×10^4 [18.6]
ΔH^o / kJ mol^{-1}	-12.3 [1.5]	-12.8 [13.9]
ΔG^o / kJ mol^{-1}	-32.2	-22.9
ΔS^o / J mol^{-1} K^{-1}	66.5	33.9

driven) and the stoichiometry is ~ 0.7 (Table 3.3). No binding interaction is observed at higher stoichiometries. All these facts indicate that B^{2+} has a unique and strong binding interaction with the PSS^{n-} and this complexation is followed by further aggregation of the polyelectrolyte chains and colloidal particle formation when injected into methanol.

3.6. Model for the Complexation and Fluorescence Enhancement

Taking into account the various spectroscopic and calorimetric investigations and the microscopy observation of the nano/microparticles, a model can be developed for the molecular systems existing in the various environments and their optical responses. Fig. 3.20 shows schematically the complexation of B^{2+} with PSS^{n-} in water and the enhancement of fluorescence as a consequence of the partial rigidification.

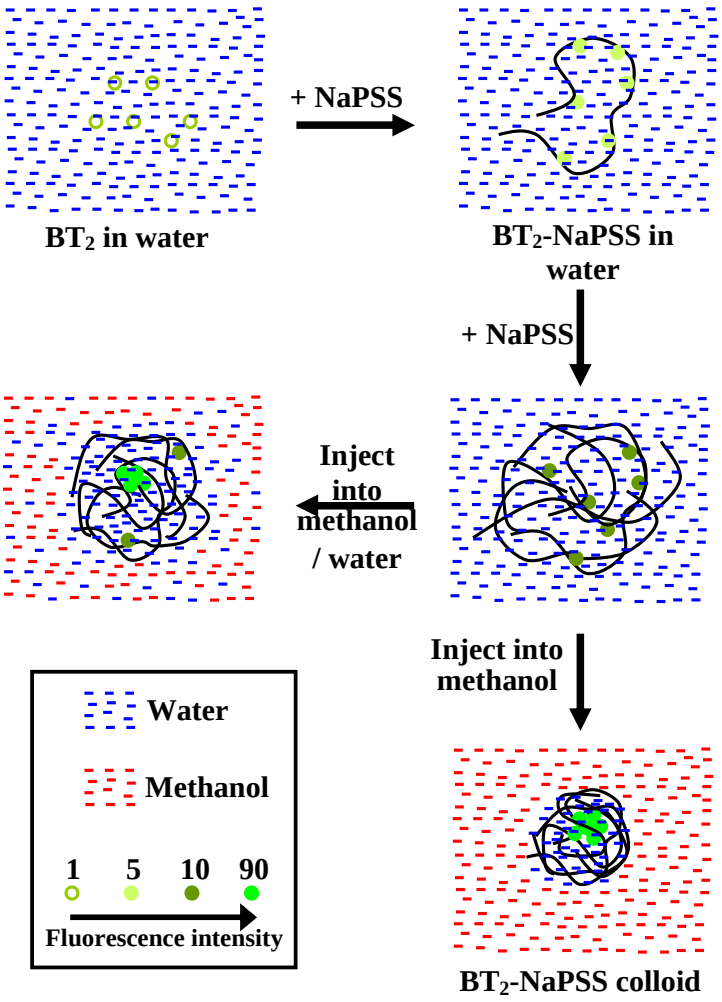

Figure 3.20. *Schematic representation of the model proposed to explain the observed fluorescence enhancement in BT_2-NaPSS systems; the symbols used are explained in the legend box.*

Upon further addition of NaPSS, the fluorescence increases further, as a result of the aggregation of the polyelectrolyte chains around the complex. Injection into methanol-water mixtures with increasing fraction of methanol causes these aggregates to tighten due to the insolubility of NaPSS in methanol, collecting water preferentially into its fold. When the medium is almost completely methanol (except for the trace quantity of water

that comes along in the injectant), the aggregation of BT_2-NaPSS or the B^{2+}-PSS^{n-} complex into particles is complete and the total rigidification of B^{2+} leads to the final enhancement of the fluorescence response.

3.7. Conclusions

We have demonstrated a polyelectrolyte-assisted reprecipitation protocol for the fabrication of highly fluorescent colloidal nanoparticles of a zwitterionic diaminodicyanoquinodimethane molecule, BT_2. This family of molecules are known to show enhanced fluorescence in the aggregated and solid states, but due to high solubility, are not amenable to the simple reprecipitation method commonly used to prepare molecular nano/microcrystals. Electrostatic binding of B^{2+} with the polyanion and the aggregation of the polyelectrolyte chains in water leads to partial rigidification of the fluorophore and enhanced emission. Transfer to methanol induces colloid formation due to the insolubility of the polyelectrolyte and aggregation of the B^{2+}, with significant enhancement of the emission intensity. Spectroscopy, microscopy and calorimetry investigations including several control experiments are used to formulate a model that helps to visualize the fundamentally interesting dye-polyelectrolyte interaction, and explain the observed emission enhancement. This method should prove generally useful for the preparation of molecular nanocrystals capable of aggregation-induced emission. Utilization of strong electrostatic interactions to achieve efficient complexation with templates may however, be required. The polyelectrolyte templating strategy allows fine tuning of the extent of molecular aggregation together with the fluorescence response. An important extension of these studies that warrants detailed exploration is the aggregation of fluorophores and enhancement of emission, in thin polymer films formed by various methods including layer-by-layer assembly.

References

1. S. Jayanty, T. P. Radhakrishnan, *Chem. Eur. J.* **2004**, *10*, 791.

2. J. N. Wilson, M. D. Smith, V. Enkelmann, U. H. F. Bunz, *Chem. Commun.* **2004**, 1700.

3. a) Y. Dong, J. W. Y. Lam, A. Qin, J. Sun, J. Liu, Z. Li, S. Zhang, J. Sun, H. S. Kwok, B. Z. Tang, *Appl. Phys. Lett.* **2007**, *91*, 011111. b) Z. Zhao, S. Chen, X. Shen, F. Mahtab, Y. Yu, P. Lu, J. W. Y. Lam, H. S. Kwok, B. Z. Tang, *Chem. Commun.* **2010**, *46*, 686.

4. a) H. Oikawa, H. Kasai, H. Nakanishi, *ACS Symp.Ser.: Anisotropic Organic Materials* **2001**, *798*, 158. b) Y. S. Zhao, H. Fu, A. Peng, Y. Ma, D. Xiao, J. Yao, *Adv. Mater.* **2008**, *20*, 2859. c) Q. Fang, F. Wang, H. Zhao, X. Liu, R. Tu, D. Wang, Z. Zhang, *J. Phys. Chem. B* **2008**, *112*, 2837.

5. a) E. I. Mal'tsev, D. A. Lypenko, B. I. Shapiro, M. A. Brusentseva, V. I. Berendyaev, B. V. Kotov, A. V. Vannikov, *Appl. Phys. Lett.* **1998**, *73*, 3641. b) L. Jinshui, W. Lun, G. Feng, L. Yongxing, W. Yun, *Anal. Bioanal. Chem.* **2003**, *377*, 346. c) E. Botzung-Appert, V. Monnier, T. Ha Duong, R. Pansu, A. Ibanez, *Chem. Mater.* **2004**, *16*, 1609. d) L. Wang, L. Wang, L. Dong, G. Bian, T. Xia, H. Chen, *Spectrochim. Acta A* **2005**, *61*, 129.

6. a) A. Patra, N. Hebalkar, B. Sreedhar, M. Sarkar, A. Samanta, T. P. Radhakrishnan, *Small* **2006**, *2*, 650; b) A. Patra, N. Hebalkar, B. Sreedhar, T. P. Radhakrishnan, *J. Phys. Chem. C* **2007**, *111*, 16184.

7. A. Patra, N. Venkatram, D. N. Rao, T. P. Radhakrishnan, *J. Phys. Chem. C* **2008**, *112*, 16269.

8. A. Patra, S. P. Anthony, T. P. Radhakrishnan, *Adv. Funct. Mater*. **2007**, *17*, 2077.

9. a) H. Nakanishi, H. Oikawa, In *Single Organic Nanoparticles*; H. Masuhara, H. Nakanishi, K. Sasaki, K., Eds.; Springer: Berlin, **2003**; pp 17-31. b) A. Patra, C. G. Chandaluri, T. P. Radhakrishnan, *Nanoscale* **2012**, *4*, 343.

10. a) F. Bertorelle, D. Lavabre, S. Fery-Forgues, *J. Am. Chem. Soc.* **2003**, *125*, 6244. b) H. Fu, D. Xiao, J. Yao, G. Yang, *Angew. Chem. Int. Ed.* **2003**, *42*, 2883. c) X. Zhang, X. Zhang, W. Shi, X. Meng, C. Lee, S. Lee, *J. Phys. Chem. B* **2005**, *109*, 18777. d) M. Abyan, D. de Caro, S. Fery-Forgues, *Langmuir* **2009**, *25*, 1651.

11. a) S. Abe, L. Chen, *J. Polym. Sci. B* **2003**, *41*, 1676. b) A. Diaspro, S. Krol, B. Campanini, F. Cannone, G. Chirico, *Opt. Exp.* **2006**, *14*, 9815. (c) S. Meyer, P. Pescador, E. Donath, *J. Phys. Chem. C* **2008**, *112*, 1427.

12. S. Jayanty, T. P. Radhakrishnan, *Chem. Mater.* **2001**, *13*, 2460.

13. C. Peyratout, E. Donath, L. Daehne, *J. Photochem. Photobiol. A* **2001**, *142*, 51.

14. D. Baigl, T. A. P. Seery, C. E. Williams, *Macromolecules* **2002**, *35*, 2318.

15. a) M. Ravi, T. P. Radhakrishnan, *J. Phy. Chem.* **1995**, *99*, 17624. b) J. M. Cole, R. C. B. Copley, G. J. McIntyre, J. A. K. Howard, M. Szablewski, G. H. Cross, *Phys. Rev. B* **2002**, *65*, 125107.

16. a) S. Hakkarainen, S. L. Gilbert, A. Kontturi, K. Kontturi, *J. Colloid Interface Sci.* **2004**, *272*, 404. b) Y. Lapitsky, M. Parikh, E. W. Kaler, *J. Phys. Chem. B* **2007**, *111*, 8379.

Synopsis

Amorphous-to-crystalline transformation (ACT) in small molecule based nanoparticles accompanied by substantial changes in some physical responses is of fundamental interest in the growth of molecular crystals and nanostructures and their materials applications. A novel protocol for controlled ACT is demonstrated using a diaminodicyanoquinodimethane based molecule. Molecular structural features that promote the formation of amorphous nanoparticles in drop-cast films of these compounds are identified. The critical steps involved in the procedure for the ACT are the partial confinement of the nanoparticles by fixing in a polymer thin film and solvent vapor fuming. The ACT is accompanied by a strong enhancement of the fluorescence and a conspicuous switching of the emission color. The whole process is monitored by spectroscopy as well as electron and confocal fluorescence microscopy; electronic structure calculations provide insight into the basis of the optical response shifts. The graphic example of the evolution of molecular nanoparticles and the associated changes in materials responses presented in this study suggest a facile route to the fabrication of amorphous molecular nanomaterials, directed transformation of these materials to the crystalline state and exploitation of the crystallinity-property correlations. The amorphous particles are potential model systems for the liquid-like clusters proposed in the two-step nucleation theory.

4.1. Introduction

The classical model for crystallization visualizes the formation of a metastable crystalline nucleus that through density fluctuations reaches a critical size and grows into a stable crystal. The two-step nucleation theory invoking a liquid-like cluster intermediate developed to explain protein crystallization,[1,2] has been shown to be of more general validity, and applicable to macromolecule as well as small molecule based crystals.[3] The amorphous-to-crystalline transformation (ACT) familiar in protein-mineral composites,[4-6] pharamaceuticals[7,8] and inorganics[9-15] including phase-change materials,[16] is of potential interest in the context of molecular crystals and nanocrystals as well. Heterogeneous nucleation and growth in confined environments[17] add a further dimension to the crystallization process.

The coexistence of amorphous/crystalline regions and the impact of crystallinity on properties in macromolecules are well known. Targeted fabrication of the amorphous state, realization of the ACT and the crystallinity-property correlation in small molecule based materials have been explored little, but are significant from the conceptual as well as application perspectives. Thermal annealing induces such changes, for example in rubrene[18] and methanofullerene[19] thin films. Crystalline and amorphous forms of (4-biphenylyl)phenyldibenzofulvene were interconverted by solvent vapor fuming, heating and cooling, the former exhibiting enhanced fluorescence.[20] Photosensitivity of dye aggregates increased when crystallinity was induced through solvent vapor fuming.[21] It is well known that the crystallinity of materials critically affect the charge mobilities in OLED's.[22] In order to explore the ACT in small molecule based materials, it is imperative to develop a molecular design and protocol for the fabrication of amorphous particles followed by their crystallization,

and monitor the transformation together with some materials response that evolves concomitantly.

The enhanced fluorescence of diaminodicyanoquinodimethane (DADQ's) in the solid state fluorescence enhancement compared to the solution state[23] has been discussed in the Chapter 2 and 3. The emission color of DADQ's can be tuned by structural variations,[24-26] and nanocrystals with strong emission have been fabricated.[24,27] The zwitterionic DADQ's crystallize easily as observed with NLO active[28] and fluorescent[23-27] derivatives in earlier studies. Present explorations show that specific structural motifs promote the formation of amorphous particles, when solutions are drop-cast on suitable substrates. As traditional methods failed to induce an ACT, we developed a novel protocol involving fuming of particles partially confined by fixing in a polymer thin film. The transformation is monitored by microscopy along with the accompanying fluorescence switching and enhancement.

4.2. Synthesis and Characterization

We have described the synthesis procedure and structural characterization of DADQ molecules in Chapter 2. We have synthesized several DADQ derivatives to explore the factors that promote the formation of amorphous nanoparticles, the aspect of interest in the present study. The compounds that were found to yield amorphous particles as drop casting dilute solution on substrates like glass are collected in Fig. 4.1. The critical structural feature common to all the derivatives is the presence of aromatic rings linked through conformationally labile bonds. The detailed studies presented below focus on 7,7-bis(2-(4-bromophenyl)ethylamino)-8,8-dicyanoquinodimethane (BBPEDQ).

Synthesis of BBPEDQ: The structure of BBPEDQ molecule and its synthesis is shown in Scheme 4.1. The general procedure used for preparation of BBPEDQ is as follows. 0.10 ml (0.75 mmol) 2-(4-bromophenyl)ethylamine was added to a warm solution of 0.05 g (0.25 mmol) 7,7,8,8-tetracyanoquinodimethane (TCNQ) in 5 ml acetonitrile (CAUTION: HCN is a byproduct in this reaction). The solution turned dark green immediately and changed to orange red subsequently. The reaction mixture was stirred at 75^{o}C for 2.5 h and then at -10^{o}C for 4 h. The light yellow product which precipitated was filtered out and dried. The compound was recrystallized twice from methanol.

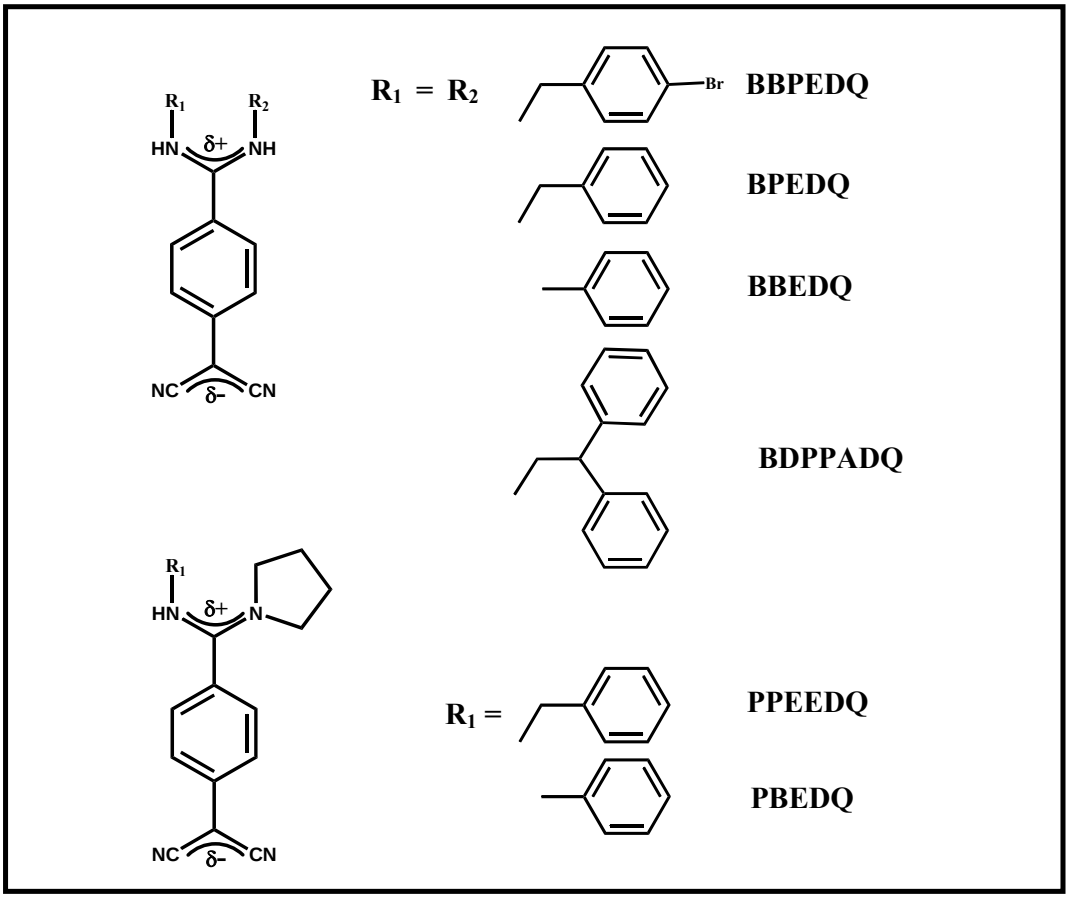

Figure 4.1. *DADQ derivatives that form amorphous nanoparticles on drop-casting on glass substrate.*

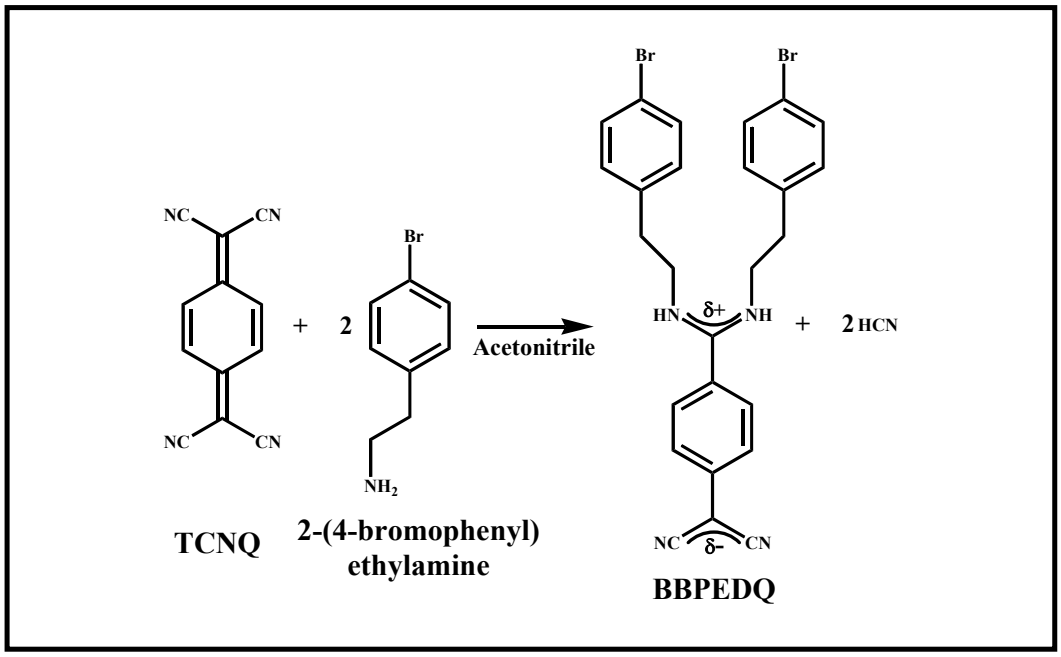

Scheme 4.1. *Synthesis of the BBPEDQ.*

Yield = 72%; M.P. (^{o}C) = 254 - 256; FTIR (KBr) : $\bar{\upsilon}$/cm^{-1} = 3040.09, 2183.62, 2133.46; ^{1}H-NMR (d_6-DMSO) : δ/ppm = 9.17 (brs, 1H), 8.66 (brs, 1H), 7.54 (d, 2H), 7.40 (d, 2H), 7.18 (d, 2H), 7.00 (d, 2H), 6.89 (d, 2H), 6.75 (d, 2H), 3.50-3.48 (m, 4H), 2.80 (t, 2H), 2.73 (t, 2H).

4.3. Crystallographic Information of BBPEDQ

We have determined the crystal structure of BBPEDQ to gain insight into the molecular level interactions in the solid state. Single crystals grown in methanol solution were found to belong to the orthorhombic crystal system and *Pbca* space group. The crystal structure reveals intermolecular amino-cyano H-bonds leading to dimer motifs and extended chains (Fig. 4.2). The crystallographic data are summarized in Table 4.1. The diaminomethylene unit is twisted with respect to the benzenoid ring

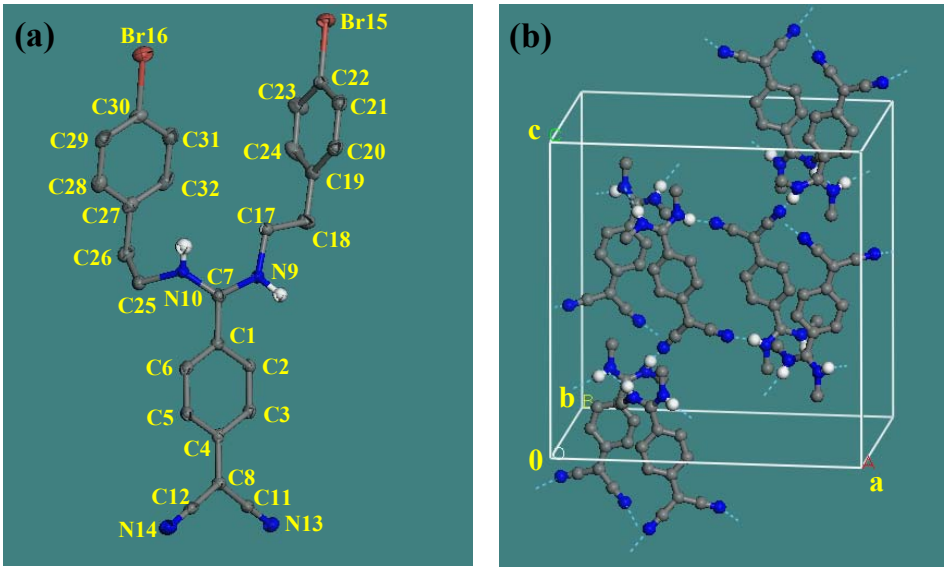

Figure 4.2. ***(a)*** *Molecular and* ***(b)*** *crystal structure of BBPEDQ from single crystal x-ray diffraction analysis; C (grey), H (white), N (blue), Br (red), intermolecular H-bond (dashed line). In (a) and (b), H atoms not involved in the H-bonds are omitted and in (b) only one C atom of the 2-(4-bromophenyl)ethyl group is retained for clarity.*

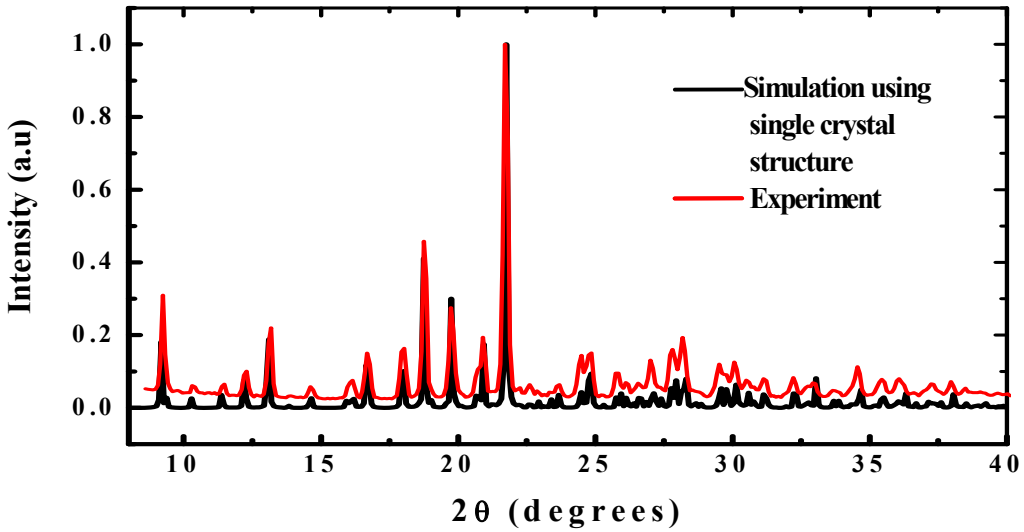

Figure 4.3. *X-ray diffraction pattern of the microcrystalline powder sample of BBPEDQ compared to the pattern obtained by simulation using single crystal structure.*

plane making dihedral angles of 38.1° and 40.3°. Powder X-ray diffraction patterns of solid BBPEDQ samples from different batches of synthesis were found to be identical and in good agreement with the one simulated using the atom coordinates from single crystal X-ray analysis (Fig. 4.3).[30] These observations confirm the purity of the bulk samples and rule out structural variations among the samples.

Table 4.1. *Crystallographic data for BBPEDQ.*

Empirical formula	$C_{26}H_{22}N_4Br_2$
Crystal system	Orthorhombic
Space group	*Pbca*
a / Å	18.7191(17)
b / Å	13.4503(12)
c / Å	19.2747(17)
V / Å^3	4852.9(8)
Z	8
$\rho_{calc.}$ / g cm^{-3}	1.506
μ / mm^{-1}	3.361
Temperature / K	100(2)
λ / Å	0.71073
Min., Max. transmission	0.2376, 0.4529
No. of reflections	4289
No. of parameters	297
GOF	1.043
R [for $I \geq 2\sigma_I$]	0.0315
wR^2	0.0801
Largest diff. peak, hole / eÅ^{-3}	0.481, -0.731

4.4. BBPEDQ Solution and Microcrystals-Spectroscopy and Computation

The optical absorption spectrum of a methanol solution of BBPEDQ has λ_{max} at 371 nm; the microcrystalline solid shows broad (300 – 420 nm) absorption (Fig. 4.4a). The fluorescence emission exhibits a clear peak shift from 485 nm (nearly green) in solution to 462 nm (nearly blue) in microcrystals (Fig. 4.4b), with the intensity increasing ~ 235 times (Fig. 4.4c). The quantum yields are 0.2% and 20.0% in solution and microcrystals respectively.

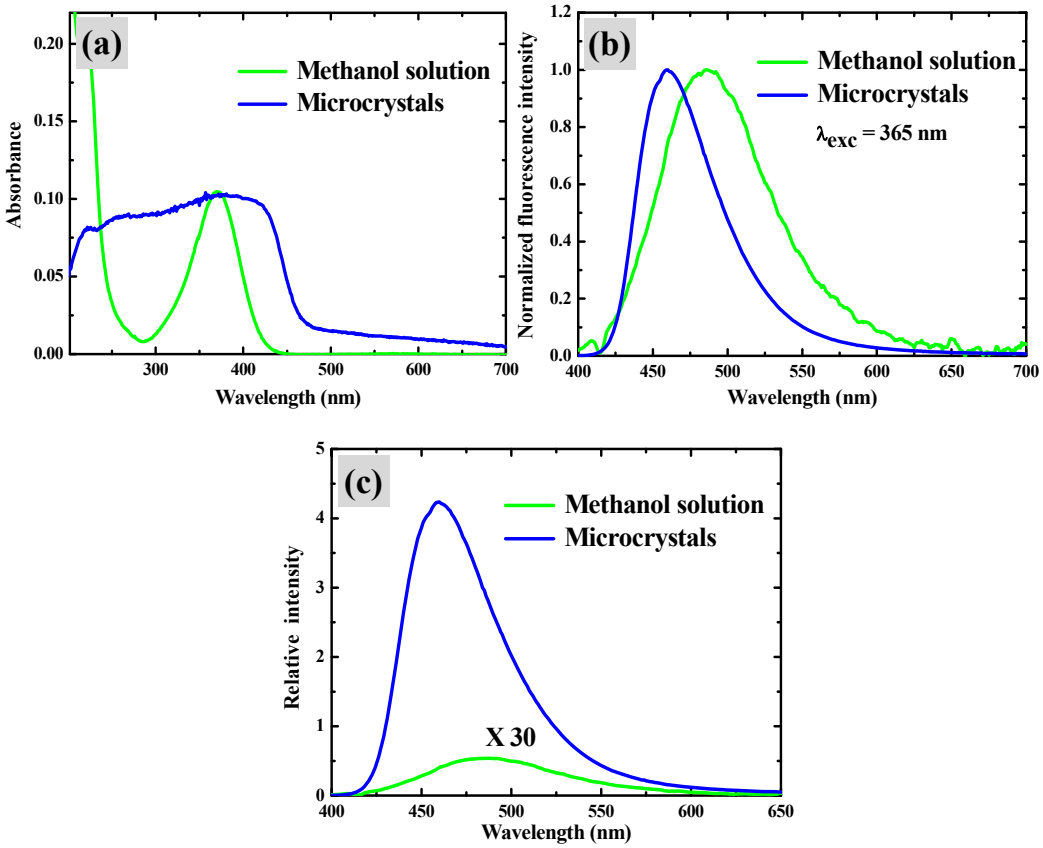

Figure 4.4. *Optical spectra of BBPEDQ:* ***(a)*** *absorption spectra of microcrystals and methanol solution (concentration adjusted to match peak absorbance);* ***(b)*** *normalized fluorescence emission spectra of microcrystals and methanol solution and* ***(c)*** *spectra of samples with matched absorbances; Excitation wavelength for the emission spectra is indicated.*

Time-dependent density functional computations were carried out using *Gaussian 03*[31] to study the electronic structure of BBPEDQ and its dimers. Different monomer geometries were considered for the computational studies (Fig. 4.5). The H-bond dimers with nearly face-on (anti-parallel dipoles) and approximately head-to-tail (quasi parallel dipoles) orientations extracted from the crystal lattice (Fig. 4.6), reminiscent of H- and J- dimers, were used in the computations.

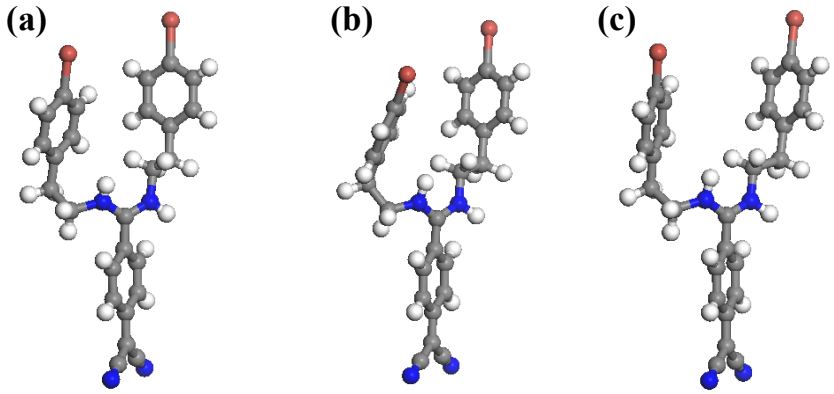

Figure 4.5. ***(a)*** *The molecular geometry taken from the crystal structure,* ***(b)*** *fully optimized in vacuum and* ***(c)*** *SCRF=methanol geometry.*

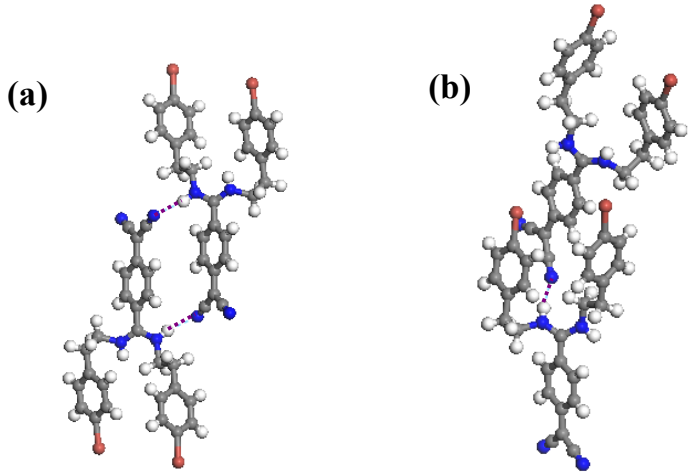

Figure 4.6. *H-bonded dimers taken from the crystal lattice (Fig. 4.2b)* ***(a)*** *with antiparallel dipoles and* ***(b)*** *quasi-parallel dipoles.*

The TD-DFT computations were carried out at the B3LYP/6-31G* level, without and with inclusion of solvation effects [SCRF (Solvent = Methanol); OFac=0.8; Rmin=0.5].

The critical geometric parameter, the dihedral twist angle between the diaminomethylene unit and the benzenoid ring (θ; the two values in the molecule and the average) and the computed excitation wavelengths (in the UV-Vis range) with appreciable oscillator strength for the different monomer structures are collected in Table 4.2. The lowest excitation energy with high oscillator strength, of the fully optimized structure of BBPEDQ in methanol environment (entry in bold font) is at 385.3 nm consistent with the solution spectrum.

It may be noted that, B3LYP/6-31G* optimization of the molecular geometry in vacuum gives a dihedral angle very different from that observed in the solid state. Imposition of a dielectric environment (equivalent to methanol) leads to a geometry in

Table 4.2. *Experimental and computed (*B3LYP/6-31G* with TD or B3LYP/6-31G* with TD, SCRF*) geometric, electronic and spectroscopic parameters of BBPEDQ monomer.*

Structure	**Twist angle θ (deg.)**	**λ_{max} (nm) [f]**	
		Vacuum	**Methanol**
Molecular geometry from crystal structure	39.2 {38.1, 40.3}	458.7 [0.65] 271.6 [0.26]	385.9 [0.84] 263.2 [0.03]
B3LYP/6-31G* Optimized (vacuum)	28.8 (27.0, 30.5}	415.0 [0.98] 261.5 [0.13]	-
B3LYP/6-31G*/SCRF Optimized (methanol)	40.3 (38.9, 41.6)	-	**385.3 [0.86] 246.3 [0.16]**

close agreement to that observed in the solid state, suggesting that the local environment of the molecule in the solid state can be mimicked using the SCRF model with the dielectric constant of methanol. This concept has been used successfully to explain the molecular structures of DADQ molecules.[32] As shown in the monomer calculations, the molecular and hence electronic structure of BBPEDQ in the solid state can be mimicked correctly using a dielectric environment (equivalent to methanol). Hence all the computations on the dimers in the solid were carried out including the solvation effect [SCRF (Solvent = Methanol); OFac=0.8; Rmin=0.5]. The computed excitation wavelengths (in the UV-Vis range) with appreciable oscillator strength are collected in the Table 4.3. The lowest energy excitations for the dimer with face-on and head-to-tail

Table 4.3. *Computed (*B3LYP/6-31G* with TD or B3LYP/6-31G* with TD, SCRF*) electronic and spectroscopic parameters of BBPEDQ dimer.*

Structure	**λ_{max} (nm) [f]**	
	Vacuum	**Methanol**
H-bonded dimer (antiparallel dipole)	406.4 [1.38] 383.9 [0.07] 333.2 [0.03] 261.1 [0.03] 259.9 [0.24] 258.1 [0.03]	**368.2 [1.62]** 262.4 [0.06] 248.0 [0.04]
H-bonded dimer (quasi-parallel dipole)	450.6 [0.98] 442.9 [0.22] 428.4 [0.19] 415.3 [0.09] 266.9 [0.29] 264.4 [0.13]	**394.7 [0.63]** **392.3 [0.28]** **377.0 [0.64]** 265.3 [0.03] 252.5 [0.05]

geometries are found to be at 368.2 nm in the former and at 394.7, 392.3 and 377.0 nm in the latter (entry in bold font). This is consistent with the broad absorption of the solid; the higher excitation energy of the latter dimer possibly leads to the blue shift of the emission. These computations clearly show that the blue shift of the absorption and fluorescence emission of BBPEDQ, from the solution to the crystalline state is a consequence of molecular assembly.

4.5. Fabrication and Optical Properties of BBPEDQ Nanoparticles

4.5.1 *Amorphous hemispherical particles*

The critical structural feature common to all the derivatives in Fig. 4.1 is the presence of aromatic rings linked through conformationally labile bonds. These molecules are found to form a thin film of hemispherical amorphous particles of uniform size when dilute solutions are drop-cast on hydrophilic substrates like glass followed by slow evaporation under ambient atmosphere and vacuum drying. Schematic representation of this process is shown in Fig. 4.7.

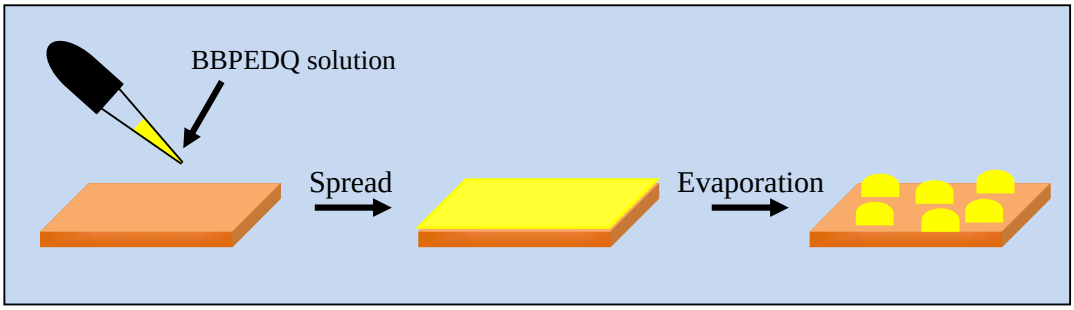

Figure 4.7. *Formation of amorphous nanoparticles by drop-cast technique.*

Molecular structure is plays a significant role in the formation of the amorphous nanoparticles. Formation of the amorphous particles is also affected by other factors

such as the solvent used and the concentration of the solution, nature of the substrate, solvent and evaporation rate. The particle size can be tuned from ~ 700 nm to 50 nm by varying the solution concentration from 1.00 to 0.01 mM (Fig. 4.8). Several interesting morphologies like network structures can be realized by changing the solvent and the substrate (Fig. 4.9). Fast evaporation of low concentration methanol solution under

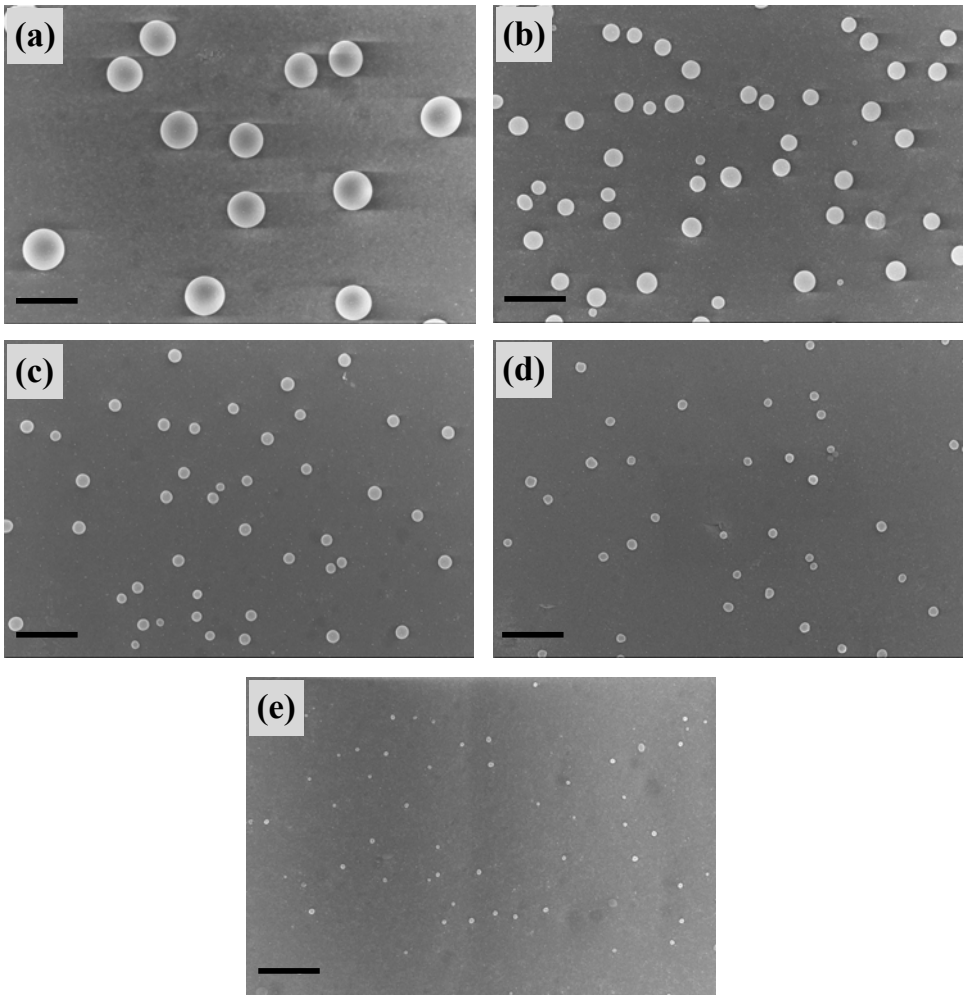

Figure 4.8. *FESEM images of BBPEDQ nanoparticles obtained by drop-casting methanol solutions of different concentrations,* ***(a)*** *1 mM,* ***(b)*** *0.5 mM,* ***(c)*** *0.1 mM,* ***(d)*** *0.05 mM,* ***(e)*** *0.01 mM, on glass substrate. Scale bar = 1 μm.*

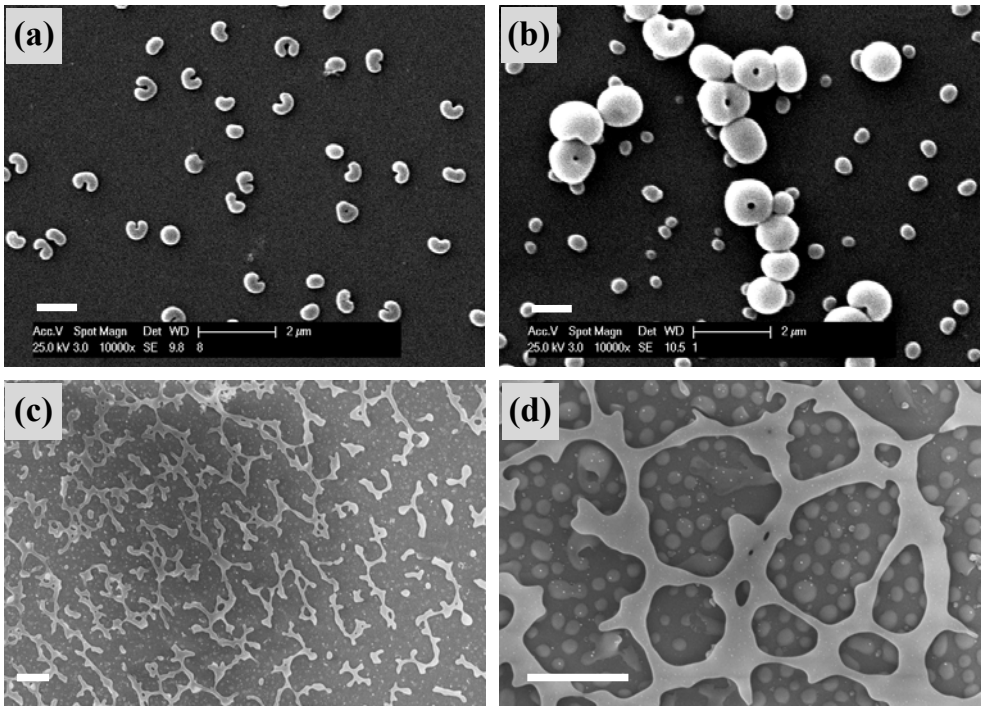

Figure 4.9. *FESEM images of films obtained by drop-casting methanol solution (0.2mM) of BBPEDQ **(a)**, **(b)** on glass, quickly dried under vacuum; **(c)** and **(d)** on hydrophobic surface (glass treated with hexamethyldisilazane), (Scale bar = 1μm).*

vacuum produces cashew and donut shaped particles (Fig. 4.9a and b). Network structures are observed on hydrophobic surfaces (Fig. 4.9c and d). This may be due to the change in the wettability of the solution on the substrate. Optical spectra of the drop-cast films on quartz are shown in Fig. 4.10a and b; λ_{max} of the absorption and emission are at 390 nm and 487 nm respectively. The films produce a green emission on illumination by a UV (365 nm) lamp. Comparison with the solution and microcrystals (Fig. 4.4) suggests that these particles, even though in the solid state, are far from crystalline. The hydrophobic substituents on BBPEDQ possibly promote dewetting on the glass and the conformational lability of the molecule leads to the amorphous assembly.

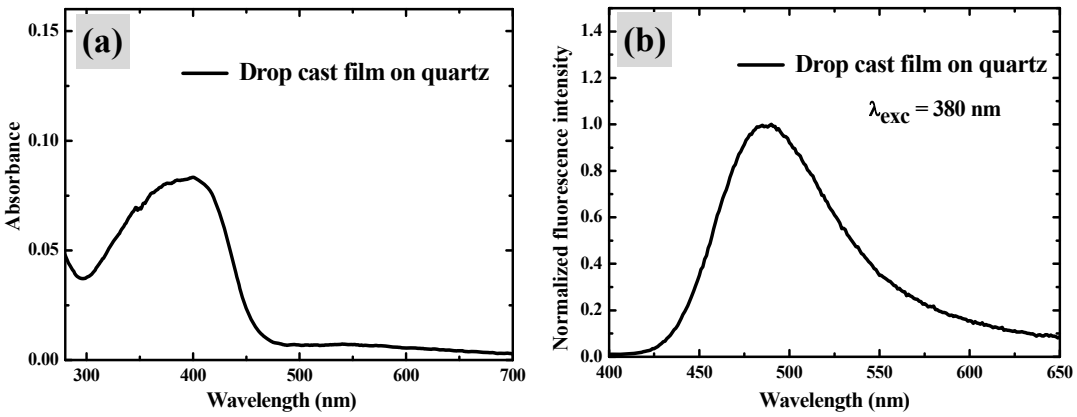

Figure 4.10. *Optical spectra of BBPEDQ:* ***(a)*** *and* ***(b)*** *are the corresponding absorption and fluorescence emission spectra of drop cast film on quartz plate. Excitation wavelength for the emission spectrum is indicated.*

4.5.2 *Amorphous-to-crystalline transformation*

Common techniques like heating and exposure to solvent fumes used to induce crystallization of amorphous particles led to the aggregation of BBPEDQ particles (Fig. 4.11), but no crystallization. The films before and after the treatment showed green fluorescence emission indicating that the amorphous nature is unchanged. We have also explored the use of other substrates such as polystyrene-coated glass to induce crystallization; however, no crystallization was observed again, but only further aggregation of the amorphous particles (Fig. 4.10).

Failure of the traditional methods is prompted us to develop a new protocol for confining the particles before attempting the ACT; the procedure is represented schematically in Fig. 4.13. A toluene solution of polystyrene (PS) was spin-coated on top of the drop-cast film on glass and dried under vacuum; it was then peeled off to give

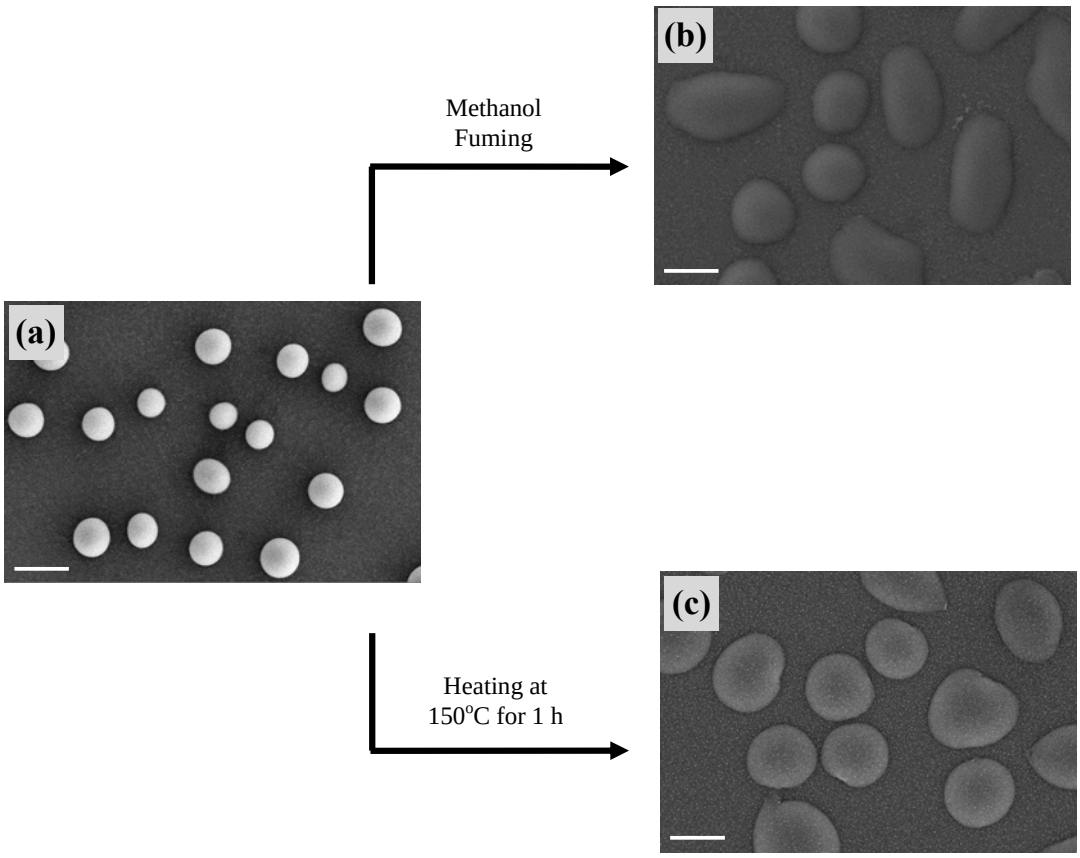

Figure 4.11. *FESEM images of BBPEDQ amorphous particles **(a)** obtained by drop-casting on glass, **(b)** after methanol fuming and **(c)** heating at 150°C for 1h.*

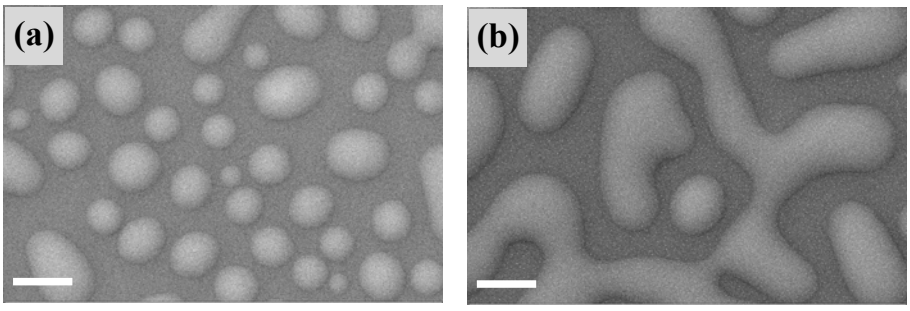

Figure 4.12. *FESEM images of BBPEDQ on PS coated on glass, **(a)** before and **(b)** after exposure to methanol vapor.*

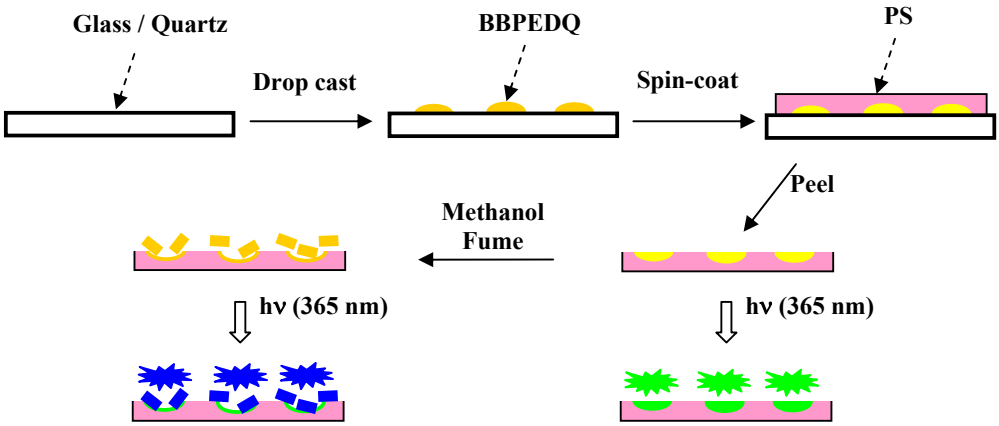

Figure 4.13. *Protocol for drop-casting, fixing in PS film and solvent vapor fuming to induce amorphous-to-crystalline transformation. Fluorescence responses of the crystalline and amorphous nanoparticles are indicated schematically.*

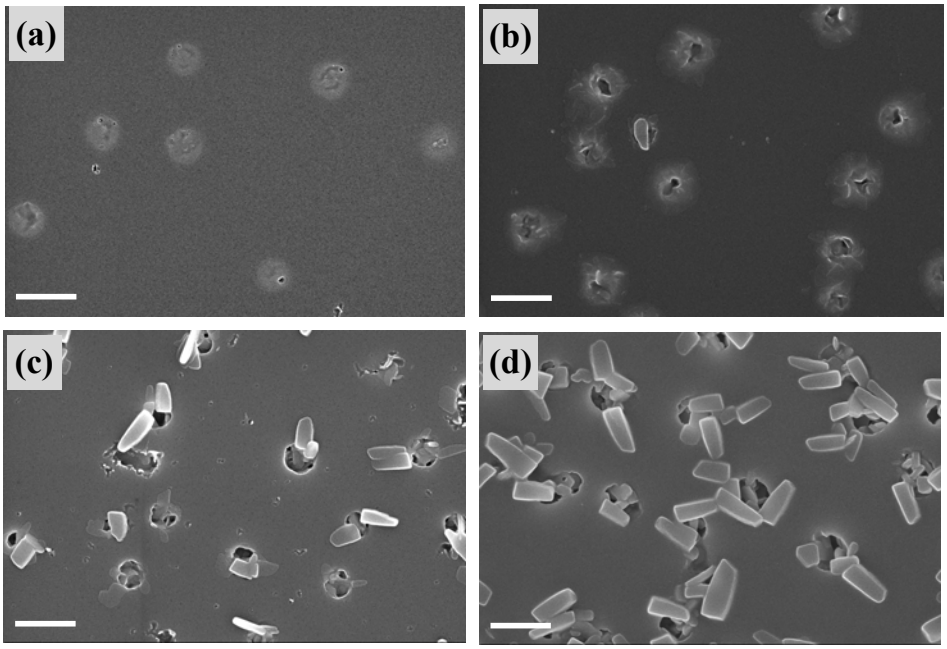

Figure 4.14. *FESEM images of BBPEDQ nanoparticles:* ***(a)*** *fixed in PS film,* ***(b - d)*** *fixed in PS film and exposed to methanol vapors for 1, 3 and 5 min, Scale bar = 1 μm.*

a free-standing film. Images of the lower side of the film reveal the circular particles fixed there (Fig. 4.14a). This side was then exposed to methanol vapors for short periods of time. Images of the film (Fig. 4.14b-d) demonstrate the formation of faceted particles and their emergence from the circular slots in the polymer which were home to the amorphous particles. This is a typical case of *square peg in a round hole.* On exposure of the film to methanol vapor, the optical absorption shifts slightly (Fig. 4.15a),

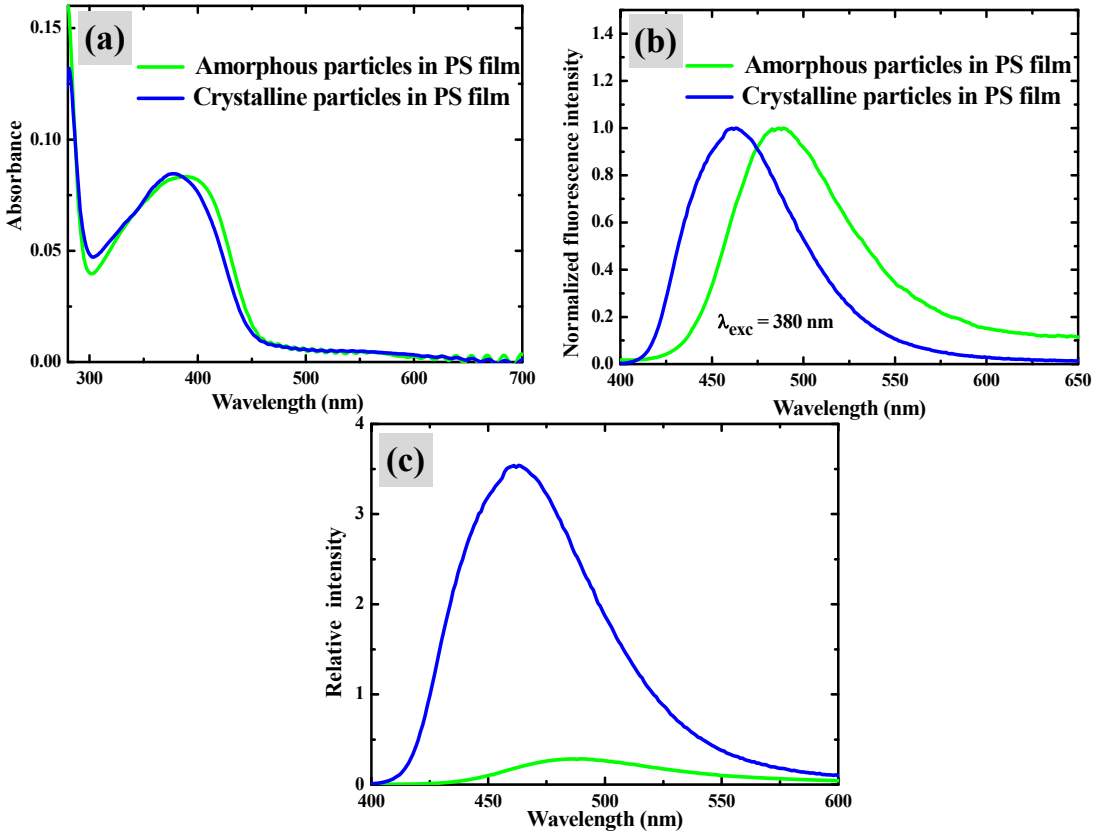

Figure 4.15. *Optical spectra of BBPEDQ:* ***(a)*** *and* ***(b)*** *are the corresponding absorption and fluorescence emission spectra of free-standing PS film with nanoparticles before (amorphous) and after 5 min exposure to methanol vapor (crystalline) and* ***(c)*** *spectra of samples with matched absorbances; Excitation wavelength for the emission spectra are indicated.*

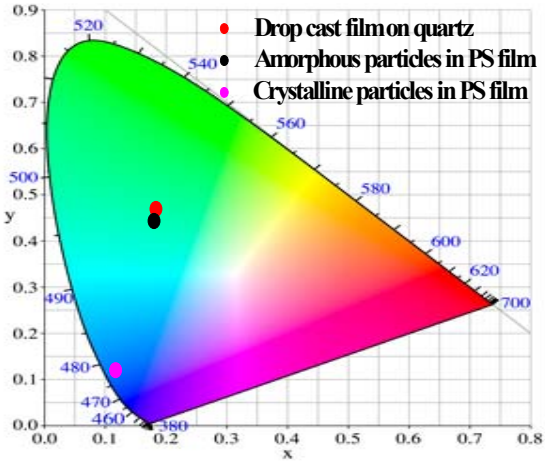

Figure 4.16. *CIE chromaticity diagram showing the color response of different BBPEDQ films.*

but the emission peak shows a definitive blue shift from 487 nm to 462 nm (Fig. 4.15b), in a manner identical to that of solution and microcrystal. The CIE chromaticity coordinates which represents the visible emission colors of the amorphous and crystalline films are shown in Fig. 4.16. The fluorescence shift is clearly indicative of an ACT. The fluorescence intensity increases ~ 13 times upon crystallization (Fig. 4.15c); quantum yields are 7.3% and 15.4% in the amorphous and crystalline forms respectively.

4.6. Characterization of Amorphous and Crystalline Particles

TEM images of the particles freed by dissolving the PS in toluene were recorded. While the circular particles showed no electron diffraction spots (Fig. 4.17a), the faceted ones obtained by exposure to methanol showed a diffraction pattern (Fig. 4.17b). The diffraction pattern is consistent with the crystal structure of BBPEDQ as shown by the indexing of the prominent spots (Fig. 4.18 and Table 4.4). This provides the final proof

for the formation of nanocrystals. It should be mentioned that, there was no definitive evidence of the ACT under electron beam irradiation, even though such a possibility exists.

Confocal fluorescence images were recorded using the emission in the 410 – 430 nm and 620 – 650 nm windows, excluding the emission from the amorphous and crystalline particles respectively (Fig. 4.15b); these are colored blue and green in Fig. 4.19. The film before exposure to methanol shows the emission from amorphous particles alone (Fig. 4.19a). Emissions from the coexisting crystalline (elongated) and amorphous (circular) particles in the exposed film are shown superposed in Fig. 4.19b. The spectral response from the different particles is depicted in Fig. 4.19c.

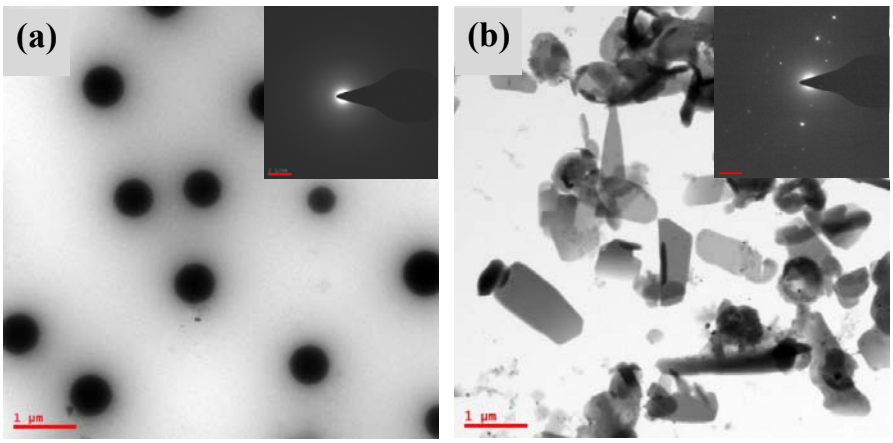

Figure 4.17. *TEM images with selected area electron diffraction (inset) of BBPEDQ nanoparticles in PS film **(a)** before and **(b)** after exposure to methanol vapor. Scale bar = 1 µm.*

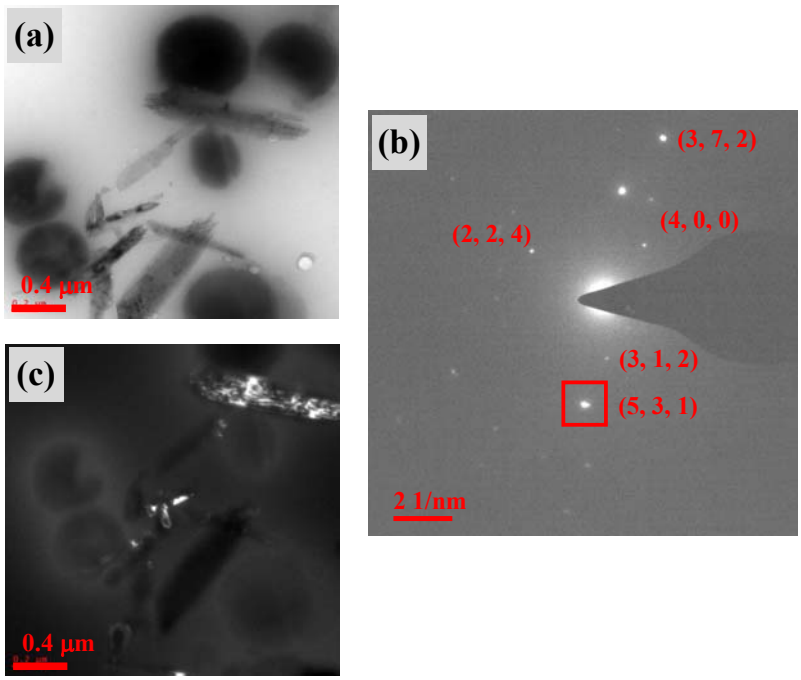

Figure 4.18. ***(a)*** *Bright field TEM image of a selected area,* ***(b)*** *corresponding electron diffraction pattern* ***(c)*** *dark field TEM image recorded using the diffraction spot indicated in (b), demonstrating that the diffraction arises from the crystalline particles.*

Table 4.4. *Indexing of the prominent spots (Fig. 4.16) using the interplanar spacing (d) values observed in the electron diffraction pattern and estimated from the crystal structure.*

d (Å) [from the electron diffraction pattern]	**d (Å) [calculated from the crystal structure]**	**h k l**
4.911	4.913	3 1 2
4.729	4.723	4 0 0
3.625	3.626	2 2 4
2.865	2.867	5 3 1
1.818	1.818	3 7 2

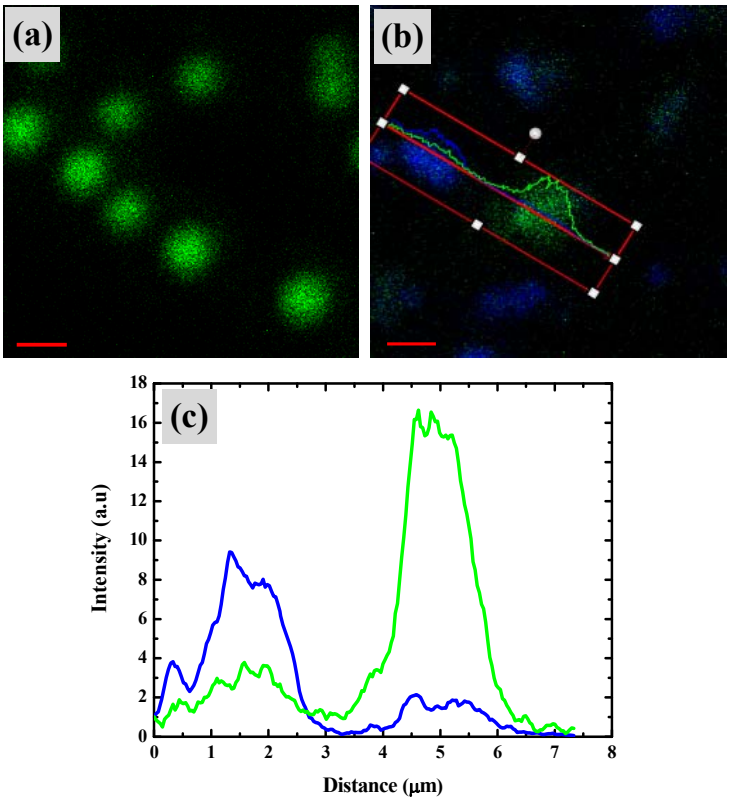

Figure 4.19. *Laser scanning confocal fluorescence images of the film **(a)** before and **(b)** after exposure to methanol vapor; blue and green colors represent emission in the 410 – 430 nm and 620 – 650 nm windows respectively, and **(c)** the spectral response in the two windows along the line shown on the image in (b). Scale bar = 1 μm.*

The amorphous and crystalline nanoparticles were isolated by dissolving the PS films in toluene, filtering through a nanoporous membrane and washing with toluene to remove any remnant PS. Particles from the film before exposure to methanol are hemispherical domes as expected (Fig. 4.20a and b). Interestingly, those from the exposed film show hemispherical shells with nanocrystals within and outside (Fig. 4.20c, d, e and f). The images suggest the following mechanism of ACT. Methanol vapor condenses on the amorphous particles fixed in the PS film forming a liquid-like cluster inside the cavities. Crystalline nuclei emerging within this cluster as visualized.

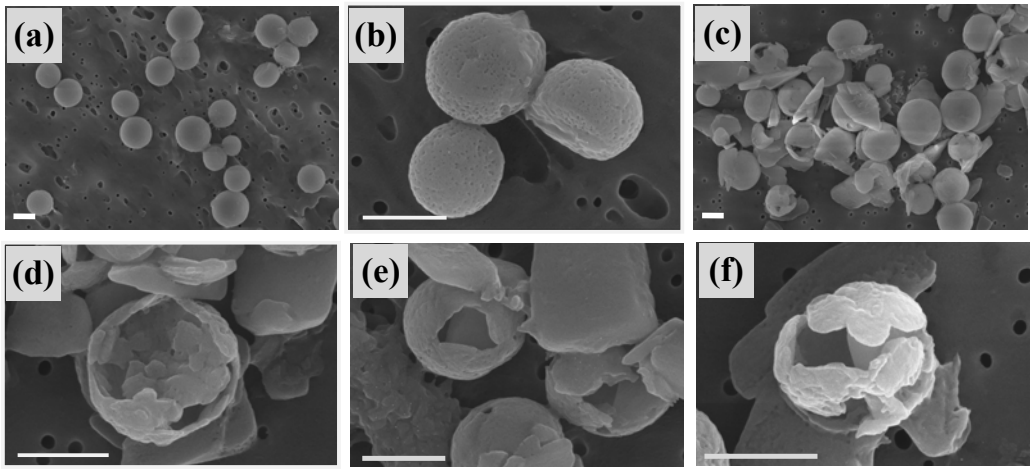

Figure 4.20. *FESEM images of the BBPEDQ nanoparticles; obtained by dissolving PS films in toluene and filtering through nanoporous polycarbonate membrane.* ***(a,b)*** *amorphous particles (before exposing) and* ***(c,d,e,f)*** *crystalline particles (after exposing to methanol vapors). Exposed film show hemispherical shells with nanocrystals within and outside (Scale bar = 500 nm).*

In the two-step nucleation model grow into stable nanocrystals. The molecules in contact with the cavity wall, possibly involved in hydrophobic interactions with the polymer, stay in amorphous state forming the shell.

Direct visualization of the liquid-like cluster proposed in the two-step nucleation model have been reported for some biological macromolecules.[33] However similar demonstration in the case of small molecule based particles are rare. The direct observation of the amorphous particles of the DADQ's expected to be a useful starting point for further investigations into the basic steps involved in the formation of molecular crystals.

4.7. Conclusions

The present study provides significant insight into the nucleation and growth of molecular nanocrystals. Molecular features and substrate characteristics conducive to the formation of amorphous particles in drop-cast films are identified. The protocol involving solvent vapor fuming of amorphous particles fixed in polymer cavities provides a facile route to the ACT and its graphic demonstration. The enhanced and shifting fluorescence emission accompanying the ACT makes BBPEDQ of considerable materials interest as well.

References

1. P. G. Vekilov, *J. Cryst. Growth* **2005**, *275*, 65.
2. P. G. Vekilov, *Nanoscale* **2010**, *2*, 2346.
3. D. Erdemir, A. Y. Lee, A. S. Myerson, *Acc. Chem. Res.* **2009**, *42*, 621.
4. X. Cheng, L. B. Gower, *Biotech. Prog.* **2006**, *22*, 141.
5. C. Wu, J. Martel, D. Young, J. D. Young, *PloS ONE* **2009,** *4*, e8058.
6. H. Peng, J. Martel, Y. Lee, D. M. Ojcius, J. D. Young, *Nanomedicine* **2011**, *6*, 643.
7. S. Strydom, W. Liebenberg, L. Yu, M. De Villiers, *Int. J. Pharm.* **2009**, *379*, 72.
8. D. Xia, J. X. Wu, F. Cui, H. Qu, T. Rades, J. Rantanen, M. Yang, *Eur. J. Pharm. Sci. A* **2012**, *46*, 446.
9. S. Hasegawa, S. Horike, R. Matsuda, S. Furukawa, K. Mochizuki, Y. Kinoshita, S. Kitagawa, *J. Am. Chem. Soc.* **2007**, *129*, 2607.
10. Y. Jeon, J. Heo, C. A. Mirkin, *J. Am. Chem. Soc.* **2007**, *129*, 7480.
11. J. Tao, H. Pan, H. Zhai, J. Wang, L. Li, J. Wu, W. Jiang, X. Xu, R. Tang, *Cryst. Growth Des.* **2009**, *9*, 3154.
12. V. B. Mortola, A. P. Ferreira, J. M. Fedeyko, C. Downing, J. M. C. Bueno, M. C. Kung, H. H. Kung, *J. Mater. Chem.* **2010**, *20*, 7517.
13. L. C. Jacobson, V. Molinero, *J. Am. Chem. Soc.* **2011**, *133*, 6458.
14. S. Jana, R. M. Rioux, *Nanoscale* **2012**, *4*, 1782.
15. J. Xiao, S. Yang, *Nanoscale* **2012**, *4*, 54.
16. S. Raoux, D. Ielmini, M. Wuttig, I. Karpov, *MRS Bull.* **2012**, *37*, 118.
17. B. D. Hamilton, J. Ha, M. A. Hillmyer, M. D. Ward, *Acc. Chem. Res.* **2012**, *45*, 414.
18. S. Park, J. Choi, K. H. Lee, H. W. Yeom, S. Im, Y. K. Lee, *J. Phys. Chem. B* **2010**, *114*, 5661.
19. L. Zheng, J. Liu, Y. Ding, Y. Han, *J. Phys. Chem. B* **2011**, *115*, 8071.

20. Y. Dong, J. W. Y. Lam, A. Qin, Z. Li, J. Sun, H. H.-Y. Sung, I. D. Williams, B. Z. Tang, *Chem. Commun.* **2007**, 40.

21. B. Z. Tang, H. Z. Chen, R. S. Xu, J. W. Y. Lam, K. K. L. Cheuk, H. N. C. Wong, M. Wang, *Chem. Mater.* **2000,** *12*, 213.

22. Y. Shirota, H. Kageyama, *Chem. Rev.* **2007**, *107*, 953.

23. S. Jayanty, T. P. Radhakrishnan, *Chem. Eur. J.* **2004**, *10*, 791.

24. A. Patra, N. Hebalkar, B. Sreedhar, M. Sarkar, A. Samanta, T. P.Radhakrishnan, *Small* **2006**, *2*, 650.

25. C. G. Chandaluri, T. P. Radhakrishnan, *Opt. Mater.* **2011**, *34*, 119.

26. A. Patra, T. P. Radhakrishnan, *Chem. Eur. J.* **2009**, *15*, 2792.

27. C. G. Chandaluri, A. Patra, T. P. Radhakrishnan, *Chem. Eur. J.* **2010**, *16*, 8699.

28. T. P. Radhakrishnan, *Acc. Chem. Res.* **2008**, *41*, 367.

29. W. R. Hertler, H. D. Hartzler, D. S. Acker, R. E. Benson, *J. Am. Chem. Soc.* **1962**, *84*, 3387.

30. PowderCell for Windows Version 2.4, W. Kraus and G. Nolze.

31. *Gaussian 03*, Revision E.01, M. J. Frisch, G. W. Trucks, H. B. Schlegel, G. E. Scuseria, M. A. Robb, J. R. Cheeseman, J. A. Jr. Montgomery, T. Vreven, K. N. Kudin, J. C. Burant, J. M. Millam, S. S. Iyengar, J. Tomasi, V. Barone, B. Mennucci, M. Cossi, G. Scalmani, N. Rega, G. A. Petersson, H. Nakatsuji, M. Hada, M. Ehara, K. Toyota, R. Fukuda, J. Hasegawa, M. Ishida, T. Nakajima, Y. Honda, O. Kitao, H. Nakai, M. Klene, X. Li, J. E. Knox, H. P. Hratchian, J. B. Cross, V. Bakken, C. Adamo, J. Jaramillo, R. Gomperts, R. E. Stratmann, O. Yazyev, A. J. Austin, R. Cammi, C. Pomelli, J. W. Ochterski, P. Y. Ayala, K. Morokuma, G. A. Voth, P. Salvador, J. J. Dannenberg, V. G. Zakrzewski, S. Dapprich, A. D. Daniels, M. C. Strain, O. Farkas, D. K. Malick, A. D. Rabuck, K. Raghavachari, J. B. Foresman, J. V. Ortiz, Q. Cui, A. G. Baboul, S. Clifford, J. Cioslowski, B. B. Stefanov, G. Liu, A. Liashenko, P. Piskorz, I. Komaromi, R. L. Martin, D. J. Fox, T. Keith, M. A. Al-Laham, C. Y. Peng, A. Nanayakkara, M. Challacombe, P. M. W. Gill, B. Johnson, W. Chen, M. W. Wong, C. Gonzalez, J. A. Pople, Gaussian, Inc., Wallingford CT, **2004**.

32. S. Jayanty, T. P. Radhakrishnan, *Chem. Mater.* **2001**, *13*, 2460.

33. O. Galkin, K. Chen, R. L. Nagel, R. E. Hirsch, G. Vekilov, *Proc. Natl. Acad. Sci.* **2002**, *99*, 8479.

Synopsis

Fabrication of an amorphous phase and its hierarchical evolution to a crystalline state offers a new dimension in the assembly of small molecule based materials. Besides the relevance to the fundamental processes of nucleation and crystal growth, this can be of practical interest if there is a parallel evolution of the materials attributes. The morphology and extent of crystallinity of the nanostructures in drop-cast thin films of a diaminodicyanoquinodimethane molecule are shown to be tunable through the variation in the composition of the solvent mixture used for drop-casting. Intermediate stages of the amorphous-to-crystalline evolution can be captured through the control of the drop-casting conditions. The different stages of assembly starting from the solvated molecule through amorphous spherical particles, crystalline nanofibers and nano/microcrystals to bulk crystals are shown to be accompanied by a smooth variation of the fluorescence emission. The color evolves from green through cyan to blue, and the efficiency increases steadily with the overall enhancement from the solution to the bulk crystalline state being ~ 400 times. Quantum chemical computations on the molecule and its H-bonded dimer and π-dimers provide a model to understand the impact of intermolecular interactions in the crystalline assemblies on the electronic structure, and provide insight into the experimental observations. The current study illustrates a significant departure from the conventional molecules-to-materials transition (Sec. 1.2.1), opening up new pathways of hierarchical evolution that enhance the flexibility and versatility of molecular materials.

5.1. Introduction

The fundamental paradigm in the fabrication of molecular materials is the transition from molecules to materials. Tailoring the materials responses and attributes is generally achieved by tuning the structure and functionalities of the molecular building blocks and through them their assemblies, an approach that could be termed as intrinsic design. The contrasting scenario would be the control of molecular assembly mediated by extrinsic factors such as template or substrate effects,[1,2] electric/magnetic fields[3,4] and mechanical constraints.[5] Organized assembly of molecules into crystalline lattices makes the elucidation of the material's structure-property correlations and further design optimization especially convenient. However an important aspect that warrants consideration is the feasibility of realizing a hierarchical assembly of molecules from the isolated (or solvated) state through an amorphous solid form to the final crystalline state, and its potential implications for the materials attributes. The amorphous state opens up a new dimension in the molecules-to-materials transition and offers the opportunity to fine-tune the properties of the molecular assembly. It is notable that the reversible transition between the amorphous and crystalline states is the basis of commercially important phase-change materials based on inorganic systems.[6] Amorphous state of molecular nanomaterials is also relevant in the context of the two-step nucleation theory of fundamental interest in crystal growth (Sec. 1.4.1).[7-9]

The coexistence of amorphous and crystalline regions in polymers and their critical role in determining the materials properties are well recognized; the extent of crystallinity is a basic characteristic of any polymeric material. A recent example of interest for light emitting materials is the tuning of the crystallinity of poly(3-hexylthiophene) nanoparticles by varying the solvent composition.[10] In the domain of

small molecule based materials, the amorphous phase and its attributes have been less widely realized and exploited as pointed out in Chapter 4. One of the few cases relates to electroluminescent systems and charge mobilities promoted by the amorphous nature.[11] Thermal and solvent vapor induced amorphous-to-crystalline transformation (ACT) has been explored in thin films[12,13] and dye aggregates.[14,15] In Chapter 4, We have described the simple protocol that we have developed for the ACT of nanoparticles of a diaminodicyanoquinodimethane (DADQ) derivative accompanied by fluorescence switching and enhancement.[16] The utility of mechanical control of the aggregation of an amphiphilic DADQ molecule at the air-water interface and its impact on the optical responses of the resulting monolayer Langmuir-Blodgett films have been investigated in our laboratory.[17]

As discussed earlier (Sec. 1.2.3), aggregation induced enhancement of fluorescence,[18,19] as opposed to its quenching, is of considerable interest from the perspectives of both molecular level interactions/assembly as well as applications such as displays and sensors. Enhancement of the fluorescence of DADQ molecules from their solution to the crystalline solid state has been investigated in detail in our laboratory.[20] The size-dependent optical responses of nano/microcrystals[21] and the enhancement of fluorescence in the solution and colloidal states of a DADQ derivative by polyelectrolyte templating have also been explored (Chapter 3).[22] Since the fluorescence emission wavelength and efficiency of DADQ's are strongly sensitive to the molecular environment as well as the rigidification of their structures, it would be interesting to explore the hierarchical assembly of these molecules through the amorphous state and monitor the consequence to the fluorescence characteristics.

In Chapter 4 we have shown that the introduction of aromatic groups through conformationally labile bonds on to the DADQ framework promotes the formation of

amorphous particles in thin films formed by drop-casting their dilute solutions on glass substrates.[16] Subsequently, we have synthesized and structurally characterized a new DADQ molecule, 7-pyrrolidino-7-benzylamino-8,8-dicyanoquinodimethane (PBEDQ). Drop-cast thin films obtained from solutions of PBEDQ with varying compositions of a good solvent and a nonsolvent revealed nanostructures ranging from amorphous spherical particles, to crystalline fibers, to faceted nano/microcrystals, and intermediate composite structures. A parallel evolution of the fluorescence emission in terms of the color as well as intensity is observed. This study demonstrates the utility of extending the hierarchical stages of molecular assembly by introducing the new dimension of the amorphous state, and its significant consequences for the materials responses.

5.2. Synthesis and Structure of PBEDQ

5.2.1 *Synthesis and characterization*

PBEDQ was synthesized in two steps as shown in Scheme 5.1 starting with 7,7,8,8-tetracyanoquinodimethane (TCNQ).

7-pyrrolidino-7,8,8,-tricyanoquinodimethane (PTCNQ): 0.10 ml (1.18 mmol) pyrrolidine was added to a warm solution of 0.3 g (1.48 mmol) TCNQ in 30 ml acetonitrile (CAUTION: HCN is a byproduct in this reaction). The solution turned purple immediately. The reaction mixture was stirred at 75^{o}C for 4 h and then kept at -10^{o}C for 1 h. The dark purple product which precipitated was filtered out and dried to give 0.26 g of PTCNQ (yield = 88%). The compound was recrystallized once from acetonitrile.

PBEDQ: 0.12 ml (1.2 mmol) benzylamine was added to a warm solution of 0.2 g (0.8 mmol) PTCNQ in 20 ml acetonitrile (CAUTION: HCN is a byproduct in this reaction).

The solution turned to light yellow immediately. The reaction mixture was stirred at 75^{o}C for 2 h and then kept at -10^{o}C for 2 h. The light yellow product which precipitated was filtered out and dried to give 0.23 g of PBEDQ (yield = 86%). It was recrystallized twice from acetonitrile.

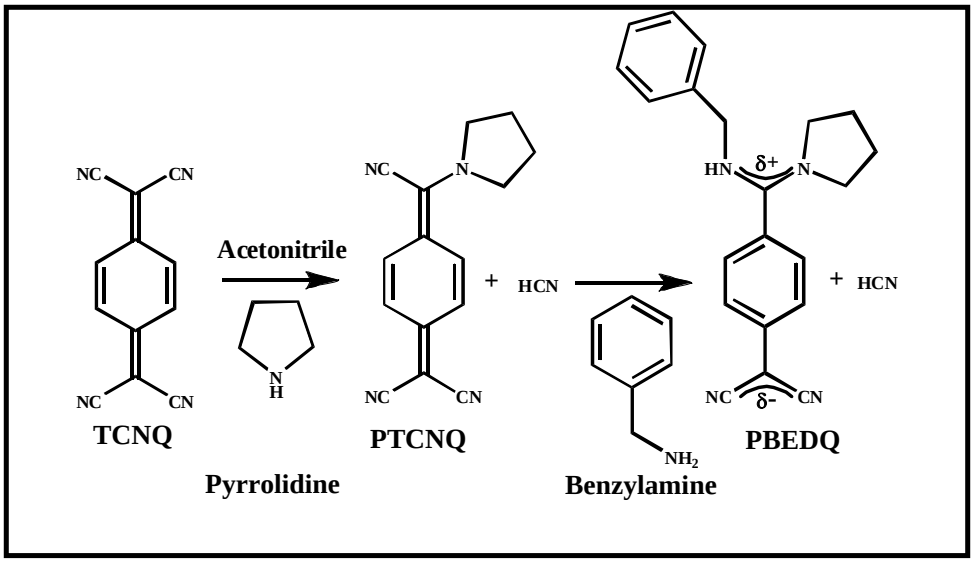

Scheme 5.1. *Synthesis of PBEDQ.*

M.P. (^{o}C) = 228 - 230; FTIR (KBr) : $\bar{\upsilon}$/cm^{-1} = 3046.3, 2169.4, 2136.5; ^{1}H-NMR (d_6-DMSO) : δ/ppm = 9.11 (s, 1H), 7.35-7.33 (m, 2H), 7.28-7.25 (m, 1H), 7.19 (d, 2H), 7.06 (d, 2H), 6.78 (d, 2H), 4.34 (s, 2H), 3.56 (t, 2H), 3.35-3.31 (m, 2H), 2.07-2.01 (m, 2H), 1.86-1.79 (m, 2H); HRMS (ESI) : m/z = 329.1766 [calc. for $C_{21}H_{21}N_4$ $(M+H)^+$: 329.1761].

5.2.2 *Crystallographic information of PBEDQ*

Crystals of PBEDQ grown from acetonitrile solution are found to belong to the *P2$_1$/n* space group with one molecule in the asymmetric unit. The molecular structure and the unit cell packing are shown in Fig. 5.1a and b respectively; the disordered carbon atom C17 is placed in the average position. Fig. 5.1c shows the disordered

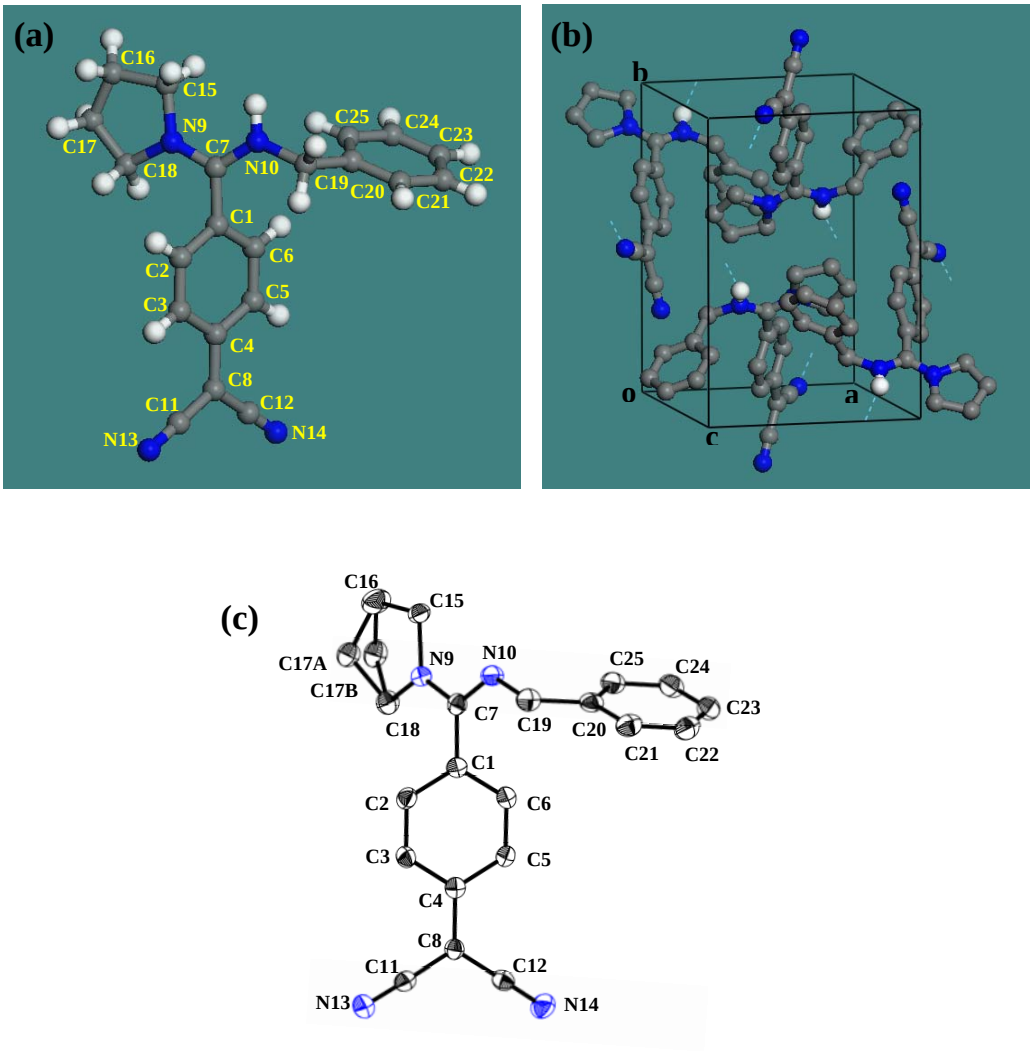

Figure 5.1. ***(a)*** *Molecular and* ***(b)*** *crystal structure of PBEDQ from X-ray diffraction analysis. C (grey), N (blue), H (white) atoms are indicated, the disordered C17 is shown in the averaged position and the H atoms (except the amine ones) are omitted in (b) for clarity and* ***(c)*** *the molecular structure showing the disorder in the position of carbon atom C17; H atom are omitted for clarity.*

structure. The significant crystallographic data are collected in Table 5.1. The molecular structure shows the prominent twist between the diaminomethylene moiety and the benzenoid ring plane (bearing the dicyanomethylene group) characteristic of DADQ molecules;[23,24] the relevant dihedral angles are $\tau_{N9\text{-}C7\text{-}C1\text{-}C2} = 54.7^{o}$, $\tau_{N10\text{-}C7\text{-}C1\text{-}C6} =$

58.3°. Intermolecular H-bonds between the amine H and one of the cyano N's [$r_{H10...N13'}$ = 2.001 Å, $\theta_{N10-10...N13'}$ = 160.2°] lead to extended supramolecular chains along the [1 0 -1] direction. The benzenoid rings show a slipped π-π contact with an interplanar distance of 2.772 Å and a centroid-centroid distance of 5.121 Å; these contacts link the H-bonded chains into sheet structures in the *ac* plane (Fig. 5.2a). Another intermolecular slipped π-π contact between the phenyl rings of the benzylamine group is also observed in the crystal structure (Fig. 5.2b).

Table 5.1. *Crystallographic data for PBEDQ*

Empirical formula	$C_{21}H_{20}N_4$
Crystal system	Monoclinic
Space group	$P2_1/n$
a / Å	9.4123 (7)
b / Å	12.9289 (10)
c / Å	14.5929 (11)
β / deg.	99.2920 (10)
V / Å^3	1752.5 (2)
Z	4
$\rho_{calc.}$ / g cm^{-3}	1.245
μ / cm^{-1}	0.76
Temperature / K	100 (2)
λ / Å	0.71073
No. of reflections	3087
No. of parameters	240
Max., Min. transmission	0.976, 0.967
GOF	1.060
R [for $I \geq 2\sigma_I$]	0.0416
wR^2	0.1090
Largest difference peak and hole / eÅ^{-3}	0.376 / -0.309

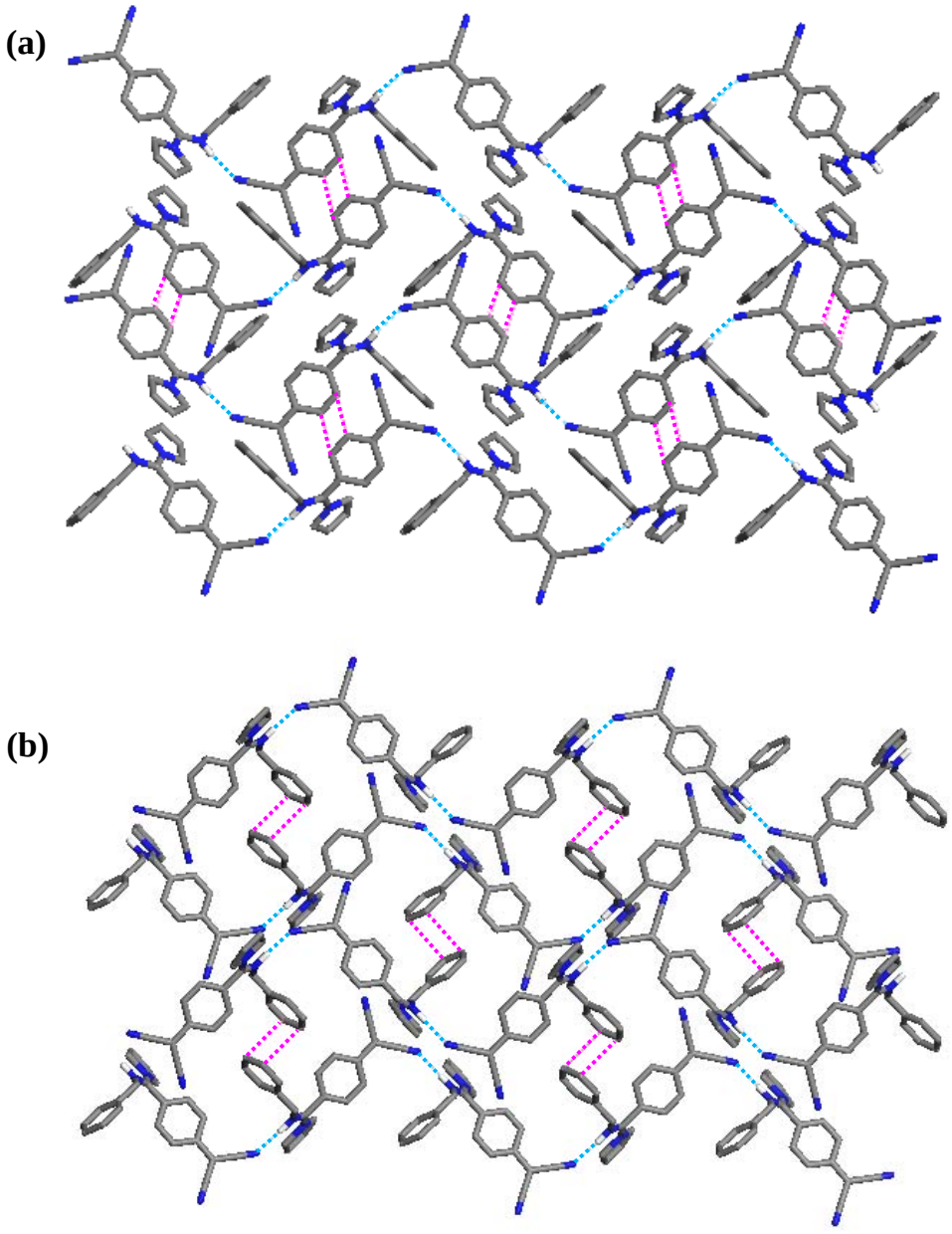

Figure 5.2. ***(a)*** *and* ***(b)*** *H-bonding (cyan broken line) and the short intermolecular contacts involved in π-π interaction (pink broken line) leading to layer structures in crystals of PBEDQ. C (grey), N (blue), H (white) atoms are indicated, the disordered C17 is shown in the averaged position and the H atoms (except those involved in H-bonding) are omitted for clarity.*

5.3. PBEDQ Solution and Microcrystals - Spectroscopy and Computation

Electronic absorption and fluorescence emission spectra of PBEDQ in acetonitrile solution and as microcrystalline solid are presented in Fig. 5.3. The solution shows an absorption with λ_{max} at 370 nm due to the characteristic intramolecular charge transfer of DADQ molecules. The solid shows a broad (320 – 400 nm) absorption in the same region. The fluorescence emission shows λ_{max} at 512 and 456 nm respectively in the solution and solid respectively. The significant blue shift of the peak in the solid is accompanied by an enhancement of intensity of ~ 400.

Ab initio quantum chemical computations were carried out using the density functional method at the B3LYP/6-31G* level; Gaussian03 program was used.[25] Geometry optimization was carried out for the isolated molecule as well as the molecule with different solvent environments using the self-consistent reaction field (SCRF) approach. Different monomer and dimer geometries were considered for the computational studies (Fig. 5.4 and Fig. 5.5).

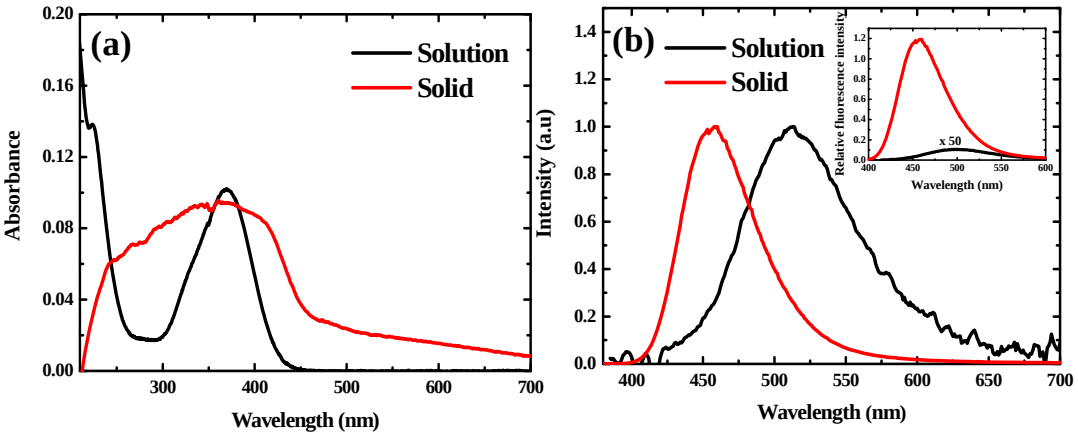

Figure 5.3. ***(a)*** *Optical absorption spectra (with concentrations adjusted to match peak absorbances) and* ***(b)*** *normalized fluorescence emission spectra of acetonitrile solution and microcrystalline solid of PBEDQ (inset: relative emission intensity of samples with matched optical density).*

Electronic excitation profiles of the molecule and its H-bonded and π-dimers extracted from the crystal lattice (Fig. 5.5) were calculated using the time-dependent density functional (TD-DFT) method; impact of the lattice environment was incorporated using the solvation model. The TD-DFT computations were carried out at the B3LYP/6-31G* level, without and with inclusion of solvent effects [SCRF (Solvent); OFac=0.8; Rmin=0.5]. The solvation model provides a useful approximation of the microscopic environment of the molecule in the crystal lattice;[23] the appropriate solvent was chosen based on the agreement of the computed structure

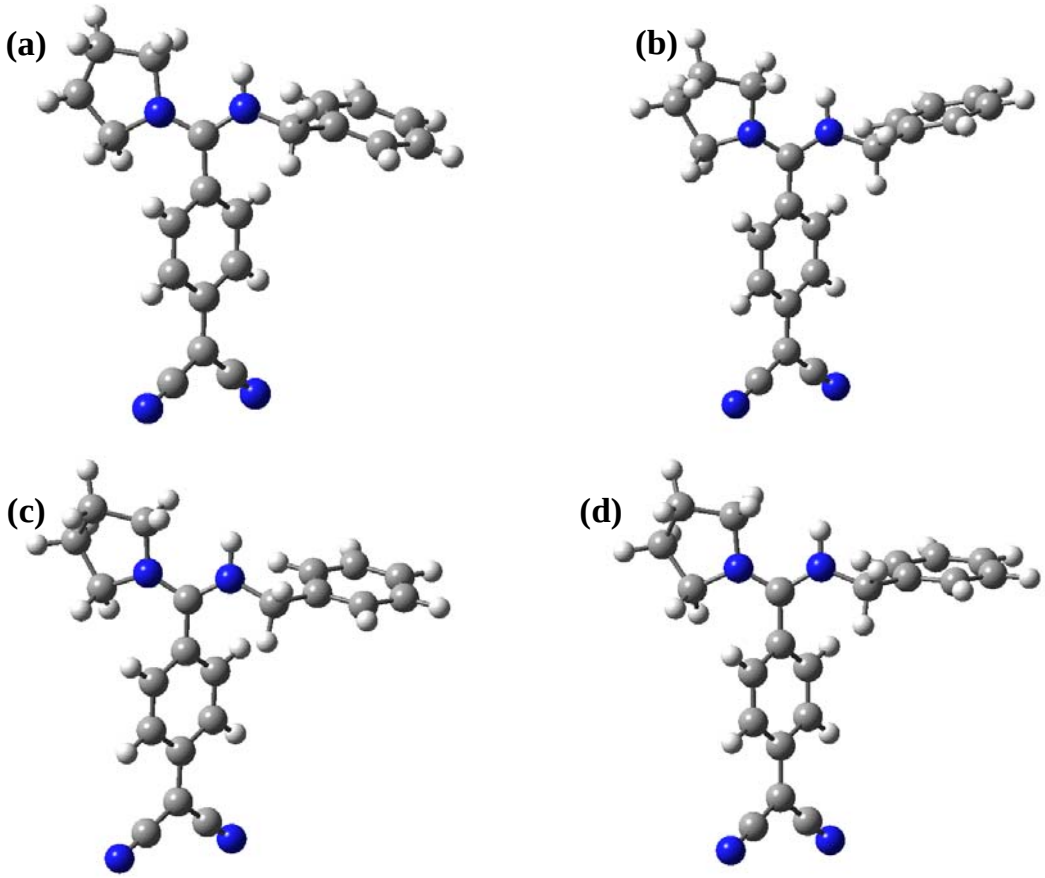

Figure 5.4. *PBEDQ monomer geometries used in the computation of excitation energies:* ***(a)*** *taken from the crystal structure,* ***(b)*** *fully optimized in vacuum,* ***(c)*** *fully optimized with SCRF= acetonitrile and* ***(d)*** *fully optimized with SCRF= water.*

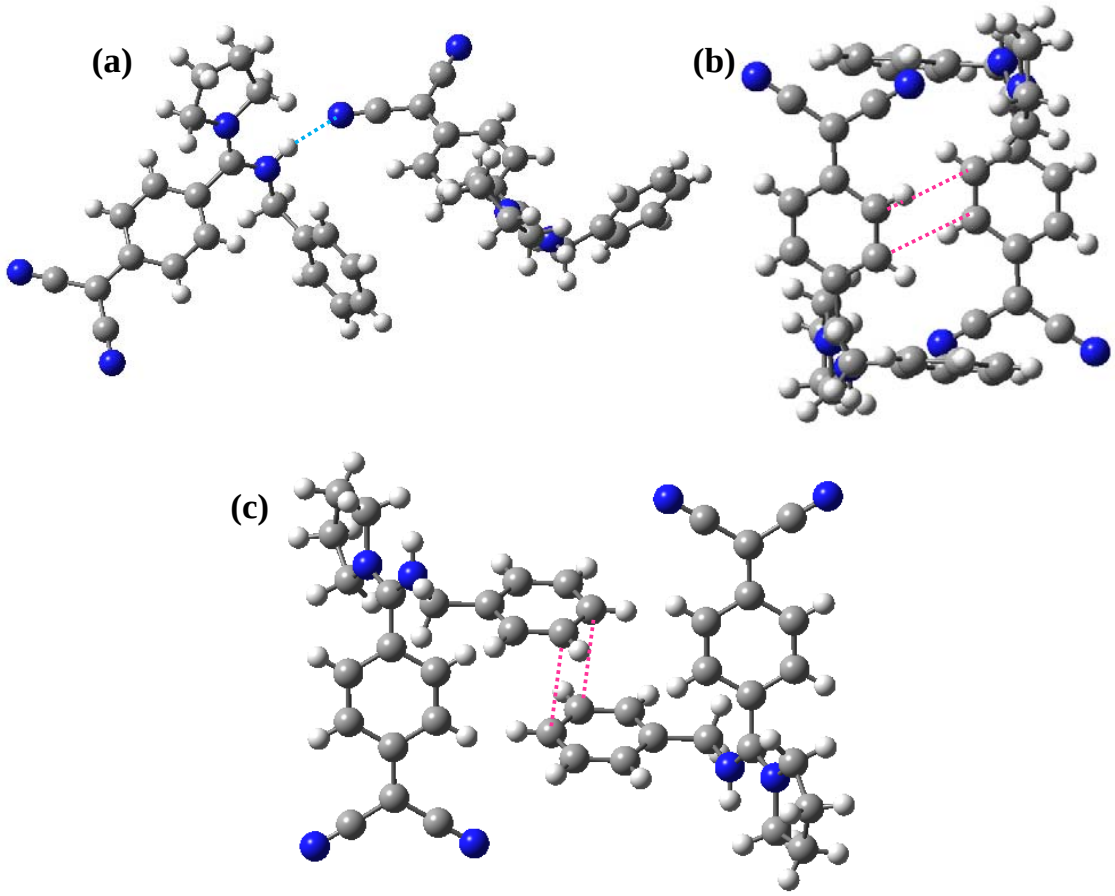

Figure 5.5. *PBEDQ dimer geometries from the crystal structure used in the computation of excitation energies:* ***(a)*** *H-bonded dimer (H-bond is shown by the cyan broken line),* ***(b)*** *π-dimer 1 and* ***(c)*** *π-dimer 2 (the π-interactions are shown by the pink broken lines).*

with that observed in the crystal, specifically in terms of the characteristic dihedral twist angle of the DADQ framework that is sensitive to the dielectric environment.

The salient results are compiled in Tables 5.2 and 5.3. The solution absorption was computed using the fully optimized structure of PBEDQ; the molecular structure from the crystal was used as the starting point for the optimization and the acetonitrile

solvent environment was included in the computation. The significant absorption λ_{max} (with high oscillator strength) is found at ~ 386 nm, in good agreement with the solution spectrum. The dihedral twist angle in the optimized molecular structure of DADQ's is sensitive to the dielectric constant of the environment imposed during the optimization.[23] In the case of PBEDQ, an environment equivalent to that of water is required to reproduce the dihedral twist of the molecule in the crystal (Table 5.2). This indicates that within this simple model, the dielectric environment of the molecule in the crystal can be mimicked using water solvation. The absorption features computed for the PBEDQ monomer and different dimers are collected in Tables 5.2 and 5.3. From the computations including water solvation, it is seen that the λ_{max} (with high oscillator strength) decreases down to ~ 354 nm. These results indicate that the molecular packing in the crystal lattice leads to the blue shift in the optical absorption and emission spectra.

Table 5.2. *Experimental and computed (B3LYP/6-31G* and B3LYP/6-31G*/SCRF) geometric, electronic and spectroscopic parameters of PBEDQ monomer. The two dihedral angles and the average value for each structure are shown and the absorptions with λ_{max} > 250 nm and oscillator strength (f) > 0.1 are listed. The specific data directly relevant to the discussion are shown in bold.*

Molecular geometry	**Twist angles, τ [Average] (deg.)**	**λ_{max} (nm) [f]**		
		Vacuum	**Acetonitrile**	**Water**
From crystal structure	58.3, 54.7 **[56.5]**	512.4 [0.33] 303.4 [0.37]	372.7 [0.47] 264.1 [0.27]	**367.6 [0.48]** 262.4 [0.26]
Optimized (vacuum)	33.6, 36.4 [35.0]	430.0 [0.80] 272.2 [0.11]	-	-
Optimized (acetonitrile)	53.4, 53.6 [53.5]	-	**386.0 [0.56]** 262.3 [0.23]	-
Optimized (water)	55.1, 54.8 **[55.0]**	-	-	378.3 [0.54] 262.4 [0.23]

Table 5.3. *Computed (B3LYP/6-31G* and B3LYP/6-31G*/SCRF) electronic and spectroscopic parameters of PBEDQ dimers. The absorptions with λ_{max} > 250 nm and oscillator strength (f) > 0.1 are listed. The specific data directly relevant to the discussion are shown in bold.*

Structure	λ_{max} (nm) [f]	
	Vacuum	**Water**
H-bonded dimer	480.8 [0.40] 470.9 [0.25] 292.4 [0.30] 291.0 [0.26]	**364.3 [0.52]** **359.6 [0.46]** 260.1 [0.26] 259.6 [0.21]
π-dimer 1	414.0 [0.55] 277.8 [0.48]	**354.2 [0.76]** 264.1 [0.17] 257.3 [0.25]
π-dimer 2	495.8 [0.63] 300.7 [0.75]	**366.4 [0.93]** 264.0 [0.38] 260.7 [0.10]

5.4. Fabrication and Optical Properties of PBEDQ Nanostructures

In a conventional reprecipitation process, injection of small amounts of an acetonitrile solution of PBEDQ into toluene (nonsolvent for PBEDQ) produced a colloid. The colloid shows a blue emission characteristic of crystalline PBEDQ. It was filtered through a nanoporous membrane and observed in an FESEM (Fig. 5.6); formation of fibrous nanostructures could be discerned clearly. The spectroscopy and microscopy observations suggest that PBEDQ molecules assemble into crystalline fibers in presence of toluene. This prompted us to explore in detail, thin films of PBEDQ fabricated by drop-casting solutions with different acetonitrile-toluene compositions.

Typically 0.3 – 0.6 mM solutions of PBEDQ in acetonitrile-toluene mixtures with varying composition (100:0 to 10:90 v/v) were drop-cast on glass/quartz substrates

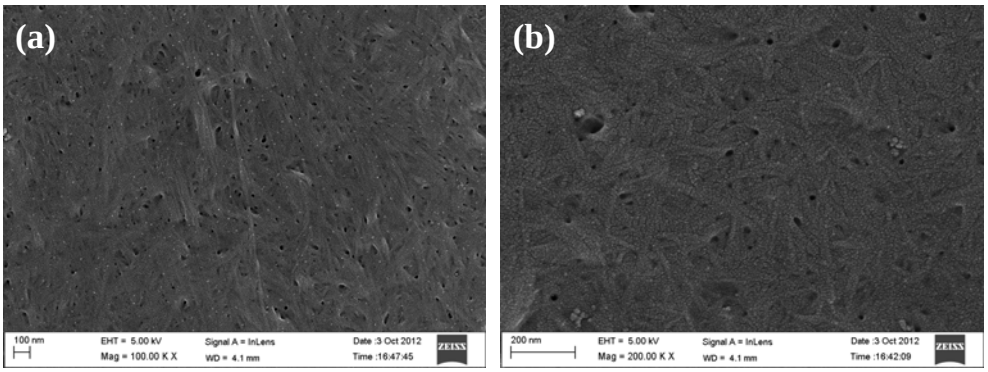

Figure 5.6. *FESEM images of the colloid of PBEDQ (images at different magnifications are shown in (a) and (b)).*

and the resulting films dried quickly under ambient atmosphere. FESEM images illustrating the morphology of the thin films formed are collected in Fig. 5.7. Shape of the particles is spherical in the case of pure acetonitrile. The morphology is characteristic of amorphous nanoparticles formed by DADQ derivatives possessing aromatic substituent groups connected through conformationally labile bonds (compare with Fig. 4.8 for BBPEDQ).[16] With the introduction of small amounts of toluene in the solvent, the drop-cast films show spherical particles together with fibrous nanostructures. The presence of toluene not only reduces the solubility of PBEDQ, but also slows down the drying of the drop-cast film. When the toluene content is increased, the nanofibers become the dominant structures, and the film is exclusively made of the fibers when the acetonitrile-toluene composition is 40:60. It may be noted that crystalline organic fibers have been fabricated earlier by the fast evaporation of capillary films.[26] Emergence of faceted nano/microcrystals of PBEDQ is observed when the solvent composition reaches 10:90.

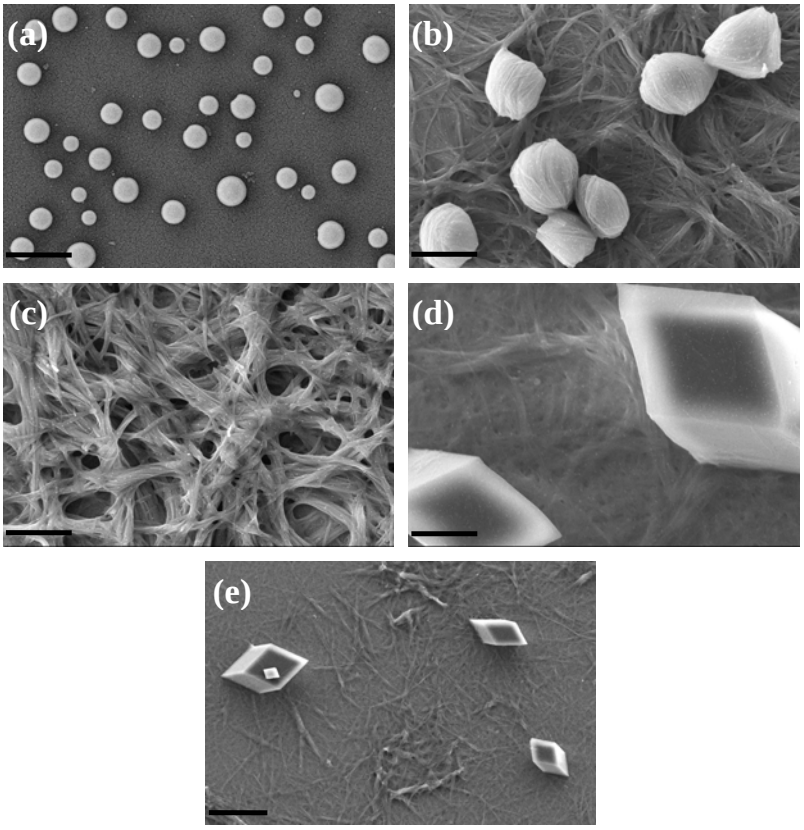

Figure 5.7. *FESEM images of thin films fabricated by drop-casting PBEDQ in acetonitrile-toluene mixtures with varying composition:* ***(a)*** *100:0,* ***(b)*** *80:20,* ***(c)*** *40:60,* ***(d)*** *and* ***(e)*** *10:90. Scale bar is 1 μm in (a) to (d) and 5 μm in (e).*

Subtle variations in the drop-casting conditions and treatment of the drop-cast films lead to the formation of a wide range of morphologies with varying amorphous/crystalline structures. The following typical examples illustrate this. Enclosing the films drop-cast from acetonitrile solution (3 mM) inside a covered petri-dish slows down the evaporation of the solvent and drying of the film leading to the formation of nanofibers (Fig. 5.8a) instead of the spherical particles. Films obtained by quick drying, made up of the spherical particles (Fig. 5.7a), when exposed again to acetonitrile vapors shows the formation of nanofibers emanating from the spherical

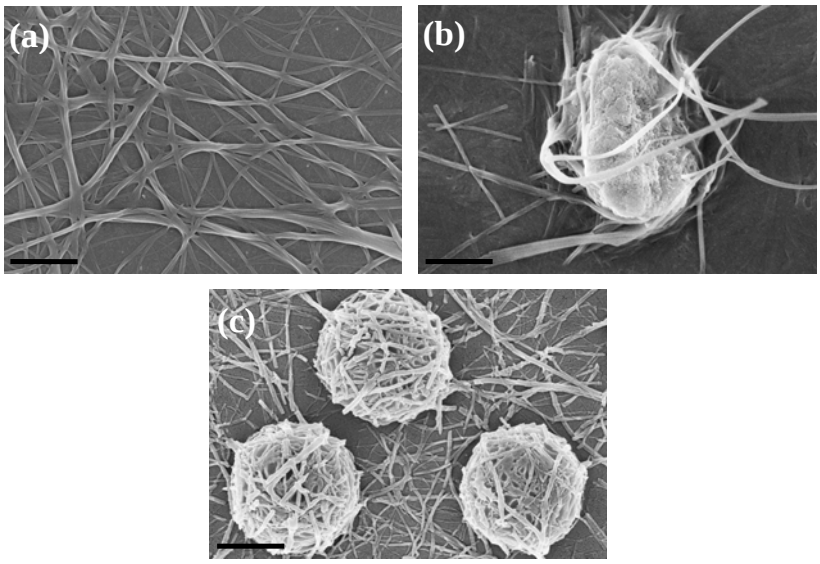

Figure 5.8. *FESEM images of thin films fabricated by drop-casting PBEDQ in* ***(a)*** *acetonitrile and evaporating the solvent slowly,* ***(b)*** *acetonitrile, evaporating the solvent quickly and then exposing to acetonitrile vapors,* ***(c)*** *methanol and evaporating the solvent slowly. Scale bar = 1 µm.*

seeds (Fig. 5.8b), a vivid illustration of the crystalline structures emerging smoothly from the amorphous ones. Slow evaporation of the solvent in the films drop-cast from methanol solutions of PBEDQ reveal spherical particles enveloped in a fiber network (Fig. 5.8c). These observations point to the rich variety of morphologies and more significantly, extents of crystallinity of the PBEDQ nanostructures that can be realized by optimization of the conditions for fabrication of the drop-cast thin films. An earlier study of some interest in this context is the control of self-assembly and long-range orientational order in H-bonded oligothiophene polymorphs through variation of solvent evaporation and crystal growth conditions.[27]

Absorption and emission spectra of the drop-cast films are collected in Fig. 5.9a and 5.9b respectively. The relatively broader spectrum with higher baseline of the film with the spherical particles can be attributed to stronger scattering from the amorphous

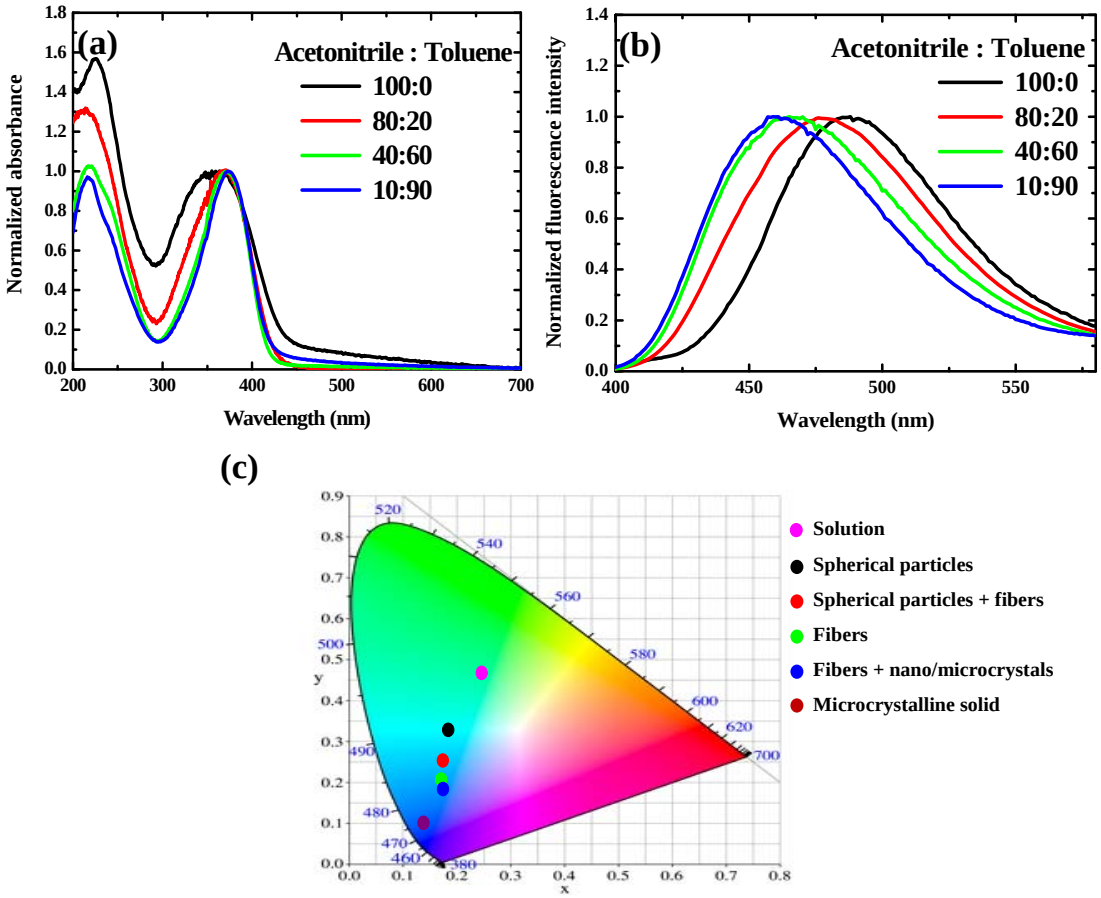

Figure 5.9. ***(a)*** *Absorption and* ***(b)*** *emission spectra of thin films fabricated by drop-casting (on quartz) PBEDQ in acetonitrile-toluene mixtures with varying composition.* ***(c)*** *CIE chromaticity plot of the thin films fabricated by drop-casting acetonitrile-toluene mixtures of different compositions [100:0 (spherical particles); 80:20 (spherical particles + fibers); 40:60 (fibers); 10:90 (fibers + nano/microcrystals)] together with that of the solution and microcrystalline solid.*

particles. The emission spectra are recorded by exciting at the maximum of the fluorescence excitation spectrum in each case (Fig. 5.10); they reveal the evolution from amorphous to crystalline nanostructures, consistent with the microscopy observations above. The film with spherical particles obtained from the acetonitrile solution shows

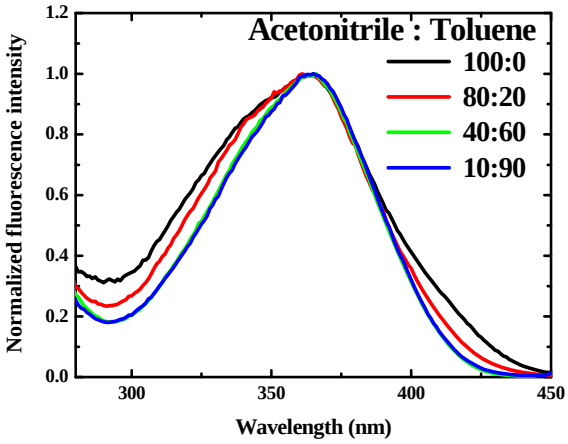

Figure 5.10. *Fluorescence excitation spectra of thin films fabricated by drop-casting PBEDQ in acetonitrile-toluene mixtures with varying composition.*

emission (λ_{max} ~ 488 nm) close to green reminiscent of the solution. With increasing toluene content in the solvent used for drop-casting, the peak shifts steadily to the blue; emission of the films with nanofibers and nano/microcrystals resemble that of the bulk microcrystalline solid (λ_{max} ~ 460 nm). Confocal fluorescence images of the films (Fig. 5.11) together with the spectral responses from the individual nanostructures (Fig. 5.12) confirm this. Fine-tuning of the emission color across the series (including also the solution and bulk solid) is clearly demonstrated by the chromaticity plot in Fig. 5.9c. Significantly, the quantum yield for the emission is also found to increase across the series (Table 5.4), in parallel to the extent of crystallinity. This is consistent with the general concept of lattice rigidification inhibiting structural (rotational) relaxation of the excited state of DADQ molecules leading to fluorescence enhancement (Fig. 2.2).[20,22] FLIM images of the drop-cast films illustrate the progression of excited state lifetimes across the series (Fig. 5.13 and 5.14, Table 5.4) consistent with the fluorescence emission enhancement.

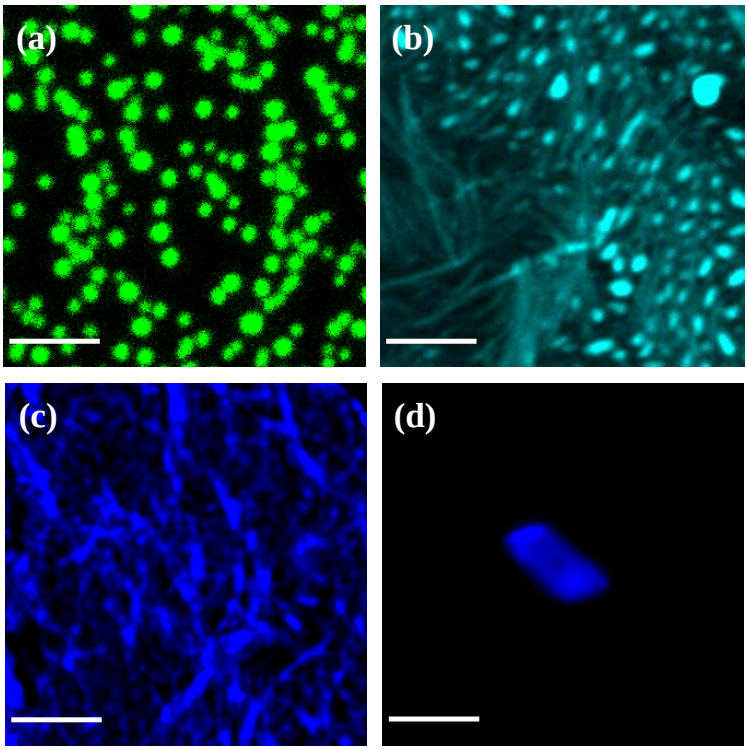

Figure 5.11. *Confocal fluorescence images of thin films fabricated by drop-casting PBEDQ in acetonitrile-toluene mixtures with varying composition:* ***(a)*** *100:0,* ***(b)*** *80:20,* ***(c)*** *40:60,* ***(d)*** *10:90. Scale bar = 5 µm.*

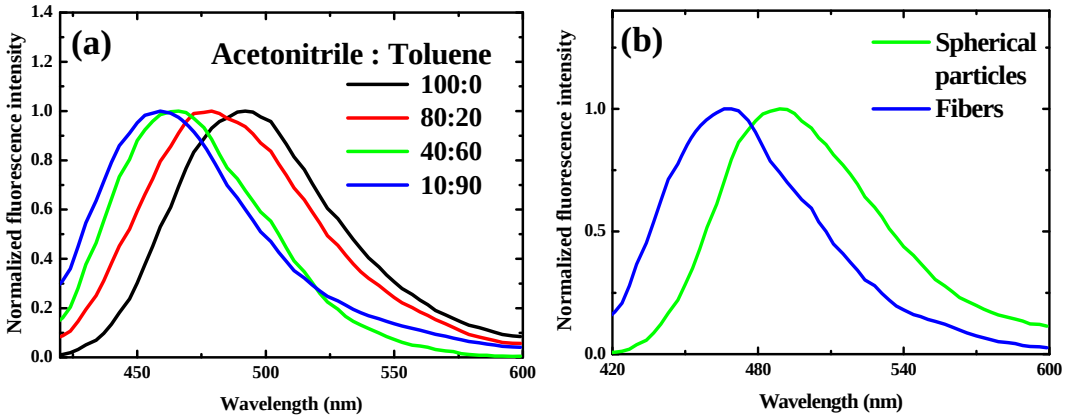

Figure 5.12. *Confocal fluorescence spectral responses of thin films fabricated by drop-casting PBEDQ* ***(a)*** *in acetonitrile-toluene mixtures with varying composition and* ***(b)*** *from the individual nanostructures in the thin film fabricated by drop-casting PBEDQ in acetonitrile-toluene mixture (80:20).*

Table 5.4. *Fluorescence quantum yield and average excited state lifetime of PBEDQ in different states, solution to drop cast films of varying amorphous/crystalline nature to microcrystalline solid.*

Acetonitrile: Toluene	Structure	Quantum yield[28] (%)	Average life time (ns)
-	Solution	0.1	< 0.18
100:0	Film (spherical particles)	1.6	0.64
80:20	Film (spherical particles + fibers)	2.2	0.89
40:60	Film (fibers)	4.4	1.02
10:90	Film (fibers + nano/microcrystals)	6.5	1.93
-	Microcrystalline solid	36.4	2.63

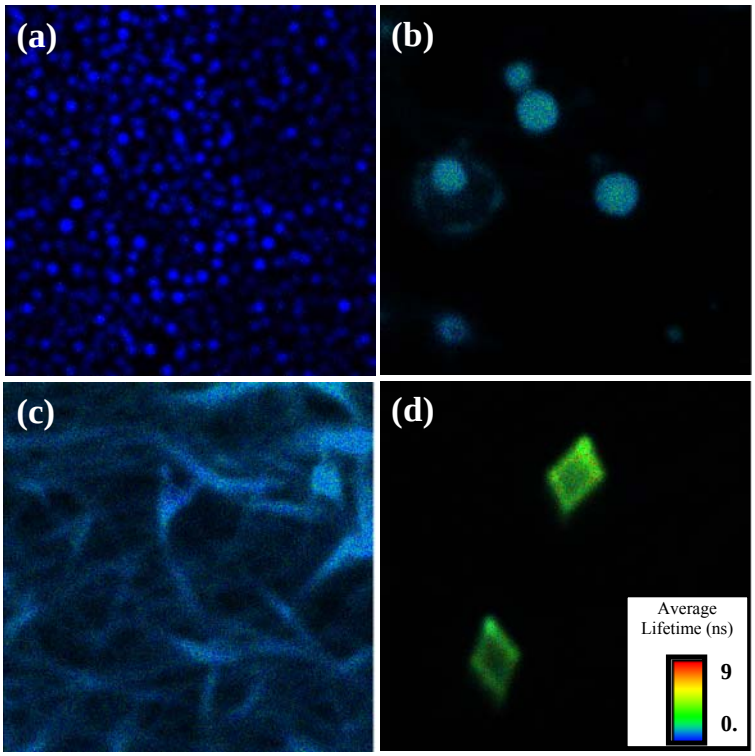

Figure 5.13. *FLIM images (20 μm × 20 μm) of thin films fabricated by drop-casting PBEDQ in acetonitrile-toluene mixtures with varying composition:* ***(a)*** *100:0,* ***(b)*** *80:20,* ***(c)*** *40:60,* ***(d)*** *10:90. The color code for the lifetime applicable to all the figures is shown in (d).*

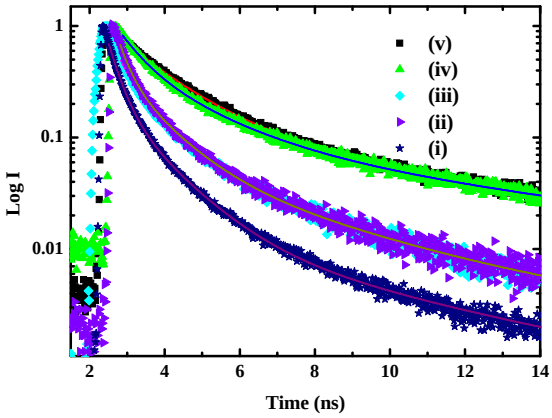

Figure 5.14. *Fluorescence emission decay profiles of thin films fabricated by drop-casting PBEDQ in acetonitrile-toluene mixtures with varying composition: (i) 100:0, (ii) 80:20, (iii) 40:60 and (iv) 10:90 and (v) the bulk solid.*

5.5. Characterization of the Amorphous and Crystalline Nanostructures

TEM and PXRD are used for characterization of the nanostructures. By coating the drop-cast films with a thin layer of polystyrene, drying and peeling off, we have fabricated free-standing films containing the nanostructures fixed in it. Placing these on a carbon-coated copper grid and dissolving the polystyrene film in toluene, TEM images of the nanostructures could be recorded. Images of the structures formed in the drop-cast films obtained using the 100:0, 40:60 and 10:90 acetonitrile-toluene mixtures are shown in Fig. 5.15; the morphologies are similar to those in the FESEM images (Fig. 5.7). The spherical particles obtained in the first case (Fig. 5.15a) gave no electron diffraction pattern; this observation is consistent with its amorphous nature. The nanofibers (Fig. 5.15b) produced a well-defined ring pattern (see inset) typical of polycrystalline materials; the lattice spacing is consistent with one of the reflections in the PBEDQ crystal, indicating a preferred growth direction. The nanocrystals (Fig. 5.15c) gave clear electron diffraction spots (see inset) which could also be indexed to the lattice structure of PBEDQ. In a separate experiment, we have enriched the content

in the acetonitrile-toluene solution (10:90) by keeping it for several hours and filtered through a nanoporous membrane; the FESEM image (Fig. 5.16) shows the formation of microcrystals and nanofibers. Powder x-ray diffraction pattern of the microparticles is fully consistent with the crystal structure of PBEDQ, confirming the crystalline nature and ruling out the formation of any polymorphic structures (Fig. 5.17).

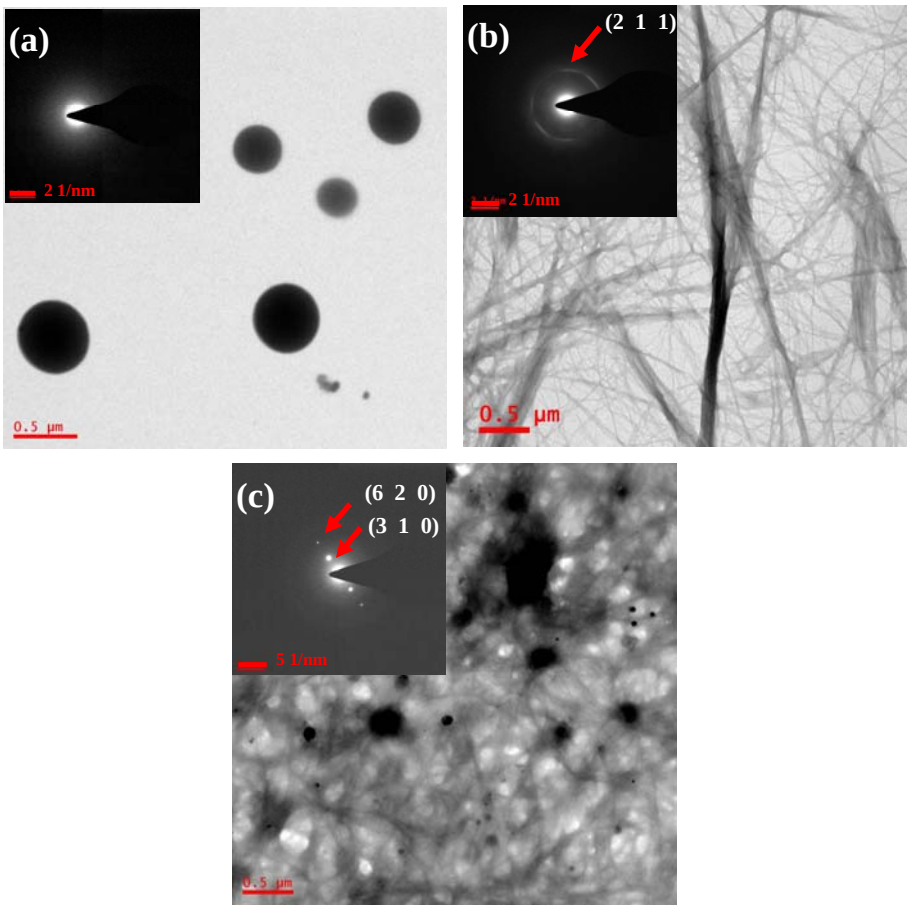

Figure 5.15. *TEM images (along with the SAED) of nanoparticles, nanofibers and nano/microcrystals fabricated by drop-casting PBEDQ in acetonitrile-toluene mixtures with the compositions:* ***(a)*** *100:0,* ***(b)*** *40:60 and* ***(c)*** *10:90. Indexing of the diffraction pattern to specific planes of the PBEDQ is indicated in the insets of (b) and (c).*

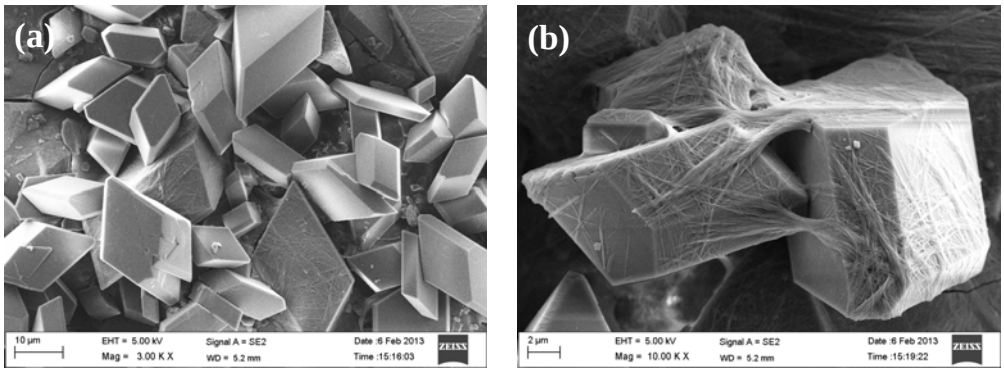

Figure 5.16. *FESEM images of microcrystals obtained from acetonitrile-toluene mixture with 10:90 composition by keeping for several hours (images at different magnifications are shown in (a) and (b)).*

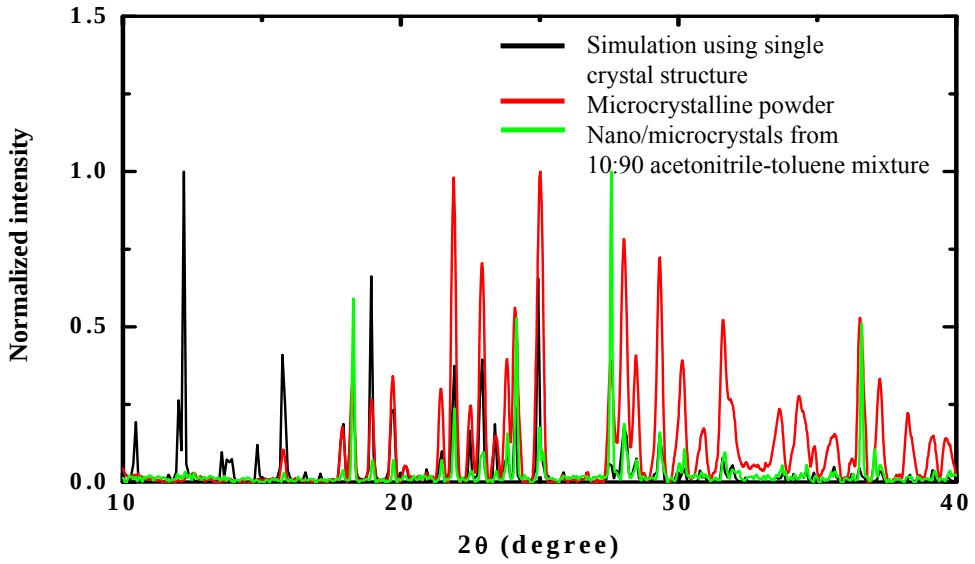

Figure 5.17. *X-ray diffraction pattern of the microcrystalline powder samples of PBEDQ compared to the pattern obtained by simulation using single crystal structure.*

5.6. Discussion

Tuning of the crystallinity and optical responses of PBEDQ nanostructures has interesting parallels and significant contrasts with the case of conjugated polymer nanoparticles of poly(3-hexylthiophene) mentioned in the Sec. 5.1.[10] In both cases, the

extent of crystallinity is controlled by the solvent composition, and increasing content of the nonsolvent enhances the crystallinity. The observation with PBEDQ is a novel illustration of such phenomena with small molecule based materials. While the extent of crystalline assembly primarily influences the electronic absorption features and photoluminescence decays in the polymer nanoparticles, the case of PBEDQ involves prominent changes in the emission characteristics in terms of the color and more significantly the quantum yields, aspects of considerable interest in practical applications.

5.7. Conclusions

A new diaminodicyanoquinodimethane derivative PBEDQ is synthesized, structurally characterized and demonstrated to be an interesting system to develop strongly fluorescent nanostructures. The nanostructures of PBEDQ in thin films fabricated by drop-casting solvent mixtures of varying composition exhibit a smooth progression of morphologies and crystallinity. While the solution and the crystalline solid state represent the two extremes of molecular materials commonly studied, the nanostructures of PBEDQ including the amorphous phase represent logical intermediates in terms of the supramolecular assembly and fluorescence characteristics, the latter in terms of both energies and efficiencies. The studies presented in the chapter establish a fundamentally interesting approach to luminescent molecular materials based on tuned assembly of a new kind.

References

1. E. Gomar-Nadal, J. Puigmartí-Luis, D. B. Amabilino, *Chem. Soc. Rev*. **2008**, *37*, 490.
2. M. J. Prakash, P. Raghavaiah, Y. S. R. Krishna, T. P. Radhakrishnan, *Angew. Chem. Int. Ed.* **2008**, *47*, 3969.
3. M. Sakai, M. Iizuka, M. Nakamura, K. Kudo, *Synth. Metals* **2005**, *153*, 293.
4. S. Dey, A. J. Pal, *Langmuir* **2011**, *27*, 8687.
5. Z. Wang, R. Bao, X. Zhang, X. Ou, C. Lee, J. C. Chang, X. Zhang, *Angew. Chem. Int. Ed.*, **2011**, *50*, 2811.
6. S. Raoux, D. Ielmini, M. Wuttig, I. Karpov, *MRS Bull.* **2012**, *37*, 118.
7. P. G. Vekilov, *J. Cryst. Growth* **2005**, *275*, 65.
8. P. G. Vekilov, *Nanoscale* **2010**, *2*, 2346.
9. D. Erdemir, A. Y. Lee, A. S. Myerson, *Acc. Chem. Res.* **2009**, *42*, 621.
10. G. Nagarjuna, M. Baghgar, J. A. Labastide, D. D. Algaier, M. D. Barnes, D. Venkataraman, *ACS nano* **2012**, *6*, 10750.
11. Y. Shirota, H. Kageyama, *Chem. Rev.* **2007**, *107*, 953.
12. S. Park, J. Choi, K. H. Lee, H. W. Yeom, S. Im, Y. K. Lee, *J. Phys. Chem. B* **2010**, *114,* 5661.
13. L. Zheng, J. Liu, Y. Ding, Y. Han, *J. Phys. Chem. B* **2011**, *115*, 8071.
14. Y. Dong, J. W. Y. Lam, A. Qin, Z. Li, J. Sun, H. H.-Y. Sung, I. D. Williams, B. Z. Tang, *Chem. Commun.* **2007**, 40.
15. X. Zhou, H. Li, Z. Chi, B. Xu, X. Zhang, Y. Zhang, S. Liu, J. Xu, *J. Fluor.* **2012**, *22*, 565.
16. C. G. Chandaluri, T. P. Radhakrishnan, *Angew. Chem. Int. Ed.* **2012**, *51*, 11849.
17. B. Balaswamy, L. Maganti, S. Sharma, T. P. Radhakrishnan, *Langmuir* **2012**, *28*, 17313.
18. Y. Hong, J. W. Y. Lam, B. Z. Tang, *Chem. Commun.* **2009**, 4332.

19. A. Patra, C. G. Chandaluri, T. P. Radhakrishnan, *Nanoscale* **2012**, *4*, 343.

20. S. Jayanty, T. P. Radhakrishnan, *Chem. Eur. J.* **2004**, *10*, 791.

21. A. Patra, N. Hebalkar, B. Sreedhar, M. Sarkar, A. Samanta, T. P. Radhakrishnan, *Small* **2006**, *2*, 650.

22. C. G. Chandaluri, A. Patra, T. P. Radhakrishnan, *Chem. Eur. J.* **2010**, *16*, 8699.

23. S. Jayanty, T. P. Radhakrishnan, *Chem. Mater.* **2001**, *13*, 2460.

24. T. P. Radhakrishnan, *Acc. Chem. Res.* **2008**, *41*, 367.

25. *Gaussian 03*, Revision E.01, M. J. Frisch, G. W. Trucks, H. B. Schlegel, G. E. Scuseria, M. A. Robb, J. R. Cheeseman, J. A. Jr. Montgomery, T. Vreven, K. N. Kudin, J. C. Burant, J. M. Millam, S. S. Iyengar, J. Tomasi, V. Barone, B. Mennucci, M. Cossi, G. Scalmani, N. Rega, G. A. Petersson, H. Nakatsuji, M. Hada, M. Ehara, K. Toyota, R. Fukuda, J. Hasegawa, M. Ishida, T. Nakajima, Y. Honda, O. Kitao, H. Nakai, M. Klene, X. Li, J. E. Knox, H. P. Hratchian, J. B. Cross, V. Bakken, C. Adamo, J. Jaramillo, R. Gomperts, R. E. Stratmann, O. Yazyev, A. J. Austin, R. Cammi, C. Pomelli, J. W. Ochterski, P. Y. Ayala, K. Morokuma, G. A. Voth, P. Salvador, J. J. Dannenberg, V. G. Zakrzewski, S. Dapprich, A. D. Daniels, M. C. Strain, O. Farkas, D. K. Malick, A. D. Rabuck, K. Raghavachari, J. B. Foresman, J. V. Ortiz, Q. Cui, A. G. Baboul, S. Clifford, J. Cioslowski, B. B. Stefanov, G. Liu, A. Liashenko, P. Piskorz, I. Komaromi, R. L. Martin, D. J. Fox, T. Keith, M. A. Al-Laham, C. Y. Peng, A. Nanayakkara, M. Challacombe, P. M. W. Gill, B. Johnson, W. Chen, M. W. Wong, C. Gonzalez, J. A. Pople, Gaussian, Inc., Wallingford CT, **2004**.

26. X. Zhang, B. Sun, *J. Phys. Chem. B* **2007**, *111*, 10881.

27. I. D. Tevis, L. C. Palmer, D. J. Herman, I. P. Murray, D. A. Stone, S. I. Stupp, *J. Am. Chem. Soc.* **2011**, *133*, 16486.

28. J. N. Demas, G. A. Crosby, *J. Phys. Chem.* **1971**, *75*, 991.

6.1. Overview of the Work Presented in the Thesis

Fluorescent molecular materials are of great interest from both fundamental and as well as application perspectives. The specific molecular assembly and interactions involved in the aggregation generally quenches the fluorescence of the supramolecular structures and hence limits their application potential. We have focused attention on a family of molecules which circumvent the quenching problem and develop into highly fluorescent materials in the form of crystals, nanocrystals, nanoparticles and colloidal formations. The salient aspects of controlling the molecular assembly through extrinsic factors such as template and substrate effects and aggregation conditions are highlighted in the thesis. The notable consequence of these steered assemblies to the fluorescence emission characteristics demonstrates the significance of these studies to materials applications. A major advancement realized through the studies presented in this thesis is the critical importance of the amorphous phase in small molecules based materials.

We have developed a family of novel molecular crystals based on the diaminodicyanoquinodimethane (DADQ) frame work. The new materials developed show strong light emission across the green to blue region exhibiting high quantum yields than that of their solution state. The new materials are particularly related for optical materials applications as they open up the blue front for the emission of DADQ's; earlier materials reported from our laboratory cover the red and green regions. These materials are characterized in detail using crystallographic, spectroscopic and computational investigations.

Nanomaterials based on the DADQ molecules fabricated by simple techniques such as reprecipitation and drop-casting form another important area of our investigations. We have addressed in the thesis, the fundamental problem in the

reprecipitation method for the fabrication of nanoparticles of molecules that show appreciable solubility in common solvents. The molecule of interest is complexed with a polyelectrolyte and solvents are chosen to be miscible as usual, but good or bad with respect to the polyelectrolyte rather than the molecule of interest. Nanoparticles formed in this approach showed large fluorescence enhancement over their solutions. Spectroscopic and calorimetric experiments were used to model the molecular level interactions and aggregation effects in this system. This approach provides a simple route for the fabrication of molecular nanoparticles of highly soluble molecules, through the reprecipitation protocol.

We have used the simple drop casting technique to fabricate nanoparticles of DADQ's. The novel finding here was that amorphous particles can be fabricated through this simple technique, if some specific structural features are incorporated in the molecule. In the case of DADQ's the presence of aromatic rings linked through conformationally labile bonds is the critical structural component. Further, we have developed a novel protocol for the controlled amorphous-to-crystalline transformation of these particles through partial confinement by fixing in a polymer thin film and solvent vapor fuming. The switching of fluorescence emission color and its strong enhancement accompanying the amorphous-to-crystalline transformation, provides a sensitive signature of the process. The tailored assembly of the amorphous nanoparticles with the small molecule based material, is of fundamental interest to the two-step nucleation theory which proposes liquid-like clusters involved in the nucleation process. The amorphous nanoparticles of the fluorescent molecules could be of interest in developing novel phase change materials.

Realization of the amorphous nanoparticles has also lead to the detailed

investigation of a hierarchical growth of DADQ crystals, starting from the amorphous phase. This was achieved by varying the composition of the good and bad solvents used for the drop-casting process. The nanoparticles could be tuned from amorphous spherical ones to fibrous crystals to faceted crystals, with several intermediate composite structures. The concomitant changes in the fluorescence color, quantum yield and excited state lifetimes were explored in order to characterize the new avenue of hierarchical assembly of molecular materials.

6.2. Future Prospects

A large library of strongly fluorescent materials based on the same fluorophore moiety, DADQ is now available. It would be interesting to explore the basic structure property correlation using this family of fluorescent materials. Basic molecular structural factors such as the dihedral twist angle affect sensitively, the electronic structure of these molecules. The fluorescence efficiency is likely to be effected by nonradiative energy loss pathways involving intramolecular vibrational and rotational relaxations. These could be sensitive to the density of molecular packing in the crystal as well as their mechanical properties. Intermolecular energy loss pathways will be controlled by the distances between molecules and their relative conformational orientations. Exploration of the impact of these various factors on the fluorescence energies and efficiencies of DADQ crystals is under way in our laboratory.

DADQ derivatives possess the advantages of simplicity of synthesis with high yields from easily available precursors, ease of crystallization and good chemical and thermal stability. It would be interesting to make dual fluorescent molecular crystals by co-crystals formation of DADQ derivatives which show different emission color.

Development of white emitting materials by tuning the noncovalent interactions or making covalent bonds between blue, green and red emitting DADQ's would be of great interest in terms of potential applications in display systems. The good solubility of DADQ's can be exploited in fabricating doped polymer films for large area applications. The strongly fluorescent DADQ nanoparticles could also be developed as fluorescent imaging probes, especially for biological systems.

Our investigations of the fabrication of amorphous nanoparticles and amorphous-to-crystalline transformation open ups a new direction of research on small molecule based materials. Utility of these amorphous particles as models to understand the nucleation and crystal growth process needs further investigation. If efficient and reversible cycling between the amorphous and crystalline phases can be achieved, these materials could prove useful for organic memory storage devices. It would also be interesting to explore mechanochromism reported in other molecules, in the case of DADQ's. The amorphous phase will be naturally relevant in the studies.

The family of DADQ molecules and the optical materials based on them hold great promise for several fundamental studies and application.

APPENDIX

Instrumentation

Filtration

Nano/microcrystals were filtered through different poro-sized membranes of mixed cellulose esters (Millipore, VMWP 01300) or polycarbonate (Millipore, VCTP 01300) using 13 mm SST Swinney Syringe filter holders (Millipore XX3001200). DMSO solutions of compounds were filtered through 100 nm pore alumina membrane (Whatman, Anodisc 13).

Spin-coating

Laurell Technologies Corporation Model WS-400B-6NPP/LITE/8K spinner was used for the fabrication of thin polymer films.

Viscosity measurements

Viscosity measurements were carried out at 25^{o}C using Brookfield Viscometers model LVDV-IIIUCP Rheometer.

Weighing

Sartorius BP211D balance was used for high precision weighing.

Melting Point

Melting temperatures of solids were determined using capillary melting point apparatus (Superfit, India); values reported are uncorrected.

Elemental Analysis

Elemental analysis was carried out on a Thermo Finnigan (Flash EA-1112 series) CHNS analyzer.

Nuclear Magnetic Resonance Spectroscopy

^{1}H and ^{13}C NMR spectra were recorded on a Bruker 400 MHz NMR spectrometer. Spectra were recorded using the solvent peaks as the internal standard.

Infrared Spectroscopy

FT-IR spectra were recorded on a Jasco5300 FTIR spectrometer. All the spectra were calibrated against polystyrene absorption at 1601 cm^{-1}. Solid samples were recorded as KBr pellets and liquid samples as thin films between NaCl plates.

Absorption Spectroscopy

Absorption spectra were recorded on a Cary 100 Bio UV-Visible spectrophotometer. Diffuse reflectance spectra of the solid samples were recorded using the DRA-CA-30I sphere accessory, and converted into absorption spectra using the Kubelka-Munk function.

Fluorescence Spectroscopy

Steady-state fluorescence emission and excitation spectra were recorded on a Horiba Jobin Yvon Model FL3-22 Fluorolog spectrofluorimeter. Fluorescence quantum yield of solutions was estimated by comparison with quinine sulfate in 1 N H_2SO_4 (ϕ = 0.546). Absolute value of the fluorescence quantum yield of thin film samples was determined using an integrating sphere and the PLQY Calculator v.3 software (Jobin

Yvon). Time-resolved fluorescence measurements were carried out using time–correlated single-photon counting spectrometer (IBH NanoLED). Diode laser (λ_{exc} = 405 nm, FWHM = 95 ps) was used as the excitation source and an MCP photomultiplier (Hamamatsu R3809U-50) as the detector. The lamp profile was recorded by placing a scatterer (dilute solution of Ludox in water) in place of the sample. Decay curves were analyzed by nonlinear least-squares iteration using IBH DAS6 (Version 2.2) decay analysis software.

Microscopy

Scanning electron microscope imaging was carried out on a Carl Zeiss model Ultra 55 microscope (FESEM) or Philips Model XL30 SEM or HITACHI model S-4300SE/N FESEM. Transmission electron microscope (TEM) imaging and selected area electron diffraction were carried out on a Tecnai G^2 FEI F12 TEM at an accelerating voltage of 120 or 200 kV. Laser scanning confocal fluorescence microscopy was carried out on a Carl Zeiss LSM 710 NLO ConfoCor 3 microscope or Leica model TCS SP2 AOBS laser scanning confocal microscope. Atomic force microscopy images was carried out on a NT-MDT model Solver Pro M AFM. Fluorescence lifetimes imaging of thin films were carried out on a time-domain technique with a MicroTime 200 Instrument (PicoQuant) coupled to an Olympus IX71 Microscope (PicoQuant). Excitation was achieved using a 405 nm pulsed laser diode and the fluorescence observed through a 430 nm long pass filter. FWHM of pulse response function was 176 ps. The intensity decays were analyzed with a multi-exponential model using SymPhoTime v. 5.0 software (PicoQuant).

Isothermal titration calorimetry

Microcal Model VP-ITC isothermal titration calorimeter was used to carry out the calorimetric experiments. Origin 7.0 based software provided by the manufacturer was used to analyze the data.

Single Crystal X-ray Diffraction

Single crystal X-ray diffraction studies were carried out at 100 K or 298 K on a Bruker SMART APEX CCD area detector system equipped with a graphite monochromator and a MoK_α fine-focus sealed tube (λ = 0.71073 Å) operated at 1500 W power (50 kV, 30 mA) or 1200 W power (40 kV, 30 mA). The detector was placed at a distance of 6.003 cm from the crystal. A total of 2400 frames were collected with a scan width of 0.3º in ω mode and an exposure time of 5 or 10 s/frame. The frames were integrated with the Bruker SAINT software using a narrow-frame integration algorithm. Analysis of the data showed negligible decay during data collection. Data was corrected for absorption effects using the multi-scan method (SADABS). The structure was solved and refined using the Bruker SHELXTL (Version 6.14) Software.

Powder X-ray Diffraction

X-ray diffraction pattern of the microcrystalline powder sample were recorded on a SMART Bruker D8 Advance X-ray diffractometer using Cu-Kα radiation (λ = 1.5406 Å) at 40 kV and 30 mA. The simulations were carried out using PowderCell for Windows version 2.4 (W. Kraus and G. Nolze).

PUBLICATIONS

1. **Ch. G. Chandaluri**, A. Patra, T. P. Radhakrishnan, *Chem. Eur. J.* **2010**, *16*, 8699-8706.
   Polyelectrolyte-Assisted Formation of Molecular Nanoparticles Exhibiting Strongly Enhanced Fluorescence

2. **Ch. G. Chandaluri**, T. P. Radhakrishnan, *Opt. Mater.* **2011**, *34*, 119-125.
   Zwitterionic Diaminodicyanoquinodimethanes with Enhanced Blue–Green Emission in the Solid State

3. A. Patra, **Ch. G. Chandaluri**, T. P. Radhakrishnan, *Nanoscale* **2012**, *4*, 343-359.
   Optical Materials Based on Molecular Nanoparticles

4. **Ch. G. Chandaluri**, T. P. Radhakrishnan, *Angew. Chem. Int. Ed.* **2012**, *51*, 11849-11852.
   Amorphous-to-Crystalline Transformation with Fluorescence Enhancement and Switching of Molecular Nanoparticles Fixed in a Polymer Thin Film

5. **Ch. G. Chandaluri**, T. P. Radhakrishnan (Submitted for publication)
   Hierarchical Assembly of a Molecular Material through the Amorphous Phase and the Evolution of its Fluorescence Emission

PRESENTATIONS

1. **Ch. G. Chandaluri**

   Oral presentation at the National Review and Coordination Meeting on Nanoscience and Nanotechnology, Kolkata, India, March 12-14, 2009.

   Fabrication and Optical Properties of Molecular Nanocrystal - Polymer Composites

2. **Ch. G. Chandaluri**

   Oral presentation at Chemfest-2011, School of Chemistry, University of Hyderabad, Hyderabad, India, February 25-26, 2011.

   Highly Fluorescent Molecular Crystals and Nanocrystals

3. **Ch. G. Chandaluri**, T. P. Radhakrishnan

   Poster presented at the International Conference on the Chemistry of the Organic Solid State (ICCOSS XX), Indian Institute of Science, Bangalore, India, June 26-30, 2011.

   Highly Fluorescent Molecular Crystals and Nanocrystals **(Received Best Poster Award)**

4. **Ch. G. Chandaluri**, T. P. Radhakrishnan

   Poster presented in International Symposium on Recent Trends in Spectroscopy and Dynamics of Chemical Systems, University of Hyderabad, Hyderabad, India, Dec 7-8, 2011.

   Highly Fluorescent Molecular Crystals and Nanocrystals: Fabrication and Application

5. **Ch. G. Chandaluri**, T. P. Radhakrishnan

   Poster presented in International Conference on Nanoscience and Technology (ICONSAT-2012), Hyderabad, India, Jan 20-23, 2012.

   Highly Fluorescent Molecular Nanocrystals: Novel Materials, Fabrication Technique and Application **(Selected for free participation)**

6. **Ch. G. Chandaluri**

   Oral presentation at the V International Conference on Molecular Materials (MOLMAT-2012), Barcelona, Spain, July 3-6, 2012.

   Highly Fluorescent Molecular Crystals and Nanocrystals: Novel Materials, Fabrication Techniques and Application

7. **Ch. G. Chandaluri**

   Participated in Indo-Japan Workshop on Recent Advances in Spectroscopy and Microscopy: Fundamentals and Applications to Materials and Biology, University of Hyderabad, Hyderabad, India, Nov 20-21, 2012.